Functionalised peptidomimetic metallohelices

By

Hualong Song

A thesis submitted in partial fulfilment of the requirements of the degree of

Doctor of Philosophy in Chemistry

Department of Chemistry, University of Warwick

September 2018

Table of Contents

List of Figures

List of Schemes

List of Tables

Acknowledgements

Firstly, I would like to thank my supervisor Prof. Peter Scott for giving me the opportunity to work on this extraordinary project. I appreciate the guidance, support and knowledge that he has provided over the last four years. I would also thank to all members of the Scott group who have offered me lots of selfless help and have made me feel welcome whilst working in the UK. I will always remember these kind people: Dr Nicola Rogers, Dr Rebecca Vipond, Dr Dan Simpson, Dr Paul Goring, Dr Connah Burnett, Dr Anish Mistry, Shaun Morris and Sasha Wallis.

I would like to offer my appreciation to Prof. Roger Philips, Dr Simon Alison and Dr Samantha Shepherd for their guidance and expertise regarding biological testing. I would also like to thank the research groups of Prof. Viktor Brabec and Prof. Xiaogang Qu. The collaboration with all three groups for biological studies has enhanced this project.

A special thanks must also go to all of my unscientific friends. They have given me assistance and mental strength whenever I have faced difficulty. I would like to thank all my family for their encouragement. Finally, I would like to thank the China Scholarship Council for the financial support.

Publication

Chapter 2

"Stereochemistry and amyloid inhibition: Asymmetric triplex metallohelices enantioselectively bind to Aβ peptide" Y. Guan, Z. Du, N. Gao, Y. Cao, X. Wang, P. Scott, **H. Song**, J. Ren and X. Qu, *Sci. Adv.*, 2018, **4**, eaao6718.

Chapter 3

"Targeting Enantiomeric G-quadruplex DNA by 10 Pairs of Triplex Metallohelices" C. Zhao, **H. Song**, P. Scott, A. Zhao, J. Ren, X. Qu, *Angew. Chem.*, **2018**, DOI: 10.1002/ange.201809207.

Declaration

The work performed in this thesis was carried out in the Department of Chemistry, University of Warwick between October 2014 and September 2018. Unless otherwise stated it is the work of the author and has not been submitted in whole or in part for any degree at this or any other university.

Summary

Chapter 1 introduces small host-defence peptides in cancer therapy. The main mechanisms proposed in their interactions with membranes and intracellular targets are discussed. The biologically relevant peptide mimetics are also reviewed.

Chapter 2 describes the synthesis and characterisation of alkyne derivatives of metallohelices. These alkyne metallohelices demonstrated promising anticancer activity *in vitro*. Investigations of click reactions on alkyne flexicates were partially successful.

Chapter 3 describes the click reaction of alkyne triplexes. A range of aromatic clicked triplexes were synthesized and characterised. These novel complexes showed potential anticancer activity and high selectivity, and antimetastatic properties. Preliminary mechanism study revealed these metallohelices inhibit Na^+/K^+ ATPase activity.

Chapter 4 describes two different methodologies to synthesize and characterise glycoconjugate metallohelices. A variety of glyco-metallohelices were then investigated for activity and selectivity in cancer cell lines and normal cell lines. The glyco-metallohelices displayed similar inhibition to the growth of human tumour xenografts, but lower side effect than cisplatin.

Chapter 5 focuses on the synthesis and characterisation of triplex metallohelices containing triazole ligands and their potential biological application.

Chapter 6 details the experimental procedures used to carry out the work in this thesis.

List of abbreviations

Most of the abbreviations and symbols used in this thesis are in common use within the scientific community. Non-standard abbreviations and symbols used in this work are given below:

CuAAC	Copper(I)-catalysed Huisgen 1,3-dipolar cycloaddation
HHH	Head-to-Head-to-Head
HHT	Head-to-Head-to-Tail
FACS	Fluorescent-activated cell sorting
HMBC	Heteronuclear Multiple-Bond Correlation
HMQC	Heteronuclear Multiple-Quantum Correlation
IC_{50}	Half-maximal inhibitory concentration
NMR	Nuclear Magnetic Resonance
ARPE-19	Human retinal pigment epithelial cells (non-cancerous)
BPY	2,2'-Bipyridine
MLCT	Metal-ligand charge transfer
MTT	3-(4,5-Dimethylthiazol-2-yl)-2,5-diphenyltetrazolium salt
CD	Circular dichroism
MRSA	Methicillin-resistant Staphylococcus aureus
PBS	Phosphate buffered saline
APT	Attached proton test
PAMC	Post-assembly modification via click chemistry
TCRP	Time-dependent cellular response profiles
TRZ	Triazole

Ligands used in this Thesis

L[1]

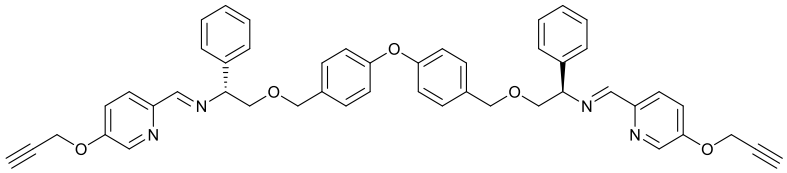

L[2]

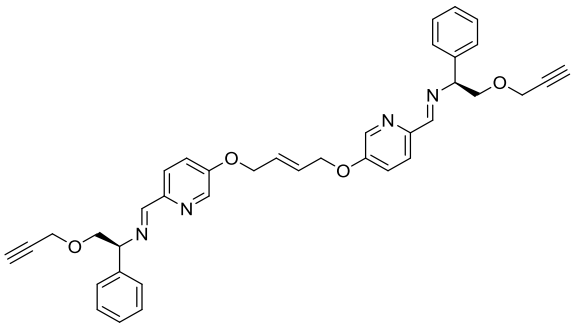

L[3]

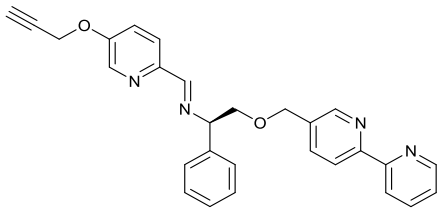

L[4a]

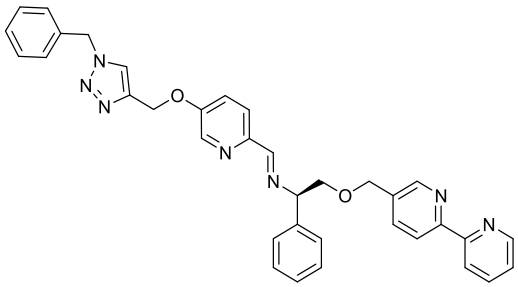

L[4b]

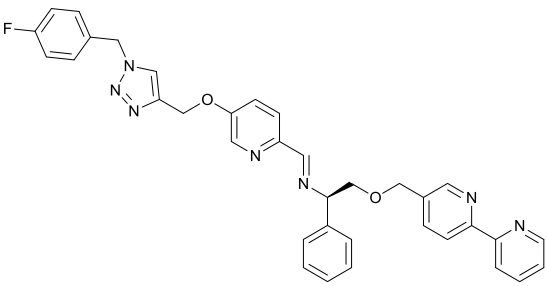

L^{4c}

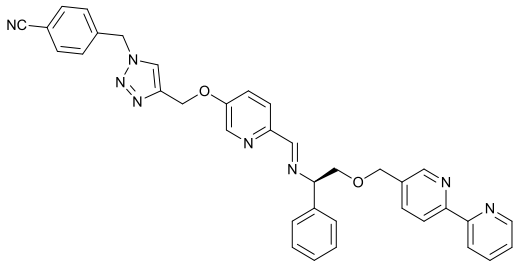

L^{4d}

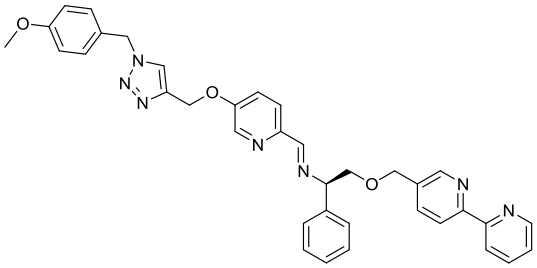

L^{4e}

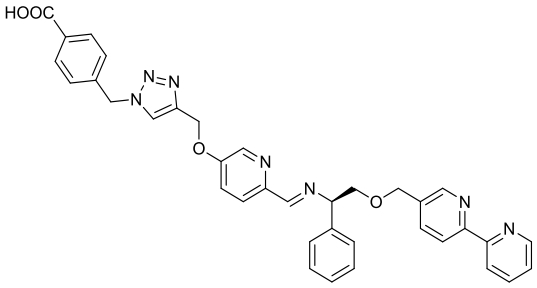

L^{5}

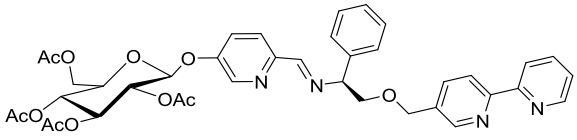

L^{6}

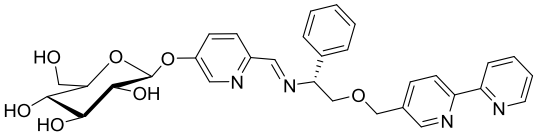

L^{7a}

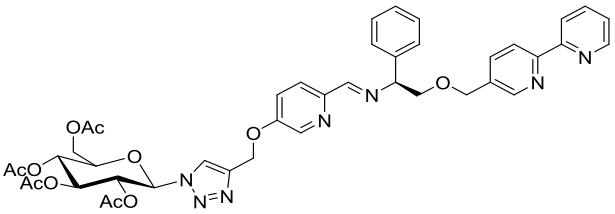

L^{7b}

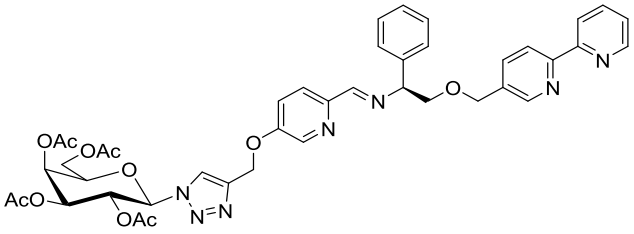

L^{7c}

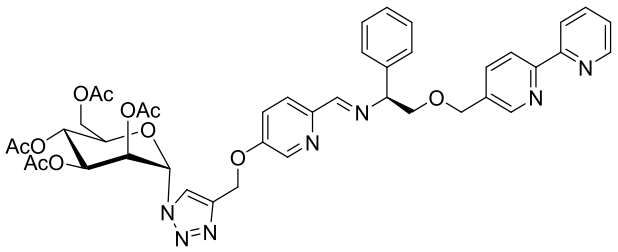

L^{7d}

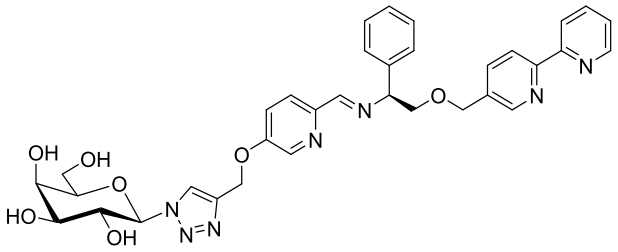

L^{7e}

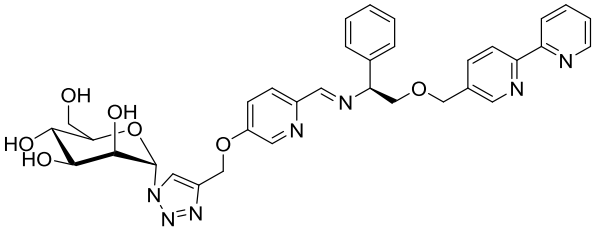

L^{7f}

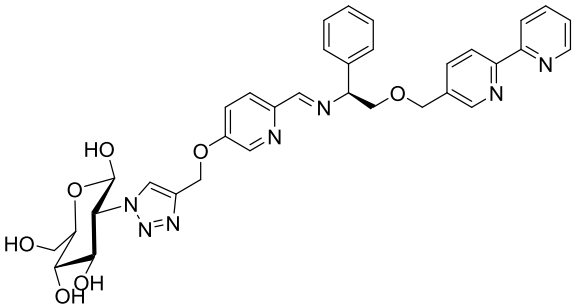

L^{7g}

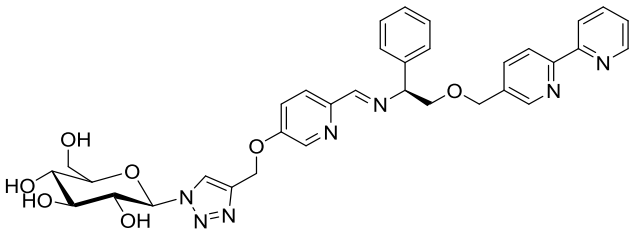

L^{7h}

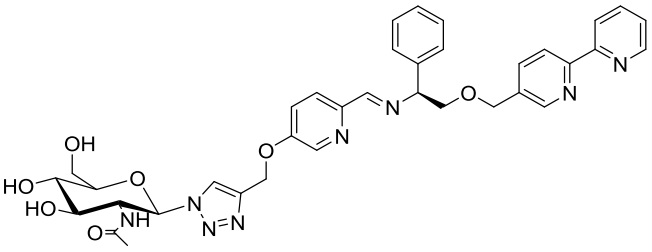

L^{7i}

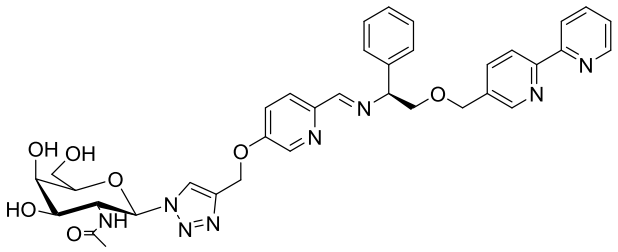

L^{8a}

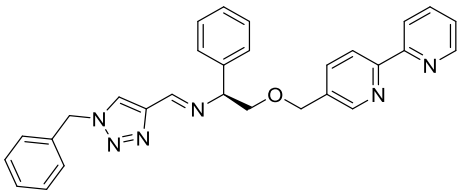

L^{8b}

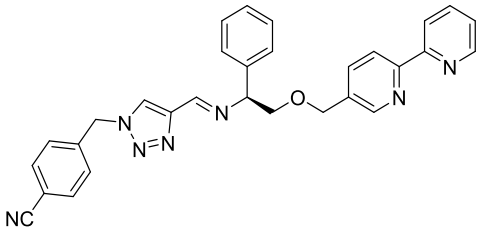

L^{8c}

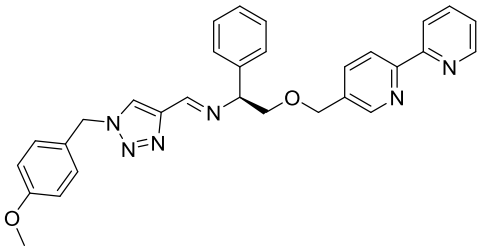

L^{8d}

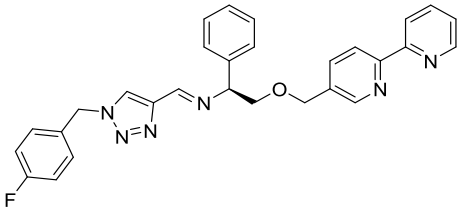

L^{8e}

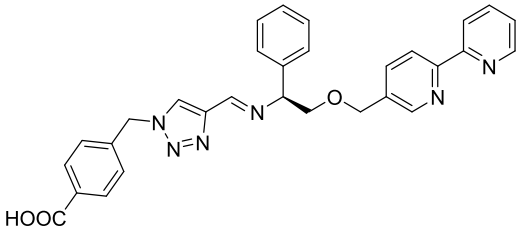

L^{9a}

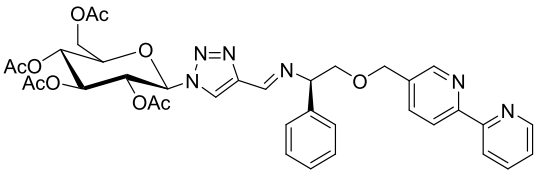

L^{9b}

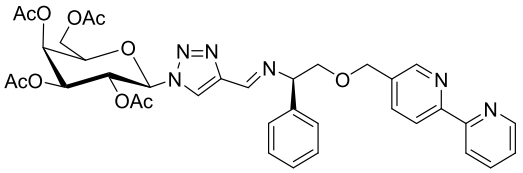

L^{9c}

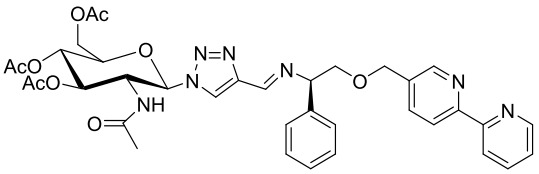

L^{10}

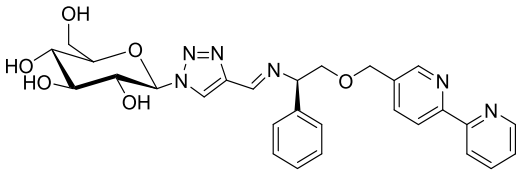

Chapter 1

Peptides and peptide mimetics in cancer therapy

1.1 Cancer therapies

As a result of dramatic improvements in understanding of disease mechanism, new therapeutics and treatment programs have been developed to the point where most cancers are no longer regarded as incurable.[1] At the same time, the battle continues to improve survival rates and the quality of life of patients.

Anticancer drug regimens used in clinic have been classified as chemotherapy, hormonal therapy and immunotherapy,[2] of which chemotherapy is the most frequently used. The common mechanism of action of classical chemotherapeutic agents involves interaction with tumour DNA.[3] The rationale for this approach was based on the notion that cancer is characterized by uncontrolled cell proliferation, and rapidly proliferating and dividing cells are generally more sensitive to chemotherapeutic compounds than are normal cells.[1b-1c] However, this relative rate of cellular division provides for weak selectivity, not least because many types of normal cell have fast proliferation rates: famously those present in hair follicles, bone marrow and the gastrointestinal tract.[4] Correspondingly, the common chemotherapy-induced side effects such as immune suppression, neuropathies, gastrointestinal conditions, hair loss, fatigue and skin disorders almost always accompany treatment.[5]

Alongside the efforts to synthesise novel DNA-targeting chemotherapy agents with minimal side effects, new classes of anticancer drug such as antibodies,[6] oligonucleotides[7] and peptides[8] are being developed. They have novel modes of action,

targeting *e.g.* tyrosine kinases,[9] mRNA and the cancer cell membrane. Since these agents are designed to have fairly specific binding targets they may have lower toxicity to the host than DNA binding/damaging drugs, resulting in a higher selectivity (therapeutic index).[10]

In this chapter we will focus on the potential use of one such group of compounds – small host-defence peptides – as cancer therapeutics; the central hypothesis of the work described in this volume is that triplex metallohelices[11] may function as structural and functional mimics of these compounds.

1.2 Peptide therapeutics

Peptides are naturally occurring biological molecules and may be defined as amino acid polymers containing no more than 50 units, and which feature secondary structures such as helices, sheets, turns and strands.[12] More than 7000 naturally occurring peptides having been identified which conduct or control crucial functions in human physiology *e.g.* hormones, neurotransmitters, growth factors, ion channel ligands, and anti-infective and cellular signallers.[13] Compared with traditional small molecule drugs, peptides may bind with exquisite specificity to their *in vivo* targets, resulting in exceptionally high potencies and dramatically reduced off-target side effects.[12] Medical markets have witnessed an upsurge in the development of peptides therapeutics such that more than 50 peptide-based drugs such as leuprorelin (Lupron)[14], peginesatide (Hematide),[15] goserelin (Zoladex),[16] octreotide (Sandostatin),[17] and enfuvirtide (Fuzeon)[18] are currently approved for clinical use. A number of other peptides are in late-stage clinical trials.[19]

A subset of the above, the Host defence peptides (HDPs), also known as antimicrobial peptides, are widespread in nature and are used by animals and plants to

fend off a range of microbes. They are known to have a broad spectrum of antimicrobial activity.[20] These peptides share some common characteristics such as low molecular weight (the majority containing < 30 amino acids), cationic or amphipathic structure[21] and low antigenicity compared to other proteins.[22] The principal modes of action are focussed on interactions with the cellular membrane (*vide infra*). In addition to antimicrobial activity, some synthetic or natural HDPs including cecropin B,[23] magainins,[24] melittin,[25] tachyplesin,[26] BMAP-28[27] and lactoferrin,[28] have been explored as a new class of anticancer agents.[29]

The cell-penetrating peptides (CPPs) are of similar size range to the HDPs but are distinguished by their ability to cross the cellular membrane via different mechanisms, providing access, as with small molecule drugs, to intracellular targets and for example promising a strategy for drug delivery.[30] The transactivator of transcription (TAT) protein of HIV, the first discovered CPP, was found to cross cell membranes and be efficiently internalized by cells *in vitro* in 1988.[31] A few years later, the *Drosophila* Antennapedia transcription factor proteins were shown to be able to translocate cell membranes and enter cells.[32] From then on, a series of natural or synthetic CPPs has been identified with the same membrane-crossing properties.[33] In recent years, various studies have revealed the applications of CCPs serving as vectors for the delivery of various cargos such as siRNA,[34] nucleic acids,[35] small molecule therapeutic agents,[36] proteins,[37] quantum dots,[38] cellular imaging agent,[39] and MRI contrast agents.[40] Meanwhile, several bioactive CPPs have been developed with notably proapoptotic or antitumor activities.[41] The main characteristics of the CPPs are low cytotoxicity, capacity to be taken up by a variety of cell types, dose-dependent efficiency, and capacity to transport a wide range of size and type of cargo.[42]

With these structure types in mind we will review the main mechanisms of action proposed in their interactions with membranes and intracellular targets.

1.3 Membrane interaction & transport mechanisms

Membrane selectivity

The outermost leaflet of the microbial cells membrane displays negative charge as a result of the preponderance of phospholipids. Electrostatic interactions with cationic peptides e.g. HDPs is proposed to be a key factor in the modes of action[43,20] as described herein. In contrast, the outer membrane of normal/healthy human cells is comprised of zwitterionic phosphatidylcholine and sphingomyelin components,[44] and the consequent relatively weak interactions with cationic peptides forms a basis for antimicrobial selectivity.

Cancer membrane components are in this sense similar to microbial systems.[45] Anionic lipid phosphatidylserine (PS), normally located in the inner leaflet of eukaryotic plasma membranes,[44] is exposed 3-7 fold more than in normal keratinocytes.[46] This has been described as a general phenomenon for cancer cells.[21] Another enhancement of negative charge on the surface of cancer cells arises because *O*-glycosylated mucins, which playing a role against oxidative stress-induced cell death, facilitating cell adhesion during tumour metastasis and alter the function of surface-interacting proteins[47] are aberrantly overexpressed in various malignancies.[48] Membrane fluidity and microvilli may also contribute to the preferential killing of cancer cells by HDPs. The increased membrane fluidity of cancer cells will enhance the lytic activity of peptides by facilitating membrane destabilization.[49] The higher

numbers of microvilli on the cancer cell increases the surface area of the tumorigenic cell membranes and allows cancer cells to bind a larger amount of HDP.[50]

Membrane disruption

Non-specific membrane disruption, also called cell lysis, refers to a mechanism by which agents, often at high concentrations, compromise the integrity of the cell membrane and thereby cause cell death. Numerous nonspecific membrane-active small molecules exist e.g. biocides, chaotropic agents and other synthetic chemicals.[51] Here, however, we are concerned with some of the more subtle membranolytic mechanisms characteristic of the action of peptides. Unsurprisingly, such mechanisms are common to many small amphipathic peptides, be they described as HDPs, CPPs *etc*. After adsorption onto the cancer cell membrane surface by electrostatic interaction as described above, peptides can induce a variety of membrane changes.[52]

Some cationic amphipathic peptides adsorb onto the membrane surface and orient parallel to the bilayer surface in a carpet-like manner.[53] These peptides cover the outer leaflet of the membrane tightly and disrupt the integrity of the supramolecular structure. Membrane fragmentation may occur when the peptide carpet accumulation is sufficiently dense, causing the leakage of the cytoplasmic contents, ions, and biomolecules.[52] Such a mechanism is clearly related to simple surfactancy, and requires a relatively high concentration of peptide in the membrane.[54]

A number of peptides cause cell lysis by pore formation. The accumulation of the peptides on the cell surface causes a thinning of the bilayer, by which outwardly facing hydrophobic residues interact with the lipid membrane, while hydrophilic groups with high curvature form a central lumen to create the transient holes which are termed toroidal pores.[55] Membrane pores result in the loss of the membrane

potential and rapid release of intracellular components, triggering cancer cell necrosis.[56]

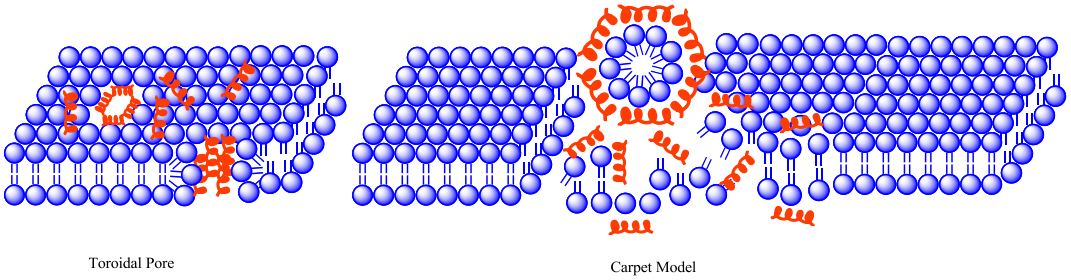

Figure 1-1 The mechanism of membrane disruption caused by peptides

Transport through the Membrane

Many mechanism have been proposed by which small molecules such as drugs enter cells, and it is worth noting that while there is a prevailing assumption that passive diffusion is the principal route of ingress, there is a highly credible argument for a carrier-mediated view of drug uptake i.e. that drugs predominantly enter cells via promiscuous proteinaceous carriers.[57] Also, it is worth noting that many of the energy independent (passive) and energy-dependent (active) mechanisms we describe below might be considered to be closely related to one another.

There are three main models described for direct translocation of peptides into the cytosol *via* energy-independent pathways: inverted micelle formation[58], adaptive translocation[59] and pore-formation (Figure 1-2).[20]

In the inverted micelle formation model it is proposed that the positively charged peptide residues interact with the negatively charged phospholipids in the plasma membrane, and subsequently, interaction of the hydrophobic segments with the membrane core induces destabilization of the bilayer forming a negative curvature.[60] The concomitant reorganization of the neighbouring lipids leads to the

formation of the inverted micelle that encapsulates peptide molecules. Membrane disruption releases the peptide on the intracellular side.[61]

Adaptive translocation describes the interaction between guanidinium-rich peptides and the phosphate lipid head-groups, which masks the peptide charge, attenuating its polarity and enabling its adaptive diffusion into and across the membrane.[59]

In the pore formation model the accumulation of the peptides on a small region of the cell surface causes a local thinning of the bilayer, eventually creating a central lumen composed principally of negatively charged phospholipids and stabilised by the cationic peptide. The passive diffusion of peptides across the plasma membrane is thus facilitated.[55a, 55b]

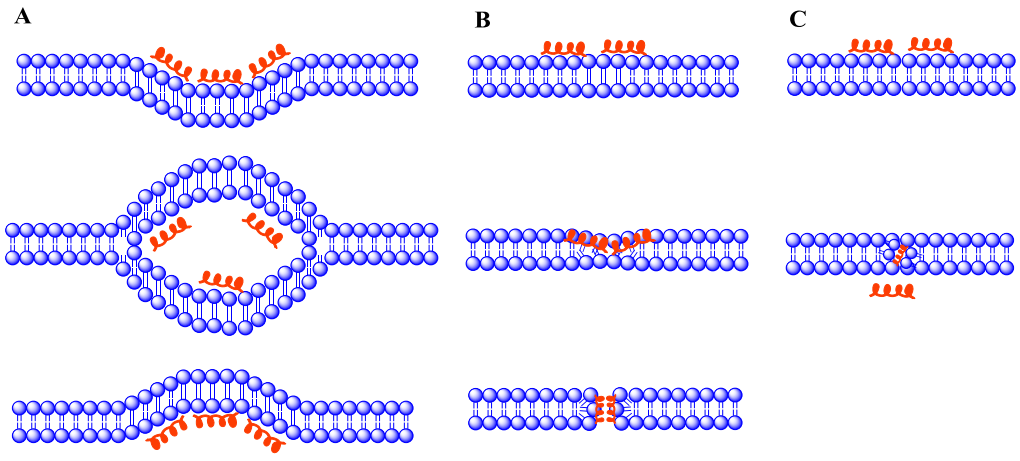

Figure 1-2 Examples of the proposed mechanisms for direct translocation. (A) Inverted micelle formation. (B) Pore-formation. (C) Adaptive translocation.

Endocytosis is an energy-dependent transport mechanism, which is used to take up large objects such as other cells, viruses and bacteria (Figure 1-3).[62] Major classes of endocytosis include clathrin- and caveolin-dependent endocytosis,[63,64] as well as macropinocytosis[65] and phagocytosis.[63, 66] The process consists of: (a) the

initial electrostatic interactions between the peptides and negatively charged components on the cellular plasma membrane, and destabilizing the bilayer to form a negative curvature,[60] (b) the concomitant reorganization of the neighbouring lipids leading to the formation of the inverted endosome that encapsulates peptides,[61] (c) endosomal escape; and (d) cytoplasmic or nuclear localization.[54] If the transported objects remain trapped inside the endosomes, they can be subjected to lysosomal degradation which negates the biological effect of the cargo. Endocytosis mechanisms cannot cause cancer death directly, but could deliver peptides into cytoplasm so as to take part in active-site type mechanisms such as those described below.

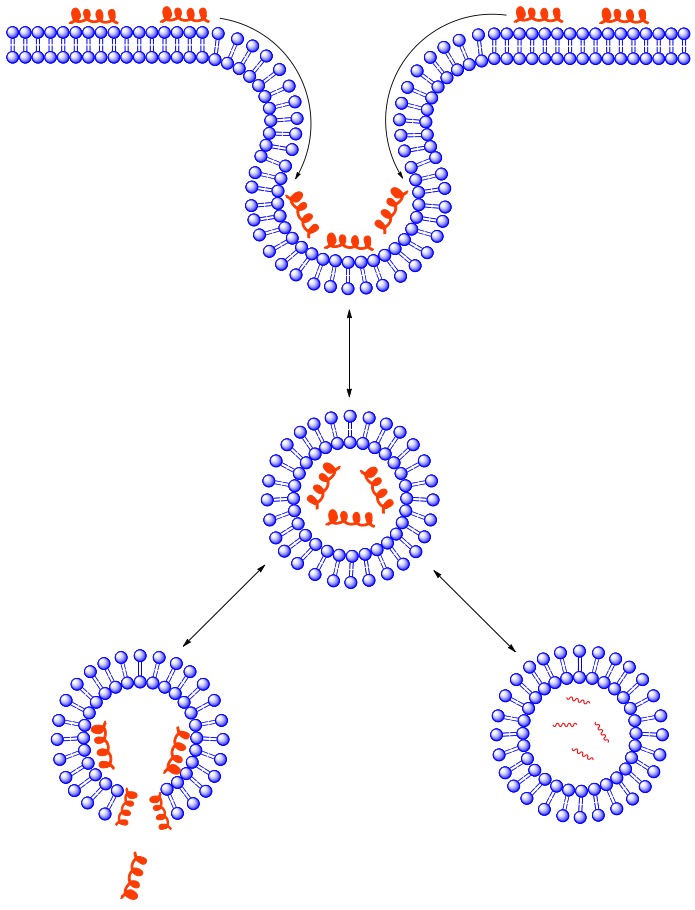

Figure 1-3 Schematic Illustration of Some of the Various Mechanisms by which a Cell Penetrating Peptide and Attached Cargo May be Internalized into a Cell

1.4 Receptor-mediated and other intracellular mechanisms

We described above the simple idea that cationic peptides are attracted to an anionic membrane, and as a result of the charge and/or the amphipathic detergent-like structure, the membrane is disrupted. Evidently however, many HDP anticancer mechanisms are of a more subtle nature.

Disruption of mitochondrial membrane

Molecules such as BH3 peptide,[67] DPI peptide,[68] pro-apoptotic peptide[69] and mitochondria penetrating peptides[70] penetrate into the cytoplasm, disrupt mitochondrial membrane and thereby release cytochrome c (Cyt c), inducing Apaf-1 oligomerization, caspase 9 activation and the subsequent conversion of pro-caspase 3 to caspase 3. Finally, caspase 3 will lead to apoptosis of cancer cells.[68, 71] Peptide mediated mitochondrial membrane perturbation is also part of the Alzheimer's disease mechanism; amyloid β-peptide acts locally in mitochondrial membranes to induce oxidative injury, leading to increased membrane permeability and subsequent release of caspase-activating factors.[72]

Inhibition of protein-protein interactions

Protein–protein interactions (PPIs) are essential for almost all cellular processes, including signal transduction, membrane transport, cell proliferation, growth, survival, and programmed death.[73] There are a total of 650,000 PPIs in the human proteome.[74] PPIs also play a critical role in a broad range of diseases, especially for cancer growth.[75] For instance, p53/HDM2 interaction has been detected in many types of cancers.[76] HDM2 downregulates the tumour suppressor p53 which induces cell cycle arrest and apoptosis in response to DNA damage and cellular stress.[77] A set of β^3-

peptides have been revealed to inhibit the p53/HDM2 interaction with nanomolar affinity in cell-free system;[78] the potencies *in vivo* are under investigation. PPIs between Bcl-2 family members contribute to tumour initiation, progression and resistance to therapy.[79] Bcl-2 binding peptide CPM-1285 showed anticancer activities inducing apoptosis *in vitro* and *in vivo*.[80]

All these researches demonstrate the significance of controlling and modulating PPIs in the development of new molecular therapeutics. Interestingly PPIs are considered to be "undruggable" by small molecules;[81] the binding surfaces between proteins are usually large (1500–3000 $Å^2$) and involve many polar and hydrophobic interactions, whereas most small molecules target well-defined cavities of enzymes or receptors.[82] In addition, binding surfaces are typically flat, with a less well-defined shape for binding of a small-molecule drug.[81] An alternative approach for the discovery of PPI inhibitors is centred on the role of protein secondary structures at protein interfaces, especially the α-helix which is the most common protein secondary structural element, and contributes to 62% of PPI interfaces.[83]

DNA binding

Anticancer mechanisms caused by DNA binding can be majorly classified into two species, DNA duplex binding and G-quadruplex binding. DNA duplex is generally considered as the molecular target for the chemotherapeutic agents.[3] DNA duplex binding, driven by intercalation, groove binding or covalent binding,[84] leads to a variety of significant biological responses, including the inhibition of DNA synthesis, G2 arrest in the cell cycle, and apoptosis.[85] DNA G-quadruplex, enriched in cancer-related genes and regions,[86] are formed by guanine-rich nucleic acid sequences through strong hydrogen-bonding.[87] DNA G-quadruplex binding could result in

downregulation of specific gene expression and telomerase inhibition, and stimulate DNA damage responses.[88]

A four-ring tripeptide has been demonstrated specifically binding six-base pair 5'-(A,T)GCGC(A,T)-3' sites in the minor groove of DNA.[89] Two peptides mimicking basic regions of natural leucine zipper proteins were uncovered to bind in the major groove of DNA.[90] DNase I footprinting experiments show that a disulphide-bonded dimer of peptide containing 27 residues of the basic region of the yeast transcriptional activator GCN4 can bind specific sequence with DNA.[91] Short peptides derived from the non-histone chromosomal protein HMG-I/Y bind specifically to the minor groove of DNA.[92] LL37 peptide can form a complex with DNA and induce DNA packaging into aggregated and condensed structures to trigger Toll-like receptor 9.[93]

1.5 Peptide mimetics

Small peptides commonly exist in random conformational states in solution, adopting active secondary structures during the binding event.[82] Despite this, they have favourable pharmacodynamics, but of course in the unfolded state they have low resistance to proteases leading to relatively poor pharmacokinetic profiles. [94] These issues have prompted studies into various strategies including helix stabilization,[81] and the design of non-peptide scaffolds.

Stapled peptide mimetics

Stabilisation of the active conformations of peptides, *i.e.* increasing the α-helical content, is expected to reduce the rate of degradation by proteases and thus improve pharmacokinetic properties, as well as improving pharmacodynamics. A number of methods involving intramolecular side chain to side chain cross-links such as intramolecular hydrogen bonds,[95] salt bridges,[96] metal chelates[97] and covalent

crosslinks have been developed (Figure 1-4).[82] Approaches including thiol-, lactam-, hydrocarbon and hydrogen-bonding surrogate staples, have been successfully applied to the generation of PPI inhibitors.

Disulfide Bridge Peptides constrained by intramolecular disulfide bridge at *i* and *i*+4 or *i*+7 residues, show an increased α-helical content compared to their acyclic counterparts [Figure 1-4 (b)].[98] However, disulfide cross-links are labile under reductive conditions in the cytoplasm. Further, the replacement of disulphide bridges with chemically more stable linkers such as *m*-xylene[99] and bisarylmethylene[100] (not shown) increased peptide cell permeability and the efficiency as PPI inhibitors.

Lactam bridge Lactam bridges linking (*i*, *i*+3), (*i*, *i*+4), or (*i*, *i*+7) amino acid residues have been used to introduce conformational constraints in peptide structures [Figure 1-4 (c)].[101] Compared with disulphide bridges, amide bonds are much more chemically inert under cellular conditions. Biological studies have focused on the potential application of lactam-bridged peptides for peptide-protein recognition, protein folding as well as interactions with cell surface receptors.[102]

Hydrocarbon bridge The building blocks here are non-proteinogenic bearing terminal olefin tethers of varying lengths which are ring-closed by metathesis using Grubbs type catalysts [Figure 1-4 (d)].[103] Dramatic improvements are observed in resistance to proteolytic degradation, cell-penetration, and *in vivo* half-life.[104]

Hydrogen-Bond Surrogates (HBS) This is closely related to the above in that ring-closing metathesis[105] is used at the position shown [Figure 1-4 (e)]. The overall outcome is that a short carbon chain replaces the NH···O=C hydrogen bond moiety [Figure 1-4 (a)] in a natural structure.[106] Compared with other cross-linkers (e.g. disulphide, lactam), the HBS approach exert the desired effect of stabilising the helical conformation without dramatically altering the surface topography of the target

helix.[107] HBS peptides have improved conformational stability and cellular uptake, increasing PPI affinity.[108]

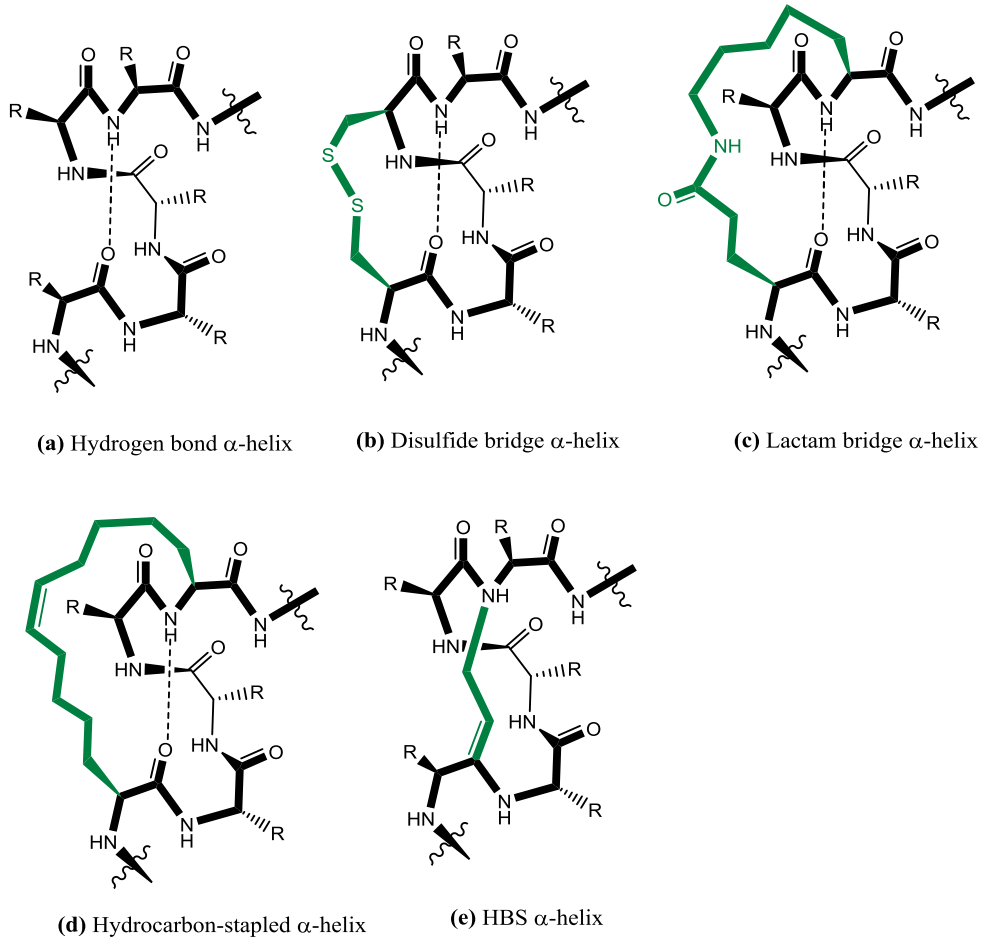

Figure 1-4 Different α-helix stabilization strategies

Non-peptide scaffolds

Non-peptide scaffolds have in the main been aimed at the production of rod-like structures with appropriately placed functional groups so as to mimic the orientation of the side-chains in α-helix peptides.[109] While this may not only accurately reproduce the same binding mode as the native protein, it does provide structural diversity, with a potentially large library of synthetic building blocks available, and the products are very likely to display resistance to proteolytic mechanisms (Figure 1-5).[82] A great number of researches have been carried out on the identification of scaffolds with more

versatile and accessible synthetic chemistry and with arguably more 'drug-like' properties than peptides i.e. principally better pharmacokinetics.[109]

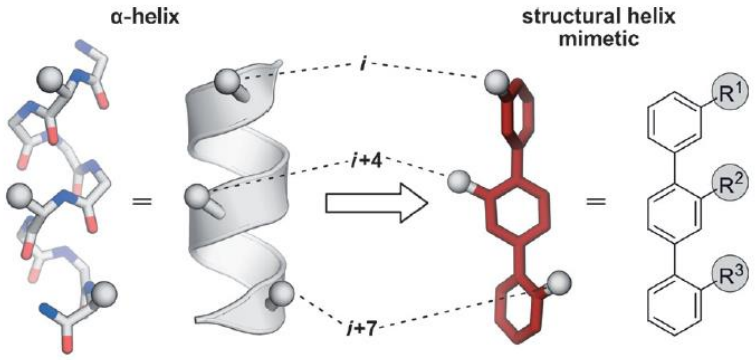

Figure 1-5 Concept of structural a-helix mimetics: Left: Stick and schematic representations of a α-helix. Right: Stick representation and chemical structure of a terphenyl structural mimetic.[82]

Based on different mechanisms by which the helix-like structure is promoted, non-peptide scaffolds have been classified in three groups: sterically enforced, hydrogen-bond guided, and covalently constrained scaffolds (Figure 1-6).[82]

Terphenyls and heterocycles are typical sterically enforced scaffolds in which the conjugation of the aromatic rings represents the major contribution to spatial preorganization.[82]

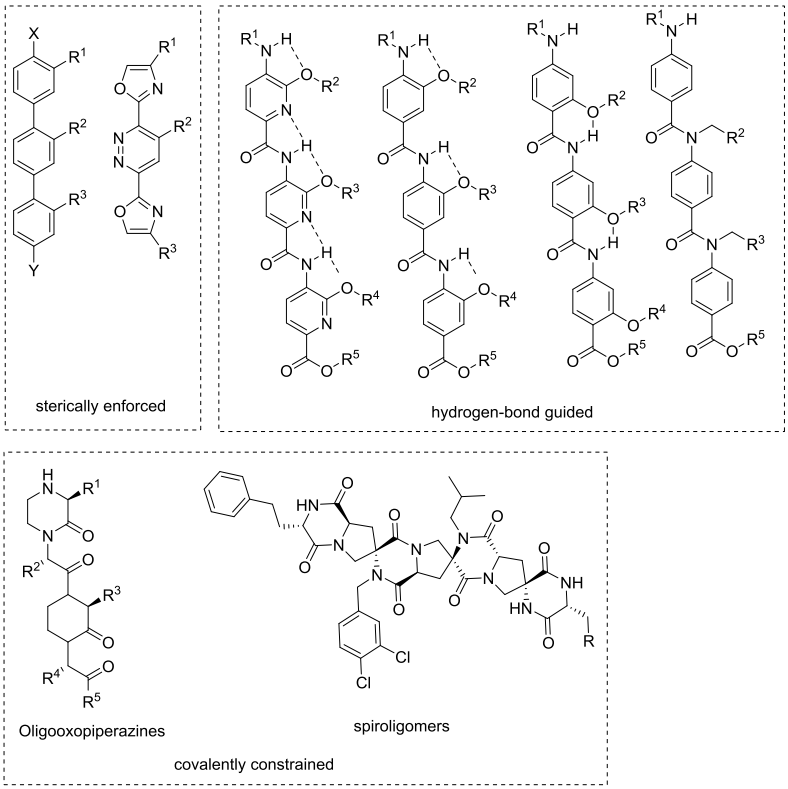

Figure 1-6 Examples of the non-peptide scaffolds[81]

Aromatic oligoamide templates including trispyridylamides,[110] 3-*O*-alkylated-,[111] 2-*O*-alkylated[112] and *N*-alkylated oligobenzamides,[113] represent hydrogen-bond guided scaffolds. The intramolecular hydrogen bonds between the NH group of the amides and the *ortho* alkoxy functionalities on the same face of the molecule induce a structural constraint, resulting in a curvature of this scaffold, thus enabling α-helix mimicry.[110]

Oligooxopiperazines[114] and spiroligomers[115] are covalently constrained scaffolds which possess a chiral backbone. The chirality of the structure has been evidenced to render a higher binding specificity.[82]

Despite improvements in such helix-proteomimetics, they are not readily able to target more than one face on the hot-spot of a PPI.[109] Furthermore, the preponderance of aromatic rings increases the hydrophobicity of these molecules and

limits aqueous solubility. Further, there is a question over their synthetic accessibility and eventual cost of goods. All these obstacles provide an impetus for the development of new scaffolds.

Helicates and other Metallohelices

Metal coordination presents great opportunities for the construction of diverse molecular architectures.[116] In principle ligands can be tailor-made for specific interactions, and the strength, reversibility and defined directionality of coordination bonds allows precise control over the three-dimensional structure and stability of the final assembly. Peptides frequently use metal ions to control structure, and indeed a number of researchers are using ligand-modified peptides to create unnatural metallated assemblies.[117] In this section we will however focus on non-peptide systems arising originally from J.-M Lehn's "helicate" concept[118] focusing on systems which are aimed at drug discovery. A large number of helicate systems have been produced and this area has been reviewed,[119] although few systems have properties that make them suitable for application as pharmaceuticals.

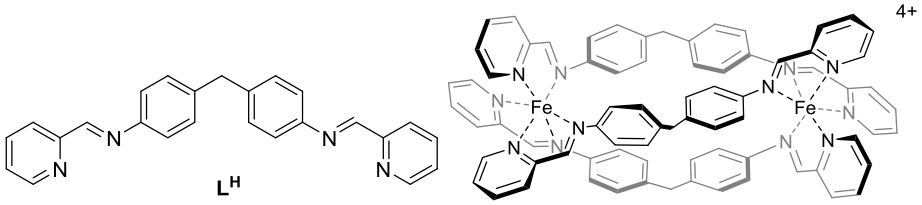

Figure 1-7 Bis-pyridylimine ligand and the helicate structure

In 1997, Hannon and co-workers simplified the well-established bipyridine helical systems of Lehn with pyridylimine binding sites linked by a central diphenylmethylene group. Reaction of methanol solutions of three equivalents of the ligand $\mathbf{L^H}$ with two equivalents of Fe(II) salts induced the formation of the triple-

helical architecture of Figure 1-7. The rigid ligand system mechanically couples the helical coordination environments, requiring them to adopt the same stereochemistry (i.e. Δ,Δ, or Λ,Λ). The ensuing triple-helix structure has a well-defined pitch.

The reported syntheses of this and closely related compounds involve the use of weakly-coordinating anions (PF_6^-) for ease of isolation, followed by exchange with chloride to provide water solubility. A number of biological studies followed using this water-soluble chloride salt "$[Fe_2\mathbf{L}^{\mathbf{H}}{}_3]Cl_4$". In fact, the synthesis and characterisation of this specific moiety has only recently been reported, and contrary to earlier reports it is a tetrahydrate.[11] Related examples of this helicate class arose from replacing the bridging -CH_2- with –O-, minor modifications to the pyridines[120] and Ru(II) analogue(s).[121] The latter, along with the original bis-Fe(II) helicate, is reported to be resolvable into enantiomers on cellulose,[120, 122] but although enantiomeric enrichment is supported by circular dichroism, the optical purity was not quantified. This might be achieved through the use of an NMR shift reagent as has been achieved in related systems.[123] Helicates with appended arginine[124] and short peptide fragments[125] were subsequently reported via multi-step routes. Helicity was seen to be controlled to within the limit of signal:noise for the NMR spectra observed.[124]

Antibacterial activity of $[Fe_2\mathbf{L}^{\mathbf{H}}{}_3]Cl_4$ was studied.[126] Unfortunately the compound was found to be unstable in standard broths[127] so a special in-house medium was devised. While this makes comparison with other compounds difficult, potencies were certainly low, with reported MICs of 32 μg/ml against Gram-positive *B. subtilis* strain 168, and 64 μg/ml against Gram-negative *E. coli* strain GM2163 respectively. In our hands,[11] and in those of others,[128] no activity was observed.

Great attention has been given to the ability of these helicate to bind DNA motifs *in vitro*, especially the B-DNA major groove[121b, 129] and three-way junctions (3WJ)[124, 130] inducing conformational changes.[121b] Inhibition of the interaction between the HIV-1 transactivator protein Tat and TAR (transactivation responsive region) RNA was reported.[131]

The anticancer activities of this metallohelicate towards human breast cancer cell (HBL-100 and T47D) are 2-5 times lower than cisplatin.[132] Qu and co-workers discovered that the helicate could specifically target the α/β-discordant stretch and strongly inhibit Alzheimer's disease β-amyloid aggregation.[133]

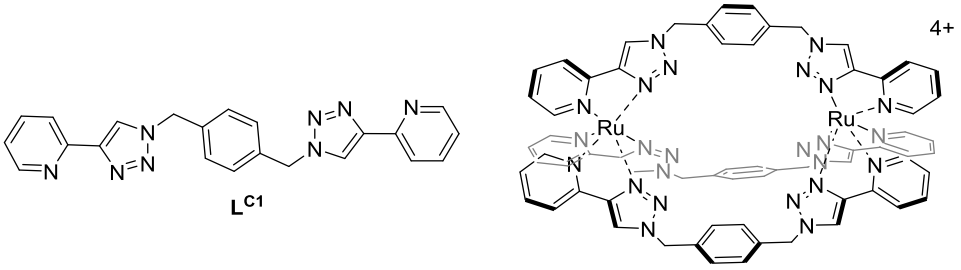

L^{C1}

Figure 1-8 Chemical structures of the pyridyl-1,2,3-triazole ligand; the molecular structure of $[Ru_2\mathbf{L^{C1}}_3](PF_6)_4$

Crowley and co-workers synthesised a ruthenium(II) triply-stranded helicate $[Ru_2\mathbf{L^{C1}}_3]^{4+}$ by using a bis-bidentate ''click'' pyridyl-1,2,3-triazole ligand $\mathbf{L^{C1}}$ and $RuCl_3$ (Figure 1-8).[128] Extremely modest antimicrobial activity *in vitro* was observed against both Gram positive (*S. aureus*) and Gram negative bacteria (*E. coli*) (MIC > 256 μg/mL).

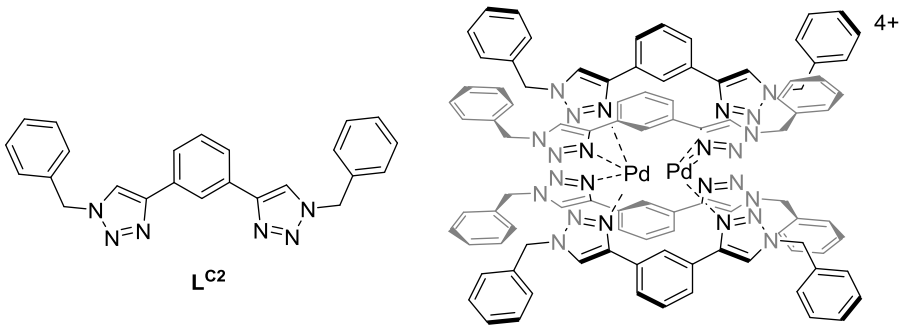

Figure 1-9 Chemical structures of the triazole (bntrz) based ligand; the molecular structure of $[Pd_2(bntrz)_4](BF_4)_4$

The same group synthesised a quadruply-stranded dipalladium architecture (Figure 1-9)[134] by simple reaction of the 1,3-phenyl linked ditriazole ligand $\mathbf{L^{C2}}$ with $[Pd(CH_3CN)_4](BF_4)_2$.[135] The helicate exhibits a range of cytotoxic properties towards A549 (lung cancer), Cisplatin resistant MDA-MB-231 (breast cancer) and DU-145 (prostate cancer). Disappointingly, the $[Pd_2(bntrz)_4](BF_4)_4$ helicate displayed no selectivity towards cancerous phenotypes.

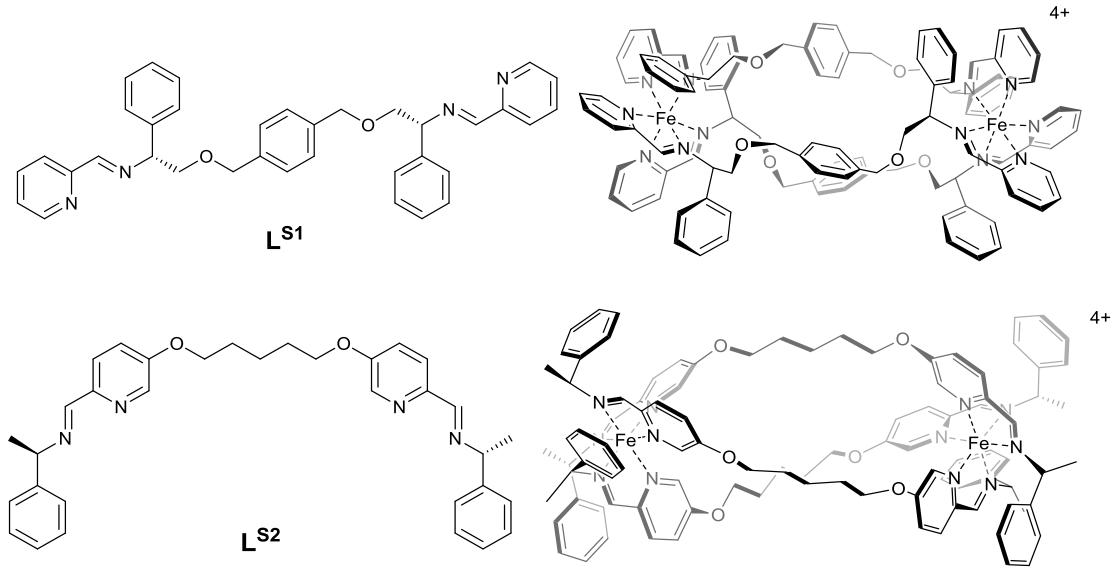

Figure 1-10 Structure of the ligands and the flexicate

Scott and co-workers designed and synthesised a series of unusually stable, optically pure and water soluble triple-stranded Fe(II) assemblies.[136] The chiral diamine linker $\mathbf{L^{S1}}$ or dialdehyde linkers $\mathbf{L^{S2}}$ assembling with pyridine aldehyde

derivative or the chiral amine in the presence of $FeCl_2$ to form two series (Figure 1-10). The helicity of the metal-complex comes from steric effects and π-stacking interactions pre-programmed in the optically pure monometallic units rather than via traditional mechanical coupling, and for this reason *i.e.* they did not use or rely on helication as a method of stereoselection, they were termed "flexicates". Preliminary anticancer screening revealed that while some flexicates have comparable activity to cisplatin against MCF7 (human breast adenocarcinoma) and A2780 (human ovarian carcinoma) they are *ca* five times more potent than cisplatin against A2780cis with no significant DNA damage.[137] Moreover, some flexicates possess excellent selectivity towards HCT116 colorectal cancer cells and healthy human retinal pigment epithelial (ARPE19) cells.[138] Qu and co-workers demonstrated the flexicates can act as a novel class of chiral amyloid-*β* inhibitors by enantioselectively inhibiting Aβ aggregation.[139] The same group also revealed flexicates can stabilize human telomeric hybrid G-quadruplex DNA and strongly inhibit telomerase activity.[140]

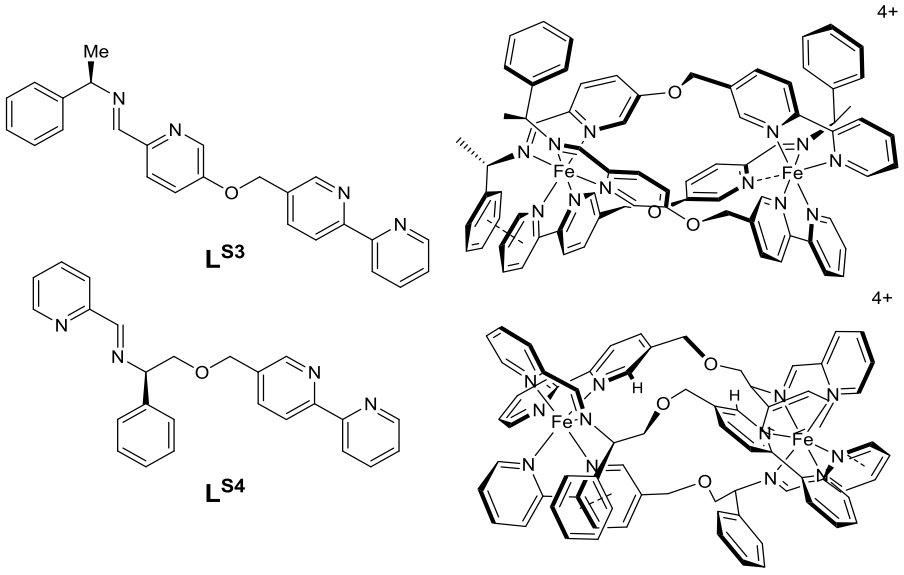

Figure 1-11 Self-assembly from versatile components of a wide range of functionalized helices in which the strands are arranged head-to-head-to-tail

The 2-phenyliminopyridine stereogenic unit in the above was also exploited to create a highly stereoselective asymmetric self-assembly of very stable, functionalized metallohelices with an antiparallel head-to-head-to-tail (HHT) "triplex" strand arrangement (dr > 98) (Figure 1-11),[11] the name being a reference to structure of triplex DNA. The compounds were synthesised by using 3 equiv. of directional ditopic ligands $\mathbf{L^{S3}}$ or $\mathbf{L^{S4}}$ in the presence of 2 equiv. $FeCl_2$. The absolute configuration of the triplex architectures as well as the uniquely selective directionality arose because this maximises the number of phenyl-bipyridine π-stacks which, according to calculations, are relatively strong. In addition, one of the two classes of ligand design also gave inter-strand bifurcated C–H···O/N interactions. The triplex systems display high structure-dependent toxicity to the human colon carcinoma cell-line HCT116 p53++ and human breast adenocarcinoma cells (MDA-MB-468), causing dramatic changes in the cell cycle without DNA damage. Interestingly, they show no significant toxicity to Gram-positive and -negative bacteria.

1.6 Proposal

Peptides such as HDPs and CPPs feature exceptionally high potencies and reduced off-target side effects as cancer therapeutics due to the ability to bind with exquisite specificity to their *in vivo* targets.[12] They are selectively absorbed onto the cancer cell membrane by electrostatic interactions[43,20] and translocated into the cytosol *via* energy-independent pathways[20,58,59] or endocytosis.[62] The main modes of action include disruption of mitochondrial membrane;[67-70] inhibition protein–protein interactions (PPIs)[78] and DNA binding.[89,90] However, due to the low resistance to proteases, natural peptides have relatively poor pharmacokinetic profiles.[94]

Alternatively, stapled peptide mimetics,[82] non-peptide scaffolds[109] including metallohelices[136,11] are being developed.

Despite the achievements thus far in the use of metallohelices as potential peptidomimetic drugs, significant barriers remain in the translation of these compounds to a clinical situation. Until recently, rather few such compounds have possessed the generic properties of drug candidates, such as optical purity, solubility in water and stability in media.[141] Several synthetic issues have also hampered their development. For instance, in order to couple the absolute configurations of adjacent metal centres (helication), rigid ligands must be used. However, the excess of aromatic rings thereby employed inevitably leads to hydrophobicity and poor aqueous solubility. Further, symmetrical ligands need to be employed so as to reduce the number of possible isomers from self-assembly, and the subsequent structures fall far short of the exquisite asymmetric topographies of natural peptides. Derivatisation of metallohelices is also great challenge; the ligands have to be relatively simple and free of extra functionality in order to avoid potential incompatibilities and interference in the self-assembly process.[142,143] All these obstacles impel us to develop new synthetic strategies for making novel asymmetrical, functionalized metallohelices.

Post assembly modification (PAM) of metal-complexes[143-145] allows the addition of a more diverse range of functional groups, potentially circumventing the limitation of self-assembly conditions, allowing facile purification and isolation, and maintains the structural identity of the system. This methodology is especially prevalent in metal-organic frameworks (MOFs) which tend to be relatively stable, and numerous functionalisation reactions such as alkyne bromination,[146] aldehyde reduction,[147] hydroxyl etherification,[148] *N*-acylation[144-145, 149] (*e.g.* Figure 1-12), *N*-alkylation,[150] and imine reduction[151] have been validated. Although the structure of

MOFs are quite different from metallohelices, these researches demonstrate that it is reasonable to apply this methodology to the derivatisation of stable complexes.[152]

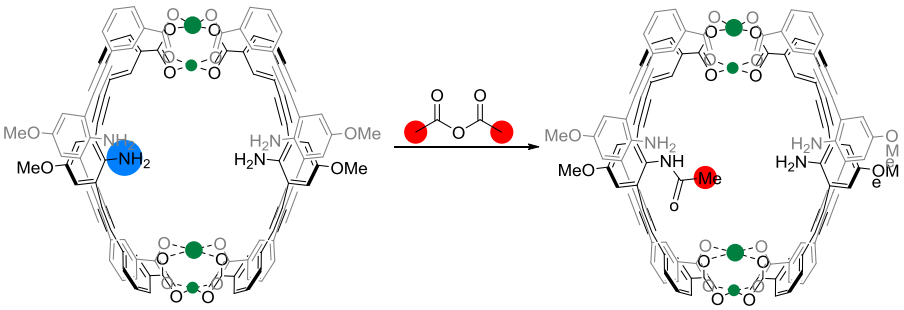

Figure 1-12 Modification of pre-formed metal-organic lantern cage[144]

The conditions of the PAM reactions above are generally rather harsh, using high temperatures or long reaction times, and it is unlikely that metallohelices based on relatively labile metal-ligand bonds will be sufficiently robust. Nevertheless, the high stability of the so-called flexicate[136] and triplex[11] metallohelices developed in this laboratory may allow them to be modified *via* relatively mild reactions such as Copper-catalysed Azide/Alkyne Click (CuAAC). Such reactions have not been achieved previously in this kind of system.

1.7 References

1. (a) R. L. Siegel, K. D. Miller and A. Jemal, *CA Cancer J. Clin.*, 2016**, 66**, 7-30; (b) D. Hanahan and R. A. Weinberg, *Cell*, 2000, **100**, 57-70; (c) D. Hanahan and R. A. Weinberg, *Cell*, 2011, **144**, 646-674.
2. (a) E. Espinosa, P. Zamora, J. Feliu and M. G. Barón, *Cancer Treat. Rev.*, 2003, **29**, 515-523; (b) C. Avendaño and J. C.Menendez, *Medicinal chemistry of anticancer drugs*. Elsevier: 2015.
3. L. H. Hurley, *Nat. Rev. Cancer*, 2002, **2,** 188-200.
4. (a) T. Reya and H.Clevers, *Nature*, 2005, **434**, 843-850; (b) E. Pérez-Herrero and A. Fernández-Medarde, *Eur. J. Pharm. Biopharm.*, 2015, **93**, 52-79.
5. (a) A. H. Partridge, H. J. Burstein and E. P. Winer, *J. Natl. Cancer Inst.*, 2001, **93**, 135-142; (b) H. J Burstein, *J. Clin. Oncol.*, 2000, **18**, 693-693; (c) D. Castellano, R. Hitt, H. Cortés-Funes, A. Romero and J. L. Rodriguez-Peralto, *J. Clin. Oncol.*, 2000, **18**, 695-695.
6. (a) A. M. Scott, J. D. Wolchok and L. J. Old, *Nat. Rev. Cancer*, 2012, **12**, 278-287; (b) E. L. Sievers and P. D. Senter, *Annu. Rev. Med.*, 2013, **64**, 15-29; (c) R. V. Chari, M. L. Miller and W. C. Widdison, *Angew. Chem. Int. Ed.*, 2014, **53**, 3796-3827.
7. F. Eckstein, *Nucleic Acid Ther.*, 2014, **24**, 374-387.
8. N. Papo and Y. Shai, *Cell. Mol. Life Sci.*, 2005, **62**, 784-790.
9. (a) A. Lasorella, R. Benezra and A. Iavarone, *Nat. Rev. Cancer*, 2014, **14**, 77-91; (b) G. Jego, A. Hazoumé, R. Seigneuric and C. Garrido, *Cancer Lett.*, 2013, **332**, 275-285; (c) Z. Wang, P. Liu, H. Inuzuka and W. Wei, *Nat. Rev. Cancer*, 2014, **14**, 233-247; (d) J. Zhang, P. L. Yang and N. S. Gray, *Nat. Rev. Cancer*, 2009, **9**, 28-39.
10. A. M. Scott, J. D Wolchok and L. J. Old, *Nat. Rev. Cancer*, 2012, **12**, 278-87.
11. A. D Faulkner,. R. A. Kaner, Q. M. Abdallah, G. Clarkson, D. J. Fox, P. Gurnani, S. E. Howson, R. M. Phillips, D. I. Roper, D. H. Simpson and P. Scott, *Nat. Chem.*, 2014, **6**, 797-803.
12. D. J. Craik, D. P. Fairlie, S. Liras and D. Price, *Chem. Biol. Drug Des.*, 2013, **81**, 136-147.
13. (a) A. Padhi, M. Sengupta, S. Sengupta, K. H. Roehm and A. Sonawane, *Tuberculosis*, 2014, **94**, 363-373; (b) H. Buchwald, R. B. Dorman, N. F. Rasmus, V. N. Michalek, N. M. Landvik and S. Ikramuddin, *Surg. Obes. Relat. Dis.*, 2014, **10**, 780-786; (c) C. Giordano, M. Marchiò, E. Timofeeva and G. Biagini, *Front. Neurol.*, 2014, **5**, 63; (d) S. D. Robinson, H. Safavi-Hemami, L. D. McIntosh, A. W. Purcell, R. S. Norton and A. T. Papenfuss, *PLoS One*, 2014, **9**, e87648.
14. M. Katsuno, H. Adachi, M. Doyu, M. Minamiyama, C. Sang, Y. Kobayashi, A. Inukai and G. Sobue, *Nat. Med.*, 2003, **9**, 768-773.
15. I. C. Macdougall, R. Provenzano, A. Sharma, B. S. Spinowitz, R. J. Schmidt, P. E. Pergola, R. I. Zabaneh, S. Tong-Starksen, M. R. Mayo and H. Tang, *N. Engl. J. Med.*, 2013, **368**, 320-332.
16. H. C. Moore, J. M. Unger, K.-A. Phillips, F. Boyle, E. Hitre, D. Porter, P. A. Francis, L. J. Goldstein, H. L. Gomez and C. S. Vallejos, *N. Engl. J. Med.*, 2015, **372**, 923-932.

17. S. Melmed, V. Popovic, M. Bidlingmaier, M. Mercado, A. J. Van Der Lely, N. Biermasz, M. Bolanowski, M. Coculescu, J. Schopohl and K. Racz, *J. Clin. Endocrinol. Metab.*, 2015, **100**, 1699-1708.
18. J. P. Lalezari, K. Henry, M. O'hearn, J. S. Montaner, P. J. Piliero, B. Trottier, S. Walmsley, C. Cohen, D. R. Kuritzkes and J. J. Eron Jr, *N. Engl. J. Med.*, 2003, **348**, 2175-2185.
19. C. Corbi-Verge, M. Garton, S. Nim and P. M. Kim, *Annu. Rev. Pharmacol. Toxicol.*, 2017, **57**, 39-60.
20. M. Zasloff, *Nature*, 2002, **415**, 389-395.
21. S. Riedl, D. Zweytick and K. Lohner, *Chem. Phys. Lipids.*, 2011, **164**, 766-781.
22. K. Lohner, *Gen. Physiol. Biophy.*, 2009, **28**, 105-116.
23. A. Moore, D. Devine and M. Bibby, *J. Pept. Res.*, 1993, **7**, 265-269.
24. M. A. Baker, W. L. Maloy, M. Zasloff and L. S. Jacob, *Cancer Res.*, 1993, **53**, 3052-3057.
25. G. Gajski, V and Garaj-Vrhovac, *Environ. Toxicol. Pharmacol.*, 2013, **36**, 697-705.
26. Y. Chen, X. Xu, S. Hong, J. Chen, N. Liu, C. B. Underhill, K. Creswell and L. Zhang, *Cancer Res.*, 2001, **61**, 2434-2438.
27. A. Risso, E. Braidot, M. C. Sordano, A. Vianello, F. Macrì, B. Skerlavaj, M. Zanetti, R. Gennaro and P. Bernardi, *Mol. Cell Biol.*, 2002, **22**, 1926-1935.
28. K. C. Mohan, P. Gunasekaran, E. Varalakshmi, Y. Hara and S. Nagini, *Cell. Biol. Int.*, 2007, **31**, 599-608.
29. C. Wang, Y. Zhou, S. Li, H. Li, L. Tian, H. Wang and D. Shang, *Life Sci.*, 2013, **92**, 1004-1014.
30. (a) F. Milletti, *Drug Discov. Today*, 2012, **17**, 850-860; (b) T. Jiang, Z. Zhang, Y. Zhang, H. Lv, J. Zhou, C. Li; L. Hou and Q. Zhang, *Biomaterials*, 2012, **33**, 9246-9258.
31. (a) A. D. Frankel and C. O. Pabo, *Cell*, 1988, **55**, 1189-1193; (b) M. Green and P. M. Loewenstein, *Cell*, 1988, **55**, 1179-1188.
32. D. Derossi,; A. H. Joliot, G. Chassaing and A. Prochiantz, *J. Biol. Chem.*, 1994, **269**, 10444-10450.
33. F. Wang, Y. Wang, X. Zhang, W. Zhang, S. Guo and F. Jin, *J. Control. Release*, 2014, **174**, 126-136.
34. (a) I. Nakase, G. Tanaka and S. Futaki, *Mol. Biosyst.*, 2013, **9**, 855-861; (b) C. J. Cheng and W. M. Saltzman, *Biomaterials*, 2011, **32**, 6194-6203; (c) K. Ezzat, E. M. Zaghloul, S. E. Andaloussi, T. Lehto, R. El-Sayed, T. Magdy, C. E. Smith and Ü. Langel, *J. Control. Release*, 2012, **162**, 1-8.
35. (a) H. Bai, Y. You, H. Yan, J. Meng, X. Xue, Z. Hou, Y. Zhou, X. Ma, G. Sang and X. Luo, *Biomaterials*, 2012, **33**, 659-667; (b) I. Nakase, H. Akita, K. Kogure, A. Gräslund, U. l. Langel, H. Harashima and S. Futaki, *Acc. Chem. Res.*, 2011, **45**, 1132-1139.
36. (a) J. Y. Lee, K. H. Bae, J. S. Kim, Y. S. Nam and T. G. Park, *Biomaterials*, 2011, **32**, 8635-8644; (b) M. Lindgren, K. Rosenthal-Aizman, K. Saar, E. Eiríksdóttir, Y. Jiang, M. Sassian, P. Östlund, M. Hällbrink and Ü. Langel, *Biochem. Pharmacol.*, 2006, **71**, 416-425.
37. (a) B. R. Liu, J.-S. Liou, Y.-J. Chen, Y.-W. Huang and H.-J. Lee, *Mar. Biotechnol.*, 2013, **15**, 584-595; (b) B. R. Liu, Y.-W. Huang and H.-J. Lee, *BMC Microbiol.*, 2013, **13**, 57.

38. S. Santra, H. Yang, J. T. Stanley, P. H. Holloway, B. M. Moudgil, G. Walter and R. A. Mericle, *Chem. Commun.*, 2005, **25**, 3144-3146.
39. (a) E. S. Olson, M. A. Whitney, B. Friedman, T. A. Aguilera, J. L. Crisp, F. M. Baik, T. Jiang, S. M. Baird, S. Tsimikas and R. Y. Tsien, *Integr. Biol.*, 2012, **4**, 595-605; (b) C.-W. Huang, Z. Li and P. S. Conti, *J. Nucl. Med.*, 2011, **52**, 1979-1986; (c) X. Zhai, M. Liu, X. Guo, S. Wang, H. Zhang and Y. Guo, *Chin. Med. J.*, 2011, **124**, 111-117; (d) N. Kamei, M. Morishita, Y. Kanayama, K. Hasegawa, M. Nishimura, E. Hayashinaka, Y. Wada, Y. Watanabe and K. Takayama, *J. Control. Release*, 2010, **146**, 16-22; (e) Q. T. Nguyen, E. S. Olson, T. A. Aguilera, T. Jiang, M. Scadeng, L. G. Ellies and R. Y. Tsien, *Proc. Natl. Acad. Sci. U. S. A.*, 2010, **107**, 4317-4322.
40. M. Lewin, N. Carlesso, C.-H. Tung, X.-W Tang,. D. Cory, D. T.Scadden and R. Weissleder, *Nat. Biotechnol.*, 2000, **18**, 410-414.
41. (a) H. J. Johansson, S. El-Andaloussi, T. Holm, M. Mäe, J. Jänes, T. Maimets and Ü. Langel, *Mol. Ther.*, 2008, **16**, 115-123; (b) J. Howl, S. Matou-Nasri, D. C. West, M. Farquhar, J. Slaninová, C.-G. Östenson, M. Zorko, P. Östlund, S. Kumar and Ü. Langel, *Cell. Mol. Life Sci.*, 2012, **69**, 2951-2966.
42. F. Heitz, M. C. Morris and G. Divita, *Br. J. Pharmacol.*, 2009, **157**, 195-206.
43. M. Dathe, M. Schümann, T. Wieprecht, A. Winkler, M. Beyermann, E. Krause, K. Matsuzaki, O. Murase and M. Bienert, *Biochemistry* 1996, **35**, 12612-12622.
44. E. Bevers, P. Comfurius and R. Zwaal, *Lupus* 1996, **5**, 480-487.
45. Y. Huang, Q. Feng, Q. Yan, X. Hao and Y. Chen, *Mini-Rev. Med. Chem.*, 2015, **15**, 73-81.
46. T. Utsugi, A. J. Schroit, J. Connor, C. D. Bucana and I. J. Fidler, *Cancer Res.*, 1991, **51**, 3062-3066.
47. S. Bafna, S. Kaur and S. Batra, *Oncogene* 2010, **29**, 2893-2904.
48. (a) W.-H. Yoon, H.-D. Park, K. Lim and B.-D. Hwang, *Biochem. Biophys. Res. Commun.*, 1996, **222**, 694-699; (b) M. D. Burdick, A. Harris, C. J. Reid, T. Iwamura and M. A. Hollingsworth, *J. Biol. Chem.*, 1997, **272**, 24198-24202.
49. (a) M. Sok, M. Šentjurc and M. Schara, *Cancer Lett.*, 1999, **139**, 215-220; (b) K. Kozłowska, J. Nowak, B. Kwiatkowski and M. Cichorek, *Exp. Toxicol. Pathol.*, 1999, **51**, 89-92.
50. (a) W. Domagala and L. Koss, *Scan. Electron. Microsc.*, 1979, **3**, 101-108; (b) J. Chaudhary and M. Munshi, *Cytopathology*, 1995, **6**, 162-167.
51. J. J. Hilliard, R. M. Goldschmidt, L. Licata, E. Z. Baum and K. Bush, *Antimicrob. Agents. Chemother.*, 1999, **43**, 1693-1699.
52. J. Li, J.-J. Koh, S. Liu, R. Lakshminarayanan, C. S. Verma and R. W. Beuerman, *Front. Neurosci.*, 2017, **11**.
53. Y. Shai, *J. Pept. Sci.*, 2002, **66**, 236-248.
54. D. M. Copolovici, K. Langel, E. Eriste and U. Langel, *ACS nano*, 2014, **8**, 1972-1994.
55. (a) H. D. Herce and A. E. Garcia, *Proc. Natl. Acad. Sci. U. S. A.*, **2007, 104**, 20805-20810; (b) H. Herce, A. Garcia, J. Litt, R. Kane, P. Martin, N. Enrique, A. Rebolledo and V. Milesi, *Biophys. J.*, 2009, **97**, 1917-1925; (c) K. Matsuzaki, O. Murase and K. Miyajima, *Biochemistry*, 1995, **34**, 12553-12559; (d) S. J. Ludtke, K. He, W. T. Heller, T. A. Harroun, L. Yang and H. W. Huang, *Biochemistry*, 1996, **35**, 13723-13728.
56. N. Papo and Y. Shai, *Biochemistry*, 2003, **42**, 9346-9354.

57. (a) D. B. Kell, *Nat. Rev. Drug Discov.*, 2016, **15**, 143-143; (b) D. B. Kell and S. G. Oliver, *Front. Pharmacol.*, 2014, **5**; (c) P. D. Dobson and D. B. Kell, *Nat. Rev. Drug Discov.*, 2008, **7**, 205-220.
58. (a) A. Prochiantz, *Curr. Opin. Neurobiol.*, 1996, **6**, 629-634; (b) A. Prochiantz, *Ann. N. Y. Acad. Sci.*, 1999, **886**, 172-179; (c) D. Derossi, S. Calvet, A.Trembleau, A.Brunissen, G. Chassaing and A. Prochiantz, *J. Biol. Chem.*, 1996, **271**, 18188-18193.
59. P. A. Wender, W. C. Galliher, E. A. Goun, L. R. Jones and T. H. Pillow, *Adv. Drug Deliv. Rev.*, 2008, **60**, 452-472.
60. I. D. Alves, N. Goasdoué, I. Correia, S. Aubry, C. Galanth, S. Sagan, S.Lavielle and G. Chassaing, *Biochim Biophys. Acta. Gen. Subj.*, 2008, **1780**, 948-959.
61. P. Joanne, C. Galanth, N. Goasdoué, P. Nicolas, S. Sagan, S. Lavielle, G. Chassaing, C. El Amri and I. D. Alves, *Biochim. Biophys. Acta. Biomembr.*, 2009, **1788**, 1772-1781.
62. J. L. Goldstein, R. G. Anderson and M. S. Brown, *Nature* 1979, **279**, 679-685.
63. S. Mayor and R. E. Pagano, *Nat. Rev. Mol. Cell Biol.*, 2007, **8**, 603-612.
64. R. E. Vandenbroucke, S. C. De Smedt, J. Demeester and N. N. Sanders, *Biochim. Biophys. Acta. Biomembr.*, 2007, **1768**, 571-579.
65. S. Futaki,; I. Nakase, A.Tadokoro, T. Takeuchi and A. T. Jones, Portland Press Limited: 2007.
66. S. D. Conner and S. L. Schmid, *Nature*, 2003, **422**, 37-44.
67. T. Kuwana, L. Bouchier-Hayes, J. E. Chipuk, C. Bonzon, B. A. Sullivan, D. R. Green and D. D. Newmeyer, *Mol. Cell*, 2005, **17**, 525-535.
68. J. C. Mai, Z. Mi, S.-H. Kim, B. Ng and P. D. Robbins, *Cancer Res.*, 2001, **61**, 7709-7712.
69. H. M. Ellerby, W. Arap, L. M. Ellerby, R. Kain, R. Andrusiak, G. Del Rio, S. Krajewski, C. R. Lombardo, R. Rao and E. Ruoslahti, *Nat. Med.*, 1999, **5**, 1032-1038.
70. K. L. Horton, K. M. Stewart, S. B.Fonseca, Q. Guo and S. O. Kelley, *Chem. Biol.*, 2008, **15**, 375-382.
71. H. Li, S. K. Kolluri, J. Gu, M. I. Dawson, X. Cao, P. D. Hobbs, B. Lin, G.-q. Chen,; J.-s. Lu and F. Lin, *Science*, 2000, **289**, 1159-1164.
72. C. M. Rodrigues, S. Solá, M. A. Brito, C. D.Brondino, D. Brites and J. J. Moura, *Biochem. Biophys. Res. Commun.*, 2001, **281**, 468-474.
73. S. Fletcher and A. D.Hamilton, *Curr. Opin. Chem. Biol.*, 2005, **9**, 632-638.
74. M. P. Stumpf, T. Thorne, E. de Silva, R. Stewart, H. J. An, M. Lappe and C. Wiuf, *Proc. Natl. Acad. Sci. U. S. A.*, 2008, **105**, 6959-6964.
75. A. A. Ivanov, F. R. Khuri and H. Fu, *Trends Pharmacol. Sci.*, 2013, **34**, 393-400.
76. B. Vogelstein, D. Lane and A. J. Levine, *Nature* 2000, **408**, 307-310.
77. M. B. Kastan, O. Onyekwere, D. Sidransky, B. Vogelstein and R. W. Craig, *Cancer Res.*, 1991, **51**, 6304-6311.
78. J. A. Kritzer, J. D. Lear, M. E. Hodsdon and A. Schepartz, *J. Am. Chem. Soc.*, 2004, **126**, 9468-9469.
79. V. Kirkin, S. Joos and M. Zörnig, *Biochim. Biophys. Acta Mol. Cell Res.*, 2004, **1644**, 229-249.
80. J.-L. Wang, Z.-J. Zhang, S. Choksi, S. Shan, Z. Lu, C. M. Croce, E. S. Alnemri, R. Korngold and Z. Huang, *Cancer Res.*, 2000, **60**, 1498-1502.

81. V. Azzarito, K. Long, N. S. Murphy and A. J. Wilson, *Nat. Chem.*, 2013, **5**, 161-173.
82. M. Pelay-Gimeno, A. Glas, O. Koch and T. N. Grossmann, *Angew. Chem. Int. Ed.*, 2015, **54**, 8896-8927.
83. B. N. Bullock, A. L. Jochim and P. S. Arora, *J. Am. Chem. Soc.*, 2011, **133**, 14220-14223.
84. L. Strekowski and B. Wilson, *Mutat. Res-Fund Mol. M.*, 2007, **623**, 3-13.
85. G. Chu, *J. Biol. Chem.*, 1994, **269**, 787-790.
86. R. Hänsel-Hertsch, D. Beraldi, S. V. Lensing, G. Marsico, K. Zyner, A. Parry, M. Di Antonio, J. Pike, H. Kimura and M. Narita, *Nat. Genet.*, 2016.
87. M. Gellert, M. N. Lipsett and D. R. Davies, *Proc. Natl. Acad. Sci. U. S. A.*, 1962, **48**, 2013-2018.
88. S. Neidle, *Nat. Rev. Chem.*, 2017, **1**, 0041.
89. B. H. Geierstanger, M. Mrksich, P. B. Dervan and D. E. Wemmer, *Science*, 1994, **266**, 646-651.
90. K. T. Neil, R. H. Hoess and W. F. DeGrado, *Science*, 1990, **249**, 774.
91. R. V. Talanian, C. J. McKnight, R. Rutkowski and P. S. Kim, *Biochemistry*, 1992, **31**, 6871-6875.
92. B. H. Geierstanger, B. F. Volkman, W. Kremer and D. E.Wemmer, *Biochemistry*, 1994, **33**, 5347-5355.
93. R. Lande, J. Gregorio, V. Facchinetti, B. Chatterjee, Y.-H. Wang, B.Homey, W. Cao, Y.-H.Wang, B. Su and F. O. Nestle, *Nature*, 2007, **449**, 564-569.
94. R. E. Hancock and H.-G. Sahl, *Nat. Biotechnol.*, 2006, **24**, 1551-1557.
95. T. Haack, M. W. Peczuh, X. Salvatella, J. Sánchez-Quesada, J. De Mendoza, A. D. Hamilton and E. Giralt, *J. Am. Chem. Soc.*, 1999, **121**, 11813-11820.
96. S. Marqusee and R. L. Baldwin, *Proc. Natl. Acad. Sci. U. S. A.*, 1987, **84**, 8898-8902.
97. A. N.Z aykov and Z. T. Ball, *Chem. Commun.*, **2011,** *47* (39), 10927-10929.
98. D. Y. Jackson, D. S. King, J. Chmielewski, S. Singh and P. G. Schultz, *J. Am. Chem. Soc.*, 1991, **113**, 9391-9392.
99. H. Jo, N. Meinhardt, Y.Wu, S.Kulkarni, X. Hu, K. E.Low, P. L.Davies, W. F.DeGrado and D. C. Greenbaum, *J. Am. Chem. Soc.*, 2012, **134**, 17704-17713.
100. A. Muppidi, K. Doi, S. Edwardraja, E. J. Drake, A. M.Gulick, H.-G. Wang and Q. Lin, *J. Am. Chem. Soc.*, 2012, **134**, 14734-14737.
101. J. W. Taylor, *Pept. Sci.*, 2002, **66**, 49-75.
102. J. W. Taylor, Q. K. Jin, M. Sbacchi, L. Wang, P. Belfiore, M. Garnier, A. Kazantzis, A. Kapurniotu, P. F. Zaratin and M. A. Scheideler, *J. Med. Chem.*, 2002, **45**, 1108-1121.
103. L. D. Walensky and G. H. Bird, *J. Med. Chem.*, 2014, **57**, 6275-6288.
104. G. L. Verdine and G. J. Hilinski, *Drug Discov. Today Technol.*, 2012, **9**, e41-e47.
105. R. N. Chapman, G. Dimartino and P. S. Arora, *J. Am. Chem. Soc.*, 2004, **126**, 12252-12253.
106. S. E. Miller, P. F.Thomson and P. S.Arora, *Curr. Protoc. Chem. Biol.*, 2014, 101-116.
107. A. B. Mahon and P. S.Arora, *Drug Discov. Today Technol.*, 2012, **9,** e57-e62.
108. C. H. Douse, S. J. Maas, J. C.Thomas, J. A. Garnett, Y. Sun, E. Cota and E. W. Tate, *ACS Chem. Biol.*, 2014, **9**, 2204-2209.
109. M. K. Jayatunga, S. Thompson and A. D. Hamilton, *Bioorg. Med. Chem. Lett.*, 2014, **24**, 717-724.

110. J. T. Ernst, J.Becerril, H. S.Park, H. Yin and A. D.Hamilton, *Angew. Chem. Int. Ed.,* 2003, **115**, 553-557.
111. N. S. Murphy, P. Prabhakaran, V. Azzarito, J. P. Plante, M. J. Hardie, C. A.Kilner, S. L. Warriner and A. J. Wilson, *Chem. Eur. J.*, 2013, **19**, 5546-5550.
112. V. Azzarito, P. Prabhakaran, A. I. Bartlett, N. S. Murphy, M. J. Hardie, C. A. Kilner, T. A. Edwards, S. L.Warriner, A. J.Wilson, *Org. Biomol. Chem.*, 2012, **10**, 6469-6472.
113. A. Barnard, K. Long, D. J. Yeo, J. A. Miles, V. Azzarito, G. M.Burslem, P. Prabhakaran, T. A. Edwards and A. J. Wilson, *Org. Biomol. Chem.*, **2014,** *12* (35), 6794-6799.
114. P. Tošovská and P. S. Arora, *Org. Lett.*, 2010, **12**, 1588-1591.
115. C. E. Schafmeister, Z. Z. Brown and S. Gupta, *Acc. Chem. Res.*, 2008, **41**, 1387-1398.
116. L. Feng, Y. Geisselbrecht, S. Blanck, A. Wilbuer, G. E. Atilla-Gokcumen, P. Filippakopoulos, K. Kräling, M. A. Celik, K. Harms and J. Maksimoska, *J. Am. Chem. Soc.*, 2011, **133**, 5976-5986.
117. R. Zou, Q. Wang, J. Wu, J. Wu, C. Schmuck and H. Tian, *Chem. Soc. Rev.*, 2015, **44**, 5200-5219.
118. J.-M. Lehn, A. Rigault, J. Siegel, J. Harrowfield, B. Chevrier and D. Moras, *Proc. Natl. Acad. Sci. U. S. A.*, 1987, **84**, 2565-2569.
119. A. J. McConnell, C. S.Wood, P. P.Neelakandan and J. R., Nitschke, *Chem. Rev.*, 2015, **115**, 7729-7793.
120. J. Kerckhoffs, J. C. Peberdy, I. Meistermann, L. J. Childs, C. J. Isaac, C. R. Pearmund, V. Reudegger, S. Khalid, N. W. Alcock, M. J. Hannon and A. Rodger, *Dalton Trans.*. 2007, **7**, 734-742.
121. (a) J. C. Peberdy, J. Malina,; S. Khalid, M. J. Hannon and A. Rodger, *J. Inorg. Biochem.*, 2007, **101**, 1937-1945; (b) M. J. Hannon, V. Moreno, M. J. Prieto, E. Moldrheim, E. Sletten, I. Meistermann, C. J. Isaac, K. J.Sanders and A.Rodger, *Angew. Chem. Int. Ed.*, 2001, **40**, 880-884.
122. M. J. Hannon, I. Meistermann, C. J. Isaac, C. Blomme, J. R. Aldrich-Wright and A. Rodger, *Chem. Commun.*, 2001, **12**, 1078-1079.
123. J. Lacour, C. Ginglinger, F. Favarger and S. TorcheHaldimann, *Chem. Commun.*, 1997, **23**, 2285-2286.
124. L. Cardo, V. Sadovnikova, S. Phongtongpasuk, N. J. Hodges and M. J. Hannon, *Chem. Commun.*, 2011, **47**, 6575-6577.
125. L. Cardo and M. J. Hannon, *Inorganica Chim. Acta*, 2009, **362**, 784-792.
126. A. D. Richards, A. Rodger, M. J. Hannon and A. Bolhuis, *Int. J. Antimicrob. Agents*, 2009, **33**, 469-472.
127. A guide to sensitivity testing. Report of the Working Party on Antibiotic Sensitivity Testing of the British Society for Antimicrobial Chemotherapy. *J. Antimicrob. Chemother.*, 1991, **27** *Suppl D*, 1-50.
128. S. V. Kumar, W. K. Lo, H. J. Brooks and J. D. Crowley, *Inorganica Chim. Acta*, 2015, **425**, 1-6.
129. (a) I. Meistermann, V. Moreno, M. J. Prieto, E. Moldrheim, E. Sletten, S. Khalid, P. M. Rodger, J. C. Peberdy, C. J. Isaac, A. Rodger and M. J. Hannon, *Proc. Natl. Acad. Sci. U. S. A.*, 2002, **99**, 5069-5074; (b) C. Uerpmann, J. Malina, M. Pascu, G. J. Clarkson, V. Moreno, A. Rodger, A. Grandas and M. J. Hannon, *Chem. Eur. J.*, 2005, **11**, 1750-1756.
130. (a) A. Oleksi, A. G. Blanco, R. Boer, I. Uson, J. Aymami, A. Rodger, M. J. Hannon and M. Coll, *Angew. Chem. Int. Ed.*, 2006, **45**, 1227-1231; (b) J.

Malina, M. J. Hannon and V. Brabec, *Chem. Eur. J.*, 2007, **13**, 3871-3877; (c) L. Cerasino, M. J. Hannon and E. Sletten, *Inorg. Chem.*, 2007, **46**, 6245-6251.
131. J. Malina, M. J. Hannon and V. Brabec, *Sci. Rep.*, 2016, **6**.
132. G. I. Pascu, A. C. Hotze, C. Sanchez-Cano, B. M. Kariuki and M. J. Hannon, *Angew. Chem. Int. Ed.*, 2007, **119**, 4452-4456.
133. H. Yu, M. Li, G. Liu, J. Geng, J. Wang, J. Ren, C. Zhao and X. Qu, *Chem. Sci.*, 2012, **3**, 3145-3153.
134. S. M. McNeill, D. Preston, J. E. Lewis, A. Robert, K. Knerr-Rupp, D. O. Graham, J. R. Wright, G. I. Giles and J. D. Crowley, *Dalton Trans.*, 2015, **44**, 11129-11136.
135. S. Ø. Scott, E. L. Gavey, S. J. Lind, K. C. Gordon and J. D. Crowley, *Dalton Trans.*, 2011, **40**, 12117-12124.
136. S. E. Howson, A. Bolhuis, V. Brabec, G. J. Clarkson, J. Malina, A. Rodger and P. Scott, *Nat. Chem.*, 2012, **4**, 31-36.
137. V. Brabec, S. E. Howson, R. A. Kaner, R. M. Lord, J. Malina, R. M. Phillips, Q. M. Abdallah, P. C. McGowan, A. Rodger and P. Scott, *Chem. Sci.*, 2013, **4**, 4407-4416.
138. R. A. Kaner, S. J. Allison, A. D. Faulkner, R. M. Phillips, D. I. Roper, S. L. Shepherd, D. H. Simpson, N. R. Waterfield and P. Scott, *Chem. Sci.*, 2016, **7**, 951-958.
139. M. Li, S. E. Howson, K. Dong, N. Gao, J. Ren, P. Scott and X. Qu, *J. Am. Chem. Soc.*, 2014, **136**, 11655-11663.
140. A. Zhao, S. E. Howson, C. Zhao, J. Ren, P. Scott, C. Wang and X. Qu, *Nucleic Acids Res.*, 2017.
141. R. A. Kaner and Scott, P. *Future Med. Chem.*, 2015, **7**, 1-4.
142. J. E. Lewis, C. J. McAdam, M. G. Gardiner and J. D. Crowley, *Chem. Commun.*, 2013, **49**, 3398-3400.
143. Z. Wang and S. M. Cohen, *Chem. Soc. Rev.*, 2009, **38**, 1315-1329.
144. V. Brega, M. Zeller, Y. He, H. P. Lu and J. K. Klosterman, *Chem. Commun.*, 2015, **51**, 5077-5080.
145. (a) D. A. Roberts, A. M. Castilla, T. K. Ronson and J. R. Nitschke, *J. Am. Chem. Soc.*, 2014, **136**, 8201-8204; (b) D. A. Roberts, B. S. Pilgrim, J. D. Cooper, T. K. Ronson, S. Zarra and J. R. Nitschke, *J. Am. Chem. Soc.*, 2015, **137**, 10068-10071; (c) T. K. Ronson, B. S. Pilgrim and J. R. Nitschke, *J. Am. Chem. Soc.*, 2016, **138**, 10417-10420; (d) R. Chakrabarty and P. J. Stang, *J. Am. Chem. Soc.*, 2012, **134**, 14738-14741; (e) K. K. Tanabe and S. M. Cohen, *Chem. Soc. Rev.*, 2011, **40**, 498-519; (f) M. Wang, W.-J. Lan, Y.-R. Zheng, T. R. Cook, H. S. White and P. J. Stang, *J. Am. Chem. Soc.*, 2011, **133**, 10752-10755; (g) M. C. Young, A. M. Johnson and R. J. Hooley, *Chem. Commun.*, 2014, **50**, 1378-1380.
146. R. J. Marshall, S. L. Griffin, C. Wilson and R. S. Forgan, *J. Am. Chem. Soc.*, 2015, **137**, 9527-9530.
147. W. Morris, C. J. Doonan, H. Furukawa, R. Banerjee and O. M. Yaghi, *J. Am. Chem. Soc.*, 2008, **130**, 12626-12627.
148. M. W. Schneider, I. M. Oppel, A. Griffin and M. Mastalerz, *Angew. Chem. Int. Ed.*, 2013, **52**, 3611-3615.
149. Z. Wang and S. M. Cohen, *J. Am. Chem. Soc.*, 2007, **129**, 12368-12369.
150. A. J. Metherell and M. D. Ward, *Polyhedron* 2015, **89**, 260-270.
151. J. Mosquera, S. Zarra and J. R. Nitschke, *Angew. Chem. Int. Ed.*, 2014, **53**, 1556-1559.

152. D. A. Roberts, B. S. Pilgrim and J. R. Nitschke, *Chem. Soc. Rev.*, 2018, **47**, 626-644.
153. (a) M. Dean, T. Fojo and S. Bates, *Nat. Rev. Cancer,* 2005, **5**, 275-284; (b) C. Holohan, S. Van Schaeybroeck, D. B. Longley and P. G. Johnston, *Nat. Rev. Cancer,* 2013, **13**, 714-726.
154. J. R. Brender, S. Salamekh and A. Ramamoorthy, *Acc. Chem. Res.,* 2012, **45**, 454.

Chapter 2

Alkyne functionalized metallohelices

2.1 Introduction

Alkyne groups, especially the terminal alkyne, are versatile units for organic and inorganic synthesis. Reactions including reduction,[1] hydration,[2] hydrohalogenation,[3] halogenation[4] and ozonolysis[5] can be used readily to introduce a range of functional groups. The recently popularised Huisgen copper-catalysed azide/alkyne cycloaddition "click" reaction CuAAC[6] allows alkynes to function as latent reactive groups, even under biologically compatible conditions, providing potential chemical tools for a wide range of applications[7] such as click modification of DNA[8] and proteins,[9] cell imaging,[10] conjugating to small peptides[11] and surface-enhanced Raman scatting detection.[12, 13] To our knowledge, no metallohelix system has previously contained terminal alkyne groups for this kind of application, although this laboratory recently developed a synthesis of optically pure heterobimetallic Fe-Cu via CuAAC,[14] and other studies have been reported on the use of click chemistry to form 1,2,3-triazole groups as active ligands[15, 16] or to derivatise metal complexes (See Chapter 3).[17]

In this chapter we will explore the synthesis of alkyne derivatives of metallohelices; two types of flexicate architecture and one triplex system. Preliminary anticancer studies of these compounds are included. The feasibility of CuAAC reactions is also addressed.

2.2 Synthesis of alkyne-decorated flexicates

In earlier work it was found that the CuAAC 'click' reactions of the monometallic complex[14] shown in Scheme 2-1(a) were very efficient, proceeding to completion with catalytic quantities of CuI. In this architecture, derived from sub-component amine **1** the structure is preorganised for coordination of the Cu(I) ion by the subsequent triazole units. Indeed, when stoichiometric amounts of CuI were added, stable Fe-Cu helicates as shown (a) were created directly, and removal of the Cu ions was not achieved without decomposition of the Fe complex.

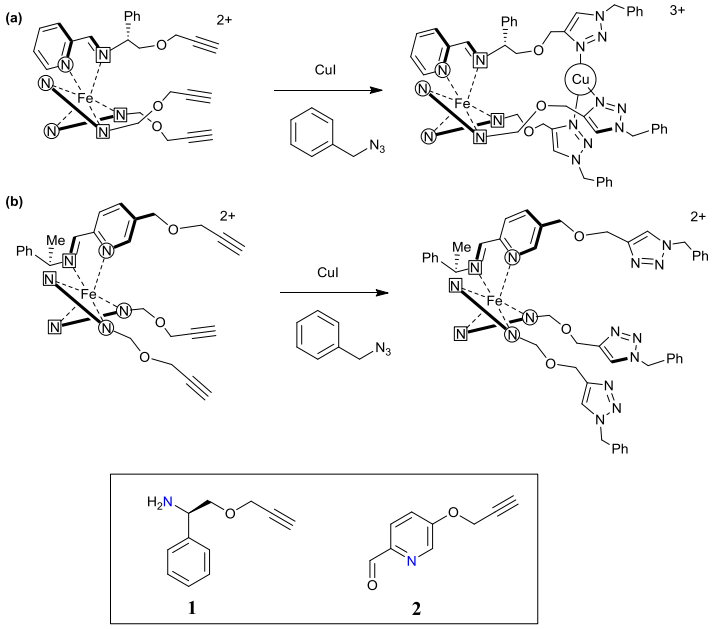

Scheme 2-1 "Click" reactions between monometallic complexes and $PhCH_2N_3$

In contrast, similar reactions in Scheme 2-1(b) of Fe(II) complexes incorporating pyridine **2** were much less efficient, requiring stoichiometric amounts of catalyst in order to proceed to completion.[14] Thus, for flexicate or triplex systems, while we might seek to incorporate alkyne groups into the ligand structure *via* either the pyridine carboxaldehyde (**2**) or chiral amine (**1**) sub-components, it is by no means clear which would be the most successful.

2.2.1 Diamine "Flexicate" alkyne derivatives

The prototype diamine flexicate architecture[18] has recently been expanded significantly in this laboratory by Dr Daniel H Simpson. The diphenylether diamine system **3** gave a flexicate with MIC of 2 μg/ml in Methicillin-resistant Staphylococcus aureus (*MRSA*). Based on this observation and the high chemical stability of the system, this bridge architecture was chosen to be exemplified as an alkyne derivative (Scheme 2-2).

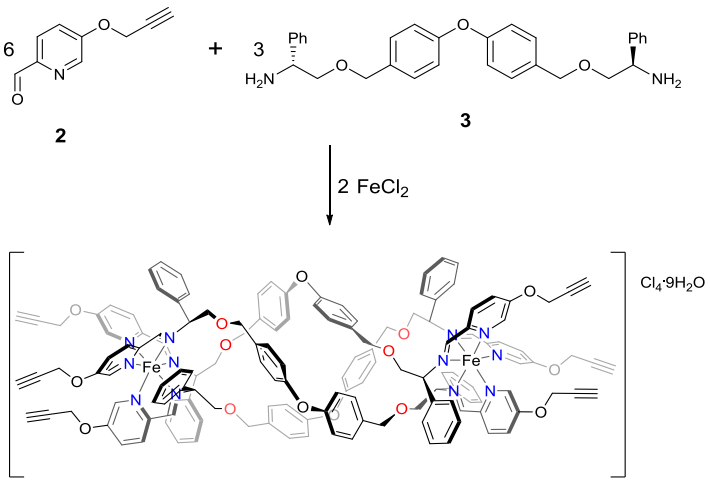

Scheme 2-2 Self-assembly of diamine alkyne flexicate

*Synthesis of the alkyne pyridine carboxaldehyde **2***

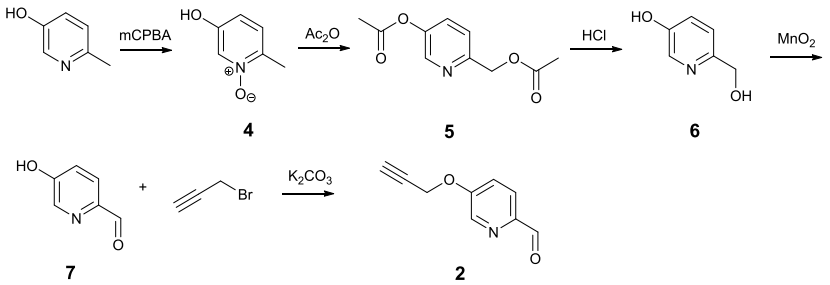

Scheme 2-3 Synthesis of the 5-(prop-2-yn-1-yloxy)picolinaldehyde

The sub-component 5-(prop-2-ynyloxy)picolinaldehyde (**2**) was synthesised as shown in Scheme2-3. Modified literature procedures were used as far as compound **7**.[19] First,

5-hydroxy-2-methylpyridine was treated with *m*-chloroperoxybenzoic acid to form 5-hydroxy-2-methylpyridine-1-oxide (**4**). Refluxing **4** in acetic anhydride yielded 2-acetoxymethyl-5-acetoxypyridine (**5**) quantitatively. Subsequently, **5** was hydrolysed in hydrochloric acid to form 6-(hydroxymethyl)pyridin-3-ol (**6**). Oxidation of **6** with activated manganese (IV) dioxide gave 5-(hydroxy)picolinaldehyde (**7**) which was converted to 5-(prop-2-ynyloxy)picolinaldehyde (**2**) in presence of with two equivalents of potassium carbonate and an equimolar amount of propargyl bromide in acetonitrile. The crude product was recrystallized in DCM:Hexane (1:4; v:v) to yield white yellow solid in overall 39% yield.

*Synthesis of phenylglycinol enantiomers **8***

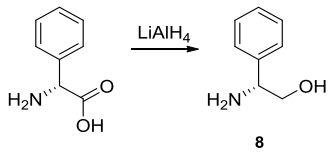

8

Scheme 2-4 Synthesis of phenylglycinol (*R*)-**8**

Reduction of optically optical pure D-phenylglycine was conducted using lithium aluminium hydride to form the phenylglycinol (*R*)-**8** (Scheme 2-4).[20, 21] The white crystalline compound was obtained by recrystallization in hot toluene. (*S*)-**8** was synthesised from L-phenylglycine but was not used in this chapter.

*Synthesis of diphenylether diamine (R,R)-**3***

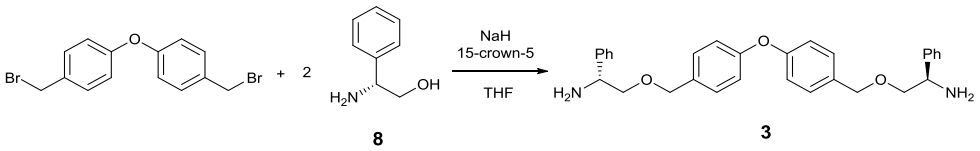

8 **3**

Scheme 2-5 Synthesis of diphenylether diamine *(R,R)*-**3**

Bis(4-(bromomethyl)phenyl)methane was supplied by Dr Daniel H Simpson. Deprotonation of (*R*)-phenylglycinol **8** was conducted using an excess of sodium hydride in the presence of *ca* one equivalent of [15]-crown-[5] (Scheme 2-5). The diamine product (*R*,*R*)-**3** was achieved by subsequent addition of the appropriate 4,4'-oxybis((bromomethyl)benzene) and was purified by silica gel column chromatography using DCM/MeOH/TEA (200/1/1; v:v:v). Diamine **7** was isolated as yellow solid in 72% yield.

Assembly of complex (R_c,Δ_{Fe})-[Fe_2**L**$^1{}_3$]Cl_4

The synthesis of the new alkyne-decorated iron(II) flexicate followed the same general method as previously reported.[18] The diamine (*R*,*R*)-**3** (3 eq.), alkyne aldehyde **2** (6 eq.) and iron(II) chloride (2 eq.) were dissolved in methanol and heated to reflux for 48 h (Scheme 2-2). The dark purple solution was filtered through celite and was evaporated carefully to dryness. The product was analysed by NMR, mass spectrometry, microanalysis, and circular dichroism.

The ^{1}H NMR spectrum of (R_c,Δ_{Fe})-[Fe_2**L**$^1{}_3$]Cl_4 in MeOD at 298 K indicates a single bimetallic flexicate (Figure 2-1). The imine peak H^a was observed at 9.24 ppm, along with the doublet peak H^b for the NCHPh proton adjacent to the imine nitrogen atom at 5.78 ppm. The propargyl protons of H^c (-CH_2C≡C) and H^d (C≡CH) were centred at 4.73 ppm and 3.22 ppm respectively. Other ^{1}H NMR and ^{13}C NMR spectra signals were fully assigned and are consistent with the presence of single, non-racemising diastereomers in solution. Notably, the alkyne C-H signal is out of phase with the rest of the CH and CH_3 signals due to the large C-H coupling constant ($^1J_{C\text{-}H}$ = 250Hz). This is observed for all alkyne groups in the thesis. In the MS, an envelope observed at *m*/*z* 594 is consistent with the presence of [$Fe_2L^1{}_3$]$^{4+}$ ion isotopomers.

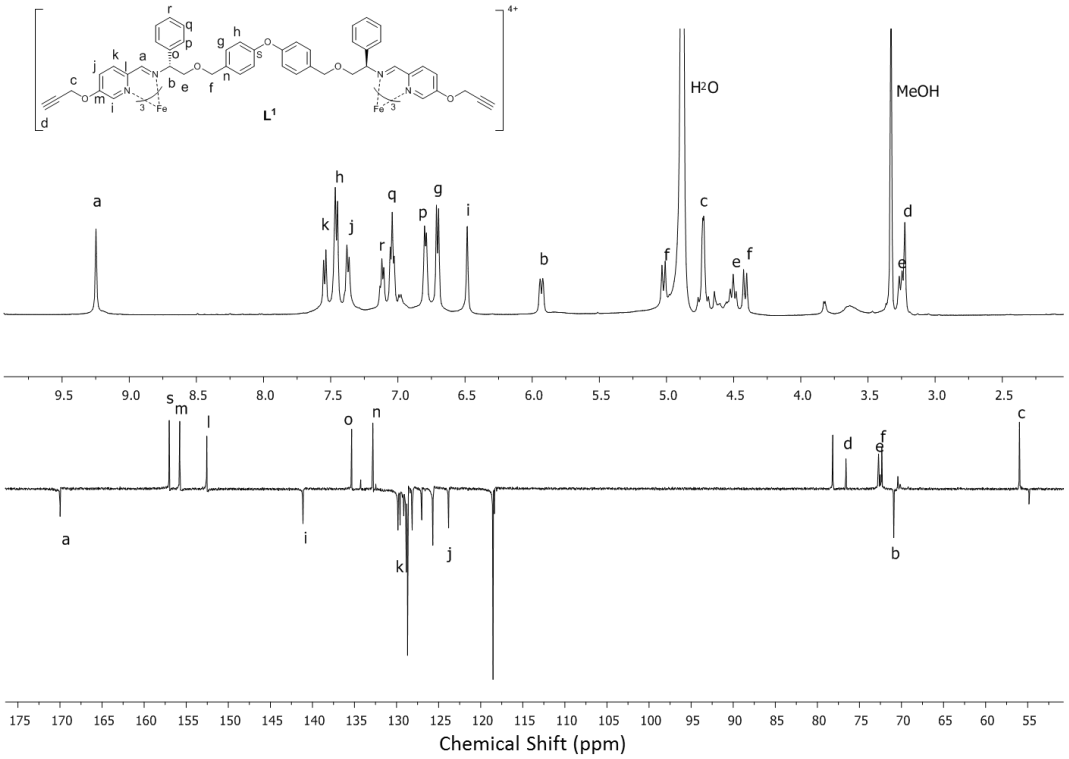

Figure 2-1 ^{1}H NMR (500 M Hz, MeOD, 298K) and ^{13}C NMR (125 M Hz, MeOD, APT, 298K) spectrum of diamine alkyne flexicate (R_c,Δ_{Fe})-[Fe_2**L**$^{1}_3$]Cl_4.

2.2.2 Dialdehyde "flexicate" alkyne derivatives

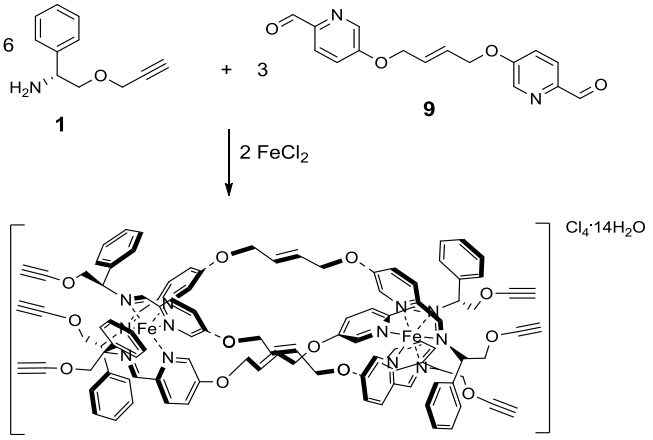

Scheme 2-6 Synthetic route to the formation of (R_c,Δ_{Fe})-[Fe_2**L**$^{2}_3$]Cl_4

A series of bimetallic flexicates have been made in presence of dialdehyde linker derivative, (*R/S*)-1-phenylethan-1-amine and $FeCl_2$ by Dr Rebecca A. Kaner in this laboratory.[22] *In vitro* cytotoxicity screening revealed that the Δ enantiomer flexicate

containing dialdehyde linker **9** was extremely active towards human tumour cell lines: MDA-MB-468, HCT116 $p53^{+/+}$ and HCT116 $p53^{-/-}$, especially for HCT116 $p53^{-/-}$ cancer cell line with IC_{50} value 40±3 nM. This flexicate also exhibited much lower toxicity to the human non-cancer retinal pigment epithelial cells (ARPE19). Therefore, the dialdehyde unit **9** was chosen to assemble with chiral alkyne amine **1** to form dialdehyde alkyne flexicate (Scheme 2-6).

*Synthesis of alkyne chiral amine enantiomers **1***

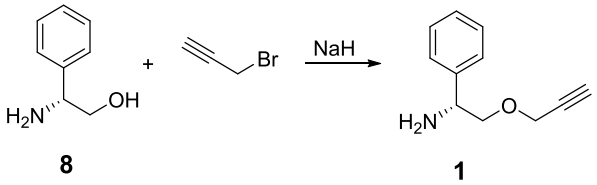

8 **1**

Scheme 2-7 Synthesis of (*R*)-1-phenyl-2-(prop-2-yn-1-yloxy)ethan-1-amine

Optically pure **8** was converted to (*R*)-1-phenyl-2-(prop-2-yn-1-yloxy)ethan-1-amine (**1**) using a modified Williamson ether synthesis in the presence of sodium hydride and propargyl bromide (Scheme 2-7).[14] This crude product was purified by silica gel column chromatography by using DCM/MeOH/TEA (500/5/2; v:v:v) as the eluent to isolate **1** as yellow oil in 75% yield.

*Synthesis of alkene dialdehyde unit **9***

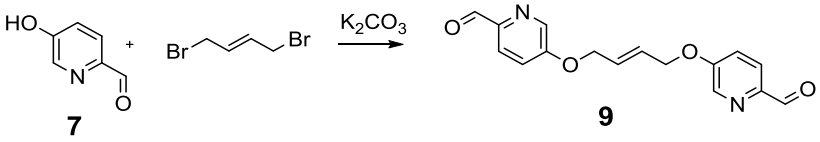

7 **9**

Scheme 2-8 Synthesis of alkene dialdehyde unit 9

The alkene (*E*)-5,5'-(but-2-ene-1,4-diylbis(oxy))dipicolinaldehyde (**9**) was synthesised *via* Williamson etherification of **7** with 1,4-trans-dibromobut-2-ene in the

presence of potassium carbonate.[22] The white solid product was obtained by silica gel column chromatography with eluent DCM/MeOH/TEA (350/5/2; v:v:v) in 85% yield.

Assembly of complex (R_c,Δ_{Fe})-[Fe_2**L**$^{2}_3$]Cl_4

Similar synthesis with diamine alkyne iron(II) flexicate (R_c,Δ_{Fe})-[Fe_2**L**$^{1}_3$]Cl_4, dialdehyde alkyne iron(II) flexicate was formed by mixing and refluxing the alkene dipicolinaldehyde linker **9** (3 eq.) and (*R*)-1-phenyl-2-(prop-2-yn-1-yloxy)ethan-1-amine (**1**) (6 eq.), with iron(II) chloride (2 eq.) in methanol (Scheme 2-6). After 48 h, the dark purple solutions were filtered through celite and evaporated carefully to dryness. The products were analysed by NMR, mass spectrometry, microanalysis, thermogravimetric analysis, infra-red, UV-vis absorption, and circular dichroism.

The ^{1}H NMR spectrum of (R_c,Δ_{Fe})-[Fe_2**L**$^{2}_3$]Cl_4 in MeOD at 298 K indicates high diastereomeric purity: the presence of single peak H^a in the imine region (9.03 ppm), *ortho* pyridine proton H^b at 6.50 ppm, alkene proton H^c at 6.03 ppm, stereogenic centre proton H^d at 5.87 ppm and alkyne proton H^e at 3.17 ppm. The ^{13}C NMR spectrum was also consistent with this and was fully assigned. (Figure 2-2).

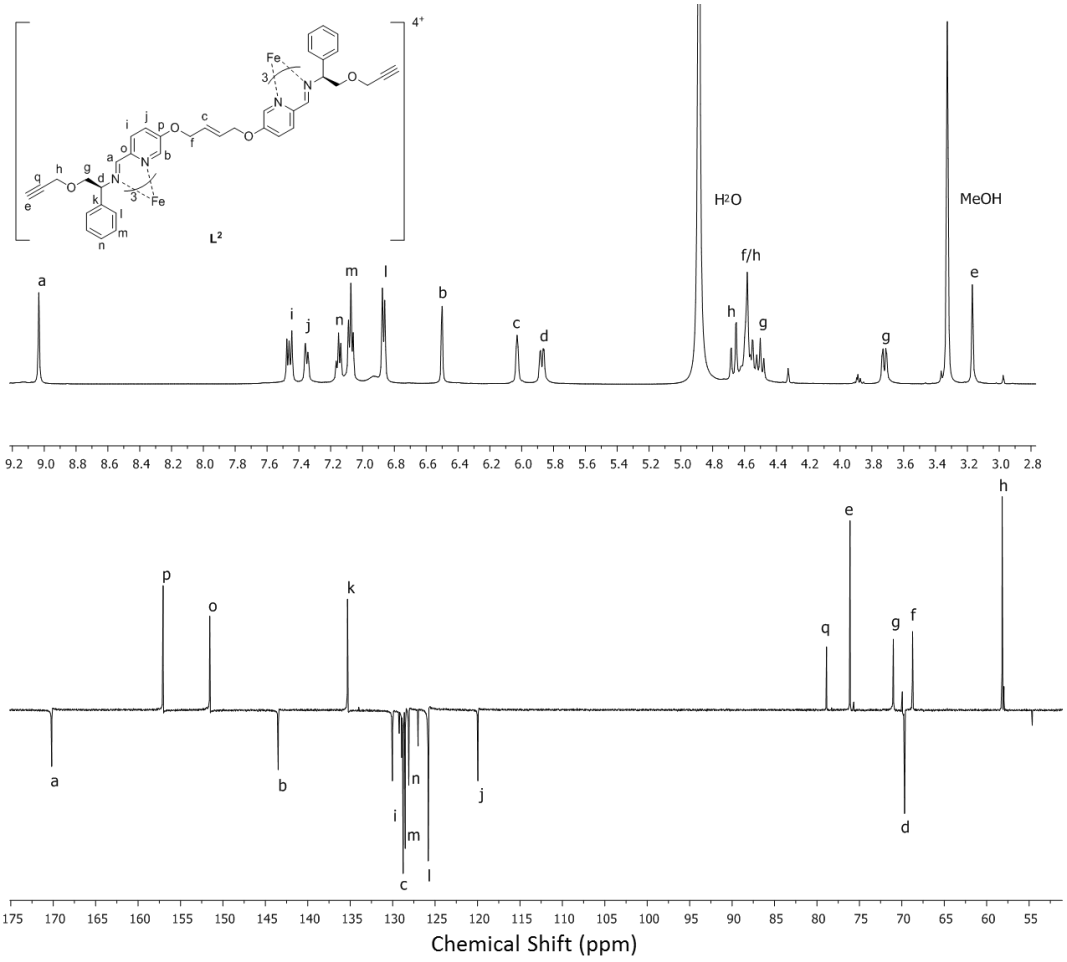

Figure 2-2 ^{1}H NMR (500 M Hz, MeOD, 298K) and ^{13}C NMR (125 M Hz, MeOD, 298K) of dialdehyde alkyne flexicate (R_c,Δ_{Fe})-[Fe_2**L²**$_3$]Cl_4

The complexes gave excellent electrospray high resolution mass spectrometry data [Figure 2-3(a)], (R_c,Δ_{Fe})-[Fe_2**L²**$_3$]Cl_4 gave a strong peak at *m/z* 487.1722 Da for the tetracationic molecular ion, which was consistent with calculated value (*m/z* 487.1724 Da). Circular dichroism spectra of each pair of enantiomers were recorded in methanol. Each displayed equal and opposite spectra, indicating that the complexes were formed in non-racemic mixtures of opposite configurations [Figure 2-3(b)].

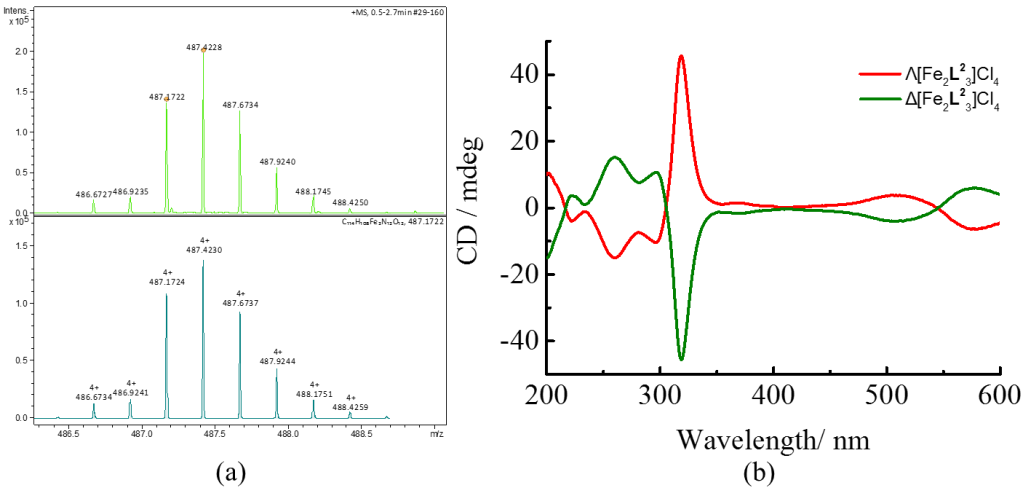

Figure 2-3 High resolution mass spectrum: top measured, below calculated (a) and CD spectrum (b) of dialdehyde alkyne flexicate $[Fe_2\mathbf{L}^{\mathbf{2}}{}_3]Cl_4$

2.2.3 Click reactions of alkyne flexicates

Both alkyne flexicates classes above were considered to be sufficiently stable to undergo click condition. Benzyl azide was employed to attempt the click reaction on alkyne flexicates. CuI was utilized as the Cu (I) catalyst with the reason that CuI is effective, low soluble in methanol and easy to remove.

Attempt to click benzyl azide onto diamine flexicate

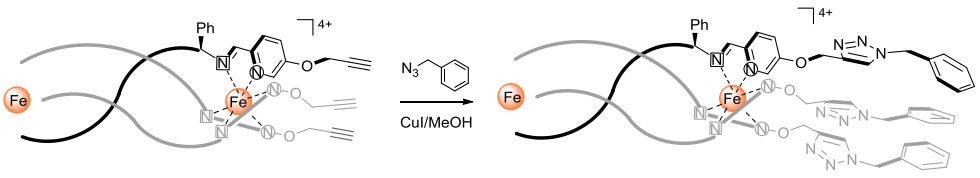

Scheme 2-9 Attempt to modify diamine alkyne flexicate by using click chemistry

The reaction of flexicate (R_c,Δ_{Fe})-$[Fe_2\mathbf{L}^{\mathbf{1}}{}_3]Cl_4$ was conducted in methanol with 1.5 equivalents of azidomethyl benzene in the presence of a catalytic amount of

copper(I) iodide (Scheme 2-9). The Cu(I) catalyst was removed by filtration and the product was recrystallized from methanol/ethyl acetate.

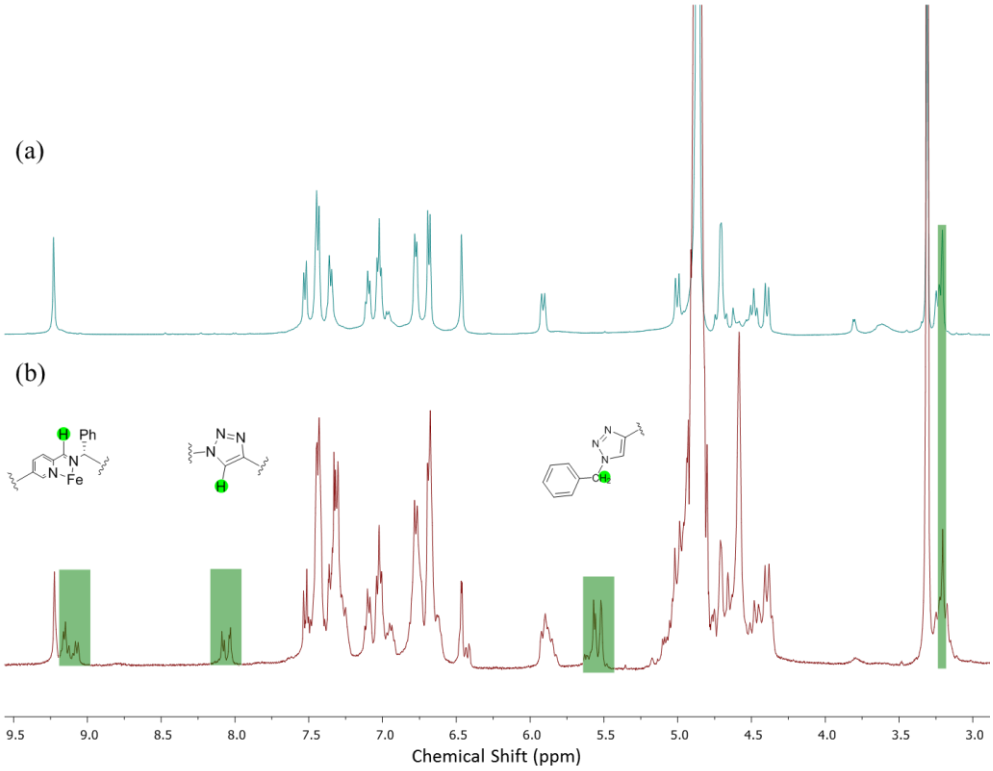

Figure 2-4 ^{1}H NMR spectra (400 MHz, 298K, MeOD) of (a) diamine alkyne flexicate, (b) benzyl azide clicked complex

^{1}H NMR spectra showed the presence of new peaks at 8.08 and 5.50 ppm assigned to the triazole and Ph-CH_2-triazole protons. [Figure 2-4(b)]. While it is clear that the reaction is incomplete any estimate of conversion has to be tentative, but on the basis that the imine singlet at 9.23 ppm is "unclicked", the progress of the reaction is calculated to be *ca* 60%. Addition of further azide did not improve conversion substantially. A similar observation was made for the monometallic analogue of optically pure heterobimetallic helicates.[14]

Attempt to click benzyl azide onto dialdehyde flexicate

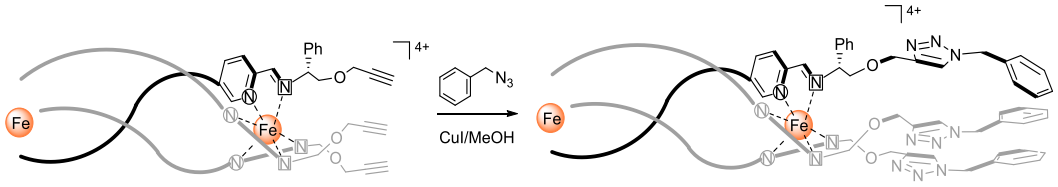

Scheme 2-10 Attempt to modify dialdehyde alkyne flexicate by using click chemistry

The flexicate (R_c,Δ_{Fe})-[Fe_2**L**$^2_3$]Cl_4 was treated with azidomethyl benzene by the same procedure as above (Scheme 2-10).

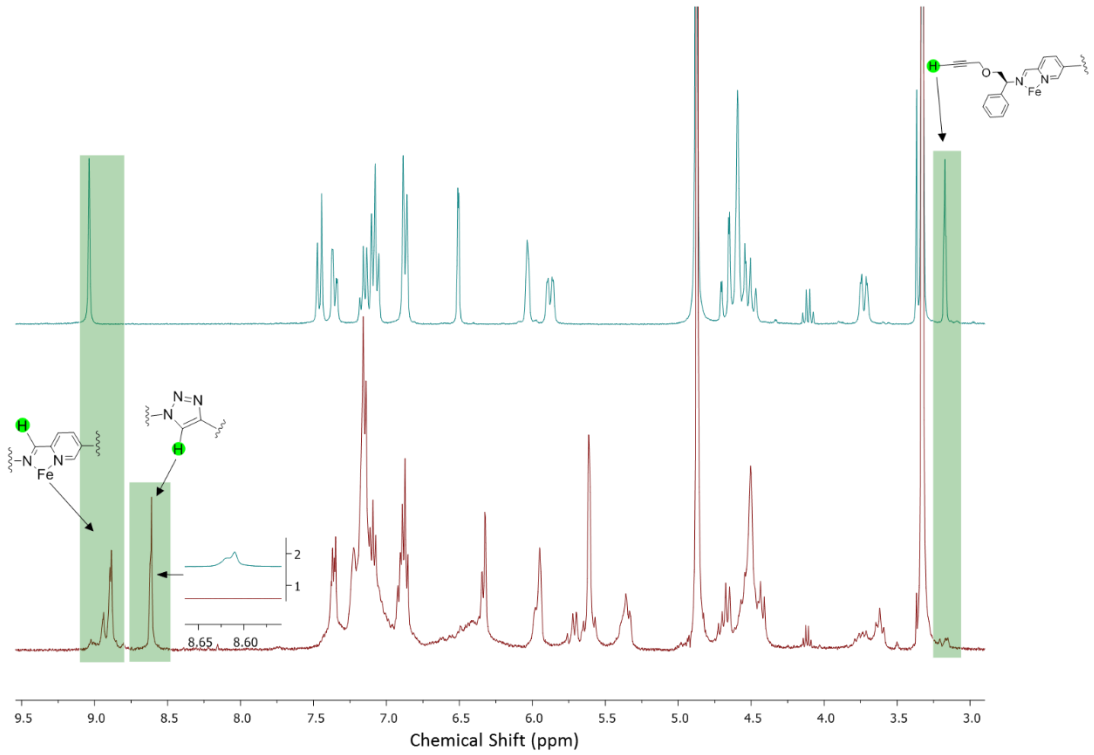

Figure 2-5 The ^{1}H NMR spectra (400 MHz, 298K, MeOD) of (a) dialdehyde alkyne flexicate, (b) benzyl azide clicked complex

The alkyne resonance at 3.17 ppm in the starting material [Figure 2-5(a)] is not present in the product [Figure 2-5(b)], suggesting that the click reaction is complete. This was also supported by the appearance of peaks assigned for the triazole proton at

8.61 ppm. However, the presence of several peaks in the imine and triazole region indicates that a number of products are present in the recrystallized sample. Addition of excess CuI to the reaction solution led to little significant change. A reasonable explanation that is consistent with these observations would be that the triazole rings coordinate to Cu(I) as observed in the monometallic clicked species.

2.3 Synthesis of alkyne triplex systems

A library of asymmetric "triplex" metallohelices have been formed in presence of 2-phenyliminopyridine and pyridine aldehyde derivative by Dr A.D. Faulkner.[23] We considered that alkyne-decorated triplexes can be accessed as above by replacing pyridine aldehyde derivative with propargyl pyridine aldehyde.

2.3.1 Synthesis of (*R*)-2-(2,2'-bipyridine-5-ylmethoxy)-1-phenylethanamine 14

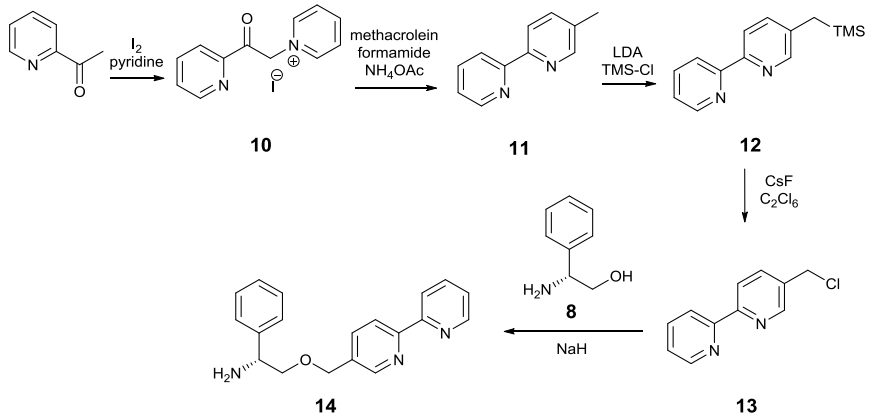

Scheme 2-11 The synthesis of (*R*)-2-(2,2'-bipyridine-5-ylmethoxy)-1-phenylethanamine **14**

The optically pure amine **14** was required for this study (Scheme 2-11). 2-Acetylpyridine was treated with iodine and pyridine at 130˚C in an inert atmosphere to form 1-(2-pyridylacetyl)pyridinium iodide (**10**).[24, 25] **10** was then treated with ammonium acetate and freshly distilled methacrolein in formamide to afford 5-methyl-2,2'-bipyridine (**11**) as a colourless oil after distillation under reduced pressure. 5-((Trimethylsilyl)methyl)-2,2'-bipyridine (**12**) was accessed *via* deprotonation of the 5-methyl-2,2'-bipyrdine with LDA at -78 ˚C, followed by the addition of 1.05 equivalents of trimethylsilyl chloride. 5-(Chloromethyl)-2,2'-bipyridine (**13**) was formed by treatment of **12** with hexachloroethane and caesium fluoride in dry acetonitrile.[26]

The direct deprotonation of one equivalent of (*R)*-phenylglycinol (**8**) with sodium hydride, followed by the addition of the same equivalents of **13** in THF gave (*R*)-2-(2,2'-bipyridine-5-ylmethoxy)-1-phenylethanamine (**14**) as crude yellow compound. After purification on silica gel [ethyl acetate/petroleum ether/trimethylamine (8/8/1; v:v:v)], pure **14** was isolated as a white solid.

2.3.2 Synthesis of Zinc alkyne triplex (R_c,Δ_{Zn})-HHT-[$Zn_2L^3_3$][ClO_4]$_4$

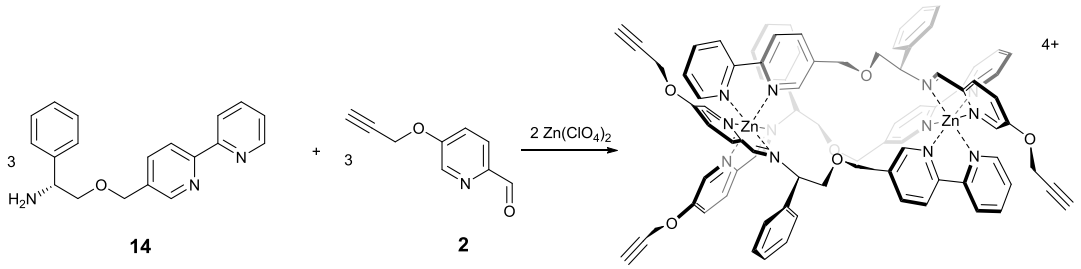

Scheme 2-12 Synthesis the alkynl Znic (II) triplex metallohelice (R_c,Δ_{Zn})-HHT-[$Zn_2\mathbf{L}^3_3$][ClO_4]$_4$

Reaction of (*R*)-2-([2,2'-bipyridin]-5-ylmethoxy)-1-phenylethan-1-amine **14** (3 eq.) with 5-(prop-2-yn-1-yloxy)picolinaldehyde **2** (3 eq.) in the present of $Zn(ClO_4)_2 \cdot 6H_2O$ (2 eq.) at ambient temperature formed terminal alkyne decorated asymmetric triplex metallohelix (Scheme 2-12).[27]

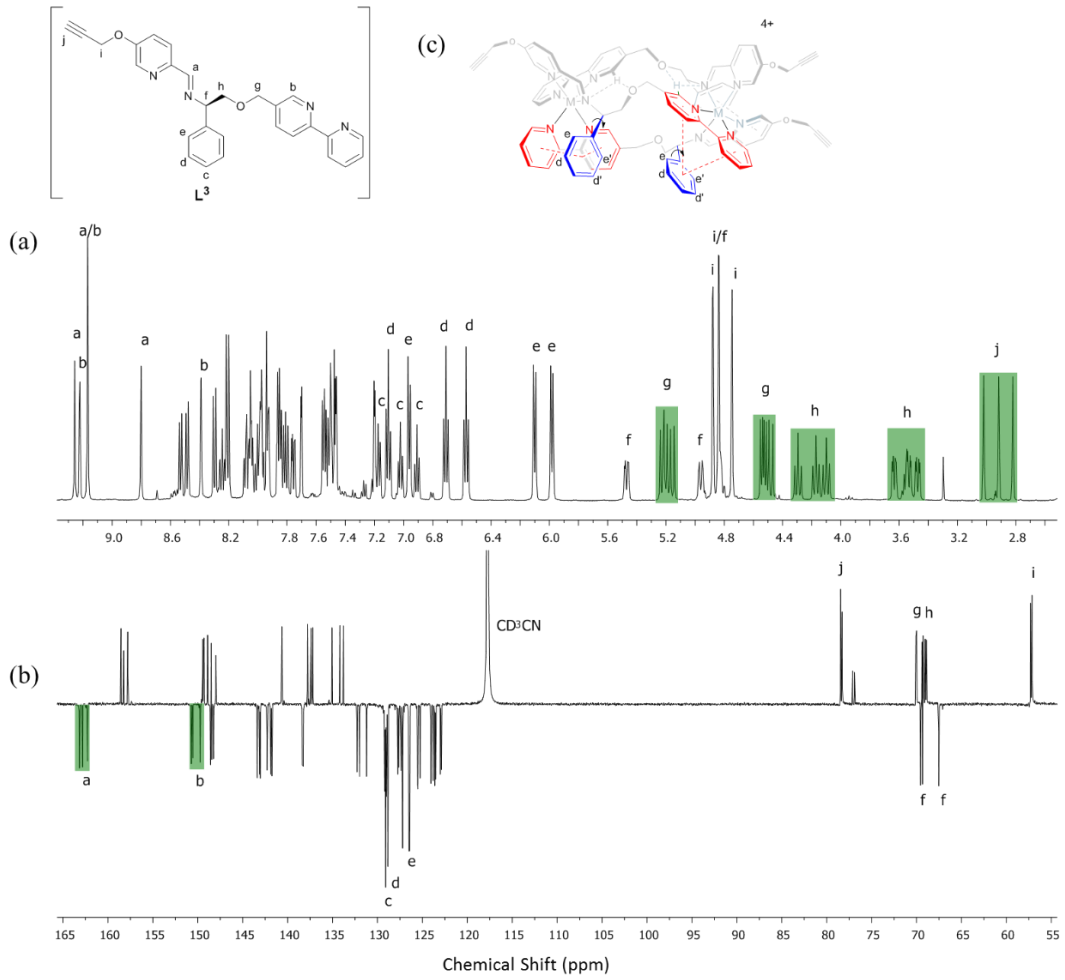

Figure 2-6 (a) ^{1}H NMR (500 MHz, CD_3CN, 298K) and (b) ^{13}C NMR spectra (125 MHz, CD_3CN, 298K) of (R_c,Δ_{Zn})-HHT-[$Zn_2\mathbf{L}^3_3$][ClO_4]$_4$; (c) two sets of phenyl ring protons H^d and H^e experienced unequally through-space shielding from the bpy unit.

^{1}H NMR spectrum confirmed the asymmetric structure with three spectroscopically unique ligand environments (Figure 2-6). The three imine singlets H^a were observed at 9.26, 9.17 and 8.80 ppm, along with the two of the bpy protons H^b at unusually low field (9.22 and 9.17ppm) which was ascribed to the intramolecular hydrogen bond with the ether oxygen atom of an adjacent ligand. The third bpy proton H^b with no such interaction was found at 8.39 ppm. Similarly, two sets of phenyl ring protons H^d and H^e (6.80–5.90 ppm) experienced through-space shielding from the bpy unit of an adjacent ligand. Whereas, the remaining set of phenyl ring protons H^d and

H^e with no such shielding effect were detected at 7.11 and 6.96 ppm, respectively. The rotation frequency of these phenyl rings is faster than the ^1H NMR timescale at room temperature (293K), and therefore the diastereotopic pairs of protons ($H^{d/d'}$, and $H^{e/e'}$) are equivalent. In the variable temperature NMR experiment, these signals begin to broaden at lower temperatures (233K) as the rotational frequency slows down with respect to the NMR timescale, and the diastereotopic pairs begin to resolve (Figure 2-7). It is interesting to note, therefore, that the π stacking of the phenyl and bipyridyl groups must be dynamic; the chemical shift due to through-space shielding is observed but the phenyl groups are rotating. The two of the benzylic protons H^f are found at 5.46 and 4.96 ppm, while the third overlaps with one of the propargyl CH_2 environments. The latter appear as apparent singlets presumably because they lie distant from the chiral architecture and are freely rotating. The rather rigid arrangement of the helicand leads to six distinct resonances for H^h, clustered at 4.42-4.10 ppm (apparent triplets) and 3.63-3.47 ppm (approximately doublets of doublets). Three singlets H^j at 3.0-2.8 ppm are assigned to alkyne protons. ^{13}C NMR spectrum was also consistent with three unique ligand environments. Three imine carbon peaks C^a were found at 163.17-162.28 ppm, three bpy carbon peaks C^b were observed at 150.72-149.37 ppm. The three benzylic carbon peaks C^f were detected at 69.54, 69.32 and 67.52 ppm. Propargyl C^i peaks were assigned at 57.30-57.14 ppm. Alkyne carbon peaks C^j were found at 78.45-78.28 ppm.

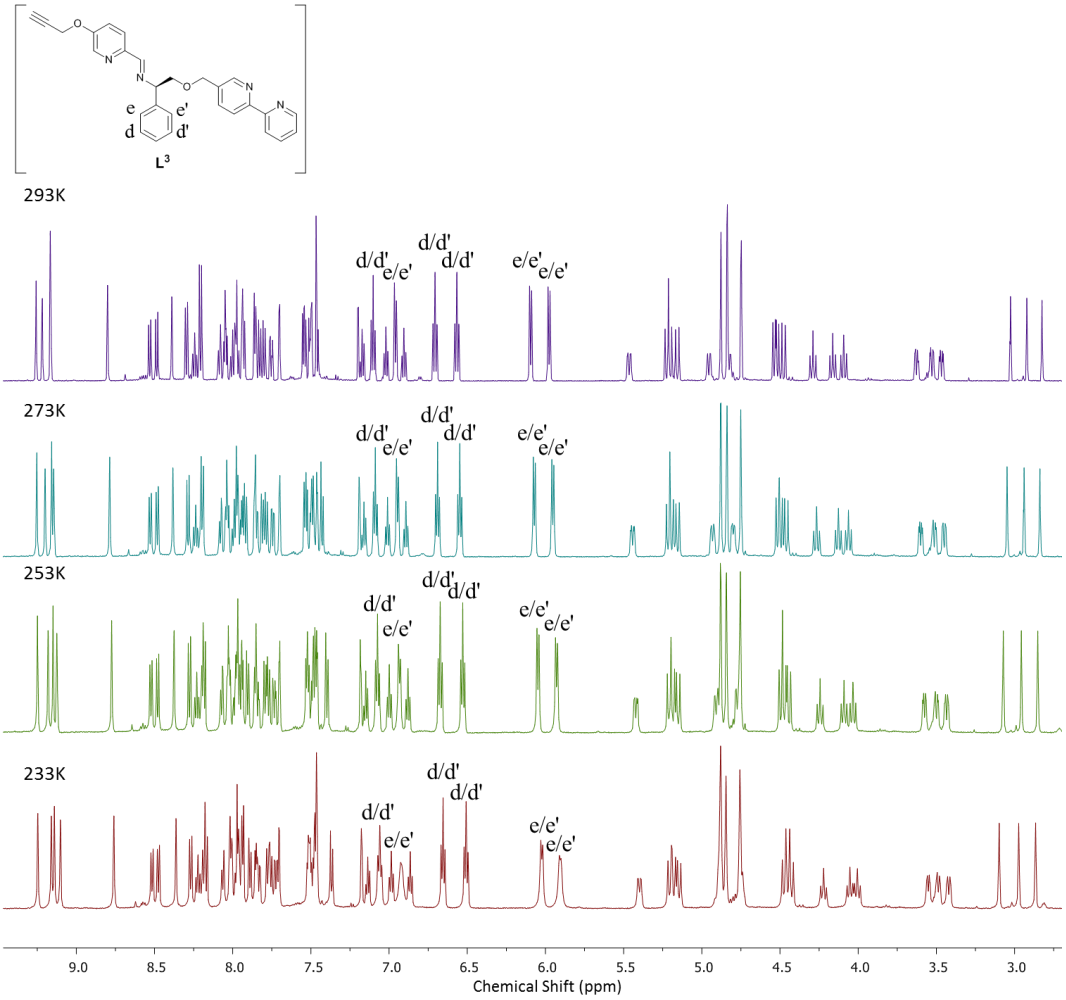

Figure 2-7 Variable temperature ^{1}H NMR spectra of (R_c,Δ_{Zn})-HHT-[Zn_2**L**$^{3}_{3}$][ClO_4]$_4$ (600 MHz, CD_3CN)

Returning for a moment to the ^{1}H NMR spectrum of Figure 2-6 we note the presence of a small singlet at 8.7 ppm. Such a peak is present in most (but not all) triplex systems prepared in this thesis, and particularly those spectra measured in acetonitrile rather than higher polarity media. We assign this to the three-fold symmetric HHH isomer of this compound and on this assumption estimate the selectivity HHT:HHH to be *ca* 99%. Other small peaks consistent with the presence of this minor isomer can be seen in the baseline. At 6.8 ppm a doublet is tentatively assigned to protons of type **e** in the HHH isomer. It is interesting to note the absence of a triplet for type **d** protons in the region 6.4-6.8 ppm in this minor component; no

such signal is expected since there is no phenyl-bpy π-stack in the HHH isomer. Similarly, no minor doublets for type **e** protons are expected around 6 ppm. As such, the appearance of these minor isomer peaks corroborates our assignments for the major isomer.

2.3.3 Synthesis of Iron alkyne triplex (R_c,Δ_{Fe})-HHT-[$Fe_2L^3_3$]Cl_4

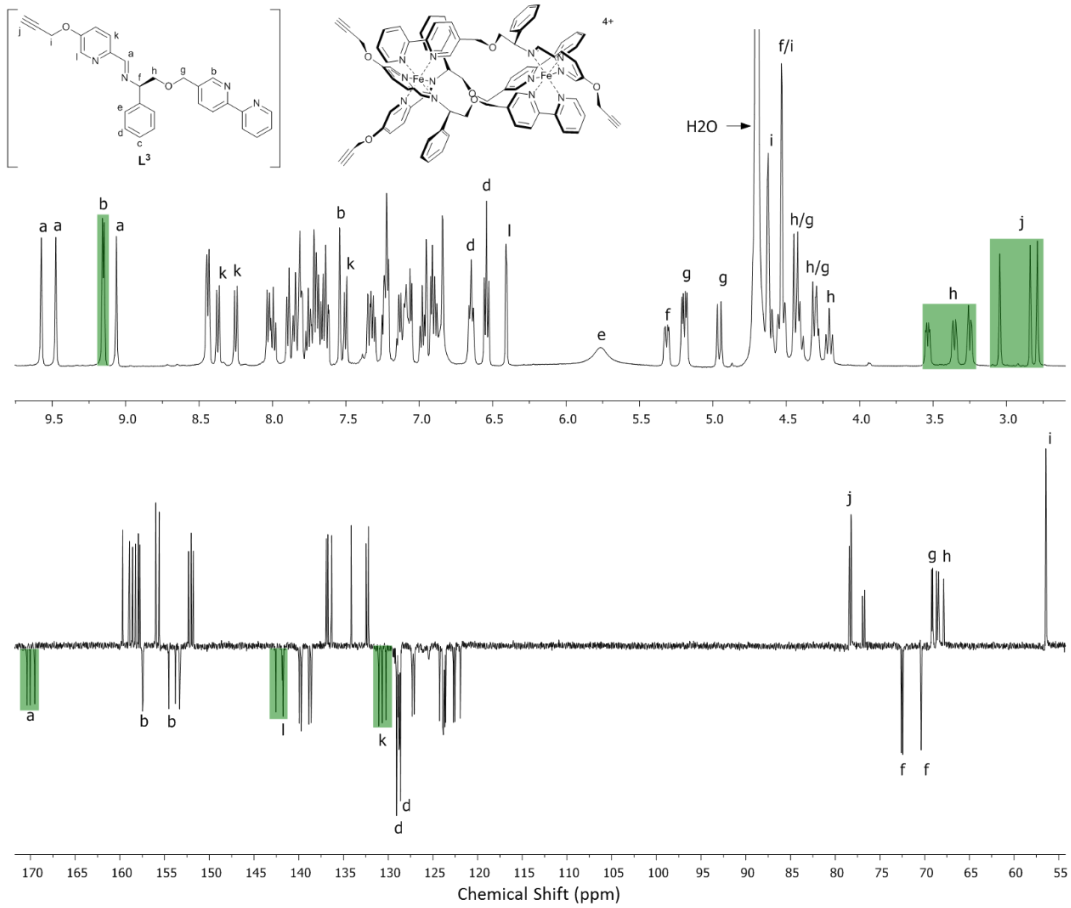

Figure 2-8 ^{1}H NMR (500 MHz, D2O, 298K) and ^{13}C NMR (125 MHz, D2O, 298K) spectra of (R_c,Δ_{Fe})-HHT-[Fe_2**L**$^3_3$]Cl_4

Mixing amine **14,** aldehyde **2** and $FeCl_2$ in 3:3:2 molar ratio led to the immediate formation of an intense purple solution. After heating at 85 ℃ for 48 h, complete conversion of a single bimetallic triplex (R_c,Δ_{Fe})-HHT-[Fe_2**L**$^3_3$]Cl_4 was observed by ^{1}H NMR spectrum. The triplex with opposite helicity (Λ_{Fe}) was prepared similarly

starting from (S)-2-phenylglycinol. As with the zinc(II) perchlorate counterparts, the characteristic peaks of three imine atoms H^a and two bpy atoms H^b were observed at low fields (9.7-9.2 ppm) (Figure 2-8). The remaining bpy proton were observed further up field at 7.54 ppm. The three alkyne atoms C≡CH are observed at the fields 3.0-2.7 ppm. ^{13}C NMR spectrum was also similar with zinc (II) perchlorate counterparts, the characteristic peaks were well assigned.

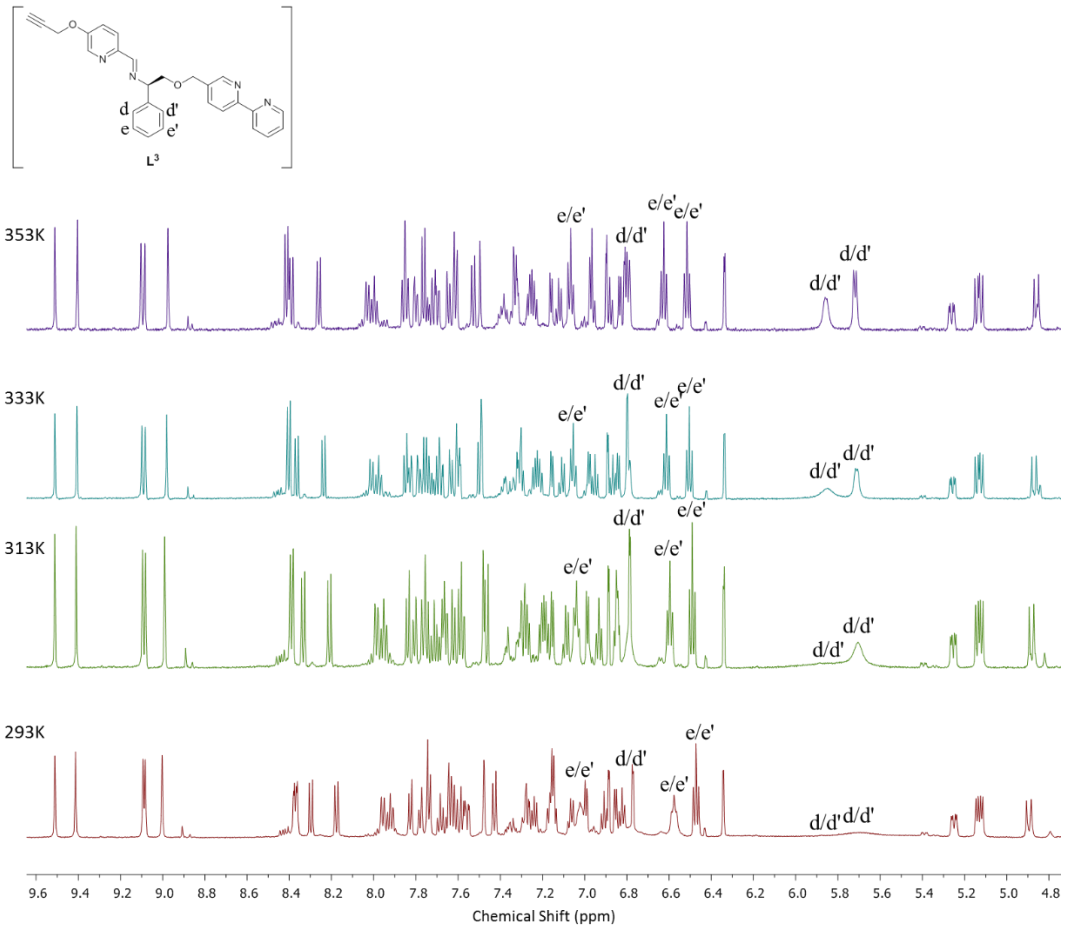

Figure 2-9 Variable temperature ^1H NMR spectra of (R_c,Δ_{Fe})-HHT-[$Fe_2\mathbf{L}^3_3$]Cl_4 (600 MHz, D_2O)

In contrast with their zinc(II) perchlorate counterparts in acetonitrile, the phenyl protons ($H^{d/d'}$ and $H^{e/e'}$) of the iron(II) triplex metallohelices in water feature broad signals in the region 5.5-6.0 ppm at 293 K (Figure 2-9), and these sharpen as the temperature is increased. This is consistent with restricted rotation on this chemical

shift timescale of the π-stacked phenyl groups. We have previously observed that such hydrophobic π-stack interactions are strengthened in more polar media.[28]

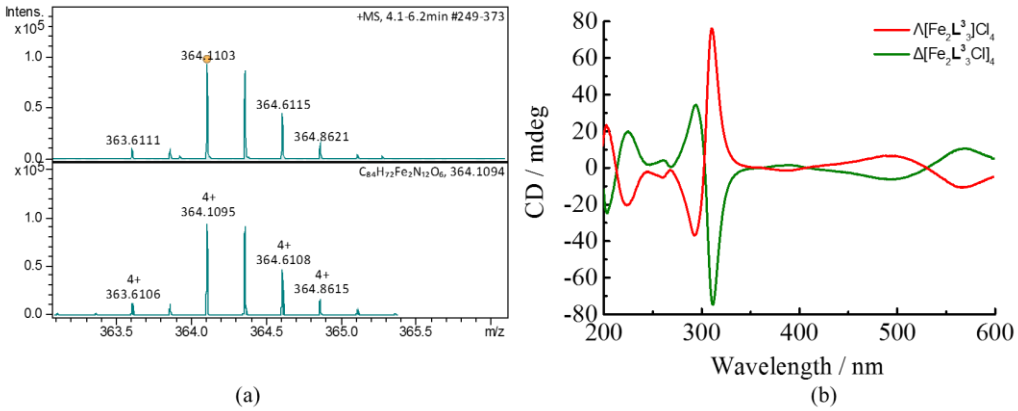

Figure 2-10 High resolution mass spectrum: top measured, below calculated (a) and CD spectrum (b) of (R_c,Δ_{Fe})-HHT-[$Fe_2\mathbf{L}^{\mathbf{3}}_3$]$Cl_4$

The complex (R_c,Δ_{Fe})-HHT-[$Fe_2\mathbf{L}^{\mathbf{3}}_3$]$Cl_4$ gave excellent electrospray mass spectrometry data, with a strong peak at *m/z* 364.1103 Da for the [$Fe_2\mathbf{L}^{\mathbf{3}}_3$]$^{4+}$ species which is consistent with the calculated value (*m/z* 364.1095 Da) [Figure 2-10(a)]. The isotope peaks observed for this molecular ion are separated by 0.25 Da, confirming the tetracationic charge. CD spectra of the alkyne iron triplex compounds Δ_{Fe}/Λ_{Fe} HHT -[$Fe_2\mathbf{L}^{\mathbf{3}}_3$]$Cl_4$ recorded in methanol contain bands spanning the whole UV-Visible region and were observed to be equal and opposite for the two enantiomers of the same complex [Figure 2-10(b)].

In the next two chapters, we will describe details of how this asymmetric configuration of the alkyne-decorated metallohelices offers the potential advantage to successfully click with aromatic azides and sugar azides respectively.

2.4 Anticancer study

2.4.1 Cytotoxicity *in vitro* evaluation.

A conventional MTT [3-(4,5-dimethylthiazol-2-yl)-2,5-diphenyltetrazolium] assay was employed to determine cytotoxicity of several drugs at different concentrations.[29] After incubation and 96 h drug exposure, a dose response curve of drug concentration *vs* % cell survival was obtained and the corresponding half maximal inhibitory concentration (IC_{50}) of each compound was calculated.

The activity of the alkyne flexicate $[Fe_2\mathbf{L^1}_3]Cl_4$, $[Fe_2\mathbf{L^2}_3]Cl_4$ and alkyne triplex (R_c,Δ_{Fe})-HHT-$[Fe_2\mathbf{L^3}_3]Cl_4$ were investigated against HCT116 $p53^{++}$ (human colon carcinoma HCT116 with wild type p53) cancer cell line. ARPE-19 (human retinal pigment epithelium), a classic noncancerous cell line,[30] was chosen for comparison of activity. Both $[Fe_2\mathbf{L^1}_3]Cl_4$ and $[Fe_2\mathbf{L^2}_3]Cl_4$ were not soluble in media, therefore 10% DMSO was added to increase the solubility. Whereas, $[Fe_2\mathbf{L^3}_3]Cl_4$ was found to be sufficiently soluble under assay conditions.

Table 2-1 Cytotoxicity assay of alkyne metallohelices against HCT116 $p53^{++}$ and ARPE-19 cell line

Cell line	**mean IC_{50} (μM) ± SD**	
	HCT116 $p53^{++}$	**ARPE-19**
Λ_{Fe},-$[Fe_2\mathbf{L^1}_3]Cl_4$	0.91 ± 0.52	1.71 ± 0.24
Δ_{Fe},-$[Fe_2\mathbf{L^1}_3][Cl]_4$	1.74 ± 0.45	2.50 ± 0.48
Λ_{Fe},-$[Fe_2\mathbf{L^2}_3]Cl_4$	3.96 ± 1.60	32.62 ± 8.49
Δ_{Fe},-$[Fe_2\mathbf{L^2}_3][Cl]_4$	2.06 ± 0.15	25.32 ± 2.52
Λ_{Fe},HHT-$[Fe_2\mathbf{L^3}_3]Cl_4$	5.02 ± 0.21	73.81 ± 13.05
Δ_{Fe},HHT-$[Fe_2\mathbf{L^3}_3]Cl_4$	2.87 ± 0.91	100.44 ± 4.67

As can be seen in Table 2-1, The alkyne flexicate $[Fe_2\mathbf{L^1}_3]Cl_4$ enantiomers demonstrated strong cytotoxicity against both HCT116 $p53^{++}$ and ARPE-19 cell line with with IC_{50} *ca* 2 μM. No obvious anticancer selectivty was observed. The flexicate

$[Fe_2\mathbf{L}^{\mathbf{2}}{}_3]Cl_4$ enantiomers showed quite high potentency against HCT116 $p53^{++}$ (IC_{50} *ca* 3 μM) and high selectivty for ARPE-19, *i.e.* the IC_{50} value was *ca* ten times higher than that of HCT116 $p53^{++}$. Triplex $[Fe_2\mathbf{L}^{\mathbf{3}}{}_3]Cl_4$ enantiomers had similar activity towards HCT116 $p53^{++}$ (average IC_{50} *ca* 4 μM), and low cytotoxicity for ARPE-19 (average IC_{50} *ca* 85 μM), therefore demonstring excellent anticancer selectivity.

2.4.2 Autophagy

(R_c,Δ_{Fe})-$[Fe_2\mathbf{L}^{\mathbf{3}}{}_3]Cl_4$ was selected for mechanistic studies due to the excellent anticancer selectivity (*SI* 35) *in vitro.* This work was conducted by Dr. Samantha Shepherd in Huddersfield University. On treating HCT116 $p53^{++}$ cells with (R_c,Δ_{Fe})-HHT-$[Fe_2\mathbf{L}^{\mathbf{3}}{}_3]Cl_4$ at the IC_{50} for 24 h, substantial autophagic vacuoles were detected by optical microscopy (Figure 2-11). Autophagy is a dynamic process of degradation of cellular proteins and cytoplasmic organelles respond to stress or stravation and is believed to play an important role in tumour development.[31] We suggest that (R_c,Δ_{Fe})-HHT-$[Fe_2\mathbf{L}^{\mathbf{3}}{}_3]Cl_4$ induces autophagy and thereby causes HCT116 $p53^{++}$ cancer cell death. More importantly, no such autophagic vacuoles were found in ARPE-19 cells; this might be the source of anticancer selectivity of (R_c,Δ_{Fe})-$[Fe_2\mathbf{L}^{\mathbf{3}}{}_3]Cl_4$. Further investigation which assesses the potency of the compounds after addition of commercial autophagy inhibitor 3MA is undergoing.

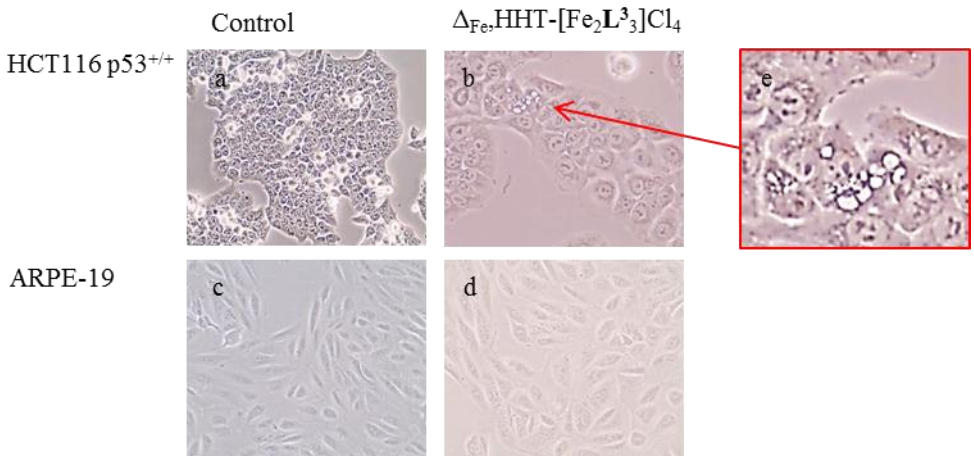

Figure 2-11 HCT116 p53++ and ARPE-19 were treated with IC50 dose of (R_c,Δ_{Fe})-HHT-[$Fe_2\mathbf{L}^3_3$]Cl_4 for 24 h. Prominent morphological change (autophagic vacuoles) was observed in HCT116 p53++ cell.

2.4.3 Drug distribution

Analysis of the drug distribution in cell can provide the clue of the mechanism. The terminal alkyne functionality of [$Fe_2\mathbf{L}^2_3$]Cl_4 enantiomers or [$Fe_2\mathbf{L}^3_3$]Cl_4 enantiomers can be tagged with fluorescent dye AlexaFluor 555 azide *via* a copper (II) mediated alkyne-azide click reaction.[32, 33] This method is highly accurate and sensitive that the fluorescent dye is only conjugated with alkyne groups to form triazole covalent bond, and thus gives no fluorescence signal in an alkyne free environment.[34, 35] In addition, 4',6-diamidino-2-phenylindole (DAPI) was utilized as second fluorescent dye to probe the potential localization of the alkyne metallohelice relative to the cell nuclei which is very common mechanism of metal drugs.[36]

HCT116 p53$^{+/+}$ cells or ARPE19 cells were cultured on eight well glass chamber slider for 48 h, then incubated with [$Fe_2\mathbf{L}^2_3$]Cl_4 or [$Fe_2\mathbf{L}^3_3$]Cl_4 at 10 μM for 1 h. The old medium was taken out with no phosphate buffered saline (PBS) wash, followed by permiabilising cells with Triton-X. The cells were then treated with Click-iT® reaction buffer cocktail containing copper (II) sulfate (2 mM) and AlexaFluor®

555 azide (5 µM) for 30 minutes in the absence of light. After that, the cells were restrained by DAPI (1µg/ml) for 5 minutes, washed with PBS for 3 times and imaged by confocal laser microscopy.[37] The control was treated with the same procedure with no drug exposure.

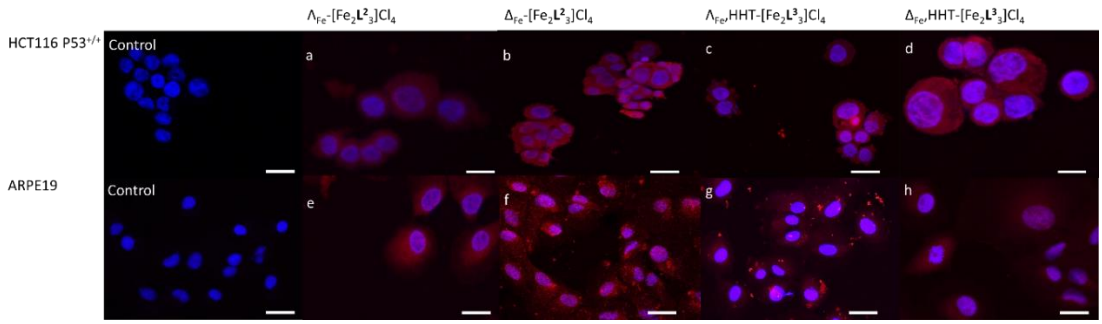

Figure 2-12 Confocal fluorescent imaging of HCT116 $p53^{++}$ co-stained with DAPI and Alexa555 dye with 10 µM of a) Λ-[$Fe_2\mathbf{L}^2_3$]Cl_4; b) Δ-[$Fe_2\mathbf{L}^2_3$]Cl_4; c) ΛHHT-[$Fe_2\mathbf{L}^3_3$]Cl_4; d) ΔHHT-[$Fe_2\mathbf{L}^3_3$]Cl_4; and ARPE19 co-stained with DAPI and Alexa555 dye with 10 µM of e) Λ-[$Fe_2\mathbf{L}^2_3$]Cl_4; f) Δ-[$Fe_2\mathbf{L}^2_3$]Cl_4; g) ΛHHT-[$Fe_2\mathbf{L}^3_3$]Cl_4; h) ΔHHT-[$Fe_2\mathbf{L}^3_3$]Cl_4; Control imagines of HCT116 $p53^{++}$ and ARPE19 were treated with DAPI and Alexa 555 dye with no drug exposure. The scale bar represents 10 µm.

As can be seen in Figure 2-12, the control confirmed the accuracy of staining method as only DAPI staining (blue fluorescene) was detected. Whereas, the strong Alexa555 staining (red fluorescence) was observed in both HCT116 $p53^{++}$ and ARPE19 cells due to the exposure of the alkyne metallohelices. Both [$Fe_2\mathbf{L}^2_3$]Cl_4 and [$Fe_2\mathbf{L}^3_3$]Cl_4 exhibit high ratio of cellular internalization (1h) (Figure 2-12, a-h). No specific cellular localisation was found in these two cell lines; [$Fe_2\mathbf{L}^2_3$]Cl_4 and [$Fe_2\mathbf{L}^3_3$]Cl_4 were detected throughout the cells including cytoplasm and nuclei (which was co-stained to identify). Interestingly, when HCT116 $p53^{++}$ cells were treated with [$Fe_2\mathbf{L}^2_3$]Cl_4 enantiomers, the cells treated with Λ enantiomer exhibited much weaker fluorescence signal than that of Δ enantiomers. This is ascribed to differential uptake of the enantiomers and may partially explain why the Δ enantiomer is much more toxic than Λ.

2.5 Conclusion

Three metallohelix systems (the diamine flexicate class $[Fe_2\mathbf{L^1}]Cl_4$, the dialdehyde class $[Fe_2\mathbf{L^2}]Cl_4$ and the triplex $[Fe_2\mathbf{L^3}_3]Cl_4$) incorporating terminally-positioned alkyne groups were prepared. Each complex was fully characterised by NMR spectroscopy, mass spectrometry, microanalysis and circular dichroism spectroscopy.

Attempts to functionlise $[Fe_2\mathbf{L^1}]Cl_4$ and $[Fe_2\mathbf{L^2}]Cl_4$ via click chemistry were partially successful in that while the products were consumed, mixtured of triazole derivatives were produced. We suggest that steric hindrance and/or intramolecular binding of Cu(I) to the products via the triazole units is responsible. The triplex system we show in subsequent chapters to be far more successful and leads to several new ranges of diverse, optically-pure, water-soluble and biologically active metallohelix.

The alkyne flexicate $[Fe_2\mathbf{L^1}_3]Cl_4$, $[Fe_2\mathbf{L^2}_3]Cl_4$ and alkyne triplex $[Fe_2\mathbf{L^3}_3]Cl_4$ have exhibited promising cytotoxcity towards the HCT116 $p53^{++}$ cancer cell line. In particular, Δ-$[Fe_2\mathbf{L^3}_3]Cl_4$ showed 35 fold selectivity between HCT116 $p53^{++}$ and ARPE-19 normal cell line. Further mechanism study demonstrated the Δ$[Fe_2\mathbf{L^3}_3]Cl_4$ can selectivetly induce prominent autophagic vacuoles in HCT116 $p53^{++}$ cancer cell line than ARPE 19 cell line, indicating that autophagy may contribute to the acitvity and selectivty of the complex. The cell localization experiment showed that both $[Fe_2\mathbf{L^2}_3]Cl_4$ and $[Fe_2\mathbf{L^3}_3]Cl_4$ enantiomers can be effectively taken up into the cancer cells and normal cells, and localized in cytoplasm and nuclei. This is the first evidence for the drug distribution of metallohelices *in cellulo*.

2.6 References

1. B. M. Trost, Z. T. Ball and T. Jöge, *J. Am. Chem. Soc.*, 2002, **124**, 7922-7923.
2. T. Tachinami, T. Nishimura, R. Ushimaru, R. Noyori and H. Naka, *J. Am. Chem. Soc*, 2013, **135**, 50-53.
3. M. R. Uehling, R. P. Rucker and G. Lalic, *J. Am. Chem. Soc.*, 2014, **136**, 8799-8803.
4. C. Chiappe, D. Capraro, V. Conte and D. Pieraccini, *Org. Lett.*, 2001, **3**, 1061-1063.
5. D. Yang, F. Chen, Z.-M. Dong and D.-W. Zhang, *J. Org. Chem.*, 2004, **69**, 2221-2223.
6. L. Jin, D. R. Tolentino, M. Melaimi and G. Bertrand, *Sci. Adv.*, 2015, **1**, e1500304.
7. N. Uhlig and C.-J. Li, *Chem. Sci.*, 2011, **2**, 1241-1249.
8. G. A. Burley, J. Gierlich, M. R. Mofid, H. Nir, S. Tal, Y. Eichen and T. Carell, *J. Am. Chem. Soc.*, 2006, **128**, 1398-1399.
9. J. Xiao and T. J. Tolbert, *Org. Lett.*, 2009, **11**, 4144-4147.
10. A. Bernardin, A. Cazet, L. Guyon, P. Delannoy, F. Vinet, D. Bonnaffé and I. Texier, *Bioconjugate Chem.*, 2010, **21**, 583-588.
11. U. Hoffmanns and N. Metzler-Nolte, *Bioconjugate Chem.*, 2006, **17**, 204-213.
12. Z.-L. Song, Z. Chen, X. Bian, L.-Y. Zhou, D. Ding, H. Liang, Y.-X. Zou, S.-S. Wang, L. Chen and C. Yang, *J. Am. Chem. Soc.*, 2014, **136**, 13558-13561.
13. K. V. Kong, C. J. H. Ho, T. Gong, W. K. O. Lau and M. Olivo, *Biosens. Bioelectron.*, 2014, **56**, 186-191.
14. S. E. Howson, G. J. Clarkson, A. D. Faulkner, R. A. Kaner, M. J. Whitmore and P. Scott, *Dalton Trans.*, 2013, **42**, 14967-14981.
15. K. A. Stevenson, C. F. Melan, O. Fleischel, R. Wang and A. Petitjean, *Cryst. Growth Des.*, 2012, **12**, 5169-5173.
16. B. Akhuli, L. Cera, B. Jana, S. Saha, C. A. Schalley and P. Ghosh, *Inorg. Chem.*, 2015, **54**, 4231-4242.
17. J. E. Lewis, A. B. Elliott, C. J. McAdam, K. C. Gordon and J. D. Crowley, *Chem. Sci.*, 2014, **5**, 1833-1843.
18. S. E. Howson, A. Bolhuis, V. Brabec, G. J. Clarkson, J. Malina, A. Rodger and P. Scott, *Nat. Chem.*, 2012, **4**, 31-36.
19. M. Seredyuk, A. B. Gaspar, V. Ksenofontov, Y. Galyametdinov, J. Kusz and P. Gütlich, *J. Am. Chem. Soc.*, 2008, **130**, 1431-1439.
20. D. Zampieri, L. Vio, M. Fermeglia, S. Pricl, B. Wuensch, D. Schepmann, M. Romano, M. G. Mamolo and E. Laurini, *Eur. J. Med. Chem.*, 2016, **121**, 712-726.
21. Y. Hsiao and L. S. Hegedus, *J. Org. Chem.*, 1997, **62**, 3586-3591.
22. R. A. Kaner, S. J. Allison, A. D. Faulkner, R. M. Phillips, D. I. Roper, S. L. Shepherd, D. H. Simpson, N. R. Waterfield and P. Scott, *Chem. Sci.*, 2016, **7**, 951-958.
23. A. D. Faulkner, R. A. Kaner, Q. M. Abdallah, G. Clarkson, D. J. Fox, P. Gurnani, S. E. Howson, R. M. Phillips, D. I. Roper and D. H. Simpson, *Nat. Chem.*, 2014, **6**, 797-803.
24. P. Das, A. Ghosh, M. K. Kesharwani, V. Ramu, B. Ganguly and A. Das, *Eur. J. Inorg. Chem.*, 2011, **2011**, 3050-3058.

25. P. Das, A. Ghosh, M. K. Kesharwani, V. Ramu, B. Ganguly and A. Das, *Eur. J. Inorg. Chem.*, 2011, **2011**, 3050-3058.
26. C. Dallaire, I. Kolber and M. Gingras, *Org. Synth.*, 2002, **78**, 42.
27. A. D. Faulkner, R. A. Kaner, Q. M. Abdallah, G. Clarkson, D. J. Fox, P. Gurnani, S. E. Howson, R. M. Phillips, D. I. Roper, D. H. Simpson and P. Scott, *Nat Chem*, 2014, **6**, 797-803.
28. S. E. Howson, L. E. Allan, N. P. Chmel, G. J. Clarkson, R. J. Deeth, A. D. Faulkner, D. H. Simpson and P. Scott, *Dalton Trans.*, 2011, **40**, 10416-10433.
29. T. Mosmann, *J. Immunol. Methods*, 1983, **65**, 55-63.
30. K. Dunn, A. Aotaki-Keen, F. Putkey and L. Hjelmeland, *Exp. Eye Res.*, 1996, **62**, 155-170.
31. Y. Kondo, T. Kanzawa, R. Sawaya and S. Kondo, *Nat. Rev. Cancer*, 2005, **5**, 726-734.
32. H. C. Kolb, M. G. Finn and K. B. Sharpless, *Angew. Chem. Int. Ed.*, 2001, **40**, 2004-2021.
33. V. V. Rostovtsev, L. G. Green, V. V. Fokin and K. B. Sharpless, *Angew. Chem. Int. Ed.*, 2002, **41**, 2596-2599.
34. A. Salic and T. J. Mitchison, *Proc. Natl. Acad. Sci. U. S. A.*, 2008, **105**, 2415-2420.
35. P. M. Clark, J. F. Dweck, D. E. Mason, C. R. Hart, S. B. Buck, E. C. Peters, B. J. Agnew and L. C. Hsieh-Wilson, *J. Am. Chem. Soc.*, 2008, **130**, 11576-11577.
36. B. Liedert, D. Pluim, J. Schellens and J. Thomale, *Nucleic Acids Res.*, 2006, **34**, e47-e47.
37. *The Molecular Probes Handbook*, 11th edn., Life Technologies, London, 2010.

Chapter 3

Click reactions of triplex metallohelices with benzylic azides

3.1 Introduction

The formation of 1,2,3-triazoles by 1,3-dipolar cycloaddition of azides and alkynes was first discovered by Arthur Michael in 1893.[1] This branch of heterocyclic chemistry was slow to reach its full potential, because initially these reactions required elevated temperatures and suffered from a lack of regioselectivity, with asymmetric alkynes yielding a mixture of the 1,4- and the 1,5-regioisomers.[2, 3] However, in 2002, Sharpless and Meldal both discovered that copper(I) salts could catalyse the reaction and afford high yields of regiospecific 1,4-disubstituted 1,2,3-triazole.[4, 5].

This copper-catalysed azide/alkyne click (CuAAC) reaction,[6, 7] has become a powerful and versatile synthetic tool in a wide variety of chemical[8] and biological applications.[9] CuAAC is most commonly performed under mild conditions *i.e.* no heat is required and the reaction can be performed in the presence of oxygen and moisture.[10] The conversion in CuAAC reactions is near-quantitative, with few or no side products, limiting the need for purification. Alkyne and azide components can be functionalised with a wide range of substituents, especially in bioconjugation, giving click chemistry enormous synthetic potential.

CuAAC chemistry has also been exploited in coordination chemistry for the synthesis of the supramolecular architectures,[11] catalysts[12] and transition metal complex drugs.[13] The versatile 1,4-functionalized 1,2,3-triazoles can be employed to

enrich ligand synthesis for metal coordination[14] or exploited for post-assembly to afford new structures that are inaccessible through traditional coordination synthesis.[15]

3.1.1 Click chemistry for ligand synthesis

The 1,2,3-triazoles have received recent interest as new ligands in coordination chemistry and have been used to generate exquisite architectures.[14,16] In principle, 1,4-disubstituted-1,2,3-triazoles can display two different *N*-donor (N2 and N3)[11] and one *C*-donor (C5) coordination modes[17] as shown in Figure 3-1 **a-c**. For instance, Schibli *et al.* developed a "click-to-chelate" approach *via* the N2, amino, and a carboxylate chelating system to form the tumour-targeting monometallic labelling precursor **d**.[18] Gautier *et al.* synthesised a cisplatin analogue in which N3 and an amine group attached at C4 coordinated to Pt(II) (**e**).[13] Gandelman *et al.* designed and prepared a tridentate pincer-type palladium complex in which the mode of coordination was generated by two phosphine groups and the C5 carbene donor of the triazole **f**.[19] The potential of a triazole moiety to act as a pyridyl surrogate and form analogues of the bis-triazole (bta) **j**, pyridine-triazole (pyta) **k** and bis-triazole-pyridine (btpy) **l** ligands is also intriguing. These trizole-containing ligands are extensively exploited to construct discrete metallomacrocycles,[20] cages[21] and helicates.[22]

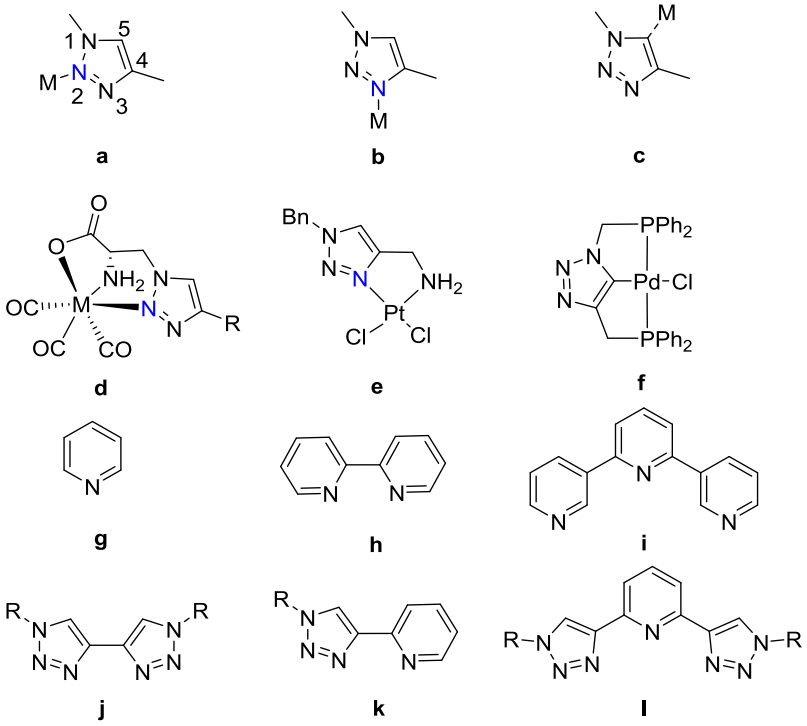

Figure 3-1 Coordination modes of 1,4-disubstituted-1,2,3-triazole ligands through: a) N2 nitrogen atom; b) N3 nitrogen atom; c) C5 carbon atom; Examples of "click-to-chelate" approach to form monometallic complex *via*: d) N2 site; e) N3 site; f) C5 site; Classic pyridine-containing chelate centre: g) pyridine; h) bipyridine; i) terpyridine; Triazole act as pyridyl surrogate: j) bis-triazole; k) pyridine-triazole; l) bis-triazole-pyridine

Relatively few examples of the establishment *via* CuAAC of intermolecular linking substituents have been reported,[23] perhaps since the triazole moiety could provide extra *N* donor sites to interfere with the self-assembly process.[24, 25] Crowley *et al*. established a facile approach to attach a variety of functional moieties to the tripyridyl ligand scaffolds and demonstrated that the presence of the 1,2,3-triazole units does not disrupt the formation of desired M_2L_4 palladium(II) cage architectures.[26,24]

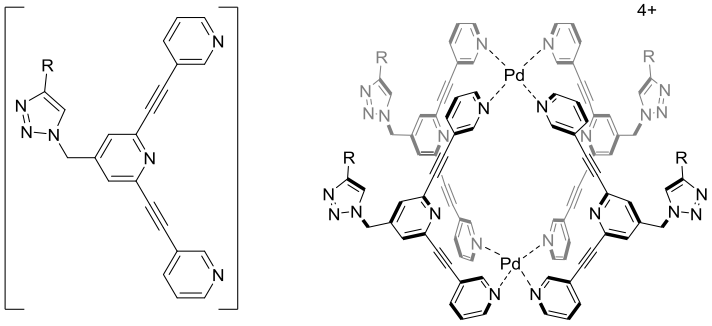

Figure 3-2 tripyridyl ligand functionalised by triazole linker and $[Pd_2L_4]^{4+}$ cage structure[26,24]

3.1.2 Click chemistry for post-assembly modification of complexes

In addition to broadening the scope of ligand synthesis, CuAAC chemistry has also been employed to introduce functionality to pre-assembled metal complexes.[27-32] There are several distinct advantages of this strategy, which can lead to rapid and modular diversification of the structures. In particular potential functional group incompatibly in the self-assembly can be circumvented, allowing access to new design configurations that are difficult to obtain by conventional ligand-plus-metal synthesis.[27] Indeed, there are several examples of successful post-assembly modifications (PAM) *via* click chemistry (referred to herein as PAMC), such as functionalised MOFs,[33] rotaxanes,[34-37] ferrocenyl complexes[38-40] and nanoparticles (Figure 3-3).[41] The general synthetic strategy used is first to establish a metal template with terminal alkyne/azide groups, and second to click the azide/alkyne derivatives on the self-assembled structure.

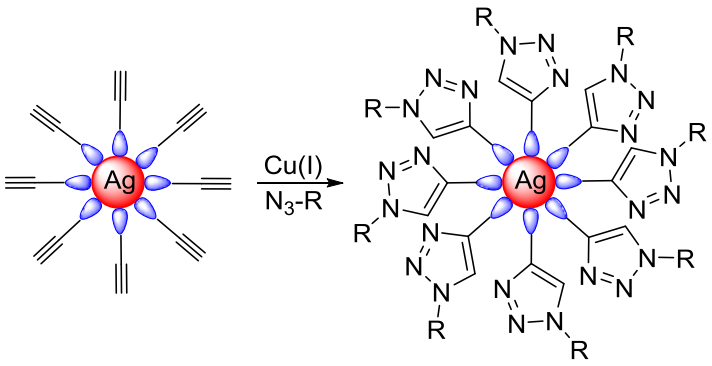

Figure 3-3 Example of PAMC for nanoparticles[42]

Compared with the widespread use of PAMC in large metal–ligand assemblies such as MOFs and nanoparticles, the application of PAMC in discrete metal complexes is far less explored.[43-45] The lack of research in this area is mainly ascribed to the fact that the Cu(I) catalyst can interfere with labile metal-ligand bonds;[44] be sequestered by multidentate binding sites of substrates;[35] and cause cytotoxicity, jeopardising biological applicability.[46] Recently, a copper-free click reaction has been developed to overcome this issue and is particularly prevalent in biochemistry.[47-52] However, only specific substrates, such as cyclooctyne derivatives or norbornenes, were able to undergoing cycloaddition in the absence of Cu(I) catalyst, and the ligand synthesis was cumbersome.[51] Therefore, structures that feature strong metal-ligand bonds and that have geometric arrangements of binding sites that do not favour Cu(I) sequestration are advantageous for PAMC.

As outlined previously in Chapter 2, the attempt to modify alkyne-terminated flexicate structures *via* PAMC failed to produce sufficiently pure species in the click reaction. In this chapter, PAMC with *triplex* systems are investigated and shown to be much more suited to this strategy.

3.2 PAMC of alkyne triplex metallohelices

3.2.1 Synthesis of benzyl azide derivatives

Benzyl azide derivatives have been chosen to validate PAMC reactions on the alkyne triplex metallohelices described in Chapter 2 due to their facile synthesis. In addition, the resulting structures allow us to elucidate whether bulky hydrophobic aromatic groups alter the biological activity of the metallohelices. Moreover, some benzyl azide derivative like 4-azidomethyl benzoic acid could offer even more powerful means of building functionalised complexes.

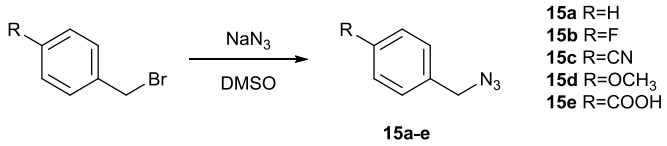

Scheme 3-1 Synthesis of benzyl azide derivative

The benzyl azide derivatives shown in Scheme 3-1 were prepared by the nucleophilic substitution of their benzyl bromide analogues (substituted by fluoro, methoxy, nitrile and carboxylic acid) with sodium azide in high yield.[53, 54]

3.2.2 Synthesis of $[Zn_2L^{4a\text{-}d}{}_3][ClO_4]_4$ triplexes *via* CuAAC

(Azidomethyl)benzene (4.5 eq.), (R_c,Δ_{Zn})-HHT-$[Zn_2\mathbf{L}^{\mathbf{3}}{}_3][ClO_4]_4$ (1 eq.) and copper (I) iodide (0.1 eq.) were heated at 65˚C under reduced pressure for 18h. The resulting suspension was filtered through celite to remove copper salts and the final product was isolated as a white/yellow solid upon the addition of ethyl acetate.

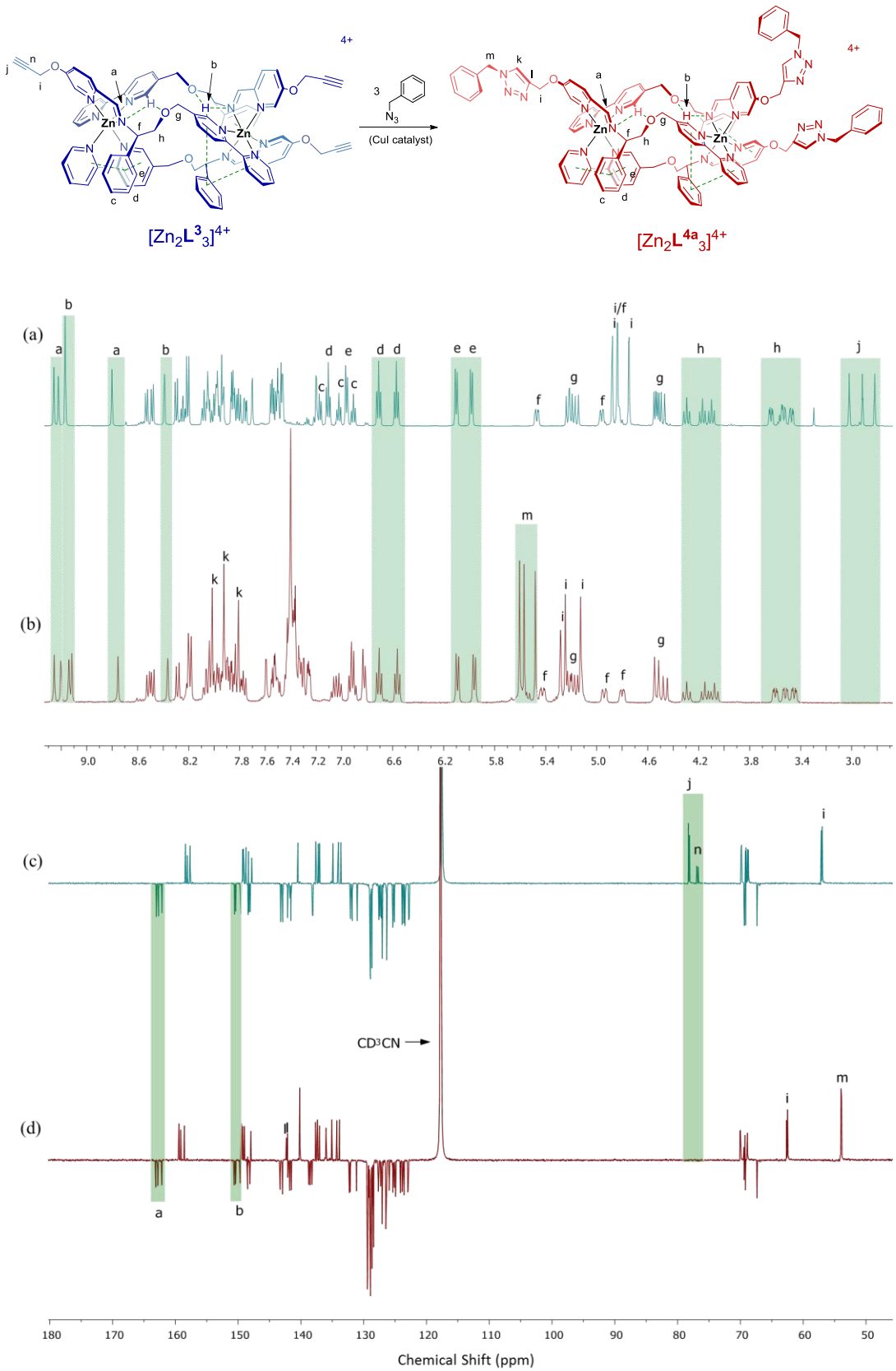

Figure 3-4 ^{1}H NMR spectra (500 MHz, CD_3CN, 298K) of (a) (R_c,Δ_{Zn})-HHT-[Zn_2**L**$^{3}_{3}$][ClO_4]$_4$, (b) (R_c,Δ_{Zn})-HHT-[Zn_2**L**$^{4a}_{3}$][ClO_4]$_4$; ^{13}C NMR spectra (125 MHz, CD_3CN, 298K) of (c) (R_c,Δ_{Zn})-HHT-[Zn_2**L**$^{3}_{3}$][ClO_4]$_4$, (d) (R_c,Δ_{Zn})-HHT-[Zn_2**L**$^{4a}_{3}$][ClO_4]$_4$;

As can be seen in the ^{1}H NMR spectra [Figure 3-4(a) and (b)], the three alkyne singlets of the zinc alkyne triplex starting material [Figure 3-4(a)] (H^{j}, between 3.0-2.8 ppm) are absent in the spectrum of the (azidomethyl)benzene CuAAC triplex product [Figure 3-4(b)]. The three methylene protons H^{i} belonging to the pyridine-O-CH_2-R group shift to higher frequency *i.e.* from *ca* 4.9 ppm in the alkyne triplex [Figure 3-4(a)] to *ca* 5.2 ppm in the product triplex [Figure 3-4(b)]. Three new singlets H^{k} at 8.01, 7.92 and 7.81 ppm are observed in Figure 3-4(b) due to the triazole protons in three separate ligand environments. In addition, the three new singlets H^{m} found at 5.61, 5.57, 5.48 ppm [Figure 3-4(b)] are assigned to the Ph-CH_2-traziole groups. The three imine peaks H^{a}, three bipyridine singlets H^{b} and the phenyl ring protons are observed with negligible shift in both ^{1}H NMR spectra, demonstrating that the structural integrity of the metallohelix was preserved during the click reaction.

The ^{13}C NMR spectra [Figure 3-4(c) and (d)] also confirm the completion of the click reaction due to the disappearance of alkyne carbon signals C^{j} and C^{n} [Figure 3-4(c)] and presence of carbon Ph-CH$_2$ peaks C^{m} at 54.2 and 54.1 (two signals) ppm [Figure 3-4(d)]. The three pyridine-O-CH$_2$-R carbons C^{i} shift to higher frequency from *ca* 57 ppm to *ca* 63 ppm as the adjacent alkyne group is replaced with the more electric withdrawing group triazole. The new signals C^{l} found at *ca* 142 ppm are assigned to triazole C4 carbon [Figure 3-4(d)].

Other similar triplex derivatives can be synthesised readily through substitution of the benzyl azide. (R_c,Δ_{Zn})-HHT-[Zn$_2$**L**$^{\mathbf{4b}}$][ClO$_4$]$_4$, (R_c,Δ_{Zn})-HHT-[Zn$_2$**L**$^{\mathbf{4c}}_3$][ClO$_4$]$_4$ and (R_c,Δ_{Zn})-HHT-[Zn$_2$**L**$^{\mathbf{4d}}_3$][ClO$_4$]$_4$ were successfully synthesised *via* CuAAC with 1-(azidomethyl)-4-fluorobenzene, 4-(azidomethyl)benzonitrile and 1-(azidomethyl)-4-methoxybenzene onto alkyne triplex (R_c,Δ_{Zn})-HHT-

$[Zn_2\mathbf{L}^{\mathbf{3}}{}_3][ClO_4]_4$ separately. The ^{1}H and ^{13}C NMR spectra were similar to that of (R_c,Δ_{Zn})-HHT-$[Zn_2\mathbf{L}^{\mathbf{4a}}{}_3][ClO_4]_4$ (Figure 3-5).

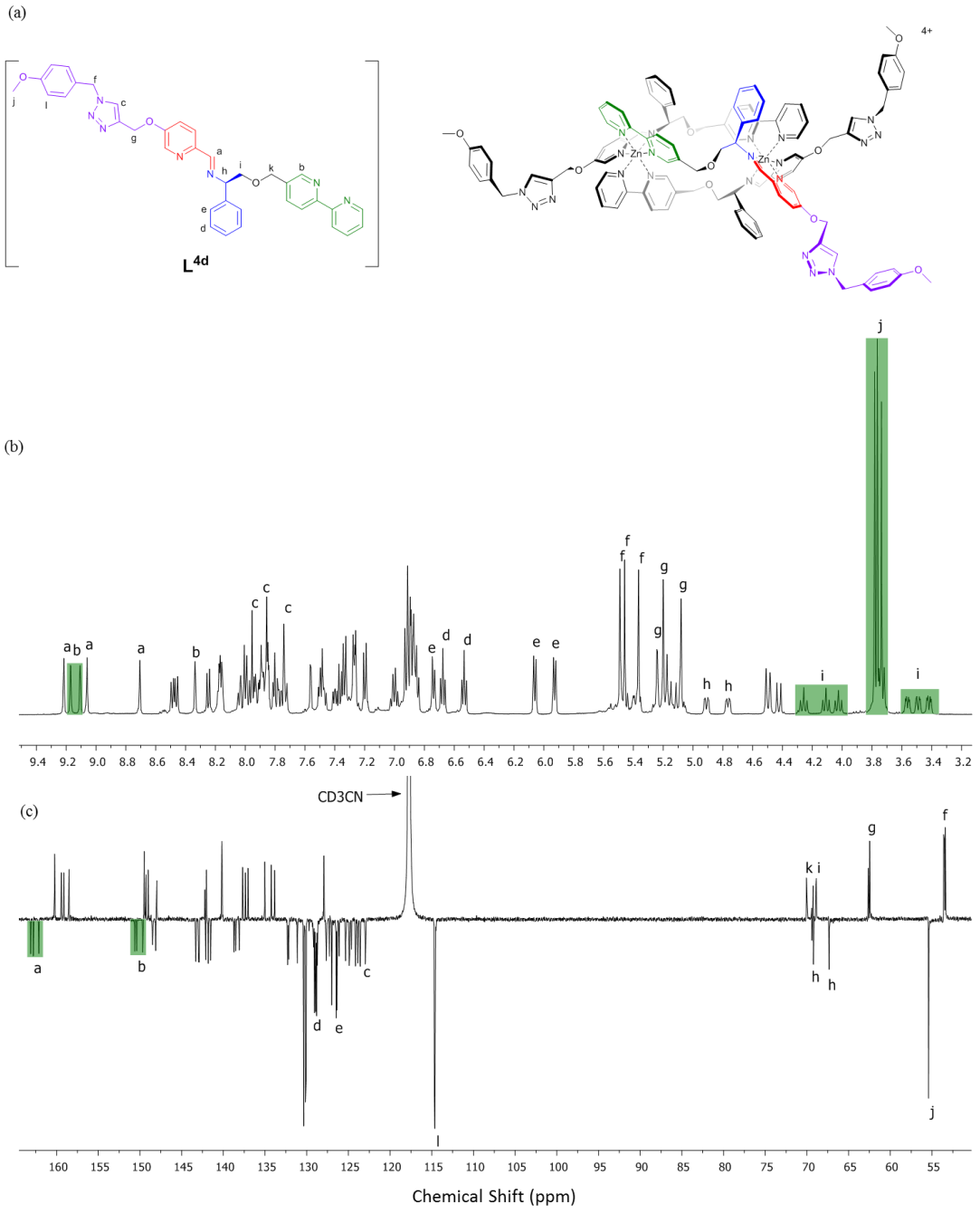

Figure 3-5 (a) Structure of $\mathbf{L}^{\mathbf{4d}}$ and (R_c,Δ_{Zn})-$[Zn_2\mathbf{L}^{\mathbf{4d}}{}_3][ClO_4]_4$; (b) ^{1}H NMR (500 MHz, 298K, CD_3CN) and (c) ^{13}C NMR (125 MHz, 298K, CD_3CN) spectra of (R_c,Δ_{Zn})-$[Zn_2\mathbf{L}^{\mathbf{4d}}{}_3][ClO_4]_4$.

3.2.3 Synthesis of water soluble iron(II) triplex systems *via* CuAAC

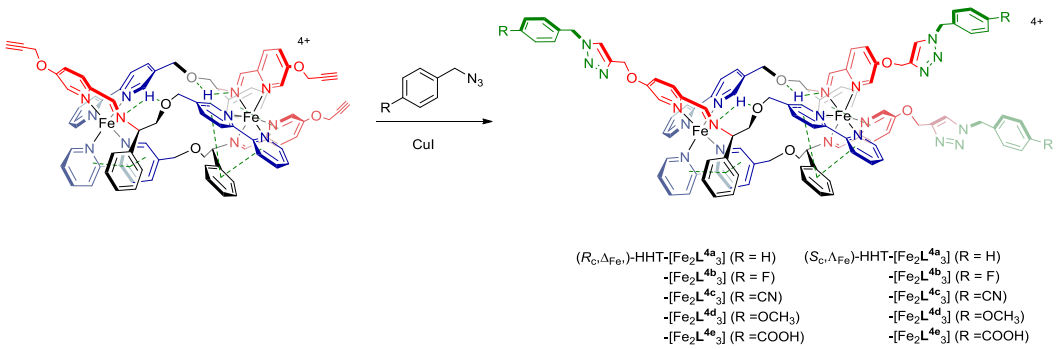

Scheme 3-2 Synthesis of CuAAC derivative iron (II) triplex metallohelices

In order to investigate the biological activities of the metallohelices, all the tested complexes must possess the solubility in aqueous media. As expected, the zinc perchlorate triplexes were insoluble in aqueous media but water-compatible triplexes were accessed by replacing zinc perchlorate with iron(II) chloride. Ten iron(II) triplex complexes Δ_{Fe}/Λ_{Fe}-[Fe_2**L**$^{\mathbf{4a\text{-}e}}{}_3$]$Cl_4$ (Scheme 3-2), were prepared *via* CuAAC reactions with benzyl azide derivatives onto the corresponding alkyne iron(II) triplex in methanol.

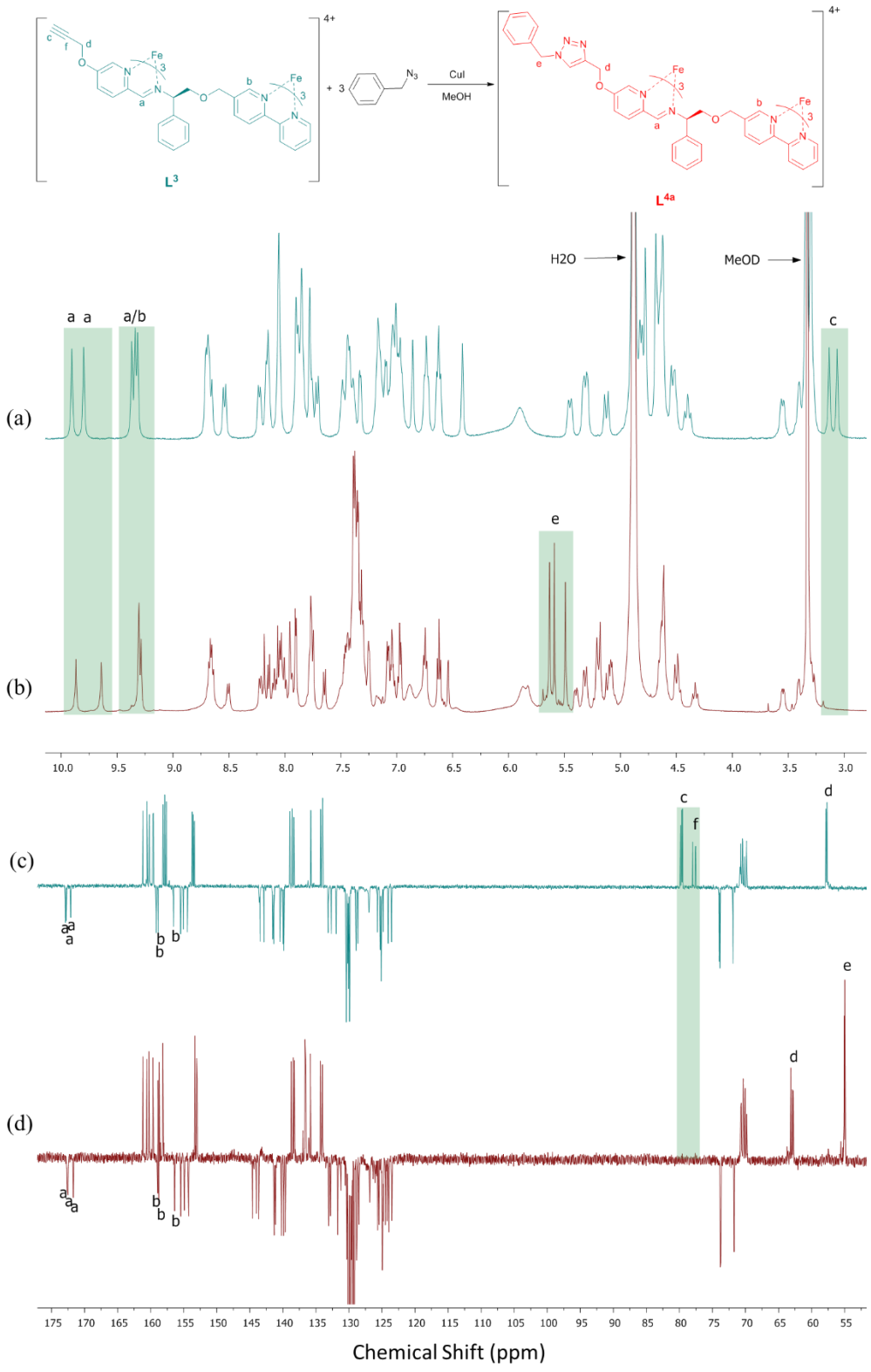

Figure 3-6 ^{1}H NMR spectra (400 MHz, MeOD, 298K) of (a) (R_c,Δ_{Fe})-HHT-[Fe_2**L**$^{3}_{3}$]Cl_4, (b) (R_c,Δ_{Fe})-HHT-[Fe_2**L**$^{4a}_{3}$]Cl_4; ^{13}C NMR spectra (125 MHz, MeOD, 298K) of (c) (R_c,Δ_{Fe})-HHT[Fe_2**L**$^{3}_{3}$]Cl_4, (d) (R_c,Δ_{Fe})-HHT-[Fe_2**L**$^{4a}_{3}$]Cl_4;

The ^{1}H-NMR spectra of all iron(II) triplex complexes were similar but broader than their Zn(II) perchlorate counterparts. However, the progress of the CuAAC reaction could still be monitored by the changes in the spectra. As seen in Figure 3-6, the alkyne singlets H^{c} at 3.19, 3.12 ppm [Figure 3-6(a)] were no longer observable in the CuAAC product triplex spectra. The triazole protons were unable to be assigned as these signals overlap with other aromatic proton signals. Three singlets H^{e} at 5.77, 5.72, 5.64 ppm [Figure 3-6(b)] appear upon completion of the reaction, and are assigned to the benzonitrile-CH_2 protons. The ^{13}C NMR spectra [Figure 3-6(c) and (d)] are also consistent with the completion of the reaction supported by the disappearance of alkyne carbon signals C^{c} and C^{f} [Figure 3-6(c)] and presence of carbon Ph-CH_2 peaks C^{e} at 55 ppm (three signals) [Figure 3-6(d)]. In a similar fashion with the zinc(II) perchlorate counterparts, the three pyridine-O-CH_2-R carbons C^{d} shift to higher frequency from *ca* 58 ppm to *ca* 63 ppm due to the adjacency of the more electron withdrawing triazole group.

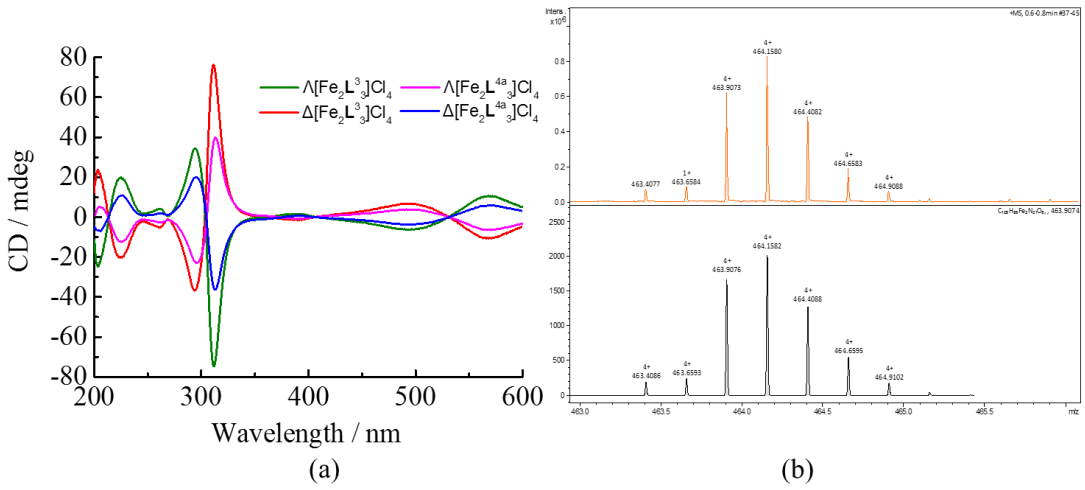

Figure 3-7 (a) CD spectra of alkyne triplex isomers $[Fe_2\mathbf{L^{3}}_3]Cl_4$ (0.1mg/ml) and (azidomethyl)benzene CuAAC product isomers $[Fe_2\mathbf{L^{4a}}_3]Cl_4$ (0.1mg/ml) in methanol; (b) High resolution mass spectrometry for (R_c,Δ_{Fe})-HHT-$[Fe_2\mathbf{L^{4a}}_3]Cl_4$: top measured, below calculated.

The CD spectra of the enantiomers in methanol were found to be equal and opposite in signal [Figure 3-7(a)]. As expected, the spectral curves were similar to the unclicked parent alkyne triplexes as the additional aromatic rings cause little effect on the chiroptic properties of the structure. The successful synthesis of all complexes $[Fe_2\mathbf{L}^{\mathbf{4}}{}_3]^{4+}$ was also confirmed by high resolution electrospray mass spectrometry. For instance, (R_c,Δ_{Fe})-HHT-$[Fe_2\mathbf{L}^{\mathbf{4a}}{}_3][Cl]_4$ gave a strong peak at *m/z* 463.9073 Da for the tetracationic molecular ion within 0.001 Da of the calculated value for $C_{105}H_{93}Fe_2N_{21}O_6$ (*m/z* 463.9076 Da) [Figure 3-7(b)]. Inductively-Coupled Plasma Atomic Absorption (ICP-MS) analysis showed only trace amounts of copper (0.527±0.005%). The isolated compounds contain water of crystallisation; *ca* 16 equivalents as has been consistently observed for this general class of compound.[55] The degree of hydration could not in most instances be determined directly by thermogravimetric analysis as the mass-loss traces contained no clear plateau. Microanalytical data are thus compared to computed figures at reasonable levels of hydration and while these gave excellent agreement for %C and N in all cases the figures for %H were consistently high (*ca* 1%).

3.3 Biological activity of the new triplex metallohelices

3.3.1 *In vitro* cytotoxicity assay

The cytotoxicity and selectivity of both enantiomers of HHT-$[Fe_2\mathbf{L}^{\mathbf{4a\text{-}e}}{}_3]Cl_4$ were screened for potency against HCT116 $p53^{++}$ (human colon carcinoma) cell lines and the human non-cancer retinal pigment epithelial cells (ARPE19). The alkyne parent compounds Δ_{Fe}/Λ_{Fe}-$[Fe_2\mathbf{L}^{\mathbf{3}}{}_3]Cl_4$ were treated as control to investigate the effect of benzyl triazole derivatives. All the compounds were found to be fully soluble in water

under assay conditions. The IC_{50} values obtained from triplicate measurements are given in Figure 3-8 and plotted in Table 3-1.

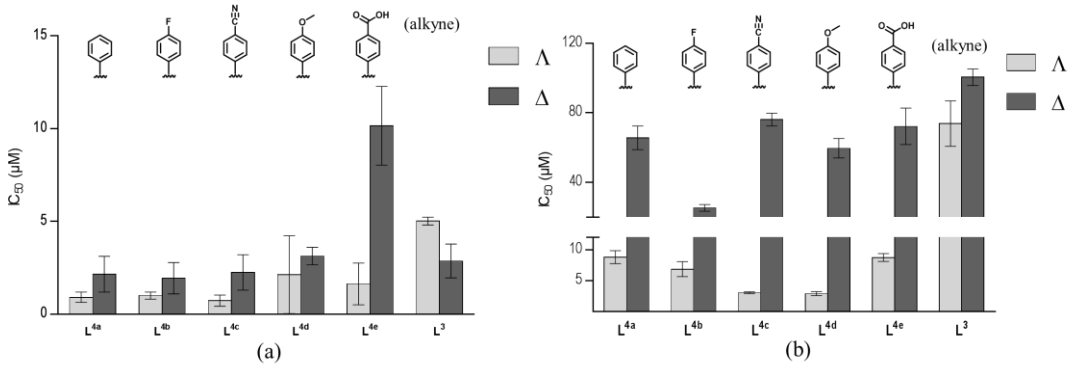

Figure 3-8 IC_{50} values for triplex $[Fe_2\mathbf{L}^{\mathbf{4a\text{-}e}}{}_3]Cl_4$ and unclicked alkyne triplex $[Fe_2\mathbf{L}^{\mathbf{3}}{}_3]Cl_4$ against: (a) HCT116 $p53^{++}$ cancer cell line; (b) ARPE19 (noncancerous cell line)

As seen in Table 3-1, all Λ $[Fe_2\mathbf{L}^{\mathbf{4a\text{-}e}}{}_3]Cl_4$ were more potent than the Δ enantiomers. The potency of these metallohelices was relatively unperturbed by the *para* substitution on the aromatic ring, except for the Δ-configured $[Fe_2\mathbf{L}^{\mathbf{4e}}{}_3]Cl_4$ complex; the substitution of the carboxylate group on the Δ enantiomer reduced the potency by a factor of *ca* 5 with respect to $\Delta[Fe_2\mathbf{L}^{\mathbf{4a}}{}_3]Cl_4$. The most potent compound is the Λ enantiomer of benzonitrile CuAAC product triplex $[Fe_2\mathbf{L}^{\mathbf{4b}}{}_3]Cl_4$ with IC_{50} = 730 nM.

While potency is an important factor, selectivity for cancer cells over "healthy" cells is crucial in potential treatments. The IC_{50} values obtained against the non-cancerous cell line ARPE19 [Table 3-1 and Figure 3-8(b)] are all significantly higher than those for HCT116 $p53^{++}$ and there was a considerable range (3 μM to 76 μM). Again, all Λ enantiomers were more toxic than Δ enantiomers. While Λ_{Fe}-$[Fe_2\mathbf{L}^{\mathbf{4c}}{}_3]Cl_4$ and Λ_{Fe}-$[Fe_2\mathbf{L}^{\mathbf{4d}}]Cl_4$ with IC_{50} 3.08, 2.94 μM respectively were the most potent, all the Δ enantiomers had IC_{50} over 25 μM and there was no clear relationship between the substituent on the aromatic ring and the activity.

Selectivity Index (SI) is defined here as the mean IC_{50} for ARPE19 divided by IC_{50} against HCT116 $p53^{++}$. While as mentioned above the Λ compounds are most potent, the most selective compounds are the Δ enantiomers, with $[Fe_2\mathbf{L^{4a}}_3]Cl_4$ and $[Fe_2\mathbf{L^{4c}}_3]Cl_4$ having SI of *ca* 30 and 34 respectively, very close to that of the parent complex Δ-$[Fe_2\mathbf{L^{3}}_3]Cl_4$ (Table 3-1)**.**

Table 3-1 Cytotoxicity and Selectivity index for triplex $[Fe_2\mathbf{L^{4a-e}}_3]Cl_4$ and unclicked alkyne triplex $[Fe_2\mathbf{L^{3}}_3]Cl_4$ against HCT116 $p53^{++}$ and ARPE-19 cell line

		mean IC_{50} (μM)		**Selectivity Index**
		HCT116 $p53^{++}$	**ARPE-19**	
$[Fe_2\mathbf{L^{4a}}_3]Cl_4$	Λ	0.91 ± 0.28	8.82 ± 1.04	10
	Δ	2.16 ± 0.97	65.58 ± 6.82	30
$[Fe_2\mathbf{L^{4b}}_3]Cl_4$	Λ	1.00 ± 0.19	6.88 ± 1.20	7
	Δ	1.94 ± 0.84	25.37 ± 1.94	13
$[Fe_2\mathbf{L^{4c}}_3]Cl_4$	Λ	0.73 ± 0.30	3.08 ± 0.15	4
	Δ	2.25 ± 0.96	76.14 ± 3.66	34
$[Fe_2\mathbf{L^{4d}}_3]Cl_4$	Λ	2.13 ± 2.10	2.94 ± 0.31	1
	Δ	3.13 ± 0.47	59.60 ± 5.60	19
$[Fe_2\mathbf{L^{4e}}_3]Cl_4$	Λ	1.63 ± 1.13	8.75 ± 0.63	5
	Δ	10.15 ± 2.12	72.23 ± 10.52	7
$[Fe_2\mathbf{L^{3}}_3]Cl_4$	Λ	5.02 ± 0.21	73.81 ± 13.05	15
	Δ	2.87 ± 0.91	100.44 ± 4.67	35

Due to their potency and selectivity towards the HCT116 $p53^{++}$ and ARPE19 cells, Δ-$[Fe_2\mathbf{L^{3}}_3]Cl_4$ and Δ-$[Fe_2\mathbf{L^{4a}}_3]Cl_4$ were further assessed by Dr Viktor Brabec in Marsaryk University for activity against additional cell lines (Table 3-2). Cisplatin was included for comparison.

As seen in Table 3-2, Δ-$[Fe_2\mathbf{L^{3}}_3]Cl_4$ and Δ-$[Fe_2\mathbf{L^{4a}}_3]Cl_4$ each showed preferential cytotoxicity towards each of the different cancer cell lines tested (derived from different cancerous tissue) compared to two non-cancerous cell lines, ARPE19 and MRC-5 pd30 (the latter is derived from fetal lung tissue). Comparing Δ-$[Fe_2\mathbf{L^{3}}_3]Cl_4$ and Δ-$[Fe_2\mathbf{L^{4a}}_3]Cl_4$, the post-assembly CuAAC addition of a benzyl had little effect on activity towards the HCT116 colon cancer cells but notably it increased

cytotoxicity towards the human ovarian and breast cancer cell lines by ~7 to 25 fold. In contrast, activity against the two non-cancer cell lines was only modestly increased {by ~1.5 fold (ARPE19) and ~2 fold (MRC-5 pd30)}. The benzyl triazole modification resulted in a ~3.75-fold increase in cytotoxicity towards the cisplatin-resistant ovarian cancer cells (A2780cis) compared to the cisplatin-sensitive parental cells. For both ovarian cell lines Δ-$[Fe_2\mathbf{L^{4a}}_3]Cl_4$ was substantially more cytotoxic and showed comparable or improved selectivity than Δ-$[Fe_2\mathbf{L^{3}}_3]Cl_4$ indicating the merits of post-assembly modification.

Table 3-2. Cell viability (IC_{50} mean values, μM) of the investigated compounds. Cell survival was evaluated using the MTT[a] assay.

Cell line	Compound Δ-$[Fe_2\mathbf{L^{3}}_3]Cl_4$	Δ-$[Fe_2\mathbf{L^{4a}}_3]Cl_4$	**cisPt**
A2780 *(ovarian cancer cells)*	6.1±0.8	0.9±0.2	3.3±0.2
A2780cisR *(ovarian cancer cells)*	6.1±0.3	0.24±0.02	20±3
HeLa *(cervical cancer cells)*	16±6	7.6±0.5	14.0±0.9
MCF-7 *(breast cancer cells)*	16±2	2.2±0.2	12.9±0.6
MDA-MB-231 *(breast cancer cells)*	22±1	2.1±0.2	22±2
HCT116 p53$^{+/+}$ *(colon cancer cells)*	2.9±0.9 [b]	2.2±1.0 [b]	3.3±0.4 [b]
HCT116 p53$^{-/-}$ *(colon cancer cells)*	3.4±0.2 [b]	3.3±0.3 [b]	7.5±0.7 [b]
ARPE-19 *(non-cancer)*	100±5 [b]	66±7 [b]	3.4±0.5 [b]
MRC-5 pd30 *(non-cancer)*	65±5	32±5	11.6±0.8

[a]The experiments were performed in triplicate or quadruplicate. The cells were treated with the compounds for 72 h, unless otherwise stated. The results are expressed as mean values ± SD from three or four independent experiments; [b]Cells were treated for 96 h.

The p53 tumour suppressor gene is one of the most commonly mutated in cancer. Loss of this function commonly increases resistance to chemotherapeutic drugs, and for example cisplatin was found here to be >2 fold less active towards HCT116 $p53^{-/-}$ than $p53^{+/+}$ (Table 3-2). Interestingly, the alkyne Δ-$[Fe_2\mathbf{L^{3}}_3]Cl_4$ and CuAAC derivative Δ-$[Fe_2\mathbf{L^{4a}}_3]Cl_4$ showed similar activity towards both cell clones.

3.3.2 Cell cycle analysis

The distribution of cell cycle during drug exposure can point to a mode of action. This work was conducted by Hannah Bridgewater. ARPE19 and HCT116 $p53^{+/+}$ cells were incubated with the enantiomers of $[Fe_2\mathbf{L}^{\mathbf{3}}{}_3]Cl_4$ and $[Fe_2\mathbf{L}^{\mathbf{4a}}{}_3]Cl_4$ at 2 × IC_{50} concentration, respectively. After 24 h, cells were analysed by fluorescence-activated cell sorting (FACS).

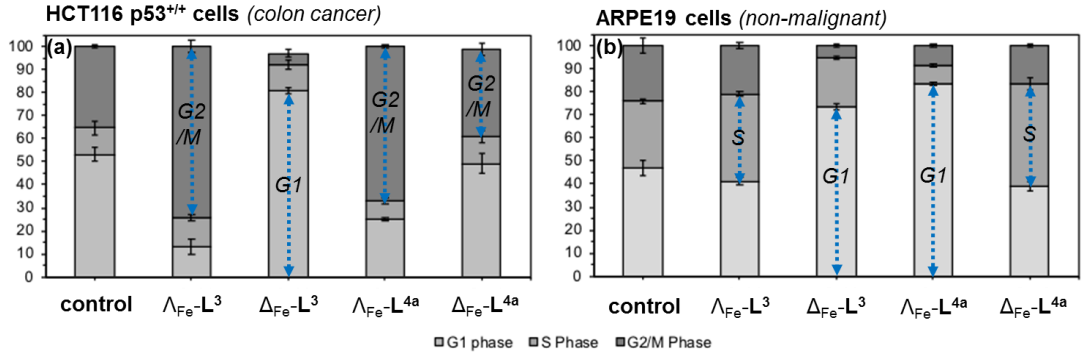

Figure 3-9 Cell cycle analysis by FACS assay using propidium iodide staining to analyse the percent population in stages of the cell cycle for untreated ARPE19 and HCT116 $p53^{++}$ cells, and those incubated with the metallohelices shown for 24 h, at twice the IC_{50} concentration.

In the HCT116 $p53^{+/+}$ cell line, Λ-$[Fe_2\mathbf{L}^{\mathbf{3}}{}_3]Cl_4$ resulted in a significant increase in G2/M cells, in comparison with the untreated (control) cells. However, the Δ-$[Fe_2\mathbf{L}^{\mathbf{3}}{}_3]Cl_4$ substantially increased the number of cells in the G1 phase, demonstrating a clear difference in cell response to the two enantiomers. In the similar fashion with Λ-$[Fe_2\mathbf{L}^{\mathbf{3}}{}_3]Cl_4$, Λ-$[Fe_2\mathbf{L}^{\mathbf{4a}}{}_3]Cl_4$ evidently led to G2/M arrest in HCT116 $p53^{+/+}$ cells. Notably, the Δ-$[Fe_2\mathbf{L}^{\mathbf{4a}}{}_3]Cl_4$ only led to a marginal increase in the proportion of cells in the G2/M phase [Figure 3-9(a)]. For the non-malignant ARPE19 cell line, Λ-$[Fe_2\mathbf{L}^{\mathbf{3}}{}_3]Cl_4$ led to marginal increase in the S phase population [Figure 3-9(b)]. In contrast, it appears that Δ-$[Fe_2\mathbf{L}^{\mathbf{3}}{}_3]Cl_4$ considerably increased the proportion of cells in the G1 phase. A significant increase in the G1 population was observed for Λ-

$[Fe_2\mathbf{L}^{\mathbf{4a}}{}_3]Cl_4$ and a slight increase in the S phase population for Δ-$[Fe_2\mathbf{L}^{\mathbf{4a}}{}_3]Cl_4$. Therefore, the post-assembly modifications of parent $[Fe_2\mathbf{L}^{\mathbf{3}}{}_3]Cl_4$ can dramatically alter the cell cycle effect in two different cell lines. Whilst effects on the cell cycle of both the enantiomer and post-assembly modifications are evident, at present the mechanisms responsible and how these relate to differential cytotoxicity and selectivity are unclear.

3.3.3 Induction of apoptosis

A hallmark of cancers is the evasion of apoptosis or programmed cell death, and the induction of this process in cancer cells is a target of many anticancer drug treatments.[56-58] We found that HCT116 $p53^{+/+}$ cells that had been incubated with $[Fe_2\mathbf{L}^{\mathbf{3}}]Cl_4$ and $[Fe_2\mathbf{L}^{\mathbf{4a}}{}_3]Cl_4$ at 2 × IC_{50} for 24 and 48 h showed no increase in membrane phosphatidylserine (PS)[59] – a key feature and quantifiable marker of early apoptosis. After 96 h a slight elevation in PS was detected. This work was conducted by Dr Samantha Shepherd in Huddersfield University.

3.3.4 Real-time cell growth and ATPase Activity

Time-dependent cellular response profiles (TCRPs) produced by impedance-based monitoring reflect cellular responses to small biologically active compounds,[60] and have been used to predict or compare the mechanism of action of small molecules.[61-63] The work below was conducted by collaborators at Marsaryk University.

The TCRPs induced in A2780 cells by the metallohelices Δ-$[Fe_2\mathbf{L}^{\mathbf{3}}{}_3]Cl_4$, Δ-$[Fe_2\mathbf{L}^{\mathbf{4a}}{}_3]Cl_4$, and Δ-$[Fe_2\mathbf{L}^{\mathbf{S}}{}_3]Cl_4$ (the triplex without terminal alkyne group[55]) were all distinct (Figure 3-10). For the parent metallohelix Δ-$[Fe_2\mathbf{L}^{\mathbf{S}}{}_3]Cl_4$ the initial rise is less

apparent than for other compounds and the period of signal elevation is the shortest. For the alkyne Δ-[Fe_2**L**$^{3}_3$]Cl_4 the CI signal increases to *ca* 1.7 × that of the control and the peak is relatively broad, the signal decreasing steadily over the measurement period. For the benzyl triazole derivative Δ-[Fe_2**L**$^{4a}_3$]Cl_4 the CI signals reach a much sharper dose-dependent maximum. A TCRP profile database search indicated a similarity with that for compounds that inhibit Na^+/K^+ stimulated ATPases (mainly cardiotonics like strophanthidin, convallatoxin, gitoxin, digoxin and/or sarmetogenin).[64]

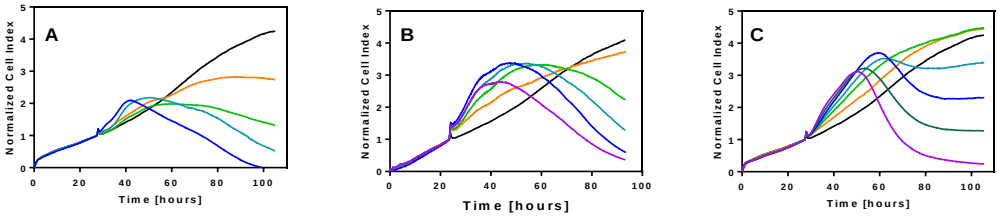

Figure 3-10 TCRPs of A2780 treated with the growing concentrations of the investigated metallohelices. The medium containing the tested compounds was added after 27.5 h of incubation. (A) Δ-[Fe_2**L**$^{S}_3$]Cl_4; (B) Δ-[Fe_2**L**$^{3}_3$]Cl_4 (C) Δ-[Fe_2**L**$^{4a}_3$]Cl_4. The concentrations of metallohelices were chosen to induce various inhibitory effects.

The above profiling study suggests that the mechanism of action of the metallohelices may involve inhibition of the activity of Na^+/K^+ ATPase; a highly conserved integral cell membrane pump expressed in virtually all cells of higher organisms that maintains ionic concentration gradients. A rubidium based assay[65] was subsequently used to evaluate Na^+/K^+ ATPase inhibition in A2780 and HCT116 $p53^{+/+}$ cell lines by Δ-[Fe_2**L**$^{S}_3$]Cl_4, Δ-[Fe_2**L**$^{3}_3$]Cl_4, Δ-[Fe_2**L**$^{4a}_3$]Cl_4 (10 μM) and ouabain. In order to secure cell viability and to mainly detect the upstream effects of the applied drug, a short incubation time (6 h) was used, after which the uptake of Rb^+ (5.4 mM) was determined by ICPMS (Figure 3-11). Δ-[Fe_2**L**$^{4a}_3$]Cl_4 was found to inhibit

rubidium uptake under the given conditions by 35-47%, which is comparable to that of the known Na^+/K^+ ATPase inhibitor ouabain[67] (39-57% inhibition). In contrast, Δ-$[Fe_2\mathbf{L}^{\mathbf{S}}{}_3]Cl_4$ and Δ-$[Fe_2\mathbf{L}^{\mathbf{3}}{}_3]Cl_4$ did not affect the rubidium uptake suggesting these compounds have a different mechanism of action to Δ-$[Fe_2\mathbf{L}^{\mathbf{4a}}{}_3]Cl_4$.

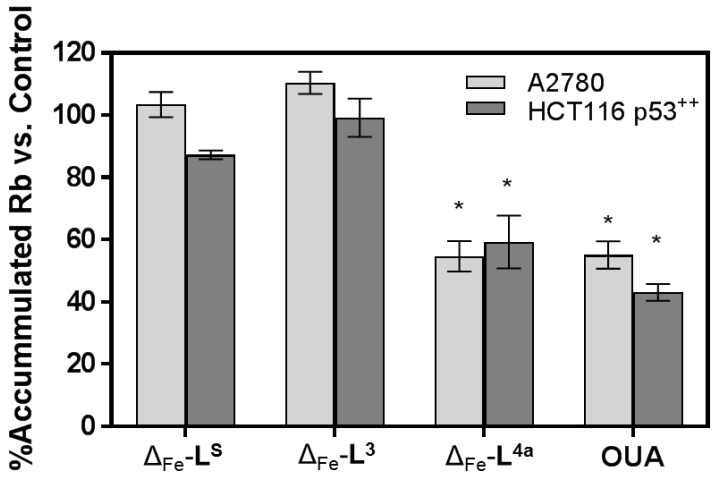

Figure 3-11 Metallohelices induced Na^+/K^+ ATPase inhibition. A2780 and HCT116 $p53^{++}$ cells were treated with metallohelices and ouabain (10 μM) for 6 h and then incubated with RbCl for 3 h. Rubidium content in cell lysates was determined with ICP-MS. All results are expressed as the mean ± SD from three independent experiments. Stars indicate significant difference from untreated control (100%) with $^*p < 0.001$ calculated by using 2way ANOVA.

3.3.5 Antimetastatic properties

Colorectal cancer is one of the four most common causes of cancer deaths and in 90% of instances, mortality is ascribed to metastasis.[68, 69] Notably, ouabain was reported to inhibit the migratory activities of various cancer cell lines,[70-73] and the antimetastatic activity was in part downstream signalling effects of Na^+/K^+ ATPase inhibition.[73] Given the comparable performance of Δ-$[Fe_2\mathbf{L}^{\mathbf{3a}}{}_3]Cl_4$ in this regard, we set out to investigate the effect of metallohelices on cell migration and invasion which are important steps in the process of metastasis.[74, 75]

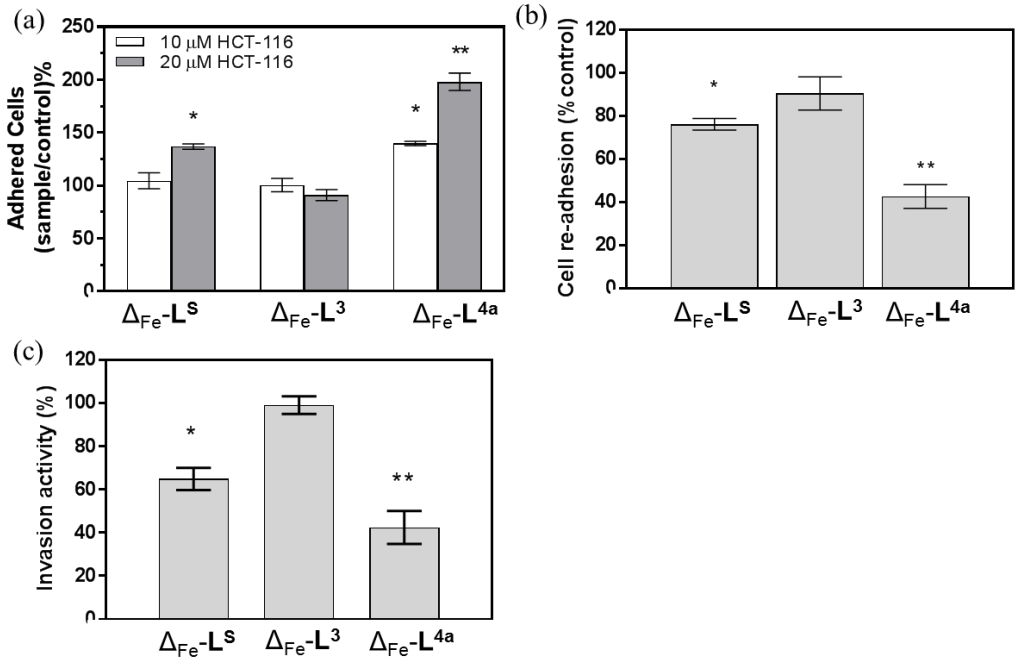

Figure 3-12 Antimetastatic activity of metallohelices against HCT116 $p53^{++}$ cells: (a) resistance to trypsin detachment, cells were treated with Δ-metallohelices at 10 μM and 20 μM respectively for 3h, (b) cell re-adhesion, cells were treated with Δ-metallohelices at 10 μM for 3h, followed by trypsin detached and re-seeded for 30 min (c) invasion activity, cells were treated with Δ-metallohelices at equitoxic ($2xIC_{50}$) concentration for 2h, followed by seeded and incubated for additional 96h. The results are expressed as the mean ± SD from three independent experiments. Stars indicate significant difference from untreated control (100%) with $^{*}p < 0.05$ or $^{**}p < 0.001$ calculated by using 2way ANOVA

We modelled the detachment of cancer cells from a primary tumour by an assay of cell resistance to trypsinization. HCT116 $p53^{++}$ cells grown in monolayer were treated with the investigated compounds for 3 h and then subjected to a diluted trypsin solution. The number of cells that resisted the treatment with trypsin (*i.e.* remained attached to the surface) was evaluated by the SRB assay. Treatment with Δ-$[Fe_2\mathbf{L}^{\mathbf{S}}{}_3]Cl_4$ reduced detachment only at higher concentrations [Figure 3-12 (a)] and Δ-$[Fe_2\mathbf{L}^{\mathbf{3}}{}_3]Cl_4$ had no significant effect. In contrast, Δ-$[Fe_2\mathbf{L}^{\mathbf{4a}}{}_3]Cl_4$ treatment of cells significantly impeded their detachment.

Re-adhesion of detached cells in a distant organ was modeled in a further assay. Cells were treated with 10 µM compound for 3 h, detached with trypsin and re-seeded at a density of 2 x 10^4 cells/well. The number of cells attached after 30 min incubation was determined with SRB assay [Figure 3-12 (b)]. While Δ-[Fe_2**L**$^{\mathbf{3}}_3$]Cl_4 did not measurably influence the ability of cells to re-attach to the new growth surface, Δ-[Fe_2**L**$^{\mathbf{S}}_3$]Cl_4 and Δ-[Fe_2**L**$^{\mathbf{4a}}_3$]Cl_4 reduced cell re-adhesion by 24% and 58%, respectively.

The effects of Δ-[Fe_2**L**$^{\mathbf{S}}_3$]Cl_4, Δ-[Fe_2**L**$^{\mathbf{3}}_3$]Cl_4, and Δ-[Fe_2**L**$^{\mathbf{4a}}_3$]Cl_4 on invasion activity were also assessed using a Matrigel^{TM} transwell assay. HCT116 $p53^{++}$ cells were treated with the investigated compounds at equitoxic ($2\times IC_{50}$) concentrations. The treatment of tumor cells for 2 h with Δ-[Fe_2**L**$^{\mathbf{4a}}_3$]Cl_4 resulted in a significantly reduced invasion activity [Figure 3-12 (c)], whereas Δ-[Fe_2**L**$^{\mathbf{3}}_3$]Cl_4 had little or no potency to inhibit HCT116 $p53^{++}$ invasiveness. Δ-[Fe_2**L**$^{\mathbf{S}}_3$]Cl_4 and Δ-[Fe_2**L**$^{\mathbf{4a}}_3$]Cl_4 reduced the invasive ability by 35% and 58%, respectively.

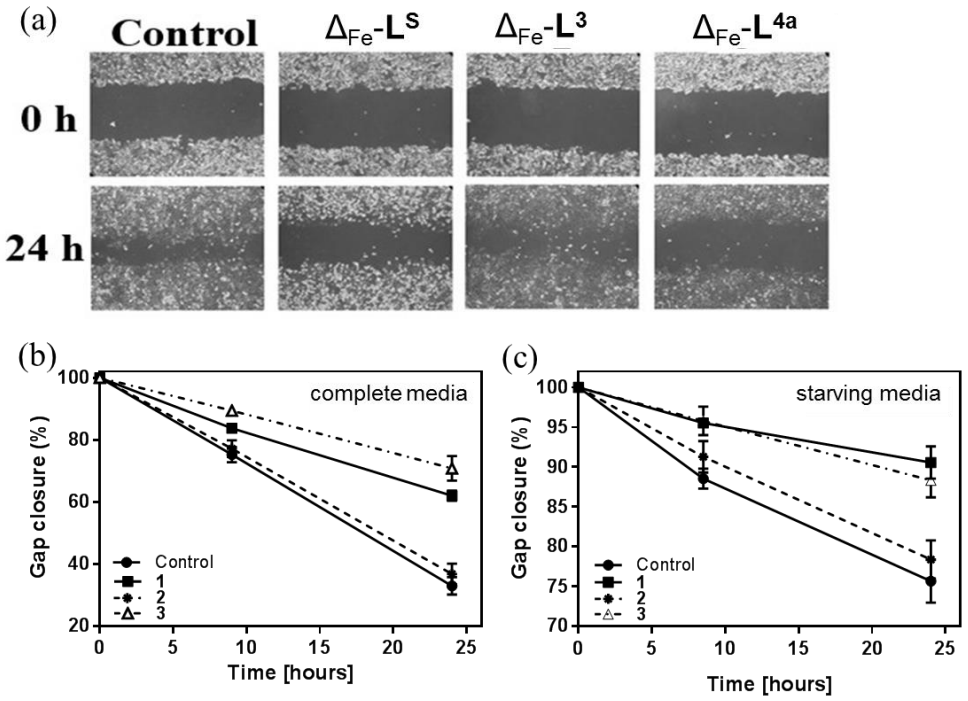

Figure 3-13 Wound healing assay of metallohelices: (a) HCT116 $p53^{+/+}$ cells were were treated with metallohelices at IC_{50} concentration. The shots were taken at times 0 h and 24 h. (b) the cells were treated in the complete medium (10% FBS, gentamycin), the shots were taken at times 0, 8.5 and 24 h. The area of a gap at time 0 h was considered 100%. (c). after growing period, the cells were incubated overnight in starving medium (1% BSA, gentamycin) and were kept in the starving medium during the rest of the assay

A wound healing assay (scratch gap closure) was also used to assess the overall ability of the compounds to influence cell migration and invasion (Figure 3-13). In complete medium, 24 h after scratching a monolayer of HCT116 $p53^{+/+}$ cells, the gap in an untreated control sample was healed to 33%, while in the presence of Δ-$[Fe_2\mathbf{L}^{S}{}_3]Cl_4$ or Δ-$[Fe_2\mathbf{L}^{4a}{}_3]Cl_4$ healing was more suppressed and 62% and 71% of the wound remained open respectively. Cells treated with Δ-$[Fe_2\mathbf{L}^{3}{}_3]Cl_4$ resembled the control [Figure 3-13 (a); (b)]. A qualitatively similar result was obtained in starving medium conditions [Figure 3-13 (c)] indicating that the suppression of wound-healing results at least in part from anti-migration/invasion rather than being due to cell proliferation resulting in closure of the scratch.

Collectively, these data show that in particular the metallohelix Δ-$[Fe_2\mathbf{L}^{\mathbf{4a}}{}_3]Cl_4$ is capable of suppressing the cellular properties characteristic of metastatic progressions, such as invasiveness, migration, and re-adherence to a substrate. Thus, these properties predestine it for further biological testing as a potential antimetastatic drug.

3.3.6 Growth-inhibitory effects on cancer stem cells (CSCs)

CSCs[76-78] have the ability to self-renew, differentiate, form secondary or tertiary tumors, exhibit up-regulated cellular defense mechanisms and are less susceptible to chemotherapy.[79] Being thus more aggressive and linked to cancer relapse and metastasis, they are the primary target for chemotherapy.[80] Recently, Qu and co-workers demonstrated that a bimetallic nickel(II) helicate could effectively eradicate breast cancer stem cells, and this led us to investigate this feature in the current system, which, being based on a non-toxic metal, not requiring chemical separation of enantiomers, and being capable of derivatisation, has several advantages over the former.[88]

We initially studied their effect on sphere formation from single cells; only self-renewing cells, stem or stem-like cells can survive and proliferate to form spheres when grown in serum-free media under low-attachment conditions. The inhibition of colonosphere formation[81-83] was tested in HCT116 $p53^{++}$ cells treated with Δ-$[Fe_2\mathbf{L}^{\mathbf{S}}{}_3]Cl_4$ and Δ-$[Fe_2\mathbf{L}^{\mathbf{4a}}{}_3]Cl_4$ at their respective IC_{30} concentrations for 72 h. These data were compared with effects of salinomycin, which is known to have CSC-selective potency.[84-86] Both Δ-$[Fe_2\mathbf{L}^{\mathbf{S}}{}_3]Cl_4$ and Δ-$[Fe_2\mathbf{L}^{\mathbf{4a}}{}_3]Cl_4$ were found to inhibit colonosphere formation in the tested HCT116 $p53^{++}$ cells, giving rise to decrease from

224±14 spheres/1000 cells and sphere diameter of 96±20 µm in the control cells, to 134±15 spheres /1000 cells and sphere diameter of 86±18 µm (Δ-$[Fe_2\mathbf{L}^{\mathbf{S}}{}_3]Cl_4$) and 94±22 spheres /1000 cells and sphere diameter of 82±16 µm (Δ-$[Fe_2\mathbf{L}^{\mathbf{4a}}{}_3]Cl_4$), both being more effective than salinomycin (142±14 spheres/1000 cells and sphere diameter of 76±17 µm) (Table 3-3).

Table 3-3. Quantification of colonosphere formation in HCT116 $p53^{++}$ cells untreated or treated with the investigated compounds at their respective IC_{30} values for 72 h.[a]

HCT116 $p53^{++}$	Spheres/1000cells	Diameter (µm)
Control	224 ± 14	96 ± 20
Salinomycin	142 ± 14	76 ± 17
Δ-$[Fe_2\mathbf{L}^{\mathbf{S}}{}_3]Cl_4$	134 ± 15	86 ± 18
Δ-$[Fe_2\mathbf{L}^{\mathbf{4a}}{}_3]Cl_4$	94 ± 22	82 ± 16

[a]The results are expressed as mean ± SD of three independent experiments.

To further study the anti-CSC potency of Δ-$[Fe_2\mathbf{L}^{\mathbf{S}}{}_3]Cl_4$ and Δ-$[Fe_2\mathbf{L}^{\mathbf{4a}}{}_3]Cl_4$, the inhibition of colonosphere formation in CSC-enriched HCT116.$CD133^+$ was also investigated, as shown in Figure 3-14.

Significant colonosphere inhibition was also observed in the CSC-enriched cells treated with both Δ-$[Fe_2\mathbf{L}^{\mathbf{S}}{}_3]Cl_4$ and Δ-$[Fe_2\mathbf{L}^{\mathbf{4a}}{}_3]Cl_4$ [Figure 3-14 (a-f)]. These data suggest that Δ-$[Fe_2\mathbf{L}^{\mathbf{S}}{}_3]Cl_4$ and Δ-$[Fe_2\mathbf{L}^{\mathbf{4a}}{}_3]Cl_4$ inhibits both the number and average size of colonospheres formed in CSC-enriched cells more effectively than salinomycin.

Monolayer human solid-tumour cell-line screening is a useful technique to garner acute toxicity information, but in order to better indicate the efficacy of anticancer drugs to kill undifferentiated CSCs, it is important to investigate their effects on clonogenic activity. The clonogenic assay is a quantitative *in vitro* technique that examines the capability of a single cell to grow into a large colony through clonal

expansion, and is a sensitive indicator of CSCs.[87] HCT116.CD133$^+$ cells incubated for 48 h with 30 µM Δ-[Fe_2**L**$^{4a}{}_3$]Cl_4, exhibited no surviving cells after being allowed to grow for 8 d; a comparable growth-inhibitory effect to that of conventional salinomycin. A more moderate growth inhibition was observed for cells treated with Δ-[Fe_2**L**$^{S}{}_3$]Cl_4 [Figure 3-14 (g)].

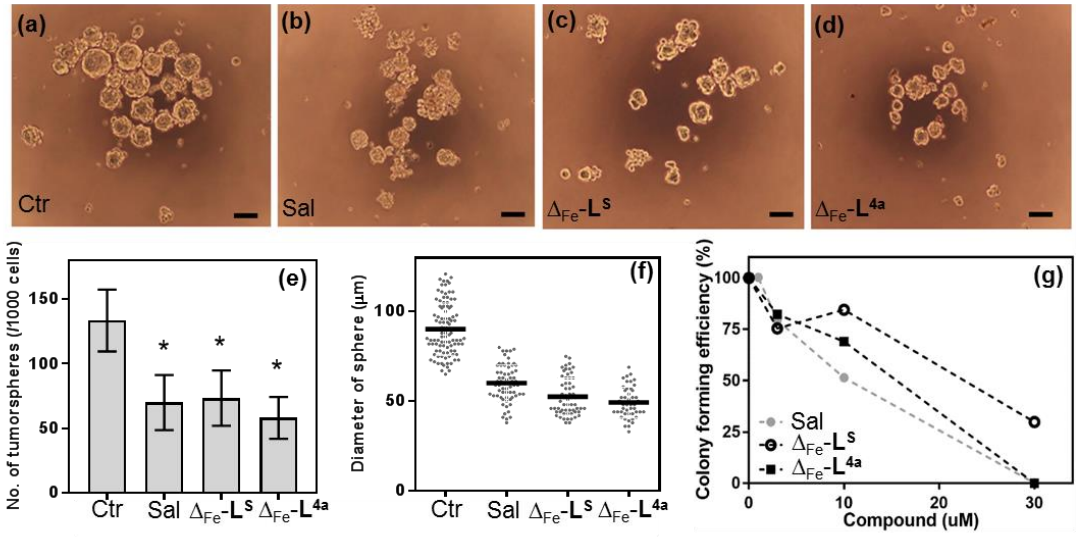

Figure 3-14 Growth inhibitory effects in HCT116.CD133$^+$ cells Representative microscopy images of the HCT116.CD133$^+$ colonospheres in the absence (a) and presence of salinomycin (b), Δ-[Fe_2**L**$^{S}{}_3$]Cl_4 (c), and Δ-[Fe_2**L**$^{4a}{}_3$]Cl_4 (d), treated at their respective IC_{30} values for 6 days (scale bar: 100 µM). Quantification of colonosphere formation (e and f) under the same conditions. Clonogenic assay on the HCT116.CD133$^+$ (g) showing the number of colonies counted after treatment with different concentrations of salinomycin, (grey circles), Δ-[Fe_2**L**$^{S}{}_3$]Cl_4 (black open circle), and Δ-[Fe_2**L**$^{4a}{}_3$]Cl_4 (black squares) for 48h, following growth for 8 days. Data represent the mean value and SD from three independent experiments. $p < 0.01$, versus control.

The cytotoxicity of Δ-[Fe_2**L**$^{4a}{}_3$]Cl_4 was also tested in isolated CD133$^+$ cells from the HCT116 p53$^{+/+}$ cell line, and an IC_{50} of 1.21±0.25 µM was measured in HCT116.CD133$^+$, using the SRB assay following a 72 h exposure (Table 3-4). This is *ca* 40% lower than the IC_{50} measured for HCT116p53$^{+/+}$ cells (2.11±0.41 µM) under the same conditions, suggesting that Δ-[Fe_2**L**$^{4a}{}_3$]Cl_4 has a strong growth-inhibitory

effect on the CSCs, in fact similar to that of salinomycin (IC_{50} {HCT116p53+/+} = 1.48±0.21 µM, IC_{50} {HCT116.CD133+} = 1.12±0.23 µM).

Table 3-4 IC_{50} values of the investigated compounds in CSC enriched HCT116.CD133^{+} cells determined with SRB assay.[a]

IC_{50} (µM)	**HCT116.CD133^{+}**	**HCT116p53^{++}**
Salinomycin	1.12 ± 0.23	1.48 ± 0.21
Δ-[Fe_2**L**$^{S}{}_3$]Cl_4	2.04 ± 0.39	3.28 ± 0.30
Δ-[Fe_2**L**$^{4a}{}_3$]Cl_4	1.21 ± 0.25	2.11 ± 0.41

[a]The cells were treated for 72 h. The results are expressed as mean ± SD of three independent experiments.

3.4 Conclusion

In this chapter, the post-assembly modification of optically pure alkyne triplex metallohelices $[Fe_2\mathbf{L^3}_3]Cl_4$ has been investigated *via* CuAAC reactions. Unlike the symmetric flexicate system $[Fe_2\mathbf{L^1}_3]Cl_4$ and $[Fe_2\mathbf{L^2}_3]Cl_4$ described in Chapter 2, the anti-parallel external alkyne functional sites of the HHT triplex metallohelices $[Fe_2\mathbf{L^3}_3]Cl_4$ offer greater geometric advantages in precluding the formation of copper(I) bonded three concurrent triazole rings,[89] allow 100% CuAAC conversion of the alkyne groups with bulky aromatic azides and preserve the helical structure. A series of new substituted triplex systems $[Fe_2\mathbf{L^{4a\text{-}e}}_3]Cl_4$ have been synthesized through the substitution of benzyl azide in high efficiency and yield, and characterised by NMR spectroscopy, microanalysis, mass spectrometry and circular dichroism spectroscopy.

In vitro cytotoxicity assay demonstrated the high potency of all the new triplex systems against HCT116 $p53^{++}$ with an average IC_{50} value 2.60 μM, similar with parent $[Fe_2\mathbf{L^3}_3]Cl_4$. A wide range of cytotoxicity (3 μM to 76 μM) was found towards noncancerous ARPE-19 cell line. Notably, the significantly enantiomeric difference was observed that all Δ enantiomers were more selective than the Λ enantiomers. The most promising compounds were Δ-$[Fe_2\mathbf{L^{4a}}_3]Cl_4$ and Δ-$[Fe_2\mathbf{L^{4c}}_3]Cl_4$ with SI *ca* 30 and 34 respectively, close to the parent complex Δ-$[Fe_2\mathbf{L^3}_3]Cl_4$. In further cytotoxicity assay, Δ-$[Fe_2\mathbf{L^{4a}}_3]Cl_4$ demonstrated high potency against multiple cancer cell lines. The cell cycle analysis revealed that the post-assembly modifications of parent $[Fe_2\mathbf{L^3}_3]Cl_4$ can dramatically alter the cell cycle effect in two different cell lines. The anticancer mechanism of Δ-$[Fe_2\mathbf{L^{4a}}_3]Cl_4$ was also demonstrated significantly different from cisplatin. Annexin V assay showed no apoptosis was induced by $[Fe_2\mathbf{L^{4a}}_3]Cl_4$ enantiomers. In contrast, they interfere with the Na+/K+ ATPase activity with

comparable potency to that of the conventional inhibitor ouabain. Moreover, Δ-$[Fe_2\mathbf{L}^{\mathbf{4a}}{}_3]Cl_4$ is the first metallohelix to show antimetastatic properties. It significantly reduces HCT116 $p53^{++}$ cell detachment, inhibits cell re-adhesion and reduces the invasion activity.

Remarkably, Δ-$[Fe_2\mathbf{L}^{\mathbf{4a}}{}_3]Cl_4$ reduces the proportion of CSCs within a heterogeneous colon cancer cell population and irreversibly inhibits the colonosphere formation in both CSC enriched cells to an similar extent to salinomycin, a natural product that targets CSCs. To our knowledge, Δ-$[Fe_2\mathbf{L}^{\mathbf{4a}}{}_3]Cl_4$ is the first metallohelix to exhibit selective toxicity for colon CSC-enriched cell populations. Given our findings and the urgent medical need for CSC-specific chemotherapies to overcome cancer relapse and metastases in the clinic, the anti-CSC properties of Δ-$[Fe_2\mathbf{L}^{\mathbf{4a}}{}_3]Cl_4$ are pre-clinically very appealing.

3.5 References

1. A. Michael, *Adv. Synth. Catal.*, 1893, **48**, 94-95.
2. R. Huisgen, *Angew. Chem. Int. Ed.*, 1963, **2**, 565-598.
3. R. Huisgen, *Angew. Chem. Int. Ed.*, 1963, **2**, 633-645.
4. V. V. Rostovtsev, L. G. Green, V. V. Fokin and K. B. Sharpless, *Angew. Chem. Int. Ed.*, 2002, **114**, 2708-2711.
5. C. W. Tornøe, C. Christensen and M. Meldal, *J. Org. Chem.*, 2002, **67**, 3057-3064.
6. H. C. Kolb, M. Finn and K. B. Sharpless, *Angew. Chem. Int. Ed.*, 2001, **40**, 2004-2021.
7. P. Wu, A. K. Feldman, A. K. Nugent, C. J. Hawker, A. Scheel, B. Voit, J. Pyun, J. M. Fréchet, K. B. Sharpless and V. V. Fokin, *Angew. Chem. Int. Ed.*, 2004, **116**, 4018-4022.
8. W. H. Binder and R. Sachsenhofer, *Macromol. Rapid Commun.*, 2007, **28**, 15-54.
9. P. Thirumurugan, D. Matosiuk and K. Jozwiak, *Chem. Rev.*, 2013, **113**, 4905-4979.
10. M. Meldal and C. W. Tornøe, *Chem. Rev.*, 2008, **108**, 2952-3015.
11. B. Schulze and U. S. Schubert, *Chem. Soc. Rev.*, 2014, **43**, 2522-2571.
12. S.-i. Fukuzawa, H. Oki, M. Hosaka, J. Sugasawa and S. Kikuchi, *Org. Lett.*, 2007, **9**, 5557-5560.
13. A. Maisonial, P. Serafin, M. Traïkia, E. Debiton, V. Thery, D. J. Aitken, P. Lemoine, B. Viossat and A. Gautier, *Eur. J. Inorg. Chem.*, 2008, **2008**, 298-305.
14. H. Struthers, T. L. Mindt and R. Schibli, *Dalton Trans.*, 2010, **39**, 675-696.
15. S. M. Cohen, *Chem. Rev.*, 2011, **112**, 970-1000.
16. R. A. Vasdev, D. Preston and J. D. Crowley, *Dalton Trans*, 2017, **46**, 2402-2414.
17. P. Mathew, A. Neels and M. Albrecht, *J. Am. Chem. Soc.*, 2008, **130**, 13534-13535.
18. T. L. Mindt, H. Struthers, L. Brans, T. Anguelov, C. Schweinsberg, V. Maes, D. Tourwé and R. Schibli, *J. Am. Chem. Soc.*, 2006, **128**, 15096-15097.
19. E. M. Schuster, M. Botoshansky and M. Gandelman, *Angew. Chem. Int. Ed.*, 2008, **47**, 4555-4558.
20. U. R. Pokharel, F. R. Fronczek and A. W. Maverick, *Nat. Commun.*, 2014, **5**, 5883.
21. P. Symmers, M. Burke, D. August, P. Thomson, G. Nichol, M. Warren, C. Campbell and P. Lusby, *Chem. Sci.*, 2015, **6**, 756-760.
22. K. A. Stevenson, C. F. Melan, O. Fleischel, R. Wang and A. Petitjean, *Cryst. Growth Des.*, 2012, **12**, 5169-5173.
23. A. L. Moore, D.-K. Bučar, L. R. MacGillivray and P. D. Benny, *Dalton Trans*, 2010, **39**, 1926-1928.
24. J. E. Lewis, A. B. Elliott, C. J. McAdam, K. C. Gordon and J. D. Crowley, *Chem. Sci.*, 2014, **5**, 1833-1843.
25. M. Jauregui, W. S. Perry, C. Allain, L. R. Vidler, M. C. Willis, A. M. Kenwright, J. S. Snaith, G. J. Stasiuk, M. P. Lowe and S. Faulkner, *Dalton Trans*, 2009, 6283-6285.

26. J. E. Lewis, C. J. McAdam, M. G. Gardiner and J. D. Crowley, *Chem. Commun.*, 2013, **49**, 3398-3400.
27. D. A. Roberts, B. S. Pilgrim and J. R. Nitschke, *Chem. Soc. Rev.*, 2018, **47**, 626-644.
28. Y.-F. Han, G.-X. Jin and F. E. Hahn, *J. Am. Chem. Soc.*, 2013, **135**, 9263-9266.
29. D. A. Roberts, A. M. Castilla, T. K. Ronson and J. R. Nitschke, *J. Am. Chem. Soc.*, 2014, **136**, 8201-8204.
30. D. A. Roberts, B. S. Pilgrim, J. D. Cooper, T. K. Ronson, S. Zarra and J. R. Nitschke, *J. Am. Chem. Soc.*, 2015, **137**, 10068-10071.
31. T. K. Ronson, B. S. Pilgrim and J. R. Nitschke, *J. Am. Chem. Soc*, 2016, **138**, 10417-10420.
32. D. Samanta, A. Chowdhury and P. S. Mukherjee, *Inorg. Chem.*, 2016, **55**, 1562-1568.
33. G. Tuci, A. Rossin, X. Xu, M. Ranocchiari, J. A. van Bokhoven, L. Luconi, I. Manet, M. Melucci and G. Giambastiani, *Chem. Mater.*, 2013, **25**, 2297-2308.
34. K. D. Hänni and D. A. Leigh, *Chem. Soc. Rev.*, 2010, **39**, 1240-1251.
35. D. G. Cabrera, B. D. Koivisto and D. A. Leigh, *Chem. Commun.*, 2007, 4218-4220.
36. J. P. Collin, S. Durot, M. Keller, J. P. Sauvage, Y. Trolez, M. Cetina and K. Rissanen, *Chem. Eur. J.*, 2011, **17**, 947-957.
37. J.-P. Collin, J. Frey, V. Heitz, J.-P. Sauvage, C. Tock and L. Allouche, *J. Am. Chem. Soc.*, 2009, **131**, 5609-5620.
38. S. Badèche, J.-C. Daran, J. Ruiz and D. Astruc, *Inorg. Chem.*, 2008, **47**, 4903-4908.
39. M. Patra, G. Gasser, D. Bobukhov, K. Merz, A. V. Shtemenko and N. Metzler-Nolte, *Dalton Trans.*, 2010, **39**, 5617-5619.
40. S. Panaka, R. Trivedi, K. Jaipal, L. Giribabu, P. Sujitha, C. G. Kumar and B. Sridhar, *J. Organomet. Chem.*, 2016, **813**, 125-130.
41. N. Li and W. H. Binder, *J. Mater. Chem.*, 2011, **21**, 16717-16734.
42. H. Li, Y. Yao, C. Han and J. Zhan, *Chem. Commun.*, 2009, 4812-4814.
43. D. A. Roberts, B. S. Pilgrim and J. R. Nitschke, *Chem. Soc. Rev.*, 2018, **47**, 626-644.
44. S. Han, Z. Ma, R. Hopson, Y. Wei, D. Budil, S. Gulla and B. Moulton, *Inorg. Chem. Commun.*, 2012, **15**, 78-83.
45. R. Chakrabarty and P. J. Stang, *J. Am. Chem. Soc.*, 2012, **134**, 14738-14741.
46. D. C. Kennedy, C. S. McKay, M. C. Legault, D. C. Danielson, J. A. Blake, A. F. Pegoraro, A. Stolow, Z. Mester and J. P. Pezacki, *J. Am. Chem. Soc.*, 2011, **133**, 17993-18001.
47. N. J. Agard, J. A. Prescher and C. R. Bertozzi, *J. Am. Chem. Soc.*, 2004, **126**, 15046-15047.
48. J. M. Baskin, J. A. Prescher, S. T. Laughlin, N. J. Agard, P. V. Chang, I. A. Miller, A. Lo, J. A. Codelli and C. R. Bertozzi, *Proc. Natl. Acad. Sci. U. S. A.*, 2007, **104**, 16793-16797.
49. P. V. Chang, J. A. Prescher, E. M. Sletten, J. M. Baskin, I. A. Miller, N. J. Agard, A. Lo and C. R. Bertozzi, *Proc. Natl. Acad. Sci. U. S. A.*, 2010, **107**, 1821-1826.
50. J. A. Codelli, J. M. Baskin, N. J. Agard and C. R. Bertozzi, *J. Am. Chem. Soc.*, 2008, **130**, 11486-11493.
51. J. C. Jewett and C. R. Bertozzi, *Chem. Soc. Rev.*, 2010, **39**, 1272-1279.

52. E. Kaya, M. Vrabel, C. Deiml, S. Prill, V. S. Fluxa and T. Carell, *Angew. Chem. Int. Ed.*, 2012, **51**, 4466-4469.
53. D. Hédou, E. Deau, C. Dubouilh-Benard, M. Sanselme, A. Martinet, E. Chosson, V. Levacher and T. Besson, *Eur. J. Org. Chem.*, 2013, **2013**, 7533-7545.
54. Y. Liu, Q. Xiao, Y. Liu, Z. Li, Y. Qiu, G. B. Zhou, Z. J. Yao and S. Jiang, *Eur. J. Med. Chem.*, 2014, **78**, 248-258.
55. A. D. Faulkner, R. A. Kaner, Q. M. Abdallah, G. Clarkson, D. J. Fox, P. Gurnani, S. E. Howson, R. M. Phillips, D. I. Roper and D. H. Simpson, *Nat. Chem.*, 2014, **6**, 797.
56. J. A. Hickman, *Cancer Metastasis Rev.*, 1992, **11**, 121-139.
57. C. M. Pfeffer and A. T. Singh, *Int. J. Mol. Sci.*, 2018, **19**, 448.
58. S. Elmore, *Toxicol. Pathol.*, 2007, **35**, 495-516.
59. G. Koopman, C. Reutelingsperger, G. Kuijten, R. Keehnen, S. Pals and M. Van Oers, *Blood*, 1994, **84**, 1415-1420.
60. Y. A. Abassi, B. Xi, W. Zhang, P. Ye, S. L. Kirstein, M. R. Gaylord, S. C. Feinstein, X. Wang, X. J. C. Xu, *Chem. Biol.*, 2009, **16**, 712-723.
61. N. Ke, B. Xi, P. Ye, W. Xu, M. Zheng, L. Mao, M.-J. Wu, J. Zhu, J. Wu and W. Zhang, *Anal. Chem.*, 2010, **82**, 6495-6503.
62. T. Pan, B. Huang, W. Zhang, S. Gabos, D. Y. Huang and V. Devendran, *Anal. Chim. Acta*, 2013, **764**, 44-52.
63. Z. Xi, S. Khare, A. Cheung, B. Huang, T. Pan, W. Zhang, F. Ibrahim, C. Jin, S. J. C. b. Gabos and chemistry, *Comput. Biol. Chem.*, 2014, **49**, 23-35.
64. Y. A. Abassi, B. Xi, W. Zhang, P. Ye, S. L. Kirstein, M. R. Gaylord, S. C. Feinstein, X. Wang and X. Xu, *Chem. Biol.*, 2009, **16**, 712-723.
65. M. V. Clausen, F. Hilbers and H. Poulsen, *Front. Physiol.*, 2017, **8**, 371.
66. D. S. Gill, R. Gill, D. Wicks, S. Despotovski and D. Liang, *Assay Drug Dev. Technol.*, 2004, **2**, 535-542.
67. J.-Q. Chen, R. G. Contreras, R. Wang, S. V. Fernandez, L. Shoshani, I. H. Russo, M. Cereijido, J. Russo, *Breast Cancer Res. Treat.*, 2006, **96**, 1-15.
68. A. M. Maffione, E. Lopci, C. Bluemel, F. Giammarile, K. Herrmann and D. Rubello, *Eur. J. Nuclear Med. Mol. Imaging*, 2015, **42**, 152-163.
69. S. Salah, F. Ardissone, M. Gonzalez, P. Gervaz, M. Riquet, K. Watanabe, J. Zabaleta, D. Al-Rimawi, S. Toubasi, E. Massad, E. Lisi and O. H. Hamed, *Ann. Surg. Oncol.*, 2015, **22**, 1844-1850.
70. N. Liu, Y. Li, S. Su, N. Wang, H. Wang and J. Li, *Oncol. Lett.*, 2013, **6**, 475-479.
71. Y. Xiao, C. Meng, J. Lin, C. Huang, X. Zhang, Y. Long, Y. Huang and Y. Lin, *Oncol. Lett.*, 2017, **14**, 6678-6684.
72. V. Pongrakhananon, P. Chunhacha and P. Chanvorachote, *PLoS One*, 2013, **8**, e68623.
73. M. A. Khajah, P. M. Mathew and Y. A. Luqmani, *PLoS One*, 2018, **13**, e0193779.
74. N. Riggi, M. Aguet and I. Stamenkovic, *Annu. Rev. Pathol. Mech.*, 2018, **13**, 117-140.
75. G. P. Gupta and J. J. C. Massagué, *Histol. Histopathol.*, 2006, **127**, 679-695.
76. J. Chen, X. Cao, Q. An, Y. Zhang, K. Li, W. Yao, F. Shi, Y. Pan, Q. Jia, W. Zhou, F. Yang, F. Wei, N. Wang and B. Yu, *Nat. Commun.*, 2018, **9**, 1406.
77. J.-H. Park, S. Chung, Y. Matsuo and Y. Nakamura, *MedChemComm*, 2017, **8**, 73-80.

78. H. Qin, C. Zhao, Y. Sun, J. Ren and X. Qu, *J. Am. Chem. Soc.*, 2017, **139**, 16201-16209.
79. M. Dean, T. Fojo and S. Bates, *Nature Rev. Cancer*, 2005, **5**, 275-284.
80. E. Batlle and H. Clevers, *Nat. Med.*, 2017, **23**, 1124.
81. S. S. Kanwar, Y. Yu, J. Nautiyal, B. B. Patel and A. P. Majumdar, *Mol. Cancer*, 2010, **9**, 212.
82. E. Chung, I. Oh and K. Y. Lee, *Ann. Surg. Treat. Res.*, 2016, **90**, 183-193.
83. S. Shaheen, M. Ahmed, F. Lorenzi and A. S. Nateri, *Stem Cell Rev. Rep.*, 2016, **12**, 492-499.
84. C. Naujokat and R. Steinhart, *J. Biomed. Biotechnol.*, 2012, **2012**, 1-17.
85. S. Zhou, F. F. Wang, E. T. Wong, E. Fonkem, T. C. Hsieh, J. M. Wu and E. Wu, *Curr. Med. Chem.*, 2013, **20**, 4095-4101.
86. P. B. Gupta, T. T. Onder, G. Jiang, K. Tao, C. Kuperwasser, R. A. Weinberg and E. S. Lander, *Cell*, 2009, **138**, 645-659.
87. V. Rajendran and M. V. Jain, *Cancer Stem Cells.*, 2018, 89-95
88. H. Qin, C. Zhao, Y. Sun, J. Ren and X. Qu, *J. Am. Chem. Soc.*, 2017, **139**, 16201-16209.
89. S. E. Howson, G. J. Clarkson, A. D. Faulkner, R. A. Kaner, M. J. Whitmore and P. Scott, *Dalton Trans.*, 2013, **42**, 14967-14981.

Chapter 4

Glycoconjugation of triplex metallohelices

4.1 Introduction

Cancer cells have significantly different metabolic requirements to most normal cells.[1] For instance, increased rates of glutaminolysis and lipid synthesis are observed in tumour tissue[2] and mitogenic signals promote nutrient uptake and the synthesis of DNA, RNA and proteins.[3] Such metabolic characteristics, which support high rates of cancer cell proliferation[4] and resist programmed cell death signals,[5] have raised interest in targeted metabolic enzymes and signalling pathways for cancer therapy.[6]

The Warburg effect, one of the most remarkable metabolic phenotypes of cancerous cells, describes the phenomenon whereby metabolism of glucose by anaerobic glycolysis (fermentation) is increased, even in the presence of oxygen.[1] This effect has been extensively studied as a hallmark of cancer over the past eight decades.[7] Two therapeutic strategies have been developed to exploit the Warburg effect: (i) interference with the signalling pathways and inhibition of metabolic enzymes involved in glycolysis by using small molecules such as 2-deoxy-D-glucose[8] and phloretin;[9] (ii) development of cytotoxins that are tethered to glucose or other sugar molecules *via* glycoconjugation in order to decrease the cytotoxicity and increase the anticancer selectivity *versus* the aglycone.[12] Substantial research has been conducted to investigate the latter strategy of glycoconjugation; the most widely exploited glycoconjugated anticancer agent is glufosfamide,[11] which demonstrated the comparable potency to that of its aglycone *in vitro* but less cytotoxicity *in vivo*. The

cellular uptake assay indicated that the entry of glufosfamide into cells was *at least partially* GLUT receptor-mediated.[12] We have not however been able to find further literature examples where any selectivity or activity improvement following glycoconjugation is shown convincingly to be a result of receptor mediation. One presumes that there are unreported examples where glycoconjugation has deleterious effects.

Nevertheless, the attempted use of glycoconjugation in cancer therapy – and the great challenge associated with synthesis of labile metal complexes with appended sugars – inspired us to design and synthesize such triplex metallohelices and explore the potential biological application. In this chapter, two different methodologies have been applied to achieve the glycoconjuation of metallohelix systems. The anticancer mechanism of activity for these compounds has been investigated both *in vitro* and *in vivo*.

4.2 Glycoconjugation of alkyne triplex metallohelices

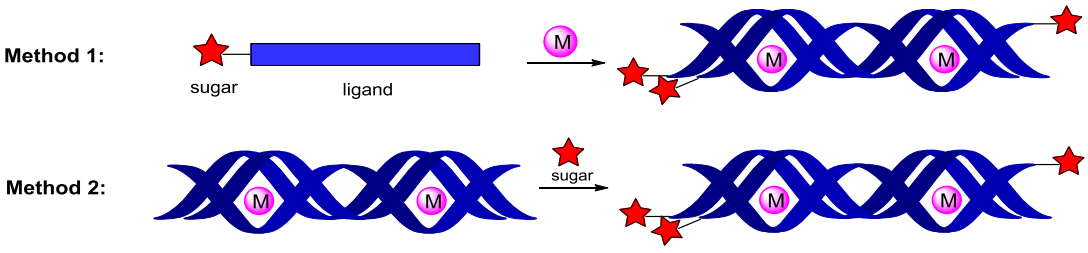

Figure 4-1 Two strategies to anchor sugars onto the triplex metallohelices

In this section, two methods for the assembly of sugar-appended triplex metallohelices are explored. (Figure 4-1). In Method 1, a sugar derivative of the single ligand strand component is synthesized initially, followed by subsequent self-assembly of the metal complex. This has the advantage of simplicity, but also some disadvantages: first, the hydroxyl or other oxygen/nitrogen donors within the sugar unit may bind to the metal

in competition with the intended diamine/bpy ligands, leading to mixtures of (paramagnetic) products; second, for each type of sugar that we wish to append to the metallohelix, a new ligand component must be synthesised. Both of these issues may be circumvented in Method 2, whereby a single triplex system synthesised by self-assembly is derivatised with a range of sugars. This of course depends on the stability of the triplex under the post-assembly reaction conditions.

4.2.1 Synthesis and self-assembly reactions of glyco-pyridine aldehydes (Method 1)

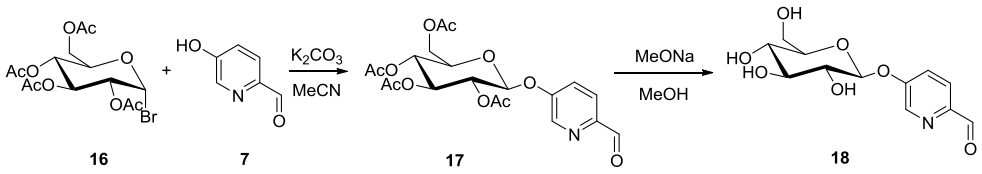

Scheme 4-1 Synthesis of glyco-pyridine aldehyde

Classically, the conjugation of sugar units to other molecules can be achieved using amide, ether, ester, thioester or glycosidic linkers;[13] such moieties are widely present in sugar-containing small organic units[14], peptides[15] and proteins.[16] For our triplex system, following a method for the etherification of similar sugar halides,[17] a prototype glycosylated sub-component was synthesised as shown in Scheme 4-1. Williamson ether synthesis using 5-(hydroxy)picolinaldehyde (**7**) and the C_1-bromo peracetylated glucose derivative **16** in the presence of K_2CO_3 in acetonitrile gave **17**. Acetyl deprotection with a catalytic amount of sodium methoxide in methanol gave **18**; as far as we aware this is the first example of a glyco-pyridine aldehyde. Notably, **18** is soluble in water, and in the presence of methanol it is in equilibrium with the hemiacetal, as observed by ^{1}H NMR spectroscopy.

Subsequently, both **17** and **18** were treated with the aminobipyridine **14** in the presence of metal salts in order to allow self-assembly of sugar-appended triplex metallohelices, as follows.

*Synthesis of $[Zn_2\boldsymbol{L^5}_3][ClO_4]_4$ from acetyl-protected sugar derivative **17***

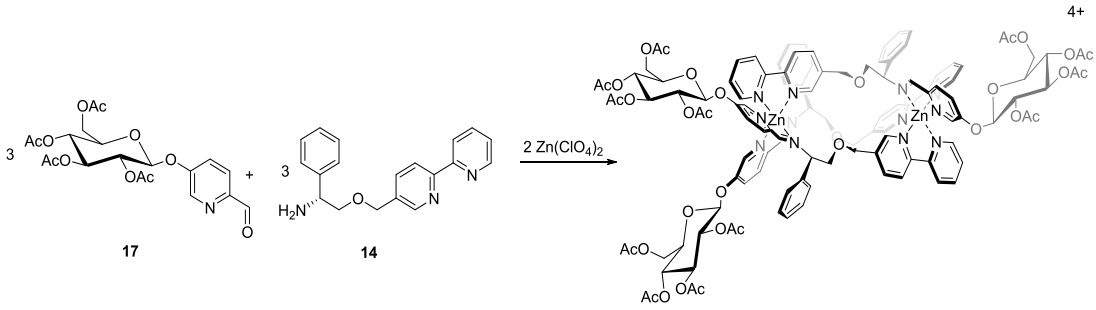

Scheme 4-2 Synthesis of the sugar appended (R_c,Δ_{Zn})-HHT-$[Zn_2L^5{}_3][ClO_4]_4$ triplex

We first attempted to synthesize zinc(II) sugar appended metallohelices since these will be rigorously diamagnetic, thus providing sharp NMR spectra in order to assist in validation of the method. The acetyl protected glycol-pyridine aldehyde was employed as it is soluble in acetonitrile. Following a similar procedure for the aglycones,[18] (*R*)-2-([2,2'-bipyridin]-5-ylmethoxy)-1-phenylethan-1-amine (**14**, 3 eq.) was added to peracetylated glyco-pyridine aldehyde **17** (3 eq.) and $Zn(ClO_4)_2{\cdot}6H_2O$ (2 eq.) in acetonitrile at ambient temperature (Scheme 4-2).

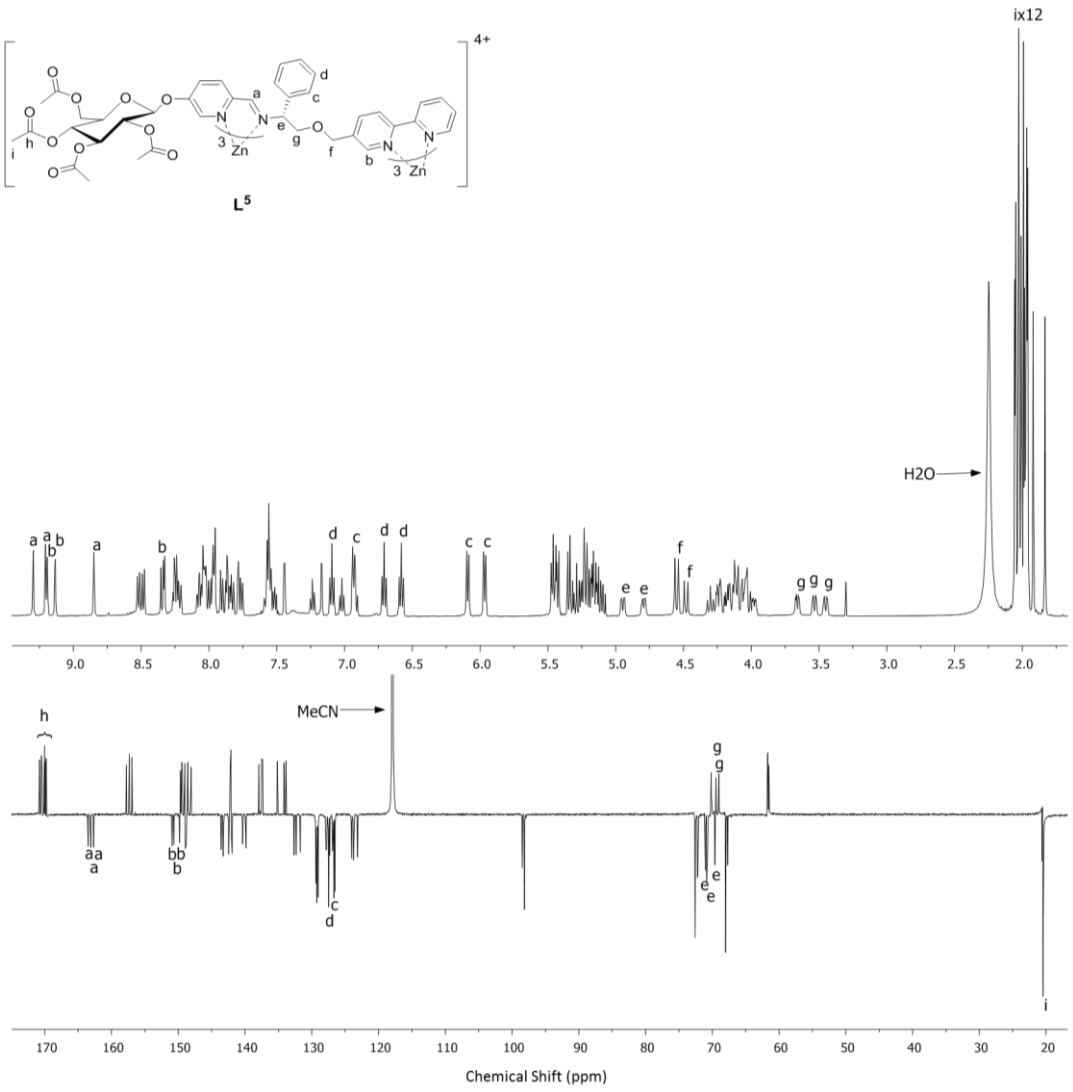

Figure 4-2 ^{1}H NMR (500 MHz, CD_3CN, 298K) and ^{13}C (125 MHz, CD_3CN, 298K) spectra of (R_c,Δ_{Zn})-HHT-[Zn_2**L**$^{5}_3$][ClO_4]$_4$.

^{1}H and ^{13}C NMR spectra are consistent with the highly selective formation of the asymmetric HHT triplex structure with three spectroscopically unique ligand environments (Figure 4-2). All the characteristic ^{1}H and ^{13}C peaks were assigned, including the presence of two bpy H resonances **b** at unusually low field indicating cross-helix H-bonding, and two sets of very high field shifted phenyl resonances **c** and **d** as a result of bifurcated π-stacking with adjacent bpy units – note that *e.g.* only one

doublet is seen for nuclei H^c for each arene as a result of flipping of the π-stack on this timescale.[19] Twelve acetyl Me (**i**) and carbonyl units (**h**) are expected and while the former overlap, most of the latter are well resolved. We also investigated whether the self-assembly reaction could withstand elevated temperatures; essentially identical ^1H and ^{13}C NMR spectra were obtained after heating to reflux for 48 h.

*Synthesis of $[Zn_2\mathbf{L^6}_3][ClO_4]_4$ from deprotected sugar derivative **18***

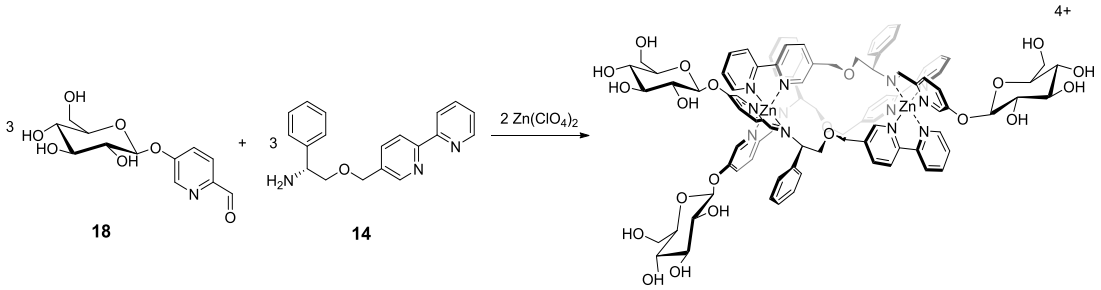

Scheme 4-3 Attempted synthesis of acetyl deprotect (R_c,Δ_{Zn})-HHT-$[Zn_2L^6_3][ClO_4]_4$

Due to the low solubility of glyco-pyridine aldehyde **18** in acetonitrile, the attempt to synthesize $[Zn_2L_3][ClO_4]_4$ from **18** and **14** in the presence of $Zn(ClO_4)_2$ was not achieved at ambient temperature (Scheme 4-3). However, following the heating of the reaction solution at reflux for 48 h, the $[Zn_2\mathbf{L^6}_3][ClO_4]_4$ was separated as yellow crystals following the addition of ethyl acetate.

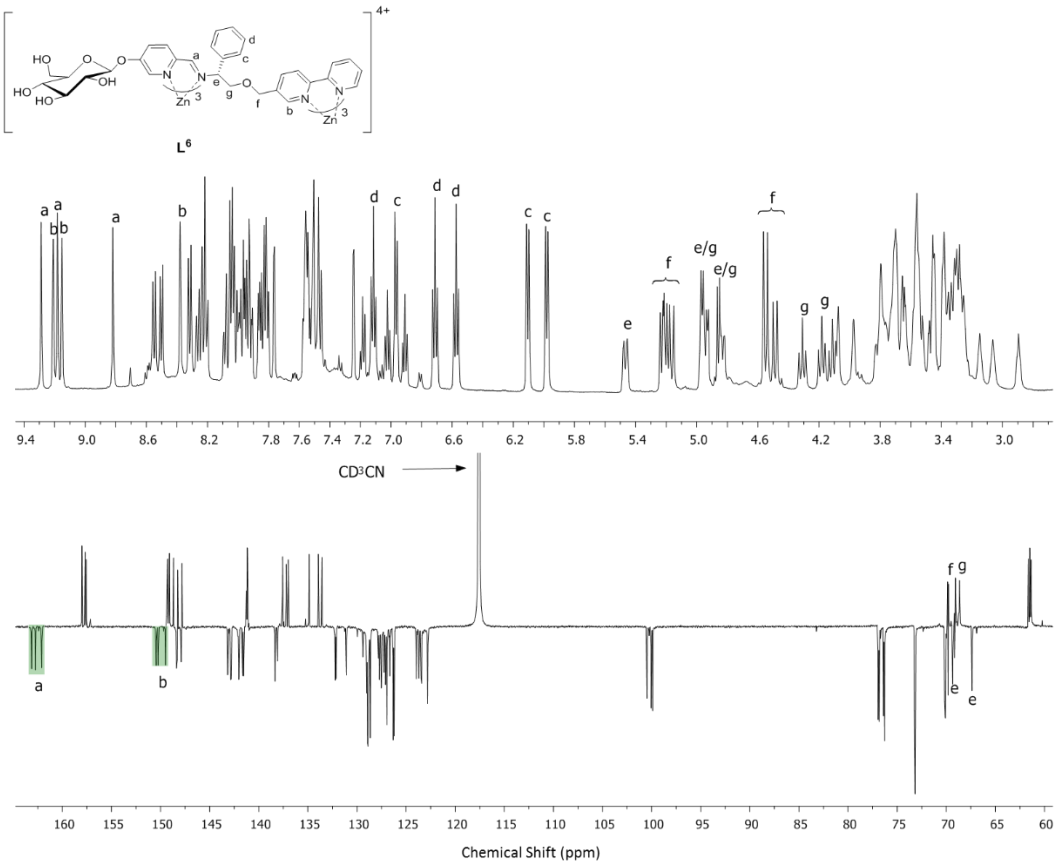

Figure 4-3 ^{1}H NMR (500 MHz, CD_3CN, 298K) and ^{13}C (125 MHz, CD_3CN, 298K) spectra of (R_c,Δ_{Zn})-HHT-[$Zn_2L^6{}_3$][ClO_4]$_4$

The ^{1}H and ^{13}C NMR spectra were well resolved and very similar to the acetyl protected compound [Zn_2**L^6**$_3$][ClO_4]$_4$ (Figure 4-3). The hydroxyl groups of the sugar dramatically increase the solubility of the zinc perchlorate complex such that NMR spectra are readily measureable in D_2O (Figure 4-4). This is the first example of a water-soluble zinc(II) metallohelix; perhaps the most astonishing aspect is that the cation in this perchlorate salt is not hydrolysed under these conditions in water, with no decomposition detected for at least one week. The prospect thus arises that we might be able to develop metallohelices for medicinal applications or biophysical studies based on colourless Zn(II) complexes rather than intensely coloured Fe(II) complexes.

These spectra (Figure 4-4) differ from those measured in CD_3CN (Figure 4-3) in that the peaks associated with the phenyl rings are significantly broadened. We suggest that this is due to the slowing of π-stack flipping in the more polar solvent. We previously noted that polar media promote the formation of π-stacked isomers in a model system.[20]

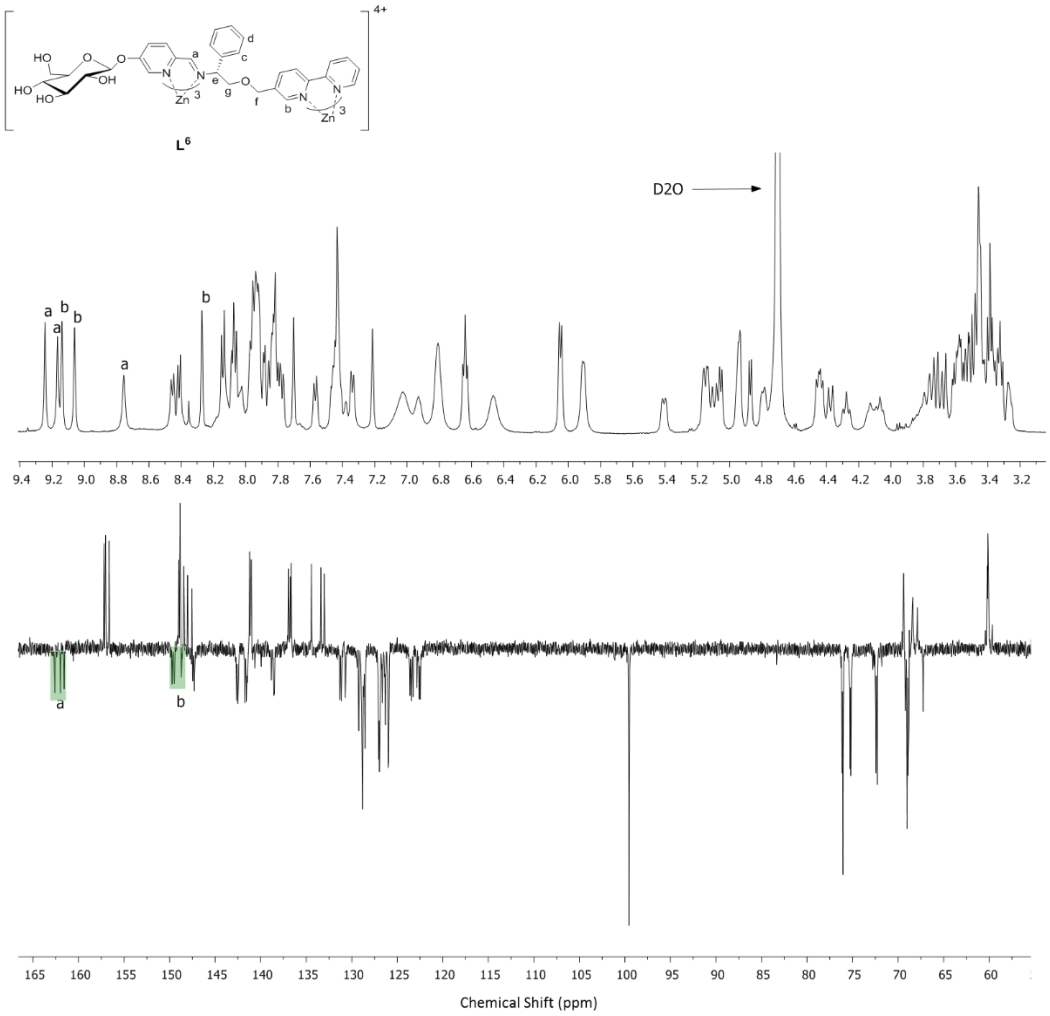

Figure 4-4 ^{1}H NMR (500 MHz, D_2O, 298K) and ^{13}C (125 MHz, D_2O, 298K) spectra of (R_c,Δ_{Zn})-HHT-$[Zn_2L^6{}_3][ClO_4]_4$

*Synthesis of [Fe_2**L**$^5{}_3$]Cl_4 from acetyl-protected sugar derivative **17***

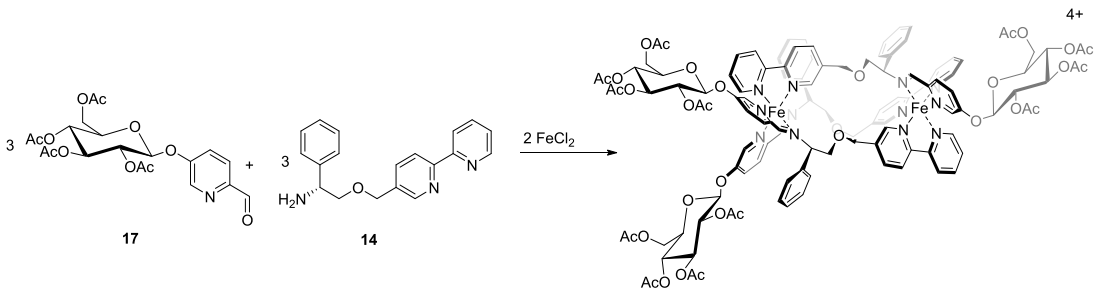

Scheme 4-4 The attempt to synthesis of the acetyl protect glucose appended (R_c,Δ_{Fe})-[$Fe_2L^5{}_3$]Cl_4 triplex

Following the successful self-assembly of the peracetylated glyco-pyridine aldehyde **17** with zinc(II) and amine **14** (Scheme 4-2), we attempted the synthesis of the iron(II) analogue (R_c,Δ_{Fe})-[Fe_2**L**$^5{}_3$]Cl_4 (Scheme 4-4). Mixing appropriate proportions of **14**, **17** and $FeCl_2$ in methanol led to the immediate formation of an intense purple solution. After heating for 48 h, the product was isolated as a semi crystalline purple solid following the addition of ethyl acetate.

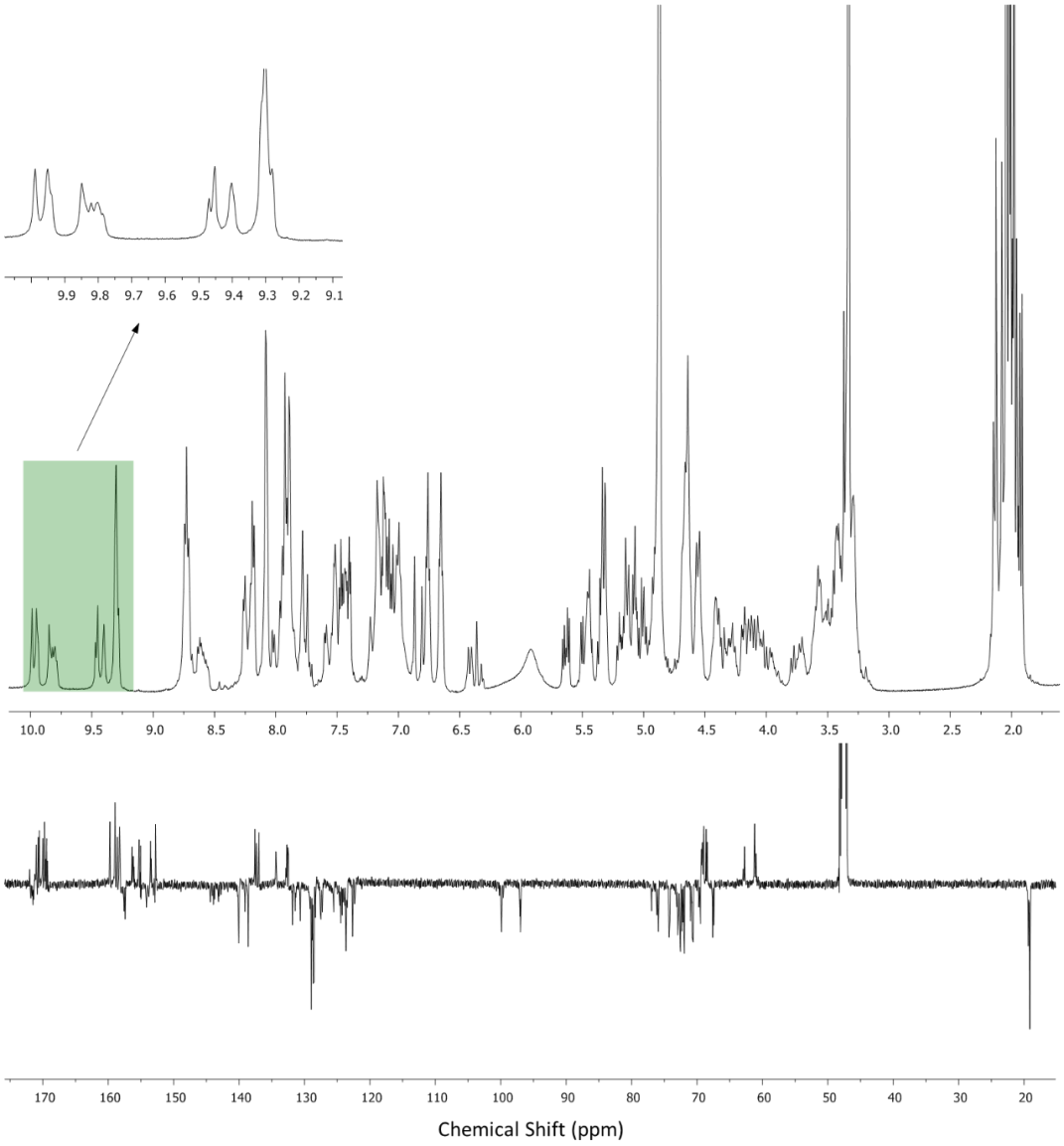

Figure 4-5 The ^{1}H NMR (500 MHz, MeOD, 298K) and ^{13}C NMR(125 MHz, MeOD, 298K) spectra of the acetyl protect glucose appended (R_c,Δ_{Fe})-[$Fe_2L^5{}_3$]Cl_4 triplex

In the region 10.0-9.2 ppm of the ^{1}H NMR spectrum, rather than the expected five singlets we observed a more complex set of peaks (Figure 4-5). The ^{13}C NMR spectrum is also more complicated than the zinc(II) perchlorate counterpart, notably with two clusters around 100 ppm arising from the sugar C_1 centres, where only one is observed above. This suggests that the phenomenon responsible for the presence of more than one species is associated with the C_1 centre.

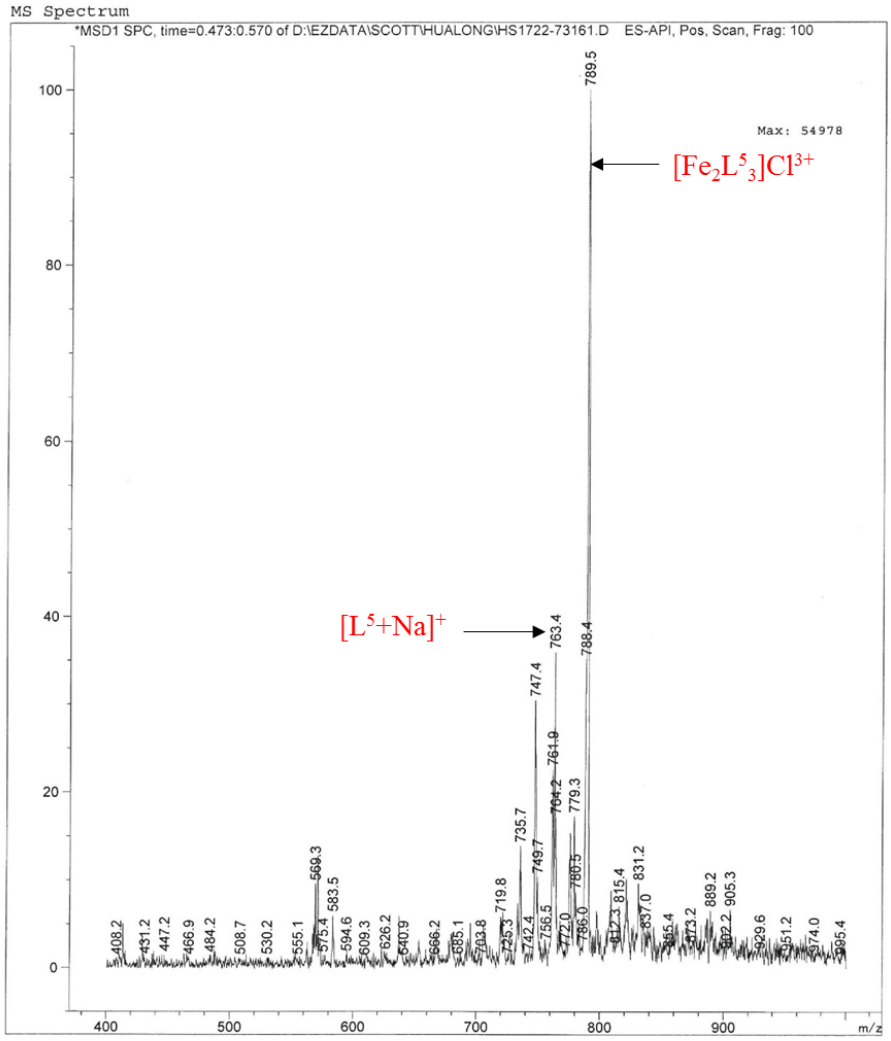

Figure 4-6 ESI mass spectrum of $[Fe_2L^5{}_3]Cl_4$ showing peaks for $[L^5+Na]^+$ and $\{[Fe_2L^5{}_3]Cl\}^{3+}$

Mass spectrometry shows the base peak of tricationic ion $\{[Fe_2\mathbf{L^5}_3]Cl\}^{3+}$ at 789.5, followed by the $[\mathbf{L^5}+Na]^+$ at 763.4 (Figure 4-6). No tetracationic molecular ion $[Fe_2\mathbf{L^5}_3]^{4+}$ was detected. The chloride ion is evidently not present in the inner coordination sphere since the NMR spectra indicate diamagnetism (*vide infra*).

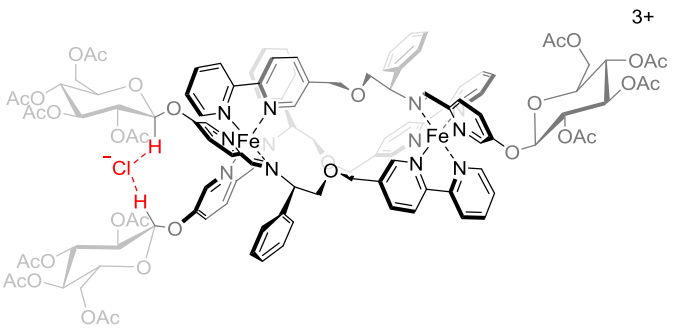

Figure 4-7 The proposed structure of the (R_c,Δ_{Fe})-$[Fe_2L^5{}_3Cl]^{3+}$ cation showing the hydrogen bonding of the chloride ion

On the basis that the tetracationic charge in the main triplex structure provides electrostatic binding, and that chelate H-bonding C_1-H···Cl^- is feasible at one end of the triplex,[21] we suggest that structures such as that shown in Figure 4-7 are responsible for the observations from mass spectrometry and the presence of unexpected species in the NMR spectra.

In order to test this idea, we explored the effects of solvent and anion. While (R_c,Δ_{Fe})-$[Fe_2\mathbf{L^5}_3]Cl_4$ is not very soluble in CD_3CN, leading to poor signal:noise, it is nevertheless clear that a similar mixture of species is present in this solvent. We were pleased to find that repeating the assembly reaction using $Fe(ClO_4)_2$ in the place of $FeCl_2$ gave essentially a single species (R_c,Δ_{Fe})-$[Fe_2\mathbf{L^5}_3][ClO_4]_4$ according to ^{1}H and ^{13}C NMR spectra, which were very similar to those of (R_c,Δ_{Zn})-$[Zn_2\mathbf{L^5}_3][ClO_4]_4$ (Figure 4-8). Unsurprisingly, no inclusion of perchlorate was detected by mass spectrometry.

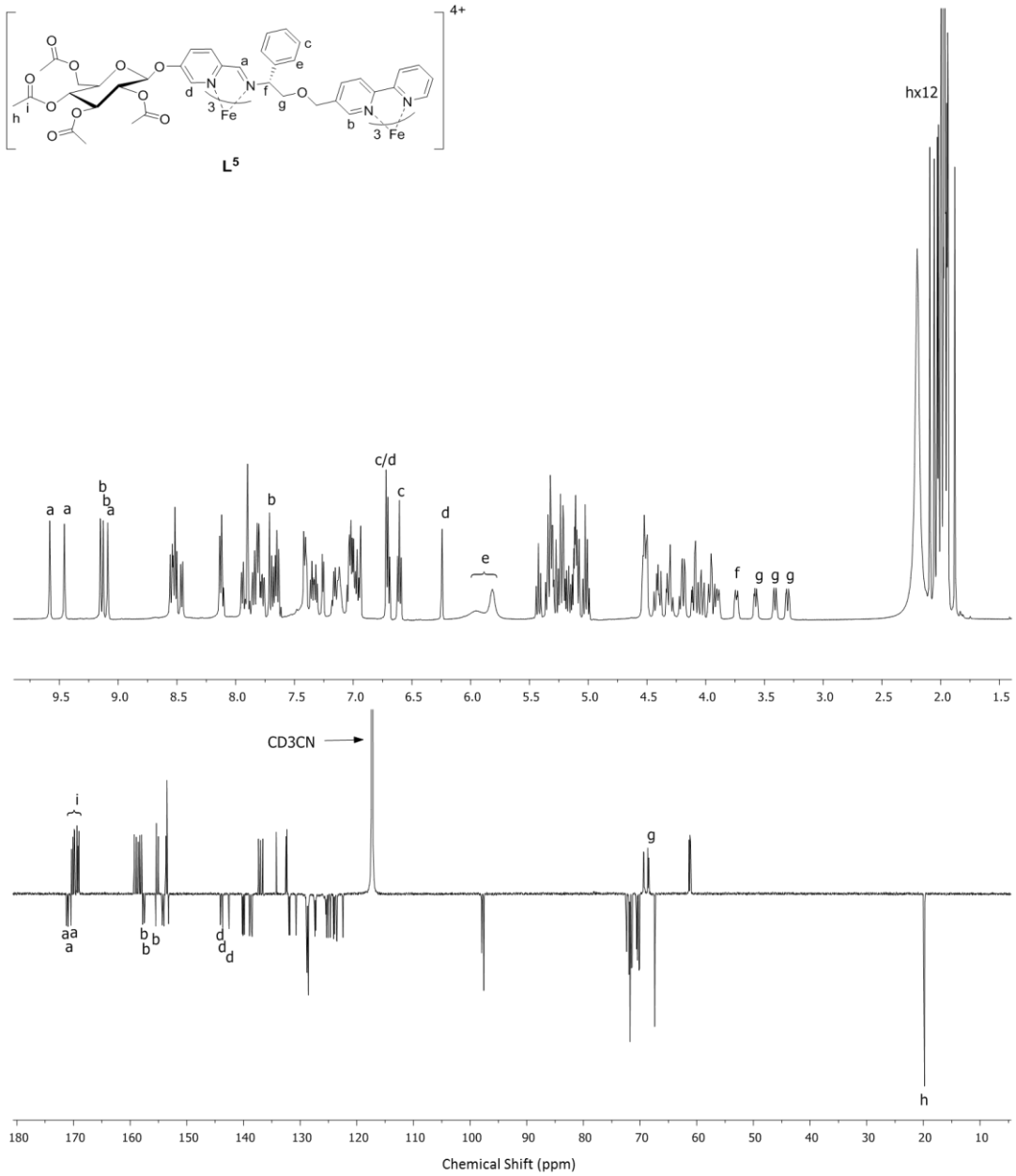

Figure 4-8 ^{1}H NMR (500 MHz, CD_3CN, 298K) and ^{13}C (125 MHz, CD_3CN, 298K) spectra of (R_c,Δ_{Fe})-HHT-[$Fe_2L^5{}_3$][ClO_4]$_4$

*Synthesis of [Fe_2**L**$^6{}_3$]Cl_4 from deprotected sugar derivative **18***

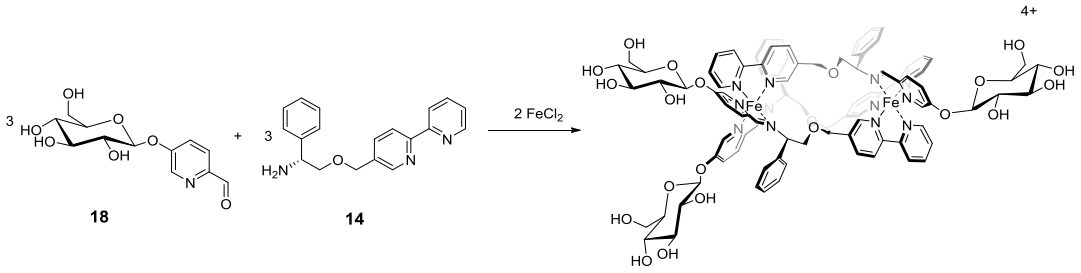

Scheme 4-5 The attempt to synthesis of (R_c,Δ_{Fe})-[$Fe_2L^6{}_3$]Cl_4 triplex

The self-assembly of glyco-pyridine aldehyde **18**, with bipyphenylamine **14** and $FeCl_2$ was also investigated, which again led to the rapid formation of purple solution from which purple microcrystals were isolated following addition of ethyl acetate after 2 d (Scheme 4-5).

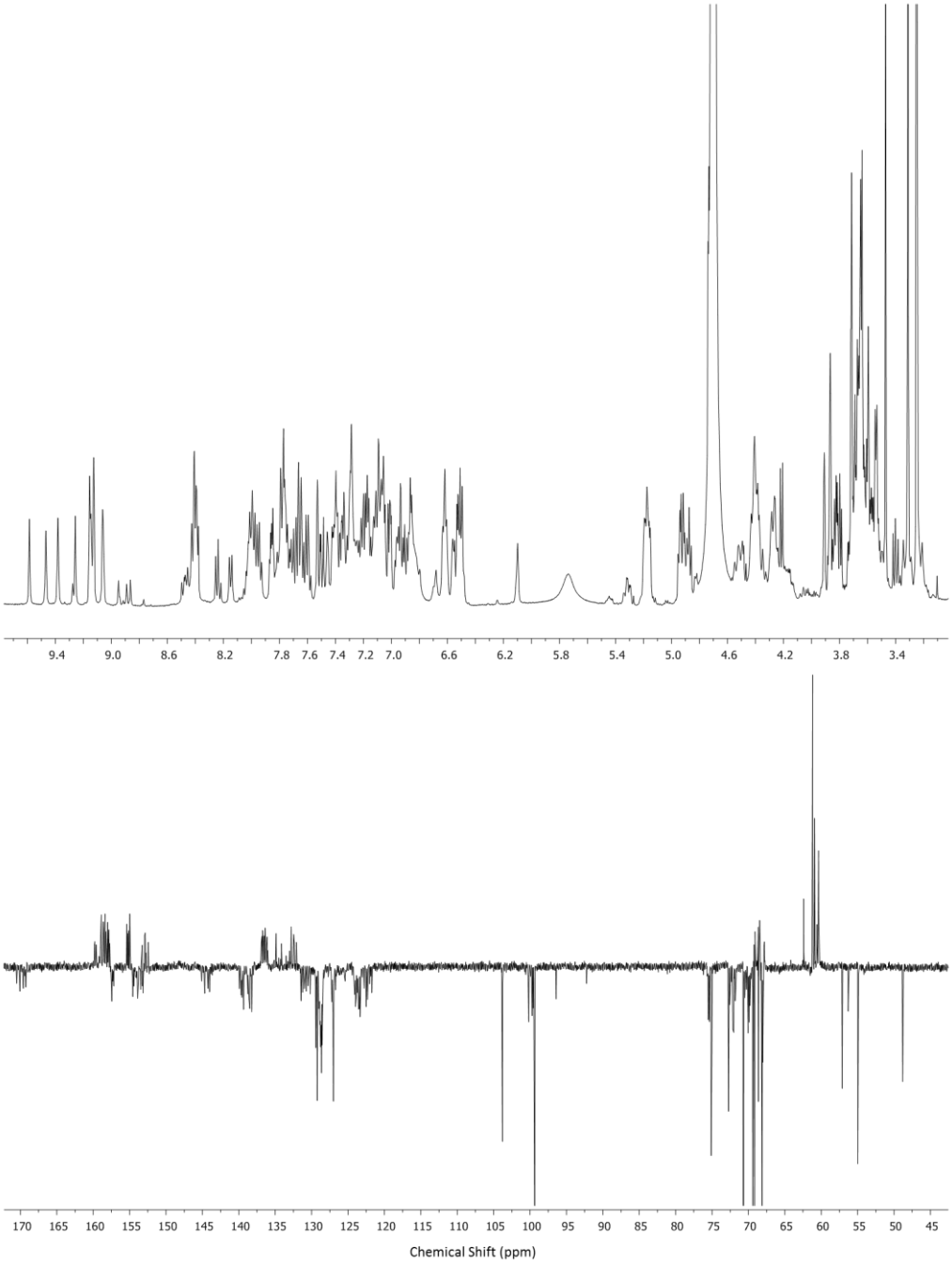

Figure 4-9 The ^{1}H NMR (500 MHz, D_2O, 298K) and ^{13}C NMR spectra (125 MHz, D_2O, 298K) of (R_c,Δ_{Fe})-[$Fe_2L^6{}_3$]Cl_4 triplex after 2 d reflux

The ^{1}H NMR spectrum (Figure 4-9) showed peaks in the low field region (9.80-8.70 ppm) consistent with the presence of two major and one minor HHT species. The ^{13}C NMR spectrum also displayed several peaks around 100 ppm which were ascribed to the C_1 carbon of various species. Coordination of Cl^- to the core triplex

tetracation is possible in the case of the deptrotected sugar via a number of modes – perhaps the above detected species differ for example in the facial coordination mode. However, the $[Fe_2\mathbf{L^6}_3Cl]^{3+}$ ion was not detected by ESI mass spectrometry.

Assembly of the same glyco-pyridine aldehyde **18** and bipyphenylamine **14** with $Fe(ClO_4)_2$ led to the formation of (R_c,Δ_{Fe})-$[Fe_2\mathbf{L^6}_3][ClO_4]_4$. The ^1H spectrum shows principally five characteristic singlets at 9.5-9.0 ppm, as for the zinc analogue (R_c,Δ_{Zn})-$[Zn_2\mathbf{L^6}_3][ClO_4]_4$ (Figure 4-10). The tetracationic molecular ion $[Fe_2\mathbf{L^6}_3]^{4+}$ was observed at 457.4 in the mass spectrum, whereas no tricationic ion $[Fe_2\mathbf{L^5}_3(ClO_4)]^{3+}$ was detected. Similar to the zinc(II) analogue, the presence of twelve hydroxyl groups improves the solubility of the structure, such that even as a perchlorate salt excellent NMR spectra could be obtained in D_2O (Figure 4-11). The presence of a minor component of apparently HHH structure is indicated in the ^1H NMR spectrum of Figure 4-10 measured in CD_3CN although the appearance of the same sample in D_2O is very different.

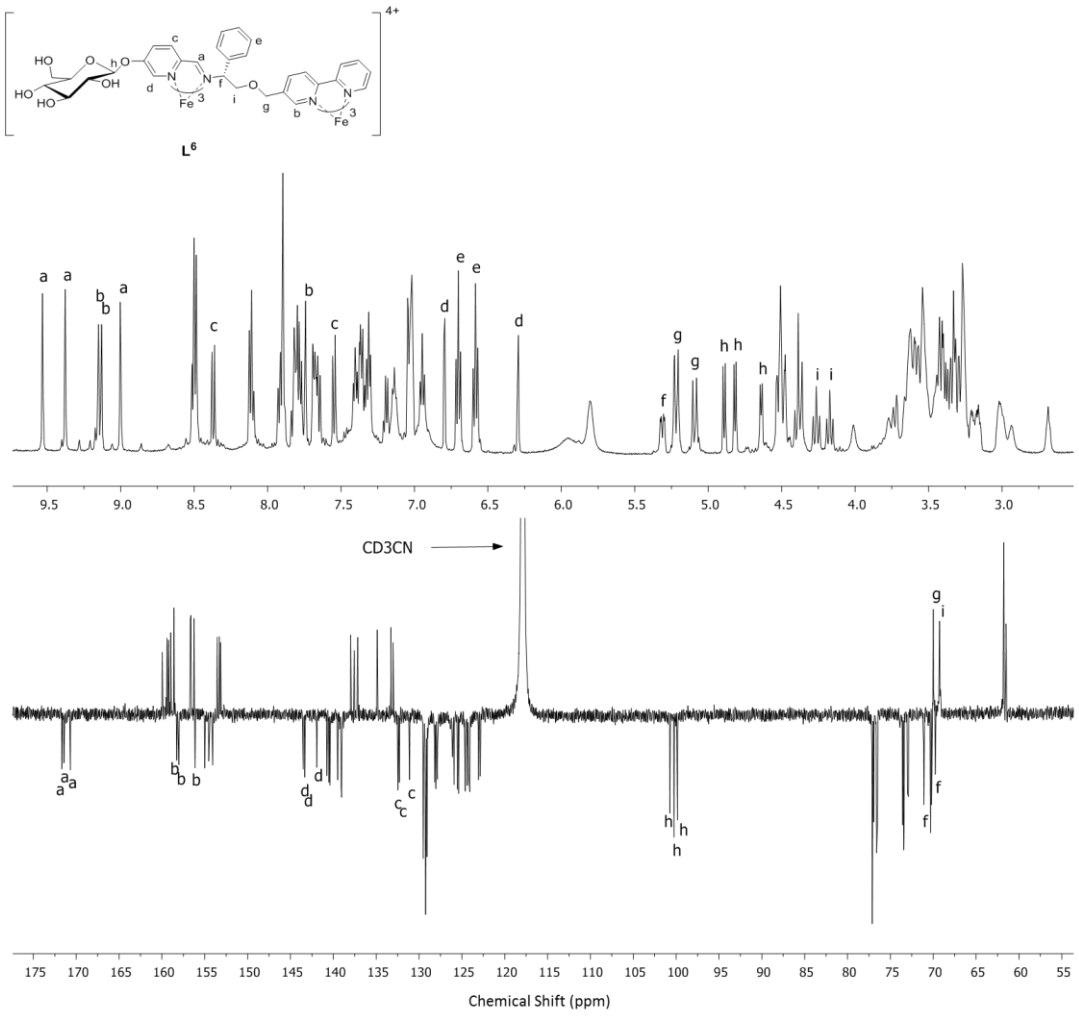

Figure 4-10 ^{1}H NMR (500 MHz, CD_3CN, 298K) and ^{13}C (125 MHz, CD_3CN, 298K) spectra of (R_c,Δ_{Fe})-HHT-[$Fe_2L^6{}_3$][ClO_4]$_4$

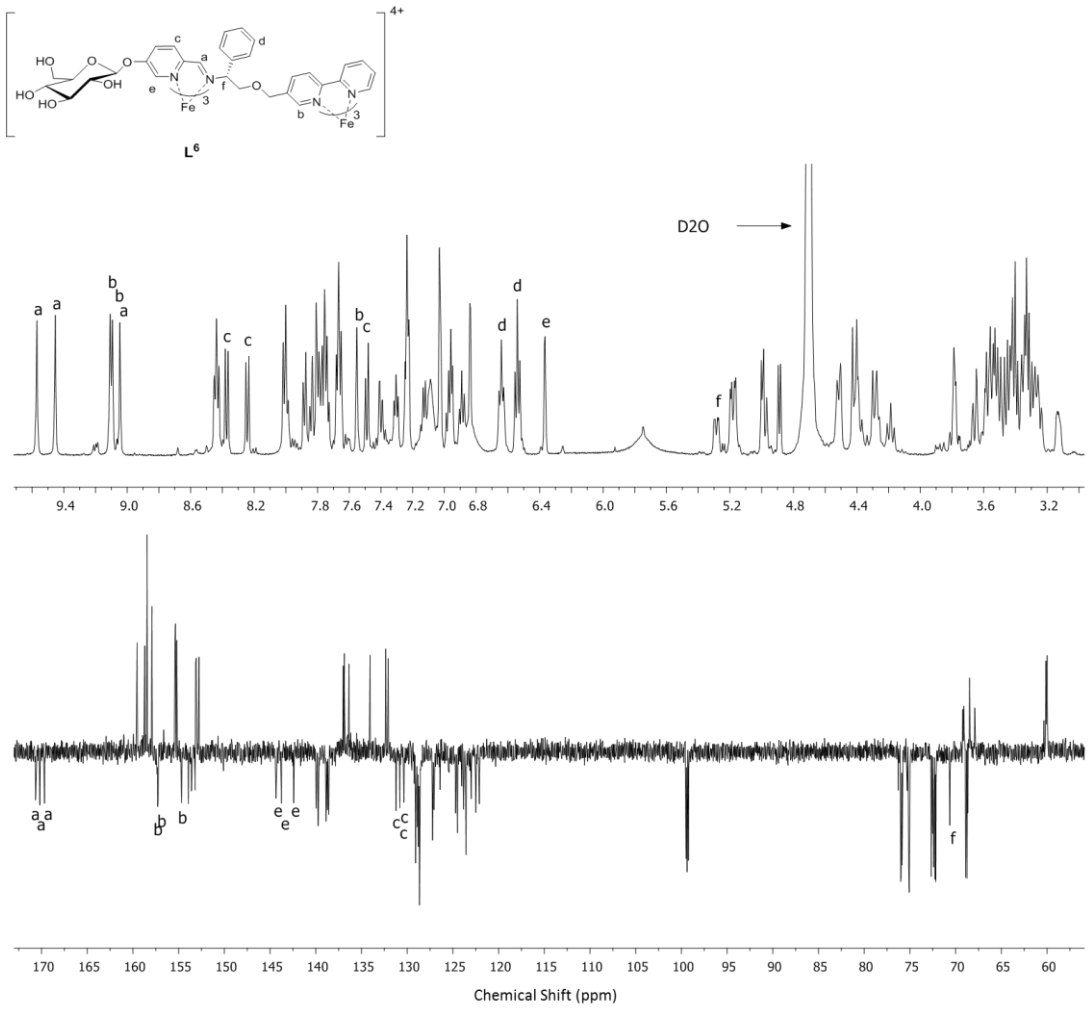

Figure 4-11 ^{1}H NMR (500 MHz, D_2O, 298K) and ^{13}C (125 MHz, D_2O, 298K) spectra of (R_c,Δ_{Fe})-HHT-$[Fe_2L^6{}_3][ClO_4]_4$

In conclusion for glycoconjugation strategy Method 1, the sugar ligand subcomponents i.e. glyco-pyridine aldehydes 17/18 have been synthesized. The acetyl protected $[M_2L^5{}_3][ClO_4]_4$ (M = Zn, Fe) and acetyl deprotected $[M_2L^6{}_3][ClO_4]_4$ metallohelices were formed and well characterized. Intriguingly, both acetyl deprotected $[Zn_2L^{63}][ClO_4]_4$ and $[Fe_2L^6{}_3][ClO_4]_4$ exhibit substantial water solubility. The same ligand components gave the mixture of species $[Fe_2L^5{}_3]Cl_4$ and $[Fe_2L^6{}_3]Cl4$ due to the presence of intramolecular hydrogen bonding between Cl^- and C1 proton or OH.

4.2.2 Method two: Synthesis of glycoconjugated triplex metallohelix *via* CuAAC

The successful use of CuAAC chemistry to attach aromatic azides to the triplex metallohelices was described in Chapter 3. In this section, we attempt to click sugar azides onto pre-formed alkyne triplex metallohelices, using the same strategy. Due to their documented involvement in cancer cell metabolism, β-glucose[23], β-galactose[24], 2-deoxy-D-glucose[25], α-mannose[26], β-*N*-acetylglucosamine[27] and β-*N*-acetylgalactosamine[28] were selected as sugar moieties to click onto the alkyne triplex metallohelices via their azide derivatives.

Synthesis of sugar azides

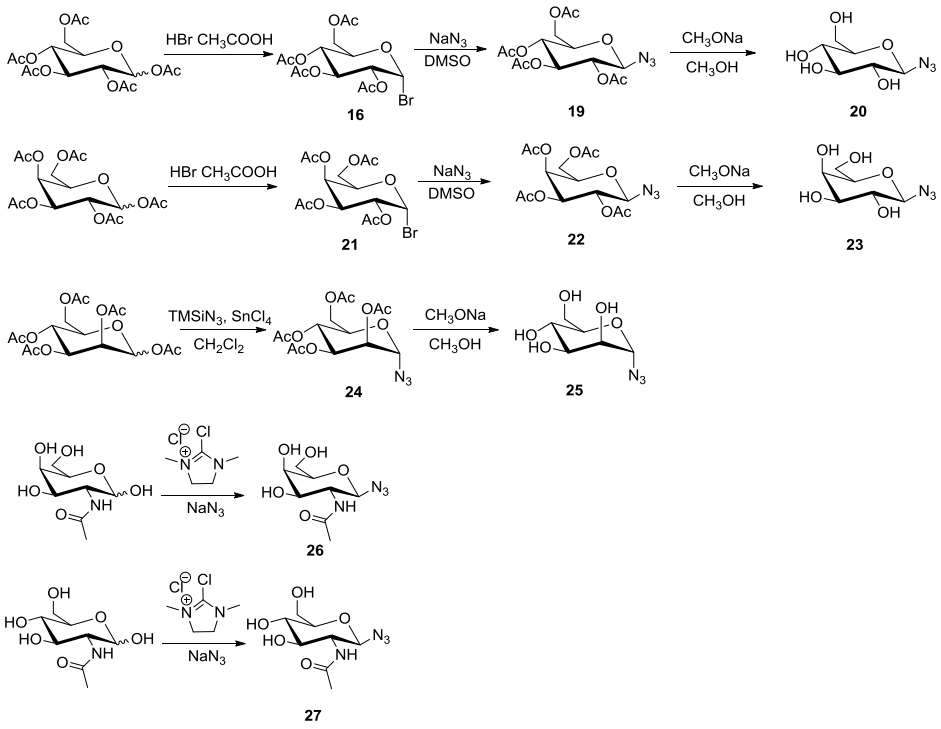

Scheme 4-6 Synthesis of the sugar azides

The synthesis of β-D-glucopyranosylazide was adapted from a literature procedure (Scheme 4-6).[29,30] D-Glucopyranosyl pentaacetate (from D-glucose and acetic anhydride) in dry CH_2Cl_2 was treated dropwise with a solution of HBr in AcOH to

form D-glucopyranosyl bromide (**16**). This was converted quantitatively to 2,3,4,6-tetra-*O*-acetyl-β-D-glucopyranosylazide (**19**) using sodium azide in DMSO. Deprotection using sodium methoxide was followed by neutralization using cationic ion-exchange resin (Dowex® 50WX4 hydrogen form), then filtration and evaporation afforded β-D-glucopyranosylazide (**20**) as a colourless oil. β-D-Galactopyranosylazide (**23**) was synthesised using the same method.[30] β-D-Mannopyranosylazide cannot be synthesised with the same method, but α-D-mannopyranosylazide (**25**) was achieved *via* the following synthetic method:[30] azidotrimethylsilane ($TMSiN_3$), tin tetrachloride ($SnCl_4$) and D-mannopyranosyl pentaacetate were added in dry CH_2Cl_2 solution under nitrogen to form 1,2,3,4,6-Penta-*O*-acetyl-α-D-mannopyranosylazide (**24**), which was deprotected with sodium methoxide to form **25**. β-*N*-acetylgalactosamine azide (**26**) and β-*N*-acetylglucosamine azide (**27**) were provided by Dr Joji Tanaka from the Perrier group, Warwick University.[31]

Synthesis of acetyl protect glucose $[Zn_2\mathbf{L}^{7a}{}_3][ClO_4]_4$ triplex via CuAAC

β-D-Glucopyranosyl pentaacetate azide (**19**) (4.5 eq.) and (R_c,Δ_{Zn})-HHT-$[Zn_2\mathbf{L}^{3}{}_3][ClO_4]_4$ (1 eq.) were dissolved in acetonitrile in the presence of copper(I) iodide (0.1 eq.). The solution was heated at 65˚C under reduced pressure for 18h. The resulting suspension was filtered through Celite to remove precipitated copper salts and the final product was isolated as a white/yellow solid upon the addition of ethyl acetate.

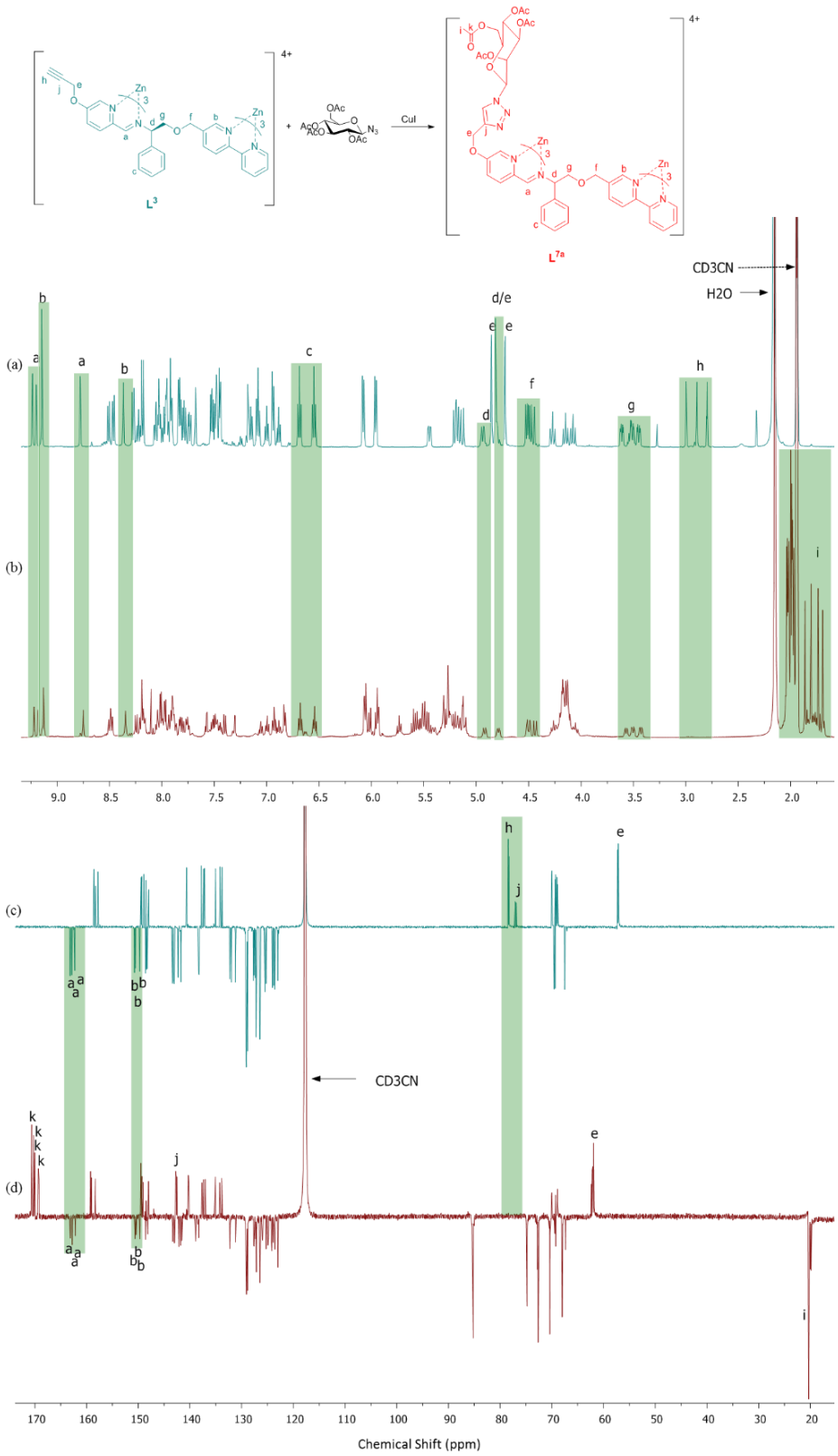

Figure 4-12 ^{1}H NMR spectra (500 MHz, CD_3CN, 298K) of (a) (R_c,Δ_{Zn})-HHT-[Zn_2**L**$^{3}_{3}$][ClO_4]$_4$, (b) (R_c,Δ_{Zn})-HHT-[Zn_2**L**$^{7a}_{3}$][ClO_4]$_4$; ^{13}C NMR spectra (125 MHz, CD_3CN, 298K) of (c) (R_c,Δ_{Zn})-HHT-[Zn_2**L**$^{3}_{3}$][ClO_4]$_4$, (d) (R_c,Δ_{Zn})-HHT-[Zn_2**L**$^{7a}_{3}$][ClO_4]$_4$;

As seen in the ^{1}H NMR spectra [Figure 4-12(a); (b)], the three alkyne singlets H^{h} (3.0-2.8 ppm) are no longer observed following the click reaction. The three sharp singlets H^{e} at 4.85, 4.81, 4.72 ppm [Figure 4-12(a)], which were assigned to the C*H*$_2$-alkyne groups, shift to higher frequency and overlap with sugar protons at *ca* 5.30 ppm [Figure 4-12(b)]. The new multiple singlets H^{i} at 2.08-1.64 ppm [Figure 4-12(b)] overlapping with CD_3CN peaks are due to acetyl groups of β-D-glucopyranosyl pentaacetate. The characteristic peaks such as three imine singlets H^{a}, three bpy singlets H^{b} and the phenyl ring protons H^{c} marginally shift in both ^{1}H NMR spectra, indicating that the core triplex architecture is retained during the click reaction.

The ^{13}C NMR spectra [Figure 4-12(c); (d)] are also consistent with complete conversion of the sugar click reaction as shown by the disappearance of alkyne carbon signals C^{h} [Figure 4-12(c)] and presence of triazole C_4 carbon C^{j} [*ca* 142 ppm Figure 4-12(d)]. Multiple signals C^{k} at *ca* 170.0 ppm are sugar carbonyl groups, accompanied with strong methyl carbon signals C^{i} found at *ca* 20.0 ppm. The three pyridine-*O*-*C*H$_2$-R carbons C^{e} shifted to higher frequency from *ca* 56.9 ppm to *ca* 62.2 ppm as a result of conjugating with the triazole, a stronger electronic withdrawing group than the alkyne. The three imine carbons C^{a} and three bpy carbons C^{b} were unperturbed by the click reaction.

Synthesis of CuAAC glycoconjugated Fe(II) triplex

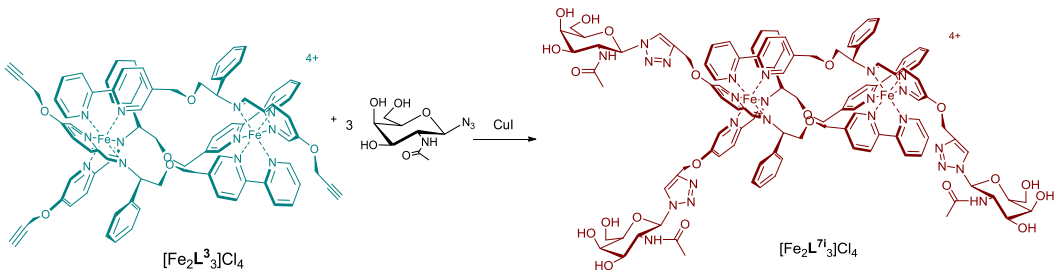

Scheme 4-7 Synthesis of CuAAC glycoconjugated Fe(II) triplex metallohelices

The Fe(II) sugar clicked triplex was synthesized in an analogous fashion to the Zn(II) sugar clicked triplex. β-*N*-Acetylgalatosmaine azide (4.5 eq.) and (R_c,Δ_{Fe})-HHT-[Fe_2**L**$^3{}_3$]Cl_4 (1 eq.) were dissolved in methanol (20 ml) in the presence of copper (I) iodide (1 eq.) (Scheme 4-7). The reaction was heated at 65˚C under reduced pressure for 18h. After cooling, the suspension was filtered and the purple product was isolated by the addition of ethyl acetate.

The ^{1}H NMR spectra [Figure 4-13(a);(b)] confirm that the click reaction has proceeded to completion alkyne singlets H$^{\mathbf{g}}$ at 3.05, 2.84 and 2.79 ppm [Figure 4-13(a)] are no longer present and triazole signals H$^{\mathbf{h}}$ at 8.28, 8.17 and 8.06 ppm **[**Figure 4-13(b)] appear. The multiplets H$^{\mathbf{i}}$ between 5.76-5.62 ppm [Figure 4-13(b)] are due to the C_1 proton of β-*N*-acetylgalactosamine units overlapping with broad phenyl protons. The three singlets H$^{\mathbf{k}}$ at 1.71, 1.55, 1.51 ppm [Figure 4-13(b)] arise from methyl protons of the acetyl groups.

The ^{13}C NMR spectra [Figure 4-13(c);(d)] also confirm the completion of the click reaction through the absence of alkyne carbon signals C$^{\mathbf{g}}$ and C$^{\mathbf{f}}$ [Figure 4-13(c)] and the presence of the triazole carbon signal C$^{\mathbf{f}}$ at *ca* 142.0 ppm [Figure 4-13(d)]. The pyridine-*O*-*C*H_2-R carbon signal C$^{\mathbf{e}}$ has shifted to higher frequency from *ca* 56.0 ppm to *ca* 60.9 ppm. The carbonyl signals C$^{\mathbf{j}}$ and methyl signals C$^{\mathbf{k}}$ of the acetyl group were found at *ca* 174.0 and *ca* 21.6 ppm, respectively.

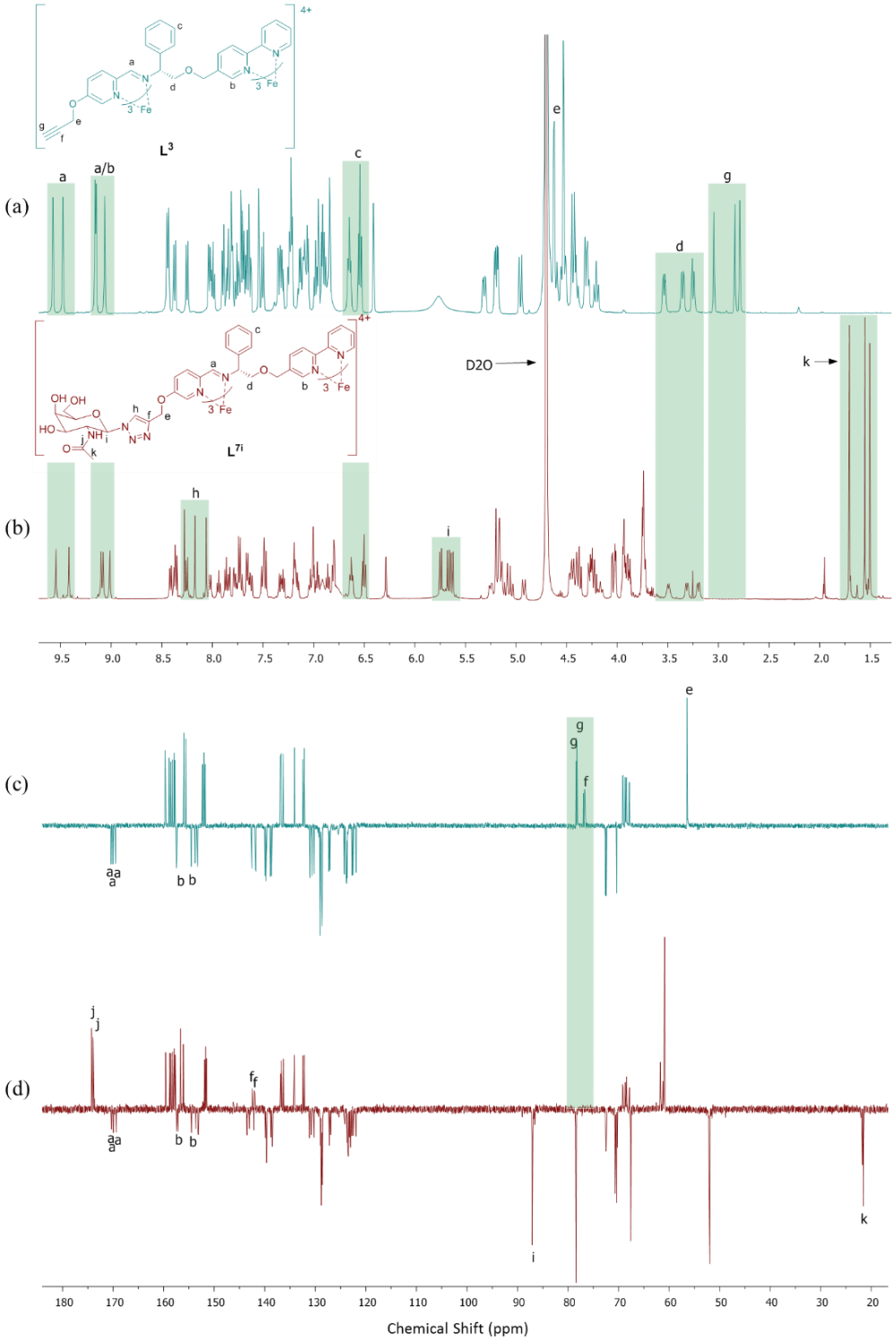

Figure 4-13 ^{1}H NMR spectra (500 MHz, D_2O, 298K) of (a) (R_c,Δ_{Fe})-HHT-[$Fe_2L^3{}_3$]Cl_4, (b) (R_c,Δ_{Fe})-HHT-[$Fe_2L^{7i}{}_3$]Cl_4; ^{13}C NMR spectra (125 MHz, D_2O, 298K) of (c) (R_c,Δ_{Fe})-HHT-[$Fe_2L^3{}_3$]Cl_4, (d) (R_c,Δ_{Fe})-HHT-[$Fe_2L^{7i}{}_3$]Cl_4

The CD spectra of the diastereomers [Fe_2**L**$^{7i}{}_3$]Cl_4 in methanol gave equal and opposite signals, and mimic the features of the aglyconic triplex isomers [Fe_2**L**$^{3}{}_3$]Cl_4

[Figure 4-14(a)]. The sugar clicked compounds were found to be remarkably stable under aqueous conditions. (R_c,Δ_{Fe})-HHT-[$Fe_2\mathbf{L}^{7i}_3$]Cl_4 gave a high resolution electrospray mass spectrometry peak at *m/z* 548.9335 Da for the tetracationic molecular ion, which is within 0.001 Da of the calculated value (548.9325) for $C_{108}H_{114}N_{24}O_{21}{}^{56}Fe_2$ [Figure 4-14(b)]; no chloride coordination was detected.

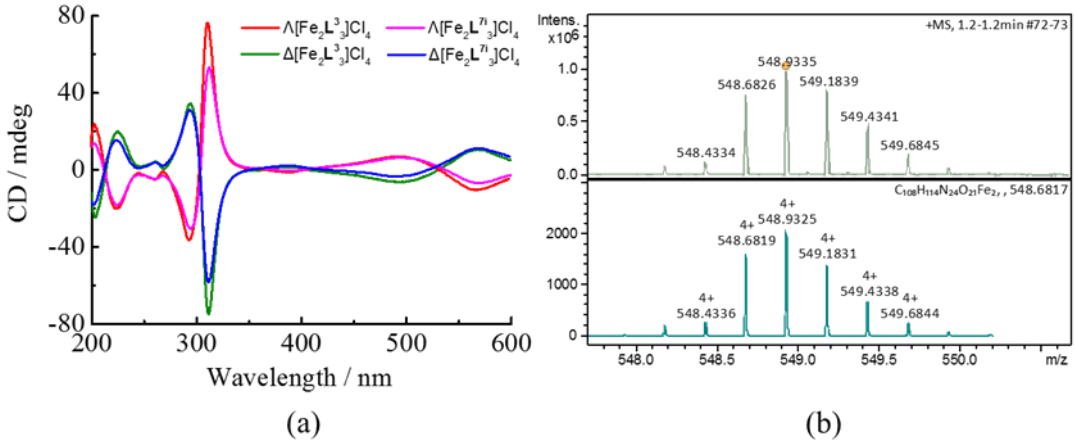

Figure 4-14 (a) CD spectra for alkyne triplex isomers [$Fe_2L^3_3$]Cl_4 and β-N-acetylgalatosmaine clicked isomers of [$Fe_2L^{7i}_3$]Cl_4 in methanol; (b) High resolution mass spectrometry for (R_c,Δ_{Fe})-HHT-[$Fe_2L^{7i}_3$]Cl_4: top measured, below calculated.

Other sugar clicked triplex metallohelices were synthesised using the same procedure. CHN elemental analyses were also consistent with the proposed formula of each metallohelix.

4.3 Biological activity of CuAAC glycoconjugated triplex metallohelices

While to our delight all the above synthetic glycoconjugation strategies were successful, Method 2 was judged to give the greatest diversity most rapidly, and did

not suffer from the complication of Cl^- coordination of some compounds from Method 1. We thus chose this small library for further study.

4.3.1 *In vitro* cytotoxicity assay

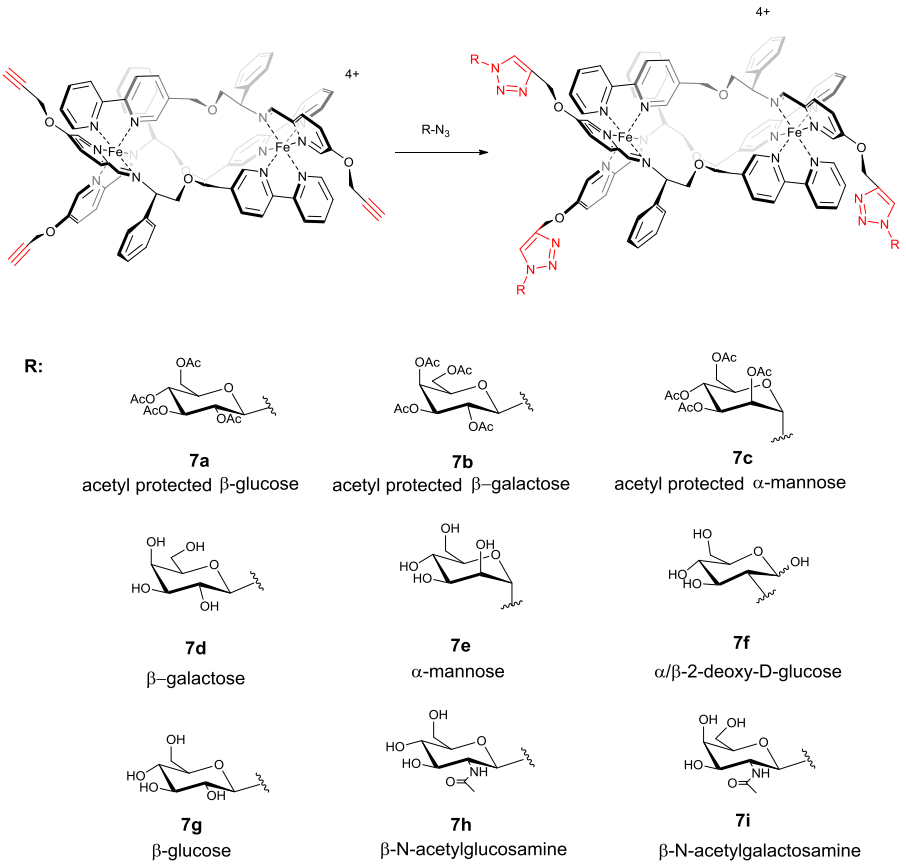

Figure 4-15 Structure of glycoconjugation triplex compounds via CuAAC

The 18 new CuAAC glycoconjugated Fe(II) triplex metallohelices of Figure 4-15 were screened alongside the alkyne triplex $[Fe_2\mathbf{L^3}_3]Cl_4$ for their activity and selectivity against cancer cell lines HCT116 $p53^{++}$ (human colon carcinoma with wild-type p53) and the healthy cell line ARPE19 (human retinal pigment epithelial cells). This work was partially conducted by Dr Samantha Shepherd in Huddersfield University. The IC_{50} values obtained from triplicate measurements are given in Figure 4-16, Figure 4-17, and are plotted in Table 4-1.

Cytotoxicity for HCT116 p53^{++} cancer cell line. The potency of all CuAAC glycoconjugated triplex metallohelices [Fe_2**L**$^{7a\text{-}i}{}_3$]Cl_4 varies from 630 nM to 10.70 μM (Figure 4-16). A significant difference in the potency was observed between diastereomers; Λ metallohelices were at least twice potent than the Δ enantiomers. The hydroxyl groups on the sugar significantly affect the drug potency as the cytotoxicity of the acetyl protected sugar compounds [Fe_2**L**$^{7a\text{-}c}{}_3$]Cl_4 decreased substantially relative to their deprotected counterparts [Fe_2**L**$^{7d\text{-}f}{}_3$]Cl_4. Investigations of structure-activity relationships revealed that the potency depended upon the sugar moiety, with activity decreasing in the following order: galactose **L**^{7d} > glucose **L**^{7g} > acetylglucosamine **L**^{7i} > deoxy-glucose **L**^{7f} > mannose **L**^{7e}> three acetyl protect sugar clicked compounds (**L**$^{7a\text{-}c}$)> acetylgalactosamine **L**^{7i}. The most potent compound is the Λ enantiomer of the galactose clicked triplex [Fe_2**L**$^{7d}{}_3$]Cl_4 with IC_{50} 630 nM.

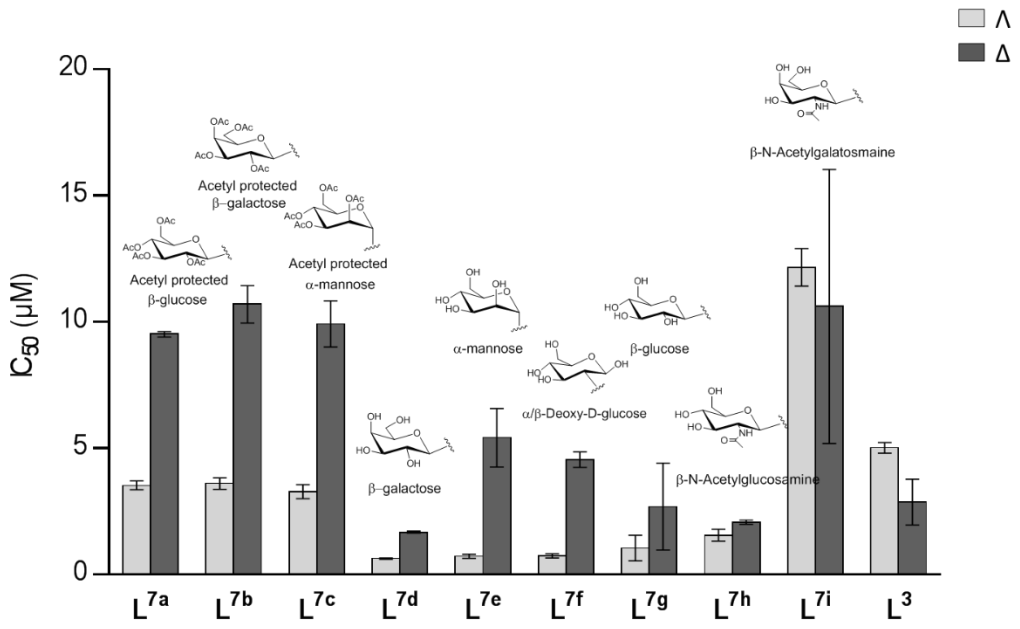

Figure 4-16 IC_{50} values of CuAAC glycoconjugated triplexes [Fe_2**L**$^{7a\text{-}i}{}_3$]Cl_4 and alkyne triplex [Fe_2**L**$^{3}{}_3$]Cl_4 against HCT116 p53^{++}

Cytotoxicity for ARPE19 noncancerous cell line. In a similar fashion to the HCT116 p53^{++} cancer cell line, the cytotoxicity difference between the enantiomers is also

remarkable *i.e.* all Λ type of metallohelices (with average IC_{50} value at 10 μM) demonstrated over 5 fold increase in toxicity with respect to the Δ diastereomers (average IC_{50} value over than 55 μM) (Figure 4-17). Compared with alkyne $[Fe_2\mathbf{L^3}_3]Cl_4$, all Λ glycoconjugated metallohelices showed increased toxicity whereas Δ counterparts possess much more moderate and similar cytotoxicity. Among the glycoconjugated metallohelices, the IC_{50} of $\Delta[Fe_2\mathbf{L^{7i}}_3]Cl_4$ (acetylgalatosmaine clicked) was extraordinarily high at 315.35 μM, which is desirable in normal cells to reduce unwanted side effects.

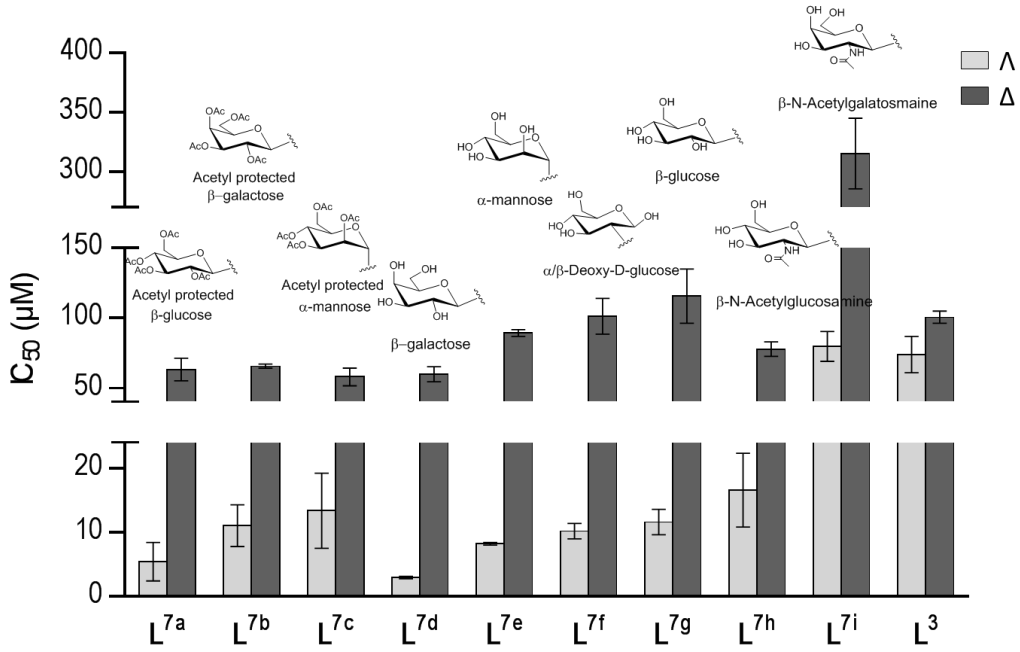

Figure 4-17 IC_{50} values of CuAAC glycoconjugated triplexes $[Fe_2\mathbf{L^{7a\text{-}i}}_3]Cl_4$ and alkyne triplex $[Fe_2\mathbf{L^3}_3]Cl_4$ against ARPE19 (noncancerous cell line)

Selectivity index. The selectivity index can be calculated by dividing the ARPE-19 IC_{50} value with that of the HCT116 $p53^{++}$cells. In conclusion, all the Δ enantiomers have much better selectivity than Λ enantiomers (Table 4-1). Structure-activity relationships demonstrated that selectivity of the sugar metallohelices decreased in the following order: glucose $\mathbf{L^{7g}}$ > acetylglucosamine $\mathbf{L^{7h}}$ > galactose $\mathbf{L^{7d}}$ >

acetylgalactosamine $\mathbf{L^{7i}}$> deoxy-glucose $\mathbf{L^{7f}}$ > mannose $\mathbf{L^{7e}}$ > all acetyl protected sugar clicked compounds $\mathbf{L^{7a\text{-}c}}$. The most potent compounds are $\Delta[Fe_2\mathbf{L^{7g}}_3]Cl_4$ (glucose clicked) and $\Delta[Fe_2\mathbf{L^{7h}}_3]Cl_4$ **(**acetylglucosamine clicked**)** with selectivity index 43 and 37.37 respectively, slightly higher than $\Delta[Fe_2\mathbf{L^{3}}_3]Cl_4$.

Table 4-1. Cytotoxicity and Selectivity index of sugar clicked triplex $[Fe_2\mathbf{L}^{7a\text{-}i}{}_3]Cl_4$ and unclicked alkyne triplex $[Fe_2\mathbf{L}^{3}{}_3]Cl_4$ against HCT116 $p53^{++}$ and ARPE-19 cell line

		mean IC_{50} (μM)		Selectivity Index
		HCT116 $p53^{++}$	ARPE-19	
$[Fe_2\mathbf{L}^{7a}{}_3]Cl_4$	Λ	3.53 ± 0.18	5.44 ± 3.01	2
	Δ	9.52 ± 0.10	63.17 ± 8.08	7
$[Fe_2\mathbf{L}^{7b}{}_3]Cl_4$	Λ	3.60 ± 0.23	11.04 ± 3.25	3
	Δ	10.70 ± 0.74	65.45 ± 1.44	6
$[Fe_2\mathbf{L}^{7c}{}_3]Cl_4$	Λ	3.28 ± 0.28	13.35 ± 5.85	4
	Δ	9.93 ± 0.92	57.90 ± 6.31	6
$[Fe_2\mathbf{L}^{7d}{}_3]Cl_4$	Λ	0.63 ± 0.02	2.96 ± 0.19	5
	Δ	1.68 ± 0.04	59.68 ± 5.44	36
$[Fe_2\mathbf{L}^{7e}{}_3]Cl_4$	Λ	0.72 ± 0.08	8.22 ± 0.19	11
	Δ	5.42 ± 1.16	89.31 ± 2.43	16
$[Fe_2\mathbf{L}^{7f}{}_3]Cl_4$	Λ	0.74 ± 0.08	10.18 ± 1.21	14
	Δ	4.54 ± 0.31	101.12 ± 12.91	22
$[Fe_2\mathbf{L}^{7g}{}_3]Cl_4$	Λ	1.05 ± 0.51	11.64 ± 1.98	11
	Δ	2.69 ± 1.71	115.55 ± 19.28	43
$[Fe_2\mathbf{L}^{7h}{}_3]Cl_4$	Λ	1.56 ± 0.23	16.56 ± 5.76	11
	Δ	2.08 ± 0.08	77.73 ± 5.28	37
$[Fe_2\mathbf{L}^{7i}{}_3]Cl_4$	Λ	12.16 ± 0.74	79.64 ± 10.67	7
	Δ	10.62 ± 5.42	315.35 ± 29.78	30
$[Fe_2\mathbf{L}^{3}{}_3]Cl_4$	Λ	5.02 ± 0.21	73.81 ± 13.05	15
	Δ	2.87 ± 0.91	100.44 ± 4.67	35

4.3.2 Pseudo-Hypoxic assay

Most cancer cells utilise anaerobic glycolysis, an inefficient way to generate energy for cellular processes.[1] This altered metabolism is due to the micro-environmental stresses of hypoxia,[33,34] which upregulates the hypoxia-inducible factor 1 (HIF1)[35] and increases the expression of glucose transporters GLUT1[36] and GLUT3.[37] We postulated that the activity and selectivity of CuAAC glycoconjugated triplex were related to glucose transporters. To validate the hypothesis, $CoCl_2$, a chemical stabilising HIF1 to mimic hypoxia conditions,[38] was added into cell culture medium, followed by the normal MTT protocol. We expected the IC_{50} value to decrease after adding $CoCl_2$ compared with normoxic conditions, as more sugar triplex would be transported into cells. This work was conducted by Dr Samantha Shepherd in Huddersfield University.

Table 4-2 Cytotoxicity of CuAAC glycoconjugated triplexes against HCT116 $p53^{++}$ with and without $CoCl_2$ exposure

	mean IC_{50} (μM)	
	HCT116 $p53^{++}$	**HCT116 $p53^{++}$ with $CoCl_2$**
Δ_{Fe},HHT-[Fe_2**L**$^{7d}{}_3$]Cl_4	1.68 ± 0.04	58.34 ± 15.14
Δ_{Fe},HHT-[Fe_2**L**$^{7e}{}_3$]Cl_4	5.42 ± 1.16	58.44 ± 14.44
Δ_{Fe},HHT-[Fe_2**L**$^{7g}{}_3$]Cl_4	2.69 ± 1.71	53.15 ± 7.09
Δ_{Fe},HHT-[Fe_2**L**$^{7h}{}_3$]Cl_4	2.08 ± 0.08	56.28 ± 12.45
Δ_{Fe},HHT-[Fe_2**L**$^{7i}{}_3$]Cl_4	10.62 ± 5.42	>100

As we can see in Table 4-2, the IC_{50} of the glycoconjugated triplex *increased* dramatically after adding $CoCl_2$. The overexpression of glucose transporters did not improve the activity of the sugar triplex. One of the reasons for this might be that hypoxia can induce drug resistance[34, 39] by effluxing xenobiotics and reducing drug retention in the cells.[40] Or, more free glucose was competitively uptaken into cells and reduced the interaction between sugar triplex and glucose transporter. Further investigations are required to verify these hypotheses.

4.3.3 *In vivo* Xenograft Studies

Based on the excellent cytotoxicity of this new series of sugar conjugated metallohelices against HCT116 $p53^{++}$ *in vitro*, the Δ_{Fe},HHT-[Fe_2**L**$^{7g}{}_3$]Cl_4 (SI>40) was chosen to evaluate the efficacy of this compound a the inhibiting tumour growth *in vivo*. Human colorectal tumour xenograft models were injected intravenously (iv) with Δ_{Fe},HHT-[Fe_2**L**$^{7g}{}_3$]Cl_4 (1.75 mg/Kg). Cisplatin (6mg/Kg) was iv administrated for comparison. These studies were conducted by Dr. Steve Shnyder at the University of Bradford.

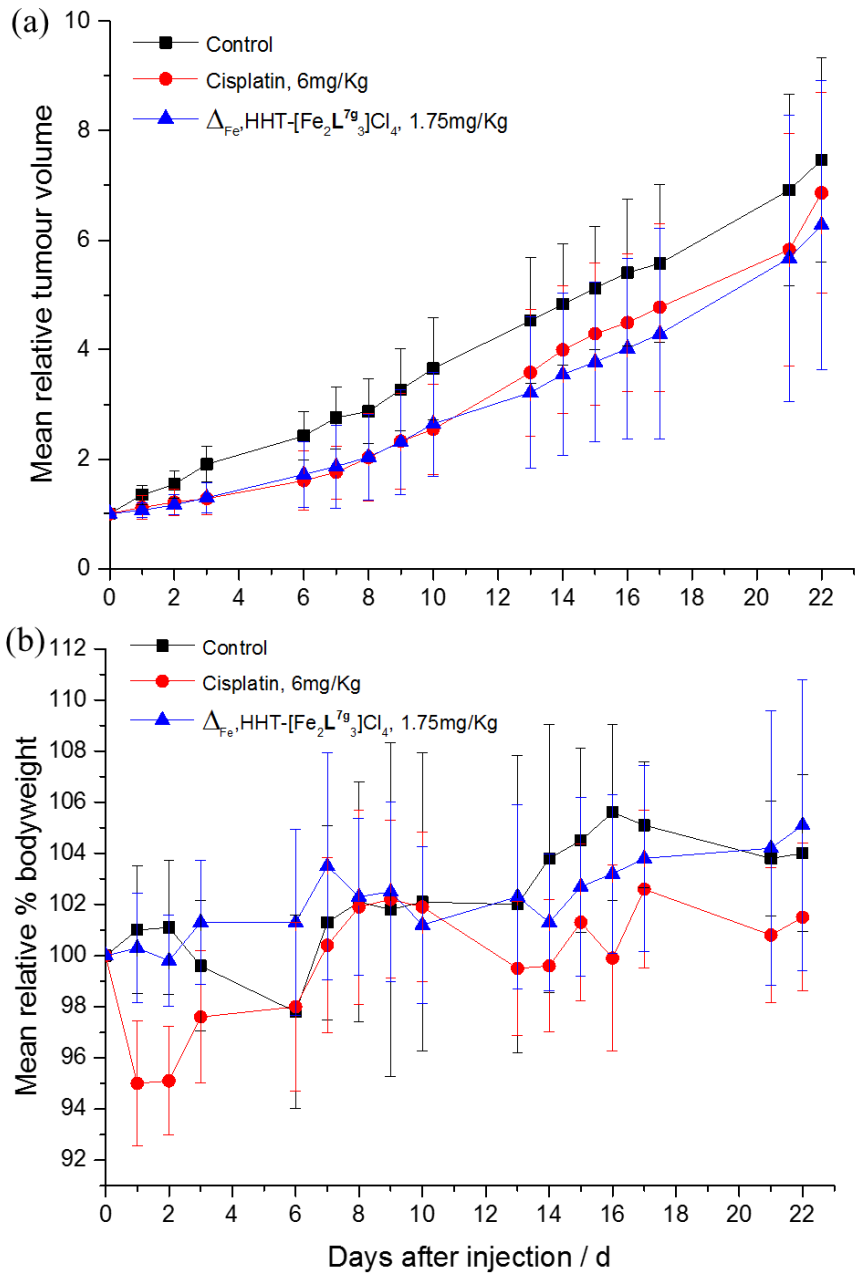

Figure 4-18 In vivo antitumor effect of Δ_{Fe},HHT-[$Fe_2L^{7g}_3$]Cl_4 on HCT116 xenograft models: Mice were administrated with Δ_{Fe},HHT-[$Fe_2L^{7g}_3$]Cl_4 (1.75mg/Kg) or cisplatin (6mg/Kg) for one dose by iv injection. (a) Mean relative tumour volumes; and (b) mean relative bodyweight were measured at different time points and plotted, and expressed with $\pm$ standard error; the significance p value < 0.01 was considered to be statistically significant.

As shown in Figure 4-18(a), Δ_{Fe},HHT-[$Fe_2\mathbf{L^{7g}}_3$]Cl_4 exhibited statistically significant tumour growth delay (4.3 days), similar to cisplatin (4.7 days). More importantly, no side effects of weight loss were observed during the treatment of

Δ_{Fe},HHT-[$Fe_2\mathbf{L}^{7g}_3$]Cl_4, which was consistent with the high selectivity observed *in vitro*. In contrast, cisplatin showed serious toxicity as indicated by up to 6% loss of body weight on day two [Figure 4-18(b), Table 4-3]. Considering that this preliminary result was obtained for only one dose injection, the antitumour activity of Δ_{Fe},HHT-[$Fe_2\mathbf{L}^{7g}_3$]Cl_4 is very promising. Multiple-dose investigation of this compound is in progress.

Table 4-3 Anti-tumour effect of Δ_{Fe},HHT-[$Fe_2L^{7g}_3$]Cl_4 and cisplatin against HCT 116 $p^{53-/-}$ tumour in vivo

Group number	Median time RTV2 (Days)	Growth delay (Days)	Significance	Maximum% weight loss
Control	4.2	-	-	2.0 (day 6)
Δ_{Fe},HHT-[$Fe_2\mathbf{L}^{7g}_3$]Cl_4	8.5	4.3	$p<0.01$	6.0 (day 2)
Cisplatin	8.9	4.7	$p<0.01$	0

4.4 Conclusion

Motivated by the Warburg effect, we attempted to make glycoconjugation of metallohelices in two different methodologies and evaluate the hypothesis that sugar appended complexes enhance the targeting and anticancer activity compared with the aglycone.

For Method 1, glyco-pyridine **17**/**18** were made as the ligand precursors to assemble with aminobipyridine **14** and metal salt in proportional ratio. For the first time, we made water soluble glyco-metallohelices $[M_2\mathbf{L}^{\mathbf{6}}{}_3][ClO_4]_4$ (M = Zn, Fe) with regard to the perchlorate salt. Whereas, the same ligand components gave a mixture of species $[Fe_2\mathbf{L}^{\mathbf{5}}{}_3]Cl_4$ and $[Fe_2\mathbf{L}^{\mathbf{6}}{}_3]Cl_4$, presumably due to the presence of intramolecular hydrogen bonding between Cl^- and C_1 proton or OH.

For Method 2, based on the success of CuAAC click post-assembly modification described in Chapter 3, the sugar azides were employed to substitute the aromatic azide. Following the same protocol, a series of sugar azides have been clicked onto the alkyne triplex $[Fe_2\mathbf{L}^{\mathbf{3}}{}_3]Cl_4$ in high yield. These new CuAAC glyco-metallohelices $[Fe_2\mathbf{L}^{\mathbf{7a\text{-}i}}{}_3]Cl_4$ demonstrated the high anticancer activity and selectivity against HCT116p53^{++} cell line and noncancerous ARPE19 cell line *in vitro*. In particular, (R_c,Δ_{Fe})-HHT-$[Fe_2\mathbf{L}^{\mathbf{7g}}{}_3]Cl_4$ displayed similar inhibition to the growth of human tumour xenografts, but reduced side effects compared to cisplatin.

4.4 References

1. M. G. Vander Heiden, L. C. Cantley and C. B. Thompson, *Science*, 2009, **324**, 1029-1033.
2. A. Schulze and A. L. Harris, *Nature*, 2012, **491**, 364-373.
3. C. Munoz-Pinedo, N. El Mjiyad and J. Ricci, *Cell Death Dis*, 2012, **3**, e248.
4. R. J. DeBerardinis, J. J. Lum, G. Hatzivassiliou and C. B. Thompson, *Cell Metab.*, 2008, **7**, 11-20.
5. A. King and E. Gottlieb, *Curr. Opin. Cell Biol.*, 2009, **21**, 885-893.
6. (a) D. A. Tennant, R. V. Durán and E. Gottlieb, *Nat. Rev. Cancer*, 2010, **10**, 267-277; (b) M. G. Vander Heiden, *Nat. Rev. Drug Discov.*, 2011, **10**, 671-684.
7. (a) O. Warburg, F. Wind and E. Negelein, *J. Gen. Physiol.*, 1927, **8**, 519; (b) O. Warburg, *Science*, 1956, **123**, 309-314.
8. R. Aft, F. Zhang and D. Gius, *Br. J. Cancer*, 2002, **87**, 805-812.
9. X. Cao, L. Fang, S. Gibbs, Y. Huang, Z. Dai, P. Wen, X. Zheng, W. Sadee and D. Sun, *Cancer Chemother. Pharmacol.*, 2007, **59**, 495-505.
10. S. Ben-Haim and P. Ell, *J. Nucl. Med.*, 2009, **50**, 88-99.
11. J. Pohl, B. Bertram, P. Hilgard, M. Nowrousian, J. Stüben and M. Wiessler, *Cancer Chemother. Pharmacol.*, 1995, **35**, 364-370.
12. E. C. Calvaresi and P. J. Hergenrother, *Chem. Sci.*, 2013, **4**, 2319-2333.
13. G. Pastuch-Gawołek, K. Malarz, A. Mrozek-Wilczkiewicz, M. Musioł, M. Serda, B. Czaplinska and R. Musiol, *Eur. J. Med. Chem.*, 2016, **112**, 130-144.
14. V. Oliveri, M. L. Giuffrida, G. Vecchio, C. Aiello and M. Viale, *Dalton Trans.*, 2012, **41**, 4530-4535.
15. S. Samantaray, U. Marathe, S. Dasgupta, V. K. Nandicoori and R. P. Roy, *J. Am. Chem. Soc.*, 2008, **130**, 2132-2133.
16. G. Stefanetti, Q. Y. Hu, A. Usera, Z. Robinson, M. Allan, A. Singh, H. Imase, J. Cobb, H. Zhai and D. Quinn, *Angew. Chem. Int. Ed.*, 2015, **54**, 13198-13203.
17. F. A. French, E. J. Blanz Jr, S. C. Shaddix and R. W. Brockman, *J. Med. Chem.*, 1974, **17**, 172-181.
18. A. D. Faulkner, R. A. Kaner, Q. M. Abdallah, G. Clarkson, D. J. Fox, P. Gurnani, S. E. Howson, R. M. Phillips, D. I. Roper and D. H. Simpson, P. Scott, *Nat. Chem.*, 2014, **6**, 797-803.
19. C. P. Sebli, S. E. Howson, G. J. Clarkson and P. Scott, *Dalton Trans.*, 2010, **39**, 4447-4454.
20. S. E. Howson, L. E. N. Allan, N. P. Chmel, G. J. Clarkson, R. J. Deeth, A. D. Faulkner, D. H. Simpson and P. Scott, *Dalton Trans.*, 2011, **40**, 10416-10433.
21. S. G. Telfer, G. Bernardinelli and A. F. Williams, *Chem. Commun.*, 2001, (**16**), 1498-1499.
22. (a) H. P. Mangunuru, J. R. Yerabolu, D. Liu and G. Wang, *Tetrahedron Lett.*, 2015, **56**, 82-85; (b) K. Upadhyaya, K. Singh, A. Arun, M. Shukla, N. Srivastava, R. Ashraf, A. Sharma, R. Mahar, S. K. Shukla and J. Sarkar, *Org. Biomol. Chem.*, 2016, **14**, 1338-1358.
23. R. B. Hamanaka and N. S. Chandel, *J. Exp. Med.*, 2012, **209**, 211-215.
24. Y. Chai, P. B. Beauregard, H. Vlamakis, R. Losick and R. Kolter, *MBio.* 2012, **3**, e00184-12.
25. B. Dwarakanath, D. Khaitan and T. Ravindranath, *Cancer Biol. Ther.*, 2004, **3**, 864-870.

26. M. L. A. de Leoz, L. J. Young, H. J. An, S. R. Kronewitter, J. Kim, S.Miyamoto, A. D. Borowsky, H. K. Chew and C. B. Lebrilla, *Mol. Cell Proteomics.*, 2011, **10**, M110. 002717.
27. T. P. Lynch, C. M. Ferrer, S. R. Jackson, K. S. Shahriari, K. Vosseller and M. J. Reginato, *J. Biol. Chem.*, 2012, **287**, 11070-11081.
28. D. Bapu, J. Runions, M. Kadhim and S. A. Brooks, *Cancer Lett.*, 2016, **375**, 367-374.
29. O. G. Adesoye, I. N. Mills, D. P. Temelkoff, J. A. Jackson and P. Norris, *J. Chem. Educ.* 2012, **89**, 943-945.
30. V. Percec, P. Leowanawat, H. J. Sun, O. Kulikov, C. D. Nusbaum, T. M. Tran, A. Bertin, D. A. Wilson, M. Peterca, S. Zhang, N. P. Kamat, K. Vargo, D. Moock, E. D. Johnston, D. A. Hammer, D. J. Pochan, Y. Chen, Y. M. Chabre, T. C. Shiao, M. Bergeron-Brlek, S. Andre,; R. Roy, H. J. Gabius and P. A. Heiney, *J. Am. Chem. Soc.*, 2013, **135**, 9055-77.
31. (a) T. Tanaka, H. Nagai, M. Noguchi, A. Kobayashi and S.-i. Shoda, *Chem. Commun.*, 2009, (**23**), 3378-3379; (b) N. Vinson, Y. Gou and C. R. Becer, *Polym. Chem.*, 2011, **2**, 107-113.
32. N. Hay, *Nat. Rev. Cancer*, **2016**.
33. W. R. Wilson, M. P. Hay, *Nat. Rev. Cancer*, 2011, **11**, 393-410.
34. J. M. Brown and W. R. Wilson, *Nat. Rev. Cancer*, 2004, **4**, 437-447.
35. (a) N. C. Denko, *Nat. Rev. Cancer*, 2008, **8**, 705-713; (b) H. Lu, R. A. Forbes and A. Verma, *J. Biol. Chem.*, 2002, **277**, 23111-23115.
36. C. Chen, N. Pore, A. Behrooz, F. Ismail-Beigi and A. Maity, *J. Biol. Chem.*, 2001, **276**, 9519-9525.
37. P. Maxwell, G. Dachs, J. Gleadle, L. Nicholls, A. Harris, I. Stratford, O. Hankinson, C. Pugh and P. Ratcliffe, *Proc. Natl. Acad. Sci. U. S. A.*, 1997, **94**, 8104-8109.
38. (a) A. Vengellur and J. LaPres, *Toxicol. Sci.*, 2004, **82**, 638-646; (b) J. P. PIRET, D. Mottet, M. Raes and C. Michiels, *Ann. N. Y. Acad. Sci.*, 2002, **973**, 443-447.
39. P. Vaupel and A. Mayer, *Cancer Metastasis Rev.*, 2007, **26**, 225-239.
40. G. Yang, S. Xu, L. Peng, H. Li, Y. Zhao and Y. Hu, *Mol. Med. Rep.*, 2016, **13**, 2583-2589.

Chapter 5

Triplex metallohelices containing triazole ligand units

5.1 Introduction

Polypyridines, such as bipyridine, terpyridine or pyridine-imine, are the most frequently employed units in discrete multinuclear coordination structures *e.g.* helicates,[1-3] cages,[4-6] and grids.[7-9] However, the limitations of pyridine-containing ligands, such as cumbersome syntheses involving toxic reagents[10] and lack of functionalization impede access to diversity.[11] Other *N*-heterocycles such as pyrazoles, imidazoles and pyrazines have also been used, but these suffer from similar problems. Alternatively, 1,2,3-triazole moieties, can in principle be much more readily functionalised than pyridines, due to the discovery of CuAAC chemistry.[12]

In addition to the synthetic advantages, 1,2,3-triazole moieties also exhibit interesting coordination behaviour. The three nitrogen atoms of the 1,2,3-triazole give rise to its distinct chemical and physical properties (*e.g.* high degree of aromaticity,[13] large polarization of electronic distribution,[14] the increased CH- acidity[15] and decreased base strength)[16] and offer two different *N*-donor (N2 and N3)[17] and one *C*-donor (C5) coordination modes.[18] In either monodentate or bidentate ligand systems, coordination through the more electron-rich (and more basic) N3 nitrogen atom is most commonly observed. Intriguingly, the isoelectronic replacement of a methine group by nitrogen leads to weaker σ-donor and π-acceptor strength of the N3-coordinated triazole ligand, with respect to pyridine.[17] These electronic differences have received considerable attention as the replacement of the pyridine by triazole

varies the photophysical,[19-21] electrochemical,[22-27] thermodynamic[28-30] and kinetic[31] properties of the metal complexes.

1,2,3-triazole ligands therefore open up an excellent route for new ligand design and can be employed in multidentate ligand systems in which the motif is treated as the pyridyl surrogate *e.g.* bidentate bis-triazole or pyridine-triazole ligands, and tridentate bis-triazole-pyridine ligands.[17, 32-34] A growing number of examples in the literature of coordination complexes with traziole-containing ligands are exploited for their applications in biology and medicine,[35-42] catalysis,[43-47] photoactive devices,[48-53] host-guest chemistry[54-57] and molecular machines.[58-61]

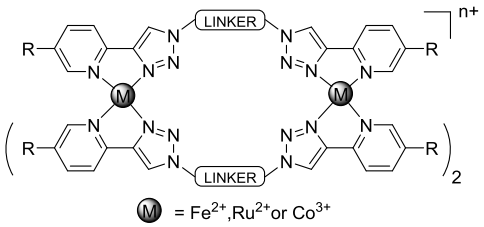

Figure 5-1 The formation of M_2L_3 helicate from bis-(2-pyridyl-1,2,3-triazole) ligands[35]

In 2012, Petitjean and co-workers first synthesized a family of M_2L_3 (M = $Fe^{2+}$and Ni^{2+}) helicates containing bis-(2-pyridyl-1,2,3-triazole) ligands and exploited the applications of magnetism and self-selection.[1,62] Crowley and co-workers employed the analogue ligand to form Fe(II) helicates and examined the biological activity. Unfortunately, no antifungal activity was observed as the complexes are not soluble in aqueous solution and decomposed instantaneously in DMSO.[36] In order to improve the solubility and stability of triazole metallohelices, the same group substituted the Fe(II) with the more inert metal Co(III); antimicrobial studies showed no activity.[37] In 2015, the same group reported a triazole-derived quadruply-stranded

helicate of Pd(II) which was 7-fold more active than cisplatin.[63] However, the complex has no selectivity towards non-malignant cells.

The majority of the triazole-containing ligands employed to date are end-to-end symmetric and contain bulky (aromatic) groups, consequently leading to symmetric, racemic, rigid and low functionality structures. More importantly, the ability to readily functionalise the triazole unit has not been exploited to its full potential to construct more flexible and asymmetric discrete metallohelices.

In this chapter, we describe the synthesis of a new directional ligand class (Figure 5-2) based on the bipyridine-imine system studied in earlier chapters, but which is derived from new triazole aldehydes. A new series of asymmetric metallohelicates is established with a range of substituents at the triazole *i.e.* on the external faces the framework. The investigations of the chemical and biological properties of these new metallohelices are also detailed.

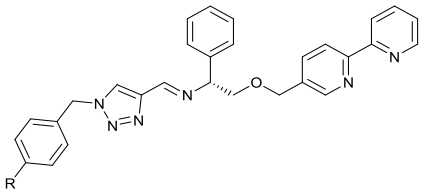

Figure 5-2 New triazole-imine/bipyridine ligand developed in this chapter.

5.2 Synthesis of benzylic triazole aldehydes 29[a-e]

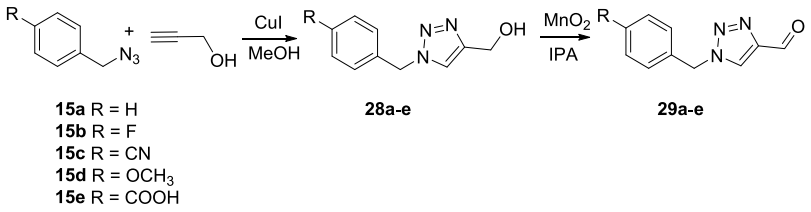

Scheme 5-1 Synthesis of aromatic triazole aldehyde

Benzyl triazole aldehyde derivatives have been reported as key intermediates for catalysis,[64,65] switchable materials,[66] antibacterial compounds,[67,68] immunostimulants,[69] anti-inflammatory compounds and anticancer drugs.[70,71] Following a literature example to make benzyl triazole aldehyde **29a** (Scheme 5-1),[72] the benzyl azide derivatives **15a-e** (1 eq.) were first treated with propargyl alcohol (1 eq.) in the present of copper iodide (0.1 eq.) to afford the respective benzyl triazole methanol derivatives **28a-e**. These derivatives were subsequently oxidised with activated manganese dioxide (3 eq.) to obtain the benzyl triazole aldehyde derivatives **29a-e**, as white solids. Of this series, **29c** and **29e** are new compounds but since characterisation of some other examples is incomplete in the literature, full data was acquired here.

5.3 Synthesis of triazole Zn(II) triplex metallohelices

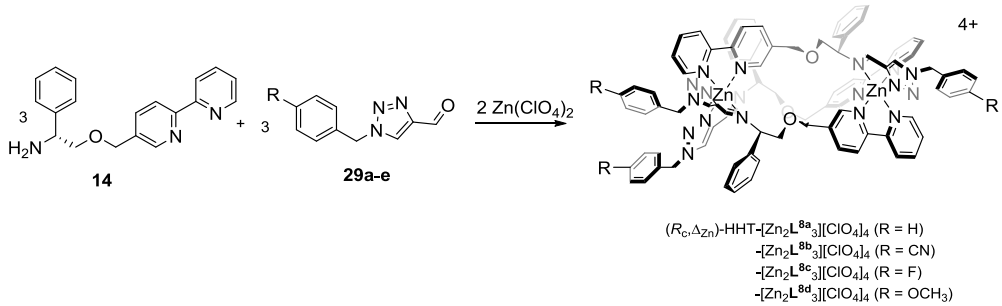

Scheme 5-2 Synthesis of benzyl triazole derivate Zn (II) triplex metallohelice

The bimetallic metallohelix (R_c,Δ_{Zn})-[Zn_2**L**$^{8a}{}_3$][ClO_4]$_4$ was synthesised by mixing (*R*)-2-([2,2'-bipyridin]-5-ylmethoxy)-1-phenylethan-1-amine (**14**, 3 eq.) with benzyl triazole aldehyde **29a** (3 eq.) and $Zn(ClO_4)_2 \cdot 6H_2O$ (2 eq.) in acetonitrile solution at ambient temperature (Scheme 5-2). After 4 h, the pure complex was isolated by dropwise addition of ethyl acetate and filtration of the microcrystalline solid formed.

The triazole-containing metallohelix (R_c,Δ_{Zn})-HHT-[Zn_2**L**$^{8a}{}_3$][ClO_4]$_4$ has an asymmetric configuration evidenced by the three spectroscopically unique ligand environments in the ^{1}H NMR spectrum (Figure 5-3). The characteristic signals of the imine proton H^{a}, bpy protons H^{b} and triazole protons H^{c} were observed at low fields (9.4-8.4 ppm) (Figure 5-3a). Two sets of phenyl ring protons H^{d} and H^{e}, found at 6.80–5.90 ppm, experience strong through-space shielding from the bpy unit of an adjacent ligand. The benzylic CH protons H^{g} were detected at 5.43, 4.88 and 4.79 ppm along with the adjacent diasterotopic CH_2 groups protons H^{i} observed at 4.30-4.00 ppm and 3.70-3.42 ppm. The clusters at 5.30-5.10 ppm and 4.55-4.40 ppm were assigned to bipyridine-CH_2 protons H^{h}. Benzyl-CH_2 atoms H^{f} were analysed at 5.62-5.40 ppm. The ^{13}C NMR spectrum (Figure 5-3b) was also consistent with three unique ligand environments. Three imine carbon peaks C^{a} were found at 157.1-156.1 ppm, and three bpy carbon peaks C^{b} were observed at 150.4-149.9 ppm. The three benzylic carbon peaks C^{g} were detected at 69.7, 69.5 and 67.8 ppm. Bipyridine-CH_2 carbon peaks C^{h} were found at 70.0, 69.9 and 69.1 ppm. Benzyl-CH_2 carbon peaks C^{f} were assigned at 55.5-50.1 ppm.

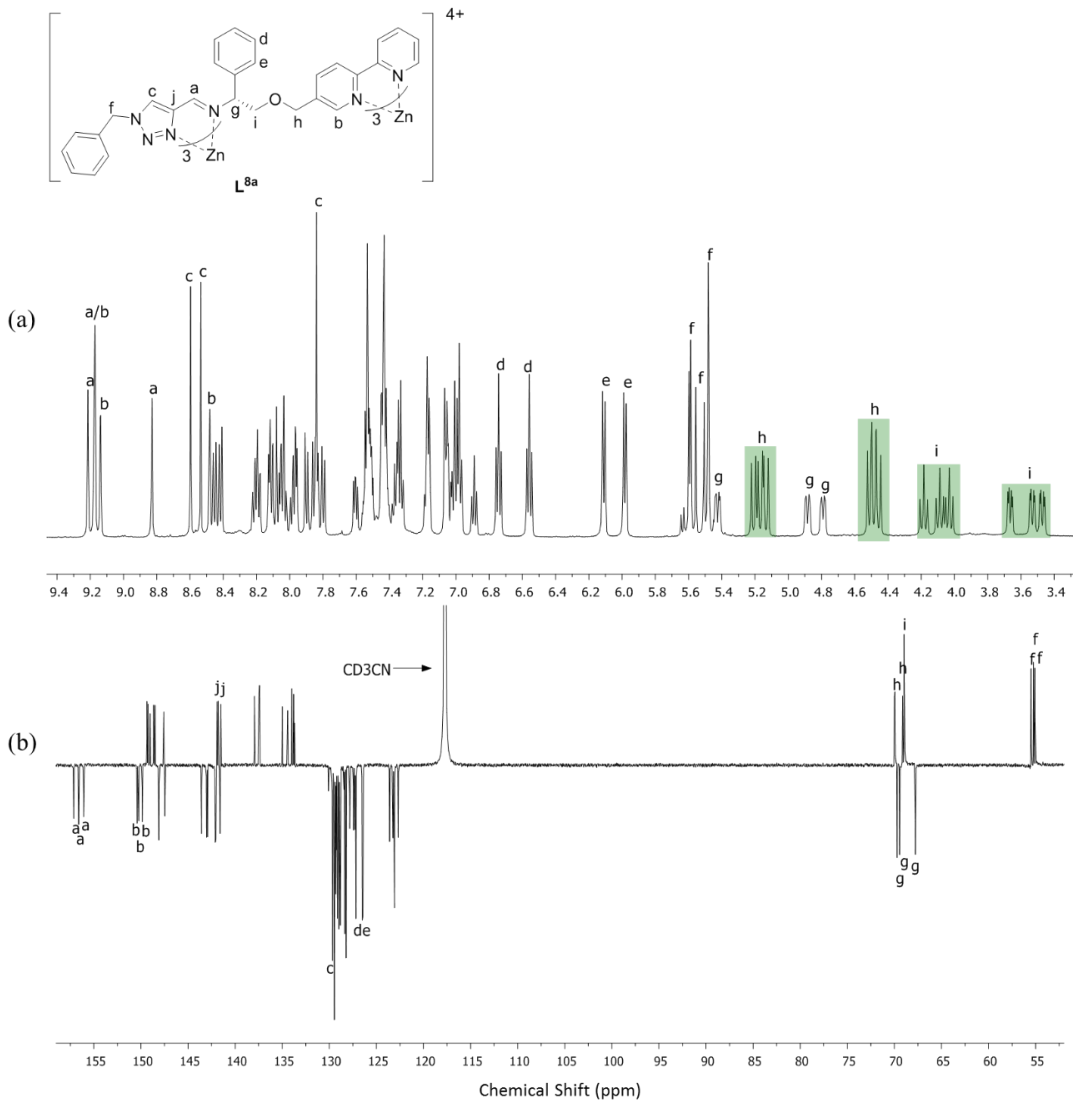

Figure 5-3 ^{1}H (500 MHz, CD_3CN, 298K) and ^{13}C (125 MHz, CD_3CN, 298K) NMR spectra of (R_c,Δ_{Zn})-HHT-[$Zn_2\mathbf{L}^{\mathbf{8a}}{}_3$][$ClO_4$]$_4$

Other aromatic triazole triplex metallohelices (Scheme 5-2) were easily accessed through use of the aldehydes shown in Scheme 5-1. The ^{1}H and ^{13}C NMR spectra (Figure 5-4) were similar to that of (R_c,Δ_{Zn})-HHT-[$Zn_2\mathbf{L}^{\mathbf{8a}}{}_3$][$ClO_4$]$_4$

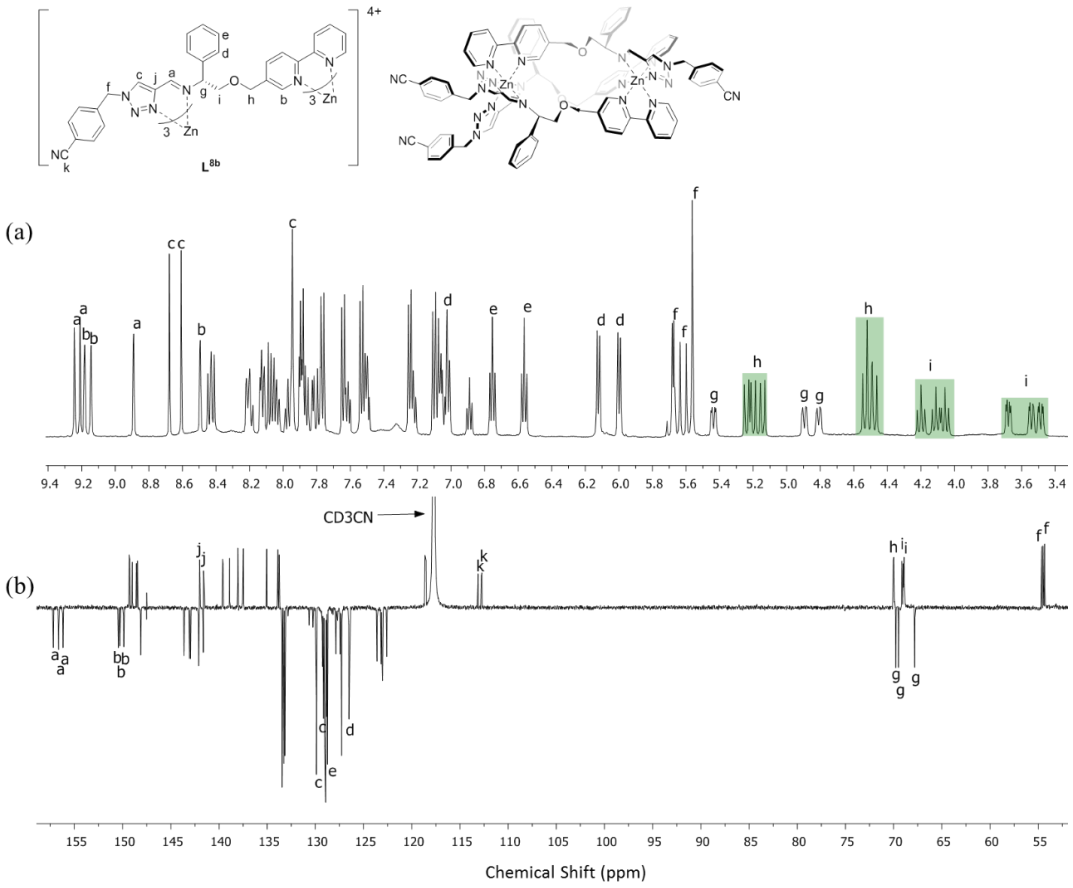

Figure 5-4 ^{1}H (500 MHz, CD_3CN, 298K) and ^{13}C (125 MHz, CD_3CN, 298K) NMR spectra of (R_c,Δ_{Zn})-HHT-[Zn_2**L**$^{8b}{}_3$][ClO_4]$_4$

5.5 Synthesis of water soluble triazole triplex metallohelices of Fe(II).

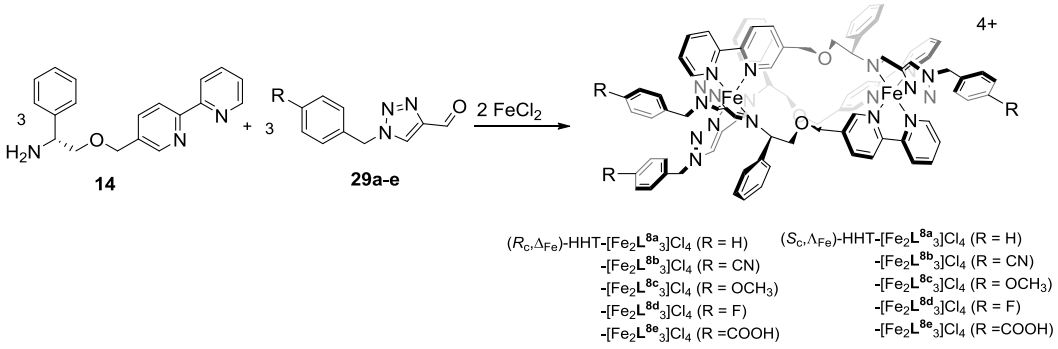

Scheme 5-3 Synthesis of triazole Fe (II) triplex metallohelices

Water soluble complexes of this class (R_c,Δ_{Fe})-HHT-[Fe_2**L**$^{8a\text{-}e}{}_3$]Cl_4 were accessed by heating (*R*)-2-([2,2'-bipyridin]-5-ylmethoxy)-1-phenylethan-1-amine (**14,** 3 eq.), the appropriate benzyl triazole aldehydes **29a-e** (3 eq.) and $FeCl_2$ (2 eq.) in methanol for 48 h (Scheme 5-3).

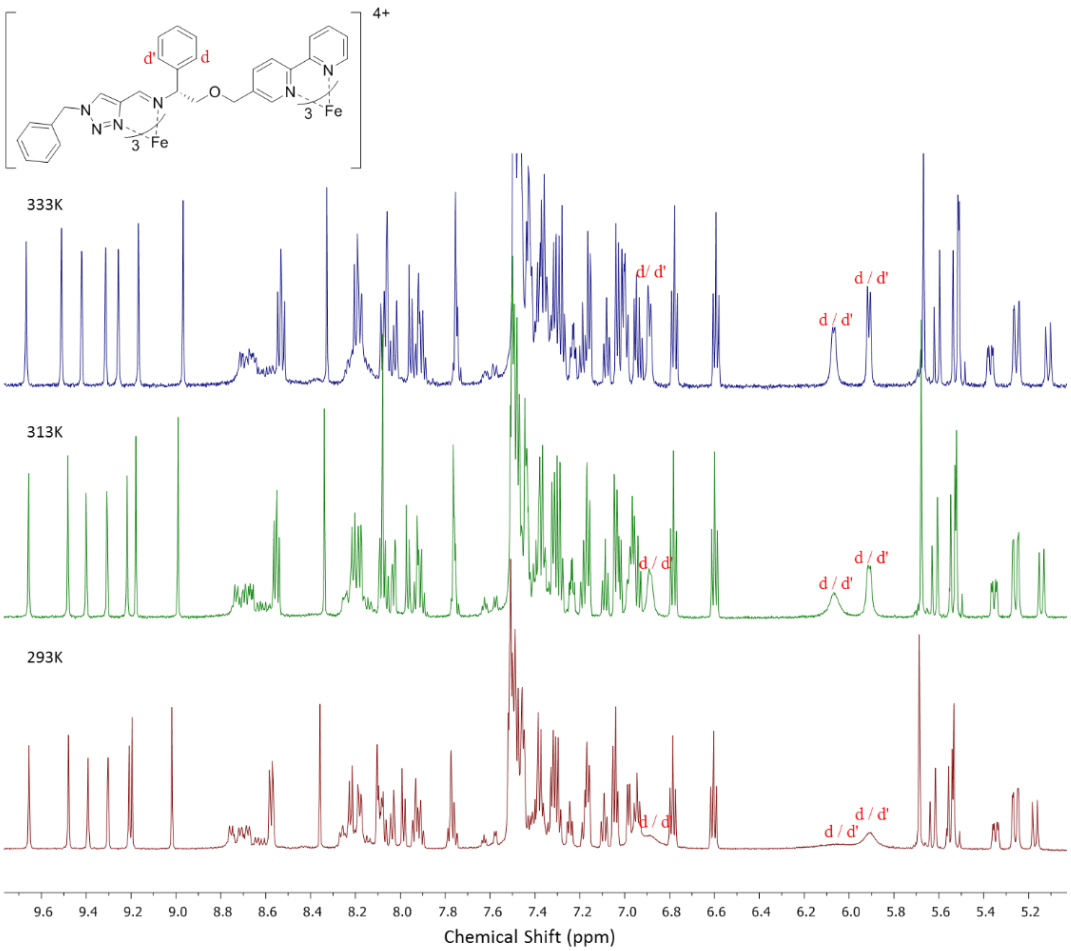

Figure 5-5 Variable temperature ^{1}H NMR spectra of (R_c,Δ_{Fe})-HHT-[Fe_2**L**$^{8a}{}_3$]Cl_4 (600 MHz, MeOD)

Compared with the Zn(II) counterparts, the ^{1}H NMR signals for the π-stacked phenyl rings (*e.g.* H$^{d/d'}$, Figure 5-5) were much broader at 293 K, presumably as a result of relatively slow rotation since on increasing the temperature the signals sharpened. These broad signals were also observed in the ^{1}H spectra of other iron(II) pyridine triplexes.

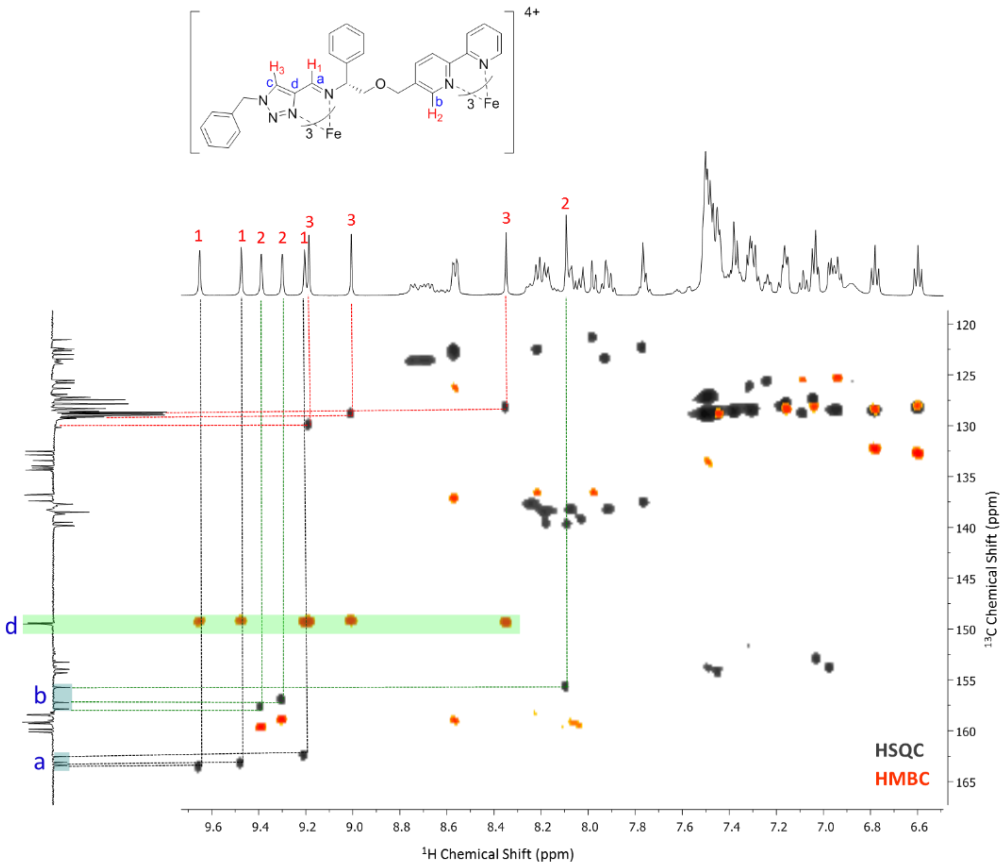

Figure 5-6 ^{1}H-^{13}C HSQC/HMBC (500 MHz, MeOD, 298K) spectra of (R_c,Δ_{Fe})-HHT-[Fe_2**L**$^{8a}{}_3$]Cl_4

In a similar fashion to the Zn(II) counterpart, nine sharp singlets were observed in the down field region of the ^{1}H NMR spectrum of (R_c,Δ_{Fe})-HHT-[Fe_2**L**$^{8a}{}_3$]Cl_4 , between 9.70-8.00 ppm, which are identified as the three imine protons **H1**, three bpy protons **H2** and three triazole protons **H3**. These assignments were confirmed by HSQC and HMBC NMR spectroscopy (Figure 5-6).

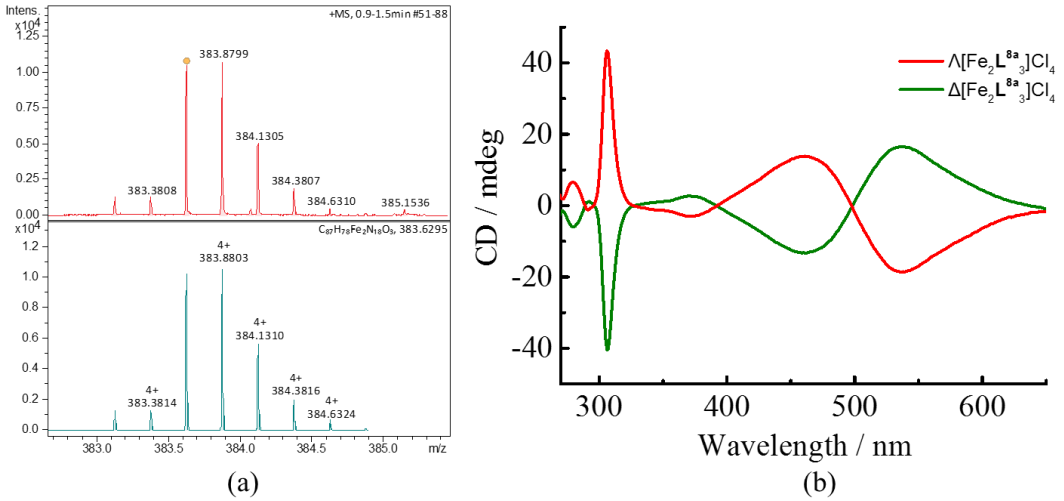

Figure 5-7 (a) High resolution mass spectrum for (R_c,Δ_{Fe})-HHT-[Fe_2**L**$^{8a}_3$]Cl_4: top measured, below calculated; (b) CD spectra of HHT-[Fe_2**L**$^{8a}_3$]Cl_4

The formation of (R_c,Δ_{Fe})-HHT-[Fe_2**L**$^{8a}_3$][Cl]$_4$ was also confirmed by high resolution electrospray mass spectrometry, with the tetracationic molecular ion being observed at *m/z* 383.8799 Da (calculated 383.8803 Da) [Figure 5-7 (a)]. The CD spectra of the two enantiomers of [Fe_2**L**$^{8a}_3$]Cl_4 in methanol were equal and opposite [Figure 5-7 (b)].

Other triazole triplex systems were synthesized using the same method. Microanalysis was also consistent with the proposed formulation. To our knowledge, this series of [M_2**L**$^{8a\text{-}d}_3$]$^{4+}$ (M= Zn^{2+} and Fe^{2+}) was the first example of optically pure and asymmetric metallohelices containing triazole chelate group.

We have noted that the selectivity for HHT-isomers over HHH in our previously reported triplex systems is *ca* 99%, but peaks consistent with the presence of the HHH isomer can nevertheless be detected (see Chapter 2 section 2.3.2). It is striking that in the ^{1}H NMR spectra of the new triazole triplex systems in this chapter, no such HHH isomer was detected. In other words, there seems to be a still stronger

preference for a mixed ligand bpy/triazole-imine metal centres over the homoleptic tris(bpy) or tris(triazole-imine).

5.6 Synthesis and self-assembly reactions of glyco-triazole aldehydes

Based on the synthetic success of benzyl triazole triplex system, we attempted to synthesize a small series of glyco-triazole aldehydes **34-39** (Scheme 5-4) and investigate their subsequent self-assembly reactions with bpy-phenylamine **14**.

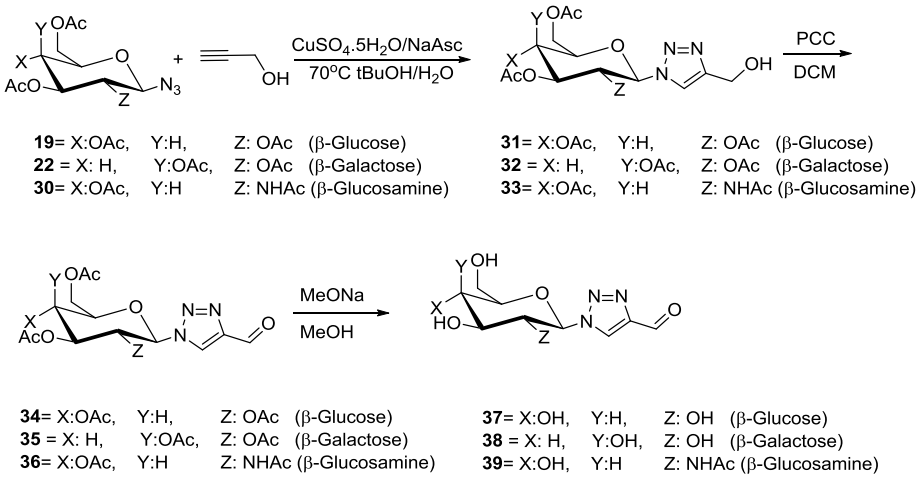

Scheme 5-4 Synthesis glyco-triazole aldehyde

Following some literature precedent on glyco-triazole derivatives,[76,77] the CuAAC reaction of β-D-pentaacetato sugar azides **19**/**22**/**30** (see Section **4.2.2**) with propargyl alcohol using $CuSO_4 \cdot 5H_2O$ as a catalyst at 70 ºC was investigated. Overnight reactions successfully led to the formation of alcohols **31-33** in *ca* 80% yield. While to our knowledge the oxidation of such compounds has not previously been achieved, we found that the use of pyridinium chlorochromate at ambient temperature gave the corresponding acetyl-protected triazole aldehydes **34-36** very

smoothly, and these were subsequently deprotected using MeONa in methanol to give **37-39** in excellent overall yield.

Synthesis of sugar triazole triplex metallohelices $[Zn_2\mathbf{L}^{9a\text{-}c}{}_3][ClO_4]_4$

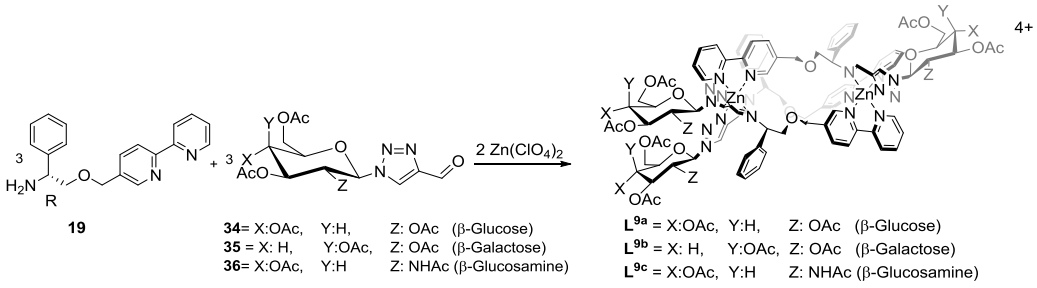

Scheme 5-5 Synthesis of glyco-triazole derivate Zn (II) triplex metallohelice

Treatment with bipyphenylamine **14** (3 eq.), glyco-triazole derivative **34-36** (3 eq.) and $Zn(ClO_4)_2$ (2 eq.) led to the rapid self-assembly of the triplex metallohelix in acetonitrile solution at ambient temperature (Scheme 5-5).

The ^{1}H NMR spectrum of the glyco-triazole zinc(II) metallohelix clearly shows three inequivalent ligand environments, indicating the formation of the asymmetric HHT configuration (Figure 5-8). For instance, the (R_c,Δ_{Zn})-HHT-$[Zn_2\mathbf{L}^{9a}{}_3][ClO_4]_4$ displayed three imine resonances $H^{\mathbf{a}}$, two bpy $H^{\mathbf{b}}$ resonances and two triazole $H^{\mathbf{c}}$ resonances at 9.40-8.70 ppm. The phenyl ring protons $H^{\mathbf{d}}$ and $H^{\mathbf{e}}$ were found at 7.00–6.00 ppm. The two benzylic environments $H^{\mathbf{f}}$ were observed at 4.92 and 4.80 ppm, while the third $H^{\mathbf{f}}$ overlapped with sugar protons. Three diasterotopic CH_2 protons $H^{\mathbf{g}}$ adjacent to benzylic centres were clustered at 3.75-3.45 ppm (approximately doublets of doublets). The twelve sugar acetyl CH_3 singlets $H^{\mathbf{h}}$ overlap with one another at high field (2.50-1.50 ppm) and were also masked slightly by the solvent peak. In the ^{13}C NMR spectrum, the acetyl C=O carbons $C^{\mathbf{i}}$ were detected

around 170.0 ppm, followed by the three imine carbon peaks C^{a} observed at 157.3-156.0 ppm. Three bpy carbon peaks C^{b} were found at 150.5-149.9 ppm. The acetyl CH_3 carbons C^{h} were assigned at 20.0 ppm. The ^{1}H and ^{13}C NMR spectra of other glyco-trizole zinc(II) metallohelices *i.e.* (R_c,Δ_{Zn})-HHT-[Zn_2**L**$^{9b}{}_3$][ClO_4]$_4$ and (R_c,Δ_{Zn})-HHT-[Zn_2**L**$^{9c}{}_3$][ClO_4]$_4$ were similar with [Zn_2**L**$^{9a}{}_3$][ClO_4]$_4$ (See Figure 5-9; Figure 5-10).

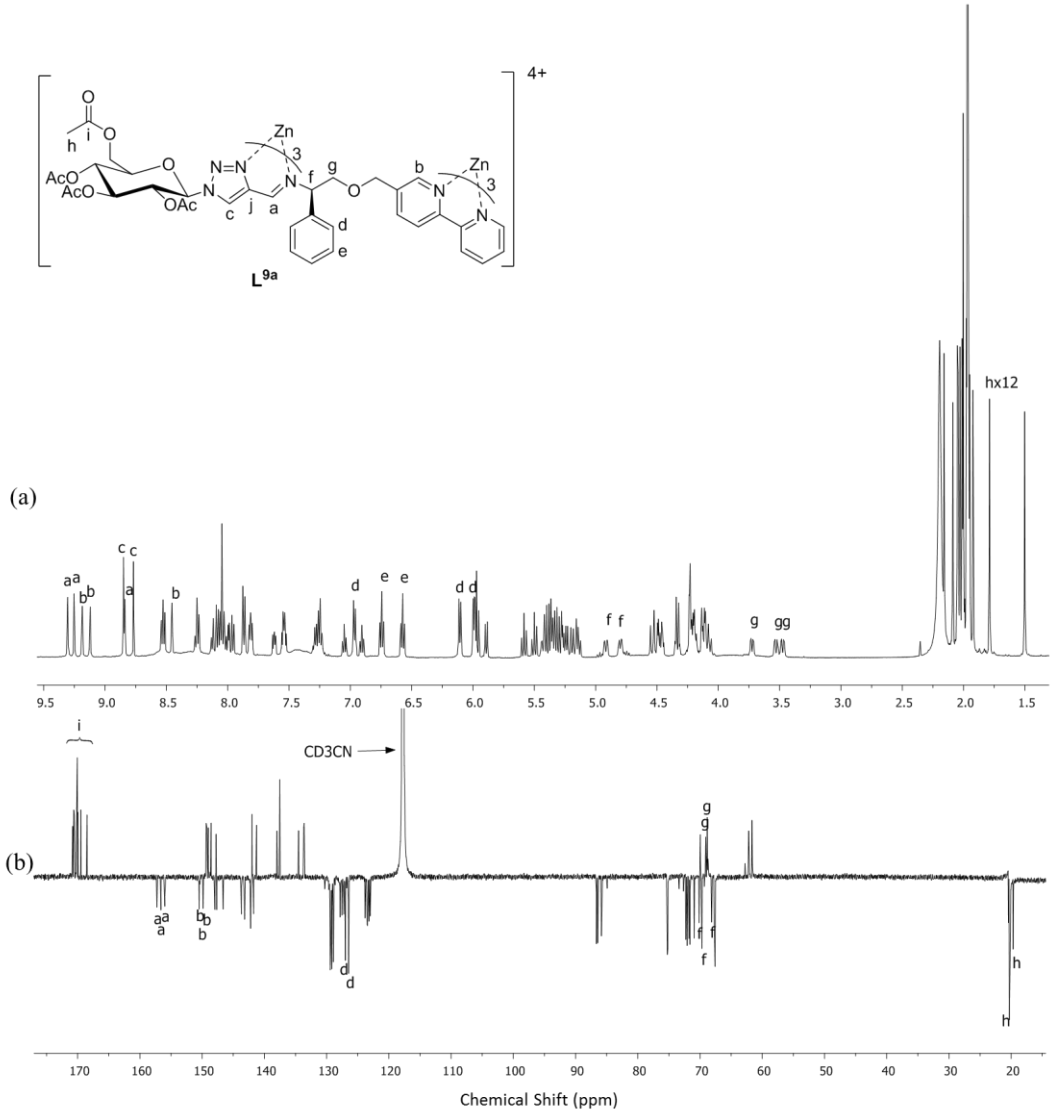

Figure 5-8 ^{1}H (500 MHz, CD_3CN, 298K) and ^{13}C (125 MHz, CD_3CN, 298K) NMR spectra of (R_c,Δ_{Zn})-HHT-[Zn_2**L**$^{9a}{}_3$][ClO_4]$_4$

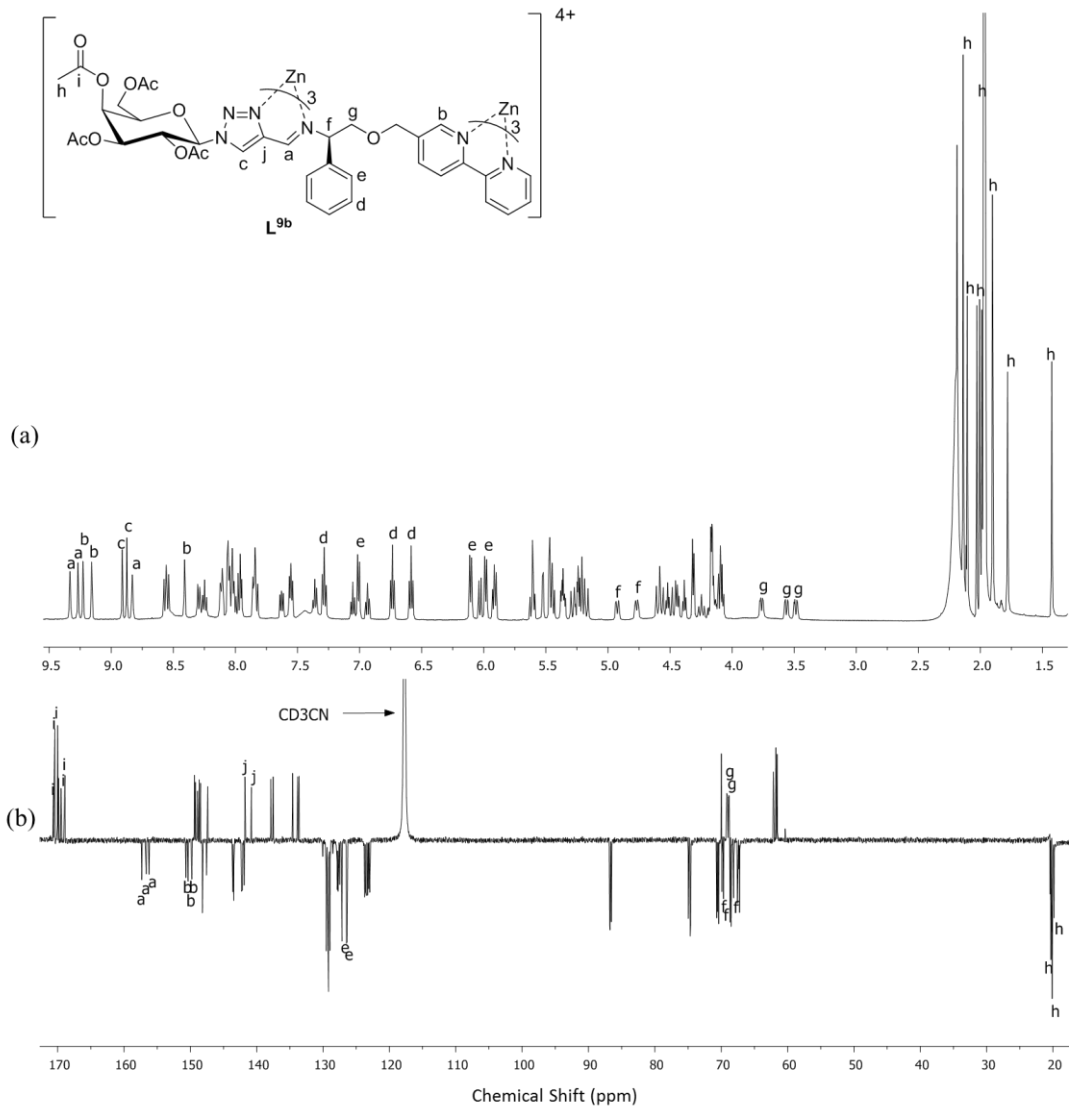

Figure 5-9 ^{1}H (500 MHz, CD_3CN, 298K) and ^{13}C (125 MHz, CD_3CN, 298K) NMR spectra of (R_c,Δ_{Zn})-HHT-[Zn_2**L**$^{9b}{}_3$][ClO_4]$_4$

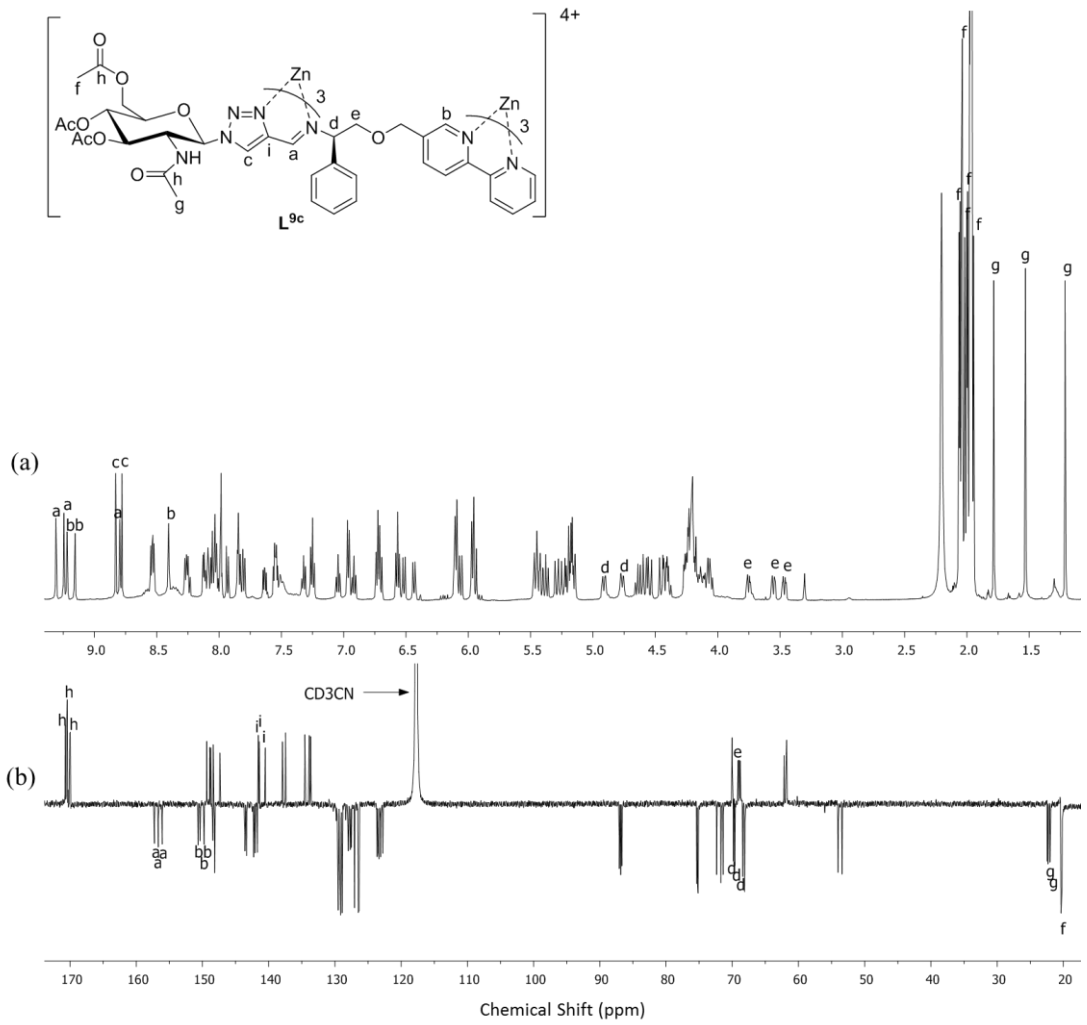

Figure 5-10 ^{1}H (500 MHz, CD_3CN, 298K) and ^{13}C (125 MHz, CD_3CN, 298K) NMR spectra of (R_c,Δ_{Zn})-HHT-[$Zn_2\mathbf{L}^{\mathbf{9c}}{}_3$] $[ClO_4]_4$

Synthesis of water soluble triazole triplex metallohelix [$Fe_2\boldsymbol{L}^{\boldsymbol{10}}{}_3$]$Cl_4$

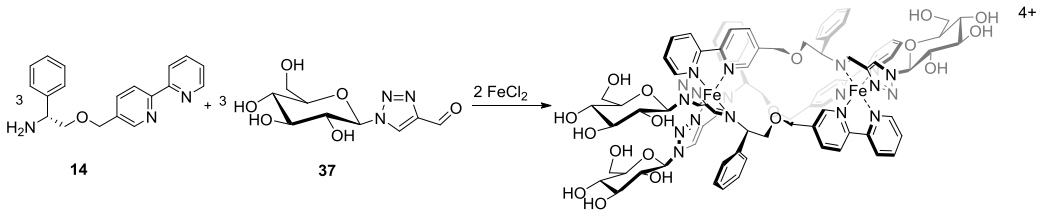

Scheme 5-6 Synthesis of no acetyl protect glucose-triazole triplex metallohelices (R_c,Δ_{Fe})-[$Fe_2\mathbf{L}^{\mathbf{10}}{}_3$]$Cl_4$

The use of three equivalents of (*R*)-2-([2,2'-bipyridin]-5-ylmethoxy)-1-phenylethan-1-amine (**14**) in a one-pot synthesis with three equivalents of the

deprotected glucose-triazole aldehyde derivative **37** and two equivalents of $FeCl_2$ led to the immediate formation of the intense orange solution (Scheme 5-6). After heating for 48 h, the pure bright orange product was isolated via the addition of ethyl acetate to the methanol solution.

The ^{1}H NMR spectrum of this product was consistent with the target triplex structure but contained relatively broad signals. The ^{13}C NMR spectrum was well-resolved and confirmed the presence of three inequivalent ligand environments (Figure 5-11). In the ^{1}H spectrum, three imine singlets H$^{\mathbf{a}}$ were observed at 9.75, 9.54 and 9.18 ppm, followed by two bpy H$^{\mathbf{b}}$ signals at 9.48 and 9.40 ppm. Two triazole singlets H$^{\mathbf{c}}$ were found at 9.54 and 9.26 ppm and two sets of the phenyl protons H$^{\mathbf{d}}$ were detected at 6.79 and 6.62 ppm. In the ^{13}C spectrum, three imine carbon peaks C$^{\mathbf{a}}$ were detected at 164.9, 164.8 and 164.0 ppm with three bpy carbon signals C$^{\mathbf{b}}$ at 159.3, 158.7 and 157.0 ppm. The triazole quaternary carbon peaks C$^{\mathbf{e}}$ were seen at 151.2, 151.1 and 150.7 ppm. Unlike the glyco-pyridine complex $[Fe_2\mathbf{L^5}_3]Cl_4$ and $[Fe_2\mathbf{L^6}_3]Cl_4$ (Chapter 4, section **4.2.1**), no tricationic ion $[Fe_2\mathbf{L^{10}}_3Cl]^{3+}$or similar were observed here, presumably because the geometry of the triazole unit is less well-disposed the Cl^- coordination. A dicationic molecular ion peak at *m/z* 910.2362 Da was observed in the high resolution electrospray mass spectrum of (R_c,Δ_{Fe})-HHT-$[Fe_2\mathbf{L^{10}}_3]Cl_4$, within 0.001 Da of the calculated value (*m/z* 910.2376).

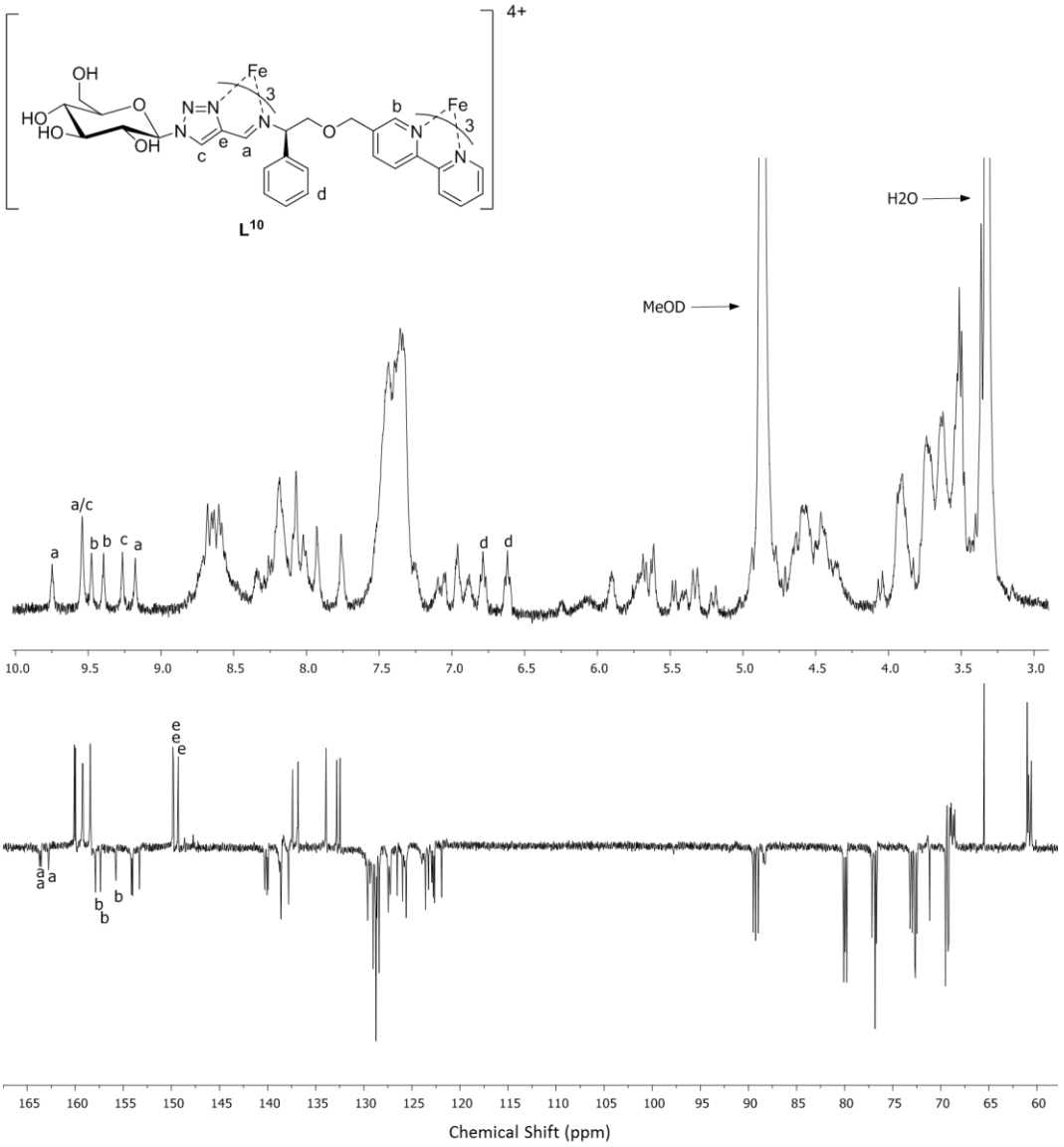

Figure 5-11 ^{1}H (500 MHz, MeOD, 298K) and ^{13}C (125 MHz, MeOD, 298K) NMR spectra of (R_c,Δ_{Fe})-HHT-[Fe_2**L**$^{10}{}_3$]Cl_4

5.7 Stability study in aqueous solution

In advance of evaluation of the compounds in biological applications, the stability of (R_c,Δ_{Fe})-HHT-[Fe_2**L**$^{8a}{}_3$]Cl_4 in aqueous solution was assessed using UV-vis spectroscopy.

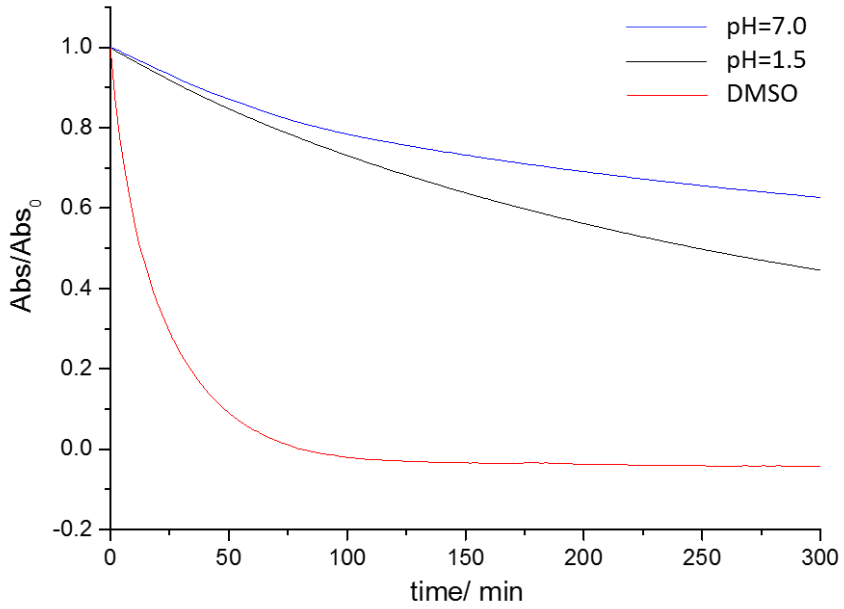

Figure 5-12 Monitoring MLCT absorption of (R_c,Δ_{Fe})-HHT-[Fe_2**L**$^{8a}{}_3$]Cl_4 in HCl/KCl buffer at pH 1.5 (green line), phosphate buffered saline (pH 7.0, black line) and DMSO λ_{max}= 485 nm (red line), concentration 0.02 mg/mL

Time-dependent photoabsorbance measurements of (R_c,Δ_{Fe})-HHT-[Fe_2**L**$^{8a}{}_3$]Cl_4 solutions were observed at 485 nm (within the MLCT band of the complex) in HCl/KCl buffer (pH 1.5), phosphate buffer saline (pH 7.0) and in DMSO. At pH 7.0, a gradual decrease in the absorbance was observed indicating (R_c,Δ_{Fe})-HHT-[Fe_2**L**$^{8a}{}_3$]Cl_4 is decomposing in neutral solution; the corresponding $t_{½}$ was calculated to be 21 h. As expected, under acidic conditions (pH 1.5) the complex decomposed more quickly ($t_{½}$ 4 h) and is rather unstable in DMSO ($t_{½}$ 36 min). It thus appears that the triaozle-imine/bpy triplex system (R_c,Δ_{Fe})-HHT-[Fe_2**L**$^{8a}{}_3$]Cl_4 is far less stable than the otherwise identical pyridine system; the compound (S_c,Λ_{Fe})-HHT-[Fe_2**L**$^{3}{}_3$]Cl_4 for example has $t_{½}$ of over 16 d in PBS at pH 7.

5.8 Biological activity of triazole iron (II) triplex metallohelices

5.8.1 *In vitro* cytotoxicity assay

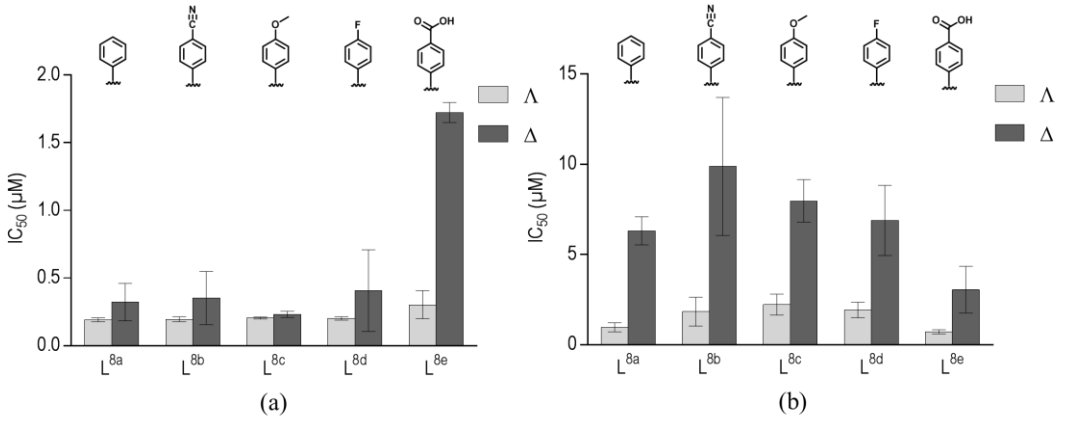

Figure 5-13 IC_{50} values of triazole derived iron (II) triplex $[Fe_2\mathbf{L}^{\mathbf{8a\text{-}e}}{}_3]Cl_4$ against: (a) HCT116 $p53^{++}$ cancer cell line; (b) ARPE19 (noncancerous cell line)

The potencies of all triazole derived iron(II) triplexes $[Fe_2\mathbf{L}^{\mathbf{8a\text{-}e}}{}_3]Cl_4$ were evaluated against the HCT116 $p53^{++}$ colon cancer cell line. As can be seen in Figure 5-13(a), with the exception of the tricarboxylic acid $[Fe_2\mathbf{L}^{\mathbf{8e}}{}_3]Cl_4$ (*vide infra*), this triplex series demonstrated excellent activity with IC_{50} values all lower than 500 nM with little effect of the *para* substituent. The Λ enantiomers were marginally more potent than the Δ enantiomers; the most potent compound was Λ-$[Fe_2\mathbf{L}^{\mathbf{8a}}{}_3]Cl_4$ with IC_{50} 191 ± 10 nM.

Notably, the *para* substitution with a carboxylate group reduces the overall charge and solubility of the $[Fe_2\mathbf{L}^{\mathbf{8a}}{}_3]Cl_4$ in aqueous solution, but no stability decrease was observed. The Δ-$[Fe_2\mathbf{L}^{\mathbf{8e}}{}_3]Cl_4$ appears to reduce the potency to HCT116 $p53^{++}$ by a factor of *ca* 5 with respect to the parent R = H compound Δ-$[Fe_2\mathbf{L}^{\mathbf{8a}}{}_3]Cl_4$, while the

same effect is not found in the Λ compound which has a similar IC_{50} (300 ± 100 nM) to the other compounds.

The compounds were also tested against the non-cancerous retinal pigment epithelial cell line ARPE19. Significant enantiomeric differences in toxicity were observed in the ARPE19 cells; the Λ enantiomers (average IC_{50} value at 1.5 μM) were more cytotoxic than the Δ enantiomers (average IC_{50} value 6.8 μM) [Figure 5-13(b)].

Table 5-1 Cytotoxicity and selectivity index of triazole triplex $[Fe_2\mathbf{L}^{\mathbf{8a\text{-}e}}{}_3]Cl_4$ against HCT116 $p53^{++}$ and ARPE-19 cell line

		mean IC_{50} (μM)		Selectivity Index
		HCT116 p^{53++}	ARPE-19	
$[Fe_2\mathbf{L}^{\mathbf{8a}}{}_3]Cl_4$	Λ	0.19 ± 0.01	0.97 ± 0.25	5
	Δ	0.32 ± 0.14	6.31 ± 0.78	20
$[Fe_2\mathbf{L}^{\mathbf{8b}}{}_3]Cl_4$	Λ	0.20 ± 0.02	1.83 ± 0.80	9
	Δ	0.35 ± 0.20	9.88 ± 3.82	28
$[Fe_2\mathbf{L}^{\mathbf{8c}}{}_3]Cl_4$	Λ	0.20 ± 0.01	2.22 ± 0.58	11
	Δ	0.23 ± 0.02	7.97 ± 1.18	34
$[Fe_2\mathbf{L}^{\mathbf{8d}}{}_3]Cl_4$	Λ	0.20 ± 0.01	1.92 ± 0.43	10
	Δ	0.40 ± 0.30	6.89 ± 1.94	17
$[Fe_2\mathbf{L}^{\mathbf{8e}}{}_3]Cl_4$	Λ	0.30 ± 0.10	0.72 ± 0.11	2
	Δ	1.72 ± 0.07	3.05 ± 1.29	2

A selectivity index (*SI*) is defined as the mean IC_{50} of ARPE19 divided by IC_{50} of HCT116 $p53^{++}$. Except for $[Fe_2\mathbf{L}^{\mathbf{8e}}{}_3]Cl_4$, significant enantiomeric selectivity was observed, with the Δ enantiomers exhibiting substantially better selectivity (SI 17-34) than Λ enantiomers (5-10).

5.8.2 Cytotoxicity of the precursor compounds

As described above, the aqueous stability of this metallohelix series is lower than that of other compounds described in this thesis, with $t_{½}$ for 21 h at pH 7 being rather shorter than the 96 h dosing time period of the MTT assay used in the IC_{50} values (Table 5-1). We thus investigated the cytotoxicity of the ligand sub-components of

$[Fe_2\mathbf{L}^{\mathbf{8a}}{}_3]Cl_4$ under similar conditions; low solubility necessitated dissolution in DMSO prior to dilution.

Table 5-2 Cytotoxicity of precursor compounds *vs* triazole triplex $[Fe_2\mathbf{L}^{\mathbf{8a}}{}_3]Cl_4$ (given per mole of ligand) against HCT116 $p53^{++}$ and ARPE-19 cell line. [a] These figures are derived from those of Table 5-1 by multiplying by 3 in order to allow direct comparison with ligand sub-components.

		mean IC_{50} (μM)		**Selectivity Index**
		HCT116 $p53^{++}$	**ARPE-19**	
14	*S*	1.13 ± 0.37	2.34 ± 0.33	2
14	*R*	2.29 ± 0.57	9.66 ± 3.61	4
29a		> 73.2	> 89.1	-
$[Fe_2\mathbf{L}^{\mathbf{8a}}{}_3]Cl_4$	Λ (*S*)	0.57[a]	2.91[a]	5
	Δ (*R*)	0.96[a]	18.93[a]	20

As seen in Table 5-2, the triazole aldehyde precursor **29a** has minimal cytotoxicity (IC_{50} > 70 μM) towards both HCT116 $p53^{++}$ and ARPE19 cells. Although the two amine enantiomers **14** (*R*/*S*) are both less toxic than their respective helical triplex metallohelix (by a factor of *ca* 2 per mole of ligand), they are both potent compounds against HCT116 $p53^{++}$cells. However, they are both more toxic towards ARPE-19 noncancerous cells than the metallohelix per mole of ligand. The Δ-$[Fe_2\mathbf{L}^{\mathbf{8a}}{}_3]Cl_4$ architecture has 5 times the selectivity than its amine precursor, over a 96 h dosing period, with the added advantage of being water-soluble. Further time-dependent cytotoxicity studies are on-going to see whether the selectivity and potency of the drug changes over time as it decomposes.

5.8 Conclusion

We initially synthesized a series of benzyl triazole aldehydes **29a-e** and investigated the self-assembly reaction with the aminobipyridine **14**. A new asymmetric HHT triazole bimetallic system was isolated and characterised. The highly stereoselective configuration is ascribed to the maximal presentation of π-stacking between the phenyl rings and triazole-imine/bpy. *In vitro* MTT assays revealed that these triazole containing iron(II) triplexes $[Fe_2\mathbf{L}^{\mathbf{8a\text{-}e}}{}_3]Cl_4$ possess excellent anticancer activity against the HCT116 $p53^{++}$ cell line with IC_{50} values under 2 μM and high selectivity towards ARPE19 cell line, whereas the precursors have moderate anticancer activity and lower selectivity.

Since the 1,2,3-triazole moiety is relatively easy to functionalise, we have synthesized glycolconjugated metallohelices from a new sugar triazole aldehyde. We developed a synthetic protocol to form a small series of sugar triazole aldehydes **34-39** and validated the assembly reaction with aminobipyridine **14**. The ^{1}H and ^{13}C NMR spectra confirmed the asymmetric arrangement of glyco-triazole triplex, and no intramolecular Cl^- coordination was observed.

Despite this class of triazole-imine chelated triplex architectures being less stable than previously designed pyridine-imine analogues, we demonstrate greater stability than other reported triazole metallohelice such as Crowley's pyridine-triazole systems which are racemic, decomposed instantaneously in DMSO and reported no biological activity.[36] This new class of structures have intermediate stability ($t_{½}$ 21 h), and it is therefore possible that the intact metallohelix can be uptaken by cells, but are expected to decompose over 24 h. We envisage that these 'metastable' triplex systems

have the potential to help deliver active compounds to the cells, and can even be used to ‘mask’ aldehydes as imines, for release within a cell.

5.9 References

1. N. Wu, C. F. Melan, K. A. Stevenson, O. Fleischel, H. Guo, F. Habib, R. J. Holmberg, M. Murugesu, N. J. Mosey and H. Nierengarten, *Dalton Trans.*, 2015, **44**, 14991-15005.
2. D. A. Roberts, A. M. Castilla, T. K. Ronson and J. R. Nitschke, *J. Am. Chem. Soc.*, 2014, **136**, 8201-8204.
3. T. Nakamura, H. Kimura, T. Okuhara, M. Yamamura and T. Nabeshima, *J. Am. Chem. Soc.*, 2016, **138**, 794-797.
4. H. Zhang, J. Lee, A. D. Lammer, X. Chi, J. T. Brewster, V. M. Lynch, H. Li, Z. Zhang and J. L. Sessler, *J. Am. Chem. Soc.*, 2016, **138**, 4573-4579.
5. A. Schmidt, M. Hollering, J. Han, A. Casini and F. E. Kühn, *Dalton Trans.*, 2016, **45**, 12297-12300.
6. M. Han, D. M. Engelhard and G. H. Clever, *Chem. Soc. Rev.*, 2014, **43**, 1848-1860.
7. S. Bala, A. Goswami, S. Sengupta, S. Ganguly, S. Bhattacharya, S. Khanra and R. Mondal, *Cryst. Growth Des.*, 2013, **13**, 5068-5075.
8. L. Zhang, J.-J. Wang and G.-C. Xu, *Inorg. Chem. Commun.*, 2014, **39**, 66-69.
9. A. M. Madalan, X.-Y. Cao, G. Rogez and J.-M. Lehn, *Inorg. Chem.*, 2014, **53**, 4275-4277.
10. U. S. Schubert, H. Hofmeier and G. R. Newkome, *Modern terpyridine chemistry*, John Wiley & Sons, 2006.
11. O. Fleischel, N. Wu and A. Petitjean, *Chem. Commun.*, 2010, **46**, 8454-8456.
12. J. E. Hein and V. V. Fokin, *Chem. Soc. Rev.*, 2010, **39**, 1302-1315.
13. C. A. Ramsden, *Tetrahedron*, 2010, **66**, 2695-2699.
14. K. Jug, S. Chiodo, P. Calaminici, A. Avramopoulos and M. G. Papadopoulos, *J. Phys. Chem. A*, 2003, **107**, 4172-4183.
15. K. Shen, Y. Fu, J.-N. Li, L. Liu and Q.-X. Guo, *Tetrahedron*, 2007, **63**, 1568-1576.
16. N. a. Kovačević and A. Kokalj, *J. Phys. Chem. C*, 2011, **115**, 24189-24197.
17. B. Schulze and U. S. Schubert, *Chem. Soc. Rev.*, 2014, **43**, 2522-2571.
18. P. Mathew, A. Neels and M. Albrecht, *J. Am. Chem. Soc.*, 2008, **130**, 13534-13535.
19. B. Schulze, D. Escudero, C. Friebe, R. Siebert, H. Görls, S. Sinn, M. Thomas, S. Mai, J. Popp and B. Dietzek, *Chem. Eur. J.*, 2012, **18**, 4010-4025.
20. I. Stengel, A. Mishra, N. Pootrakulchote, S.-J. Moon, S. M. Zakeeruddin, M. Grätzel and P. Bäuerle, *J. Mater. Chem.*, 2011, **21**, 3726-3734.
21. B. Schulze, D. G. Brown, K. C. Robson, C. Friebe, M. Jäger, E. Birckner, C. P. Berlinguette and U. S. Schubert, *Chem. Eur. J.*, 2013, **19**, 14171-14180.
22. J. s. M. Fernández-Hernández, C.-H. Yang, J. I. Beltrán, V. Lemaur, F. Polo, R. Fröhlich, J. Cornil and L. De Cola, *J. Am. Chem. Soc.*, 2011, **133**, 10543-10558.
23. J. s. M. Fernández-Hernández, J. I. Beltrán, V. Lemaur, M.-D. Gálvez-López, C.-H. Chien, F. Polo, E. Orselli, R. Fröhlich, J. r. m. Cornil and L. De Cola, *Inorg. Chem.*, 2013, **52**, 1812-1824.
24. K. N. Swanick, S. Ladouceur, E. Zysman-Colman and Z. Ding, *Chem. Commun.*, 2012, **48**, 3179-3181.
25. M. Mydlak, C. Bizzarri, D. Hartmann, W. Sarfert, G. Schmid and L. De Cola, *Adv. Funct. Mater.*, 2010, **20**, 1812-1820.

26. J. M. Fernández-Hernández, S. Ladouceur, Y. Shen, A. Iordache, X. Wang, L. Donato, S. Gallagher-Duval, M. de Anda Villa, J. D. Slinker and L. De Cola, *J. Mater. Chem. C*, 2013, **1**, 7440-7452.
27. K. N. Swanick, S. Ladouceur, E. Zysman-Colman and Z. Ding, *Angew. Chem.*, 2012, **124**, 11241-11244.
28. Y. Li, J. C. Huffman and A. H. Flood, *Chem. Commun.*, 2007, 2692-2694.
29. N. Ségaud, J.-N. l. Rebilly, K. Sénéchal-David, R. g. Guillot, L. Billon, J.-P. Baltaze, J. Farjon, O. Reinaud and F. d. r. Banse, *Inorg. Chem.*, 2013, **52**, 691-700.
30. A. Bastero, D. Font and M. A. Pericàs, *J. Org. Chem.*, 2007, **72**, 2460-2468.
31. S.-i. Aizawa, K. Matsuda, T. Tajima, M. Maeda, T. Sugata and S. Funahashi, *Inorg. Chem.*, 1995, **34**, 2042-2047.
32. R. A. Vasdev, D. Preston and J. D. Crowley, *Dalton Trans.*, 2017, **46**, 2402-2414.
33. M. Juríček, P. H. Kouwer and A. E. Rowan, *Chem. Commun.*, 2011, **47**, 8740-8749.
34. H. Struthers, T. L. Mindt and R. Schibli, *Dalton Trans.*, 2010, **39**, 675-696.
35. Q. V. van Hilst, N. R. Lagesse, D. Preston and J. D. Crowley, *Dalton Trans.*, 2018.
36. S. K. Vellas, J. E. Lewis, M. Shankar, A. Sagatova, J. D. Tyndall, B. C. Monk, C. M. Fitchett, L. R. Hanton and J. D. Crowley, *Molecules*, 2013, **18**, 6383-6407.
37. R. A. Vasdev, D. Preston, S. Ø. Scottwell, H. J. Brooks, J. D. Crowley and M. P. Schramm, *Molecules*, 2016, **21**, 1548.
38. S. C. Hockey, G. J. Barbante, P. S. Francis, J. M. Altimari, P. Yoganantharajah, Y. Gibert and L. C. Henderson, *Eur. J. Med. Chem.*, 2016, **109**, 305-313.
39. B. J. Pages, J. Sakoff, J. Gilbert, Y. Zhang, F. Li, D. Preston, J. D. Crowley and J. R. Aldrich-Wright, *J. Inorg. Biochem.*, 2016, **165**, 92-99.
40. P. R. Florindo, D. M. Pereira, P. M. Borralho, P. J. Costa, M. Piedade, C. M. Rodrigues and A. C. Fernandes, *Dalton Trans.*, 2016, **45**, 11926-11930.
41. S. Clède, F. Lambert, R. Saint-Fort, M. A. Plamont, H. Bertrand, A. Vessières and C. Policar, *Chem. Eur. J.*, 2014, **20**, 8714-8722.
42. A. Prokop, J. A. Czaplewska, M. Clausen, M. König, A. Wild, R. Thorwirth, B. Schulze, K. Babiuch, D. Pretzel and U. S. Schubert, *Eur. J. Inorg. Chem.*, 2016, **2016**, 3480-3488.
43. S. Hohloch, L. Suntrup and B. Sarkar, *Organometallics*, 2013, **32**, 7376-7385.
44. S. Jindabot, K. Teerachanan, P. Thongkam, S. Kiatisevi, T. Khamnaen, P. Phiriyawirut, S. Charoenchaidet, T. Sooksimuang, P. Kongsaeree and P. Sangtrirutnugul, *J. Organomet. Chem.*, 2014, **750**, 35-40.
45. K. E. Djernes, O. Moshe, M. Mettry, D. D. Richards and R. J. Hooley, *Org. Lett.*, 2012, **14**, 788-791.
46. K. E. Djernes, M. Padilla, M. Mettry, M. C. Young and R. J. Hooley, *Chem. Commun.*, 2012, **48**, 11576-11578.
47. U. R. Pokharel, F. R. Fronczek and A. W. Maverick, *Nat. Commun.*, 2014, **5**, 5883.
48. P. A. Scattergood, A. Sinopoli and P. I. Elliott, *Coord. Chem. Rev.*, 2017.
49. P. A. Scattergood and P. I. Elliott, *Dalton Trans.*, 2017, **46**, 16343-16356.
50. Y. Li, L. Zhao, A. Y. Y. Tam, K. M. C. Wong, L. Wu and V. W. W. Yam, *Chem. Eur. J.*, 2013, **19**, 14496-14505.

51. Y. Li, L. Chen, Y. Ai, E. Y.-H. Hong, A. K.-W. Chan and V. W.-W. Yam, *J. Am. Chem. Soc.*, 2017, **139**, 13858-13866.
52. A. K.-W. Chan, D. Wu, K. M.-C. Wong and V. W.-W. Yam, *Inorg. Chem.*, 2016, **55**, 3685-3691.
53. B. Schulze, A. Winter, C. Friebe, E. Birckner and U. S. Schubert, *ACS Macro Lett.*, 2017, **6**, 181-184.
54. J. Zhang, M. J. Junk, J. Luo, D. Hinderberger and X. Zhu, *Langmuir*, 2010, **26**, 13415-13421.
55. Y. H. Lau, P. J. Rutledge, M. Watkinson and M. H. Todd, *Chem. Soc. Rev.*, 2011, **40**, 2848-2866.
56. J. Han, Y. Zheng, S. Zheng, S. Li, T. Hu, A. Tang and C. Gao, *Chem. Commun.*, 2014, **50**, 8712-8714.
57. K. H. L. Ho, I. Hijazi, L. Rivier, C. Gautier, B. Jousselme, G. de Miguel, C. Romero-Nieto, D. M. Guldi, B. Heinrich and B. Donnio, *Chem. Eur. J.*, 2013, **19**, 11374-11381.
58. P. Waelès, B. Riss-Yaw and F. Coutrot, *Chem. Eur. J.*, 2016, **22**, 6837-6845.
59. C. Cheng, P. R. McGonigal, S. T. Schneebeli, H. Li, N. A. Vermeulen, C. Ke and J. F. Stoddart, *Nat. Nanotechnol.*, 2015, **10**, 547.
60. J. D. Crowley, S. M. Goldup, A.-L. Lee, D. A. Leigh and R. T. McBurney, *Chem. Soc. Rev.*, 2009, **38**, 1530-1541.
61. K. D. Hänni and D. A. Leigh, *Chem. Soc. Rev.*, 2010, **39**, 1240-1251.
62. K. A. Stevenson, C. F. Melan, O. Fleischel, R. Wang and A. Petitjean, *Cryst. Growth Des.*, 2012, **12**, 5169-5173.
63. S. M. McNeill, D. Preston, J. E. Lewis, A. Robert, K. Knerr-Rupp, D. O. Graham, J. R. Wright, G. I. Giles and J. D. Crowley, *Dalton Trans.*, 2015, **44**, 11129-11136.
64. P. R. Bagdi, R. S. Basha and A. T. Khan, *RSC Adv.*, 2015, **5**, 61337-61344.
65. R. H. Tale, V. B. Gopula and G. K. Toradmal, *Tetrahedron Lett.*, 2015, **56**, 5864-5869.
66. H. Hagiwara and S. Okada, *Chem. Commun.*, 2016, **52**, 815-818.
67. G. L. Goud, S. Ramesh, D. Ashok and V. P. Reddy, *Russ. J. Gen. Chem.*, 2016, **86**, 1419-1423.
68. Z.-C. Dai, Y.-F. Chen, M. Zhang, S.-K. Li, T.-T. Yang, L. Shen, J.-X. Wang, S.-S. Qian, H.-L. Zhu and Y.-H. Ye, *Org. Biomol. Chem.*, 2015, **13**, 477-486.
69. T. Ismail, S. Shafi, I. Hyder, T. Sidiq, A. Khajuria, S. M. Alam and M. Halmuthur, *Arch. Pharm.*, 2015, **348**, 796-807.
70. P. S. Rao, C. Kurumurthy, B. Veeraswamy, G. S. Kumar, Y. Poornachandra, C. G. Kumar, S. B. Vasamsetti, S. Kotamraju and B. Narsaiah, *Eur. J. Med. Chem.*, 2014, **80**, 184-191.
71. M. R. Gannarapu, S. B. Vasamsetti, N. Punna, S. Kotamraju and N. Banda, *MedChemComm*, 2015, **6**, 1494-1500.
72. M. M. Pisal, R. A. Annadate, M. C. Athalye, D. Kumar, S. P. Chavan, D. Sarkar and H. B. Borate, *Bioorg. Med. Chem. Lett.*, 2017, **27**, 979-988.
73. H. Hagiwara, R. Minoura, S. Okada and Y. Sunatsuki, *Chem. Lett.*, 2014, **43**, 950-952.
74. H. Hagiwara, T. Tanaka and S. Hora, *Dalton Trans.*, 2016, **45**, 17132-17140.
75. H. Hagiwara, T. Masuda, T. Ohno, M. Suzuki, T. Udagawa and K.-i. Murai, *Cryst. Growth Des.*, 2017, **17**, 6006-6019.
76. H. P. Mangunuru, J. R. Yerabolu, D. Liu and G. Wang, *Tetrahedron Lett.*, 2015, **56**, 82-85.

77. K. Upadhyaya, K. Singh, A. Arun, M. Shukla, N. Srivastava, R. Ashraf, A. Sharma, R. Mahar, S. K. Shukla and J. Sarkar, *Org. Biomol. Chem.*, 2016, **14**, 1338-1358.

Chapter 6

Experimental

6.1 Chemicals and solvents

All solvents and chemicals purchased from commercial sources (Sigma-Aldrich, Acros, Fisher Scientific or Alfa Aesar) were used without further purification unless otherwise stated. Sodium hydride dispersions in mineral oil were placed in a Schlenk vessel under an inert atmosphere and washed three times with diethyl ether to remove the oil. The sodium hydride powder was then dried and stored in an MBraun glove box at <5 ppm O_2. Necessary solvents were dried by heating to reflux for 3 d under dinitrogen over the appropriate drying agents (potassium for tetrahydrofuran, and calcium hydride for acetonitrile, pyridine, diisopropyl amine and triethylamine) and degassed before use. Tetrahydrofuran and diethyl ether were additionally pre-dried over sodium wire. All dried and degassed solvents were stored in glass ampoules under argon. Deuterated solvents were purchased from Sigma-Aldrich or Cambridge Isotope Laboratories Inc and pre-dried over molecular sieves (3A for methanol, dimethyl sulfoxide and acetonitrile; 4A for chloroform), for 24 h prior to use.

6.2 Equipment and instrumentation

All glassware and cannulae were stored in an oven at > 375 K. Where appropriate, reactions were carried out under argon using a dual manifold argon/vacuum line and standard Schlenk techniques or using an MBraun glove box at <5 ppm O_2.

NMR spectra were recorded on Bruker Spectrospin 300/400/500/600 spectrometers and Bruker AV II DRX-300/500 spectrometers. Routine NMR assignments were confirmed by ^{1}H-^{1}H (COSY) and ^{13}C-^{1}H (HMQC) correlation experiments where necessary. The spectra were internally referenced using the residual protio solvent ($CDCl_3$, CD_3CN *etc.*) resonance relative to tetramethylsilane (δ = 0 ppm). ESI mass spectra were recorded on Bruker Esquire 2000 or Bruker MicroTOF spectrometers. Infra-Red spectra were measured using a Bruker Alpha-P FTIR spectrometer. Elemental analyses were performed by MEDAC Ltd. Chobham, Surrey GU24, 8JB, UK.

UV-Visible absorbance spectra were recorded using a Jasco V-660 spectrometer. Measurements were collected in a 1 cm path-length quartz cuvette using the following standard parameters: bandwidth 1 nm, response time 1 sec, wavelength scan range 200 – 800 nm, data pitch 0.2 nm, scanning speed 200 nm/min and accumulation 1. CD spectra were measured on a Jasco J-815 spectrometer. Measurements were collected in a 1 cm path-length quartz cuvette using the following standard parameters: bandwidth 1 nm, response time 1 sec, wavelength scan range 200 – 800 nm, data pitch 0.2 nm, scanning speed 100 nm/min and accumulation 10.

6.3 Ligand components

(*S*)-2-(prop-2-ynyloxy)-1-phenylethanamine[1] (**1**)

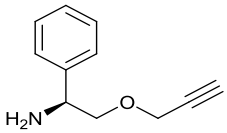

(*S*)-2-Phenylglycinol (0.50 g, 3.6 mmol) was dissolved in dry THF (15 ml) and added to a stirred suspension of sodium hydride (0.17 g, 7.3 mmol, 2.0 eq.) in dry THF (10 ml). The solution was stirred for 1 h at ambient temperature, followed by addition of propargyl bromide (0.43 ml, 3.8 mmol, 1.05 eq.). The solution was stirred for 1 h at ambient temperature then heated to reflux (65°C) under partial vacuum overnight. After cooling to ambient temperature, the solution was poured into brine (30 ml). The crude product was extracted with diethyl ether (4 × 50 ml), dried over sodium sulfate and isolated under reduced pressure. This crude product was purified by flash chromatography (DCM/MeOH/Triethylamine, 500:5:2; R_f = 0.50) to furnish (*S*)-2-(prop-2-ynyloxy)-1-phenylethanamine as a yellow oil.

Yield 0.70 g, 55%.

^{1}H NMR (400 MHz, 298 K, $CDCl_3$) δ_H ppm 7.52-7.19 (5H, m, Ph), 4.30-4.19 (3H, m, CH, CH_2), 3.72 (1H, dd, $^3J_{HH}$ = 9.0 Hz, $^4J_{HH}$ = 3.7 Hz), 3.50 (1H, t, $^3J_{HH}$ = 9.0 Hz, CH_2), 2.46 (1H, t, $^4J_{HH}$ = 2.4 Hz, C≡H), 1.76 (2H, s, NH_2).

^{13}C {^{1}H} NMR (100 MHz, 298 K, $CDCl_3$) δ_C ppm 142.26, 128.48, 127.50, 126.84 (Ph), 74.58 (CH), 58.45 (CH_2), 55.39 (CH).

MS (ESI) *m/z* 176 $[M+H]^+$

5-(propargyloxy)picolinaldehyde[2] (**2**).

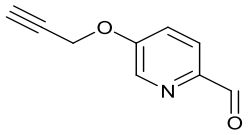

5-(Hydroxy)picolinaldehyde (1.23 g, 10.0 mmol) was dissolved in acetonitrile (40 ml), followed by the addition of potassium carbonate (1.45 g, 10.5 mmol) and propargyl bromide (80 wt% in toluene, 1.17 ml). The solution was stirred at reflux (*ca*. 85°C) overnight, cooled to ambient temperature and filtered through a short column of silica. The solvent was removed under reduced pressure to leave the crude product as a dark orange solid. The pure product was recrystalised from n-hexane/dichloromethane (80:20 v/v).

Yield = 0.45 g, 80%.

^{1}H NMR (400 MHz, 298 K, DMSO) δ_H ppm 9.90 (1H, s, HC=O), 8.54 (1H, d, $^{4}J_{HH}$ = 2.8 Hz), 7.98 (1H, d, $^{3}J_{HH}$ = 8.7 Hz), 7.64 (1H, dd, $^{3}J_{HH}$ = 8.7 Hz, $^{4}J_{HH}$ = 2.8 Hz, Py), 5.05 (2H, d, $^{4}J_{HH}$ = 2.3 Hz, CH_2–C≡C), 3.71 (1H, t, $^{4}J_{HH}$ = 2.3 Hz, C≡CH).

^{13}C {^{1}H} NMR (100 MHz, 298 K, DMSO) δ_C ppm 192.50 (CO), 157.22, 146.69, 139.40, 123.85, 122.27 (Py), 79.96 (C≡*C*H), 78.45 (*C*≡CH), 56.80 (CH_2).

MS (ESI) *m/z* 162 $[M+H]^+$

IR υ cm^{-1} 3210 w, 1690 s, 1570 s, 1485 w, 1380 w, 1305 m, 1276 w, 1260 s, 1200 s, 1005 s, 970 m, 914 w, 830 s, 802 s, 730 m, 693 s, 661 s.

Elemental Analysis found (Calculated for $C_9H_7NO_2$) % C 66.75 (67.08), H 4.32 (4.38), N 8.61 (8.69).

(*R*,*R*)-4,4'-bis[(2-amino-2-phenylethoxy)methyl]-diphenyl ether[3] (**3**)

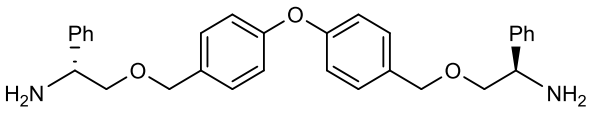

(*R*)-2-phenylglycinol (0.66 g, 4.8 mmol, 2.1 eq.) and 15-crown-5 (0.67 g, 3.0 mmol, 1.3 eq.) were dissolved in dry THF (30 ml) under inter atmosphere and was added dropwise to a stirred suspension of sodium hydride (0.25 g, 10.4 mmol, 4.6 eq.). The reaction mixture was stirred under partial vacuum for 1 h at ambient temperature. This was followed by dropwise addition of the *bis*-4-(bromomethyl)phenyl ether (0.8 g, 2.3 mmol, 1.0 eq.) in dry THF (30 ml). The solution was then heated to reflux (65˚C) for 4h. After cooled to ambient temperature, the reaction was quenched with brine (20 ml). The product was extracted into diethyl ether (3 × 100 ml), dried over sodium sulphate and the solvent was removed under reduced pressure to leave a yellow oil. The pure product was obtained by Kügelrohr distillation to remove unreacted excess (*R*)-2-phenylglycinol and 15-crown-5 at 155 ˚C under high vacuum, to give a yellow oil.

Yield: 0.85 g, 78%

^{1}H NMR (300 MHz, 298 K, $CDCl_3$) δ_H 7.42-7.29 (14H, m, Ph), 7.00 (4H, d, $^{3}J_{HH}$ = 8.5 Hz, Ph), 4.55 (4H, s, CH_2Ph), 4.27 (2H, dd, $^{2}J_{HH}$ = 9.0 Hz, $^{3}J_{HH}$ = 4.0 Hz,CHPh), 3.65 (2H, dd, $^{2}J_{HH}$ = 9.0 Hz, $^{3}J_{HH}$ = 4.0 Hz, C$\underline{H}_2$CHPh), 3.49 (2H, t, $^{2}J_{HH}$/ $^{3}J_{HH}$ = 9.0 Hz, C$\underline{H}_2$CHPh), 1.80 (4H, s, NH_2)

^{13}C {^{1}H} NMR (75 MHz, 298K, $CDCl_3$) δ_C 156.3, 141.9, 132.5, 128.8, 127.8, 126.8, 126.2, 118.1 (Ph), 76.0 ($\underline{C}H_2$CHPh), 72.3 (CH_2Ph), 55.0 (CHPh)

ESI-MS (+) *m/z* 469.2 $[M+H]^+$, 491.2 $[M+Na]^+$

IR υ (cm^{-1}): 3028 w, 2850 w, 1603 m, 1500 s, 1450 w, 1355 w, 1238 s, 1160 w, 1077 s, 1015 w, 874 m, 760 s, 700 s.

Elemental Analysis found (Calculated for $C_{30}H_{32}N_2O_3$) % C 76.47 (76.90), H 7.14 (6.88), N 5.65 (5.98).

5-hydroxy-2-methylpyridine-1-oxide[4] (**4**).

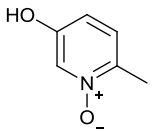

5-Hydroxy-2-mehylpyridine (25.0 g, 0.23 mol) was suspended in a solution of *m*-chlorperbenzoic acid (43 g, 0.23 mol) in chloroform (250 ml) and heated to reflux for 2 h. After cooling down to ambient temperature and stirred for a further 2 h, the solvents were removed under reduced pressure. The crude product was washed with ethyl acetate, isolated by filtration and dried to give the pure compound as a pale yellow solid.

Yield 15.6 g, 54%

^{1}H NMR (400 MHz, 298 K, DMSO) δ_H ppm 10.22 (1H, s, OH), 7.81 (1H, d, $^4J_{HH}$ = 2.3 Hz, Py), 7.24 (1H, d, $^3J_{HH}$ = 8.5 Hz, Py), 6.77 (1H, dd, $^3J_{HH}$ = 8.5 Hz, $^4J_{HH}$ = 2.3 Hz, Py), 2.23 (3H, s, Me).

^{13}C {^{1}H} NMR (75 MHz, 298 K, DMSO) δ_C ppm 153.97, 138.96, 127.33, 126.07, 113.64 (Py), 16.26 (CH_3).

MS (ESI) *m/z* 126 $[M+H]^+$ 148 $[M+Na]^+$.

IR υ cm^{-1} 2360 m, 1623 w, 1571 m, 1526 m, 1456 m, 1385 m, 1308 m, 1273 w, 1227 m, 1163 m, 1114 s, 963 w, 859 s, 822 s, 775 m, 741 w, 690 w.

6-(acetoxymethyl)pyridin-3-yl acetate[4] (**5**).

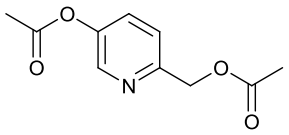

5-Hydroxy-2-methylpyridine-1-oxide (**4**) (15.60 g, 0.13 mol) was suspended in acetic anhydride (400 ml) and heated to reflux for 4 h. After cooling down to ambient temperature, the solvent was removed under reduced pressure to give the titular product as a black oil which was suitable for use without further purification.

Yield 24.8, 95%

^{1}H NMR (400 MHz, 298 K, DMSO) δ_H ppm 8.39 (1H, d, $^{4}J_{HH}$ = 2.5 Hz, Py), 7.66 (1H, dd, $^{3}J_{HH}$ = 8.5 Hz, $^{4}J_{HH}$ = 2.5 Hz, Py), 7.50 (1H, d, $^{3}J_{HH}$ = 8.5 Hz, Py), 5.14 (2H, s, CH_2), 2.31 (3H, s, CH_3) 2.12 (3H, s, CH_3).

^{13}C {^{1}H} NMR (75 MHz, 298 K, DMSO) δ_C ppm 170.0 (C=O), 169.1 (C=O) 152.9, 146.4, 142.8, 130.2, 122.4 (Py), 65.6 (CH_2), 20.7 (CH_3), 20.6 (CH_3).

MS (ESI) *m/z* 232 $[M+Na]^+$.

6-(hydroxymethyl)pyridine-3-ol[4] (**6**)

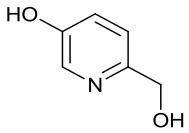

6-[(Acetyloxy)methyl]pyridine-3-yl acetate (**5**) (26.40 g, 0.13 mol) was dissolved in concentrated hydrochloric acid (36%, 100 ml) and stirred at reflux (110 °C) for 24 h. The volatile was removed under reduced pressure to 20 ml and the solution was neutralised with sodium hydroxide solution (1 M, 50 ml) to pH7. The solvent was removed under reduced pressure to yield a brown solid which was dried *in vacuo* (50

^{o}C). The crude compound was dissolved in acetonitrile (3 × 150 ml) and heated reflux for 1 h, filtered hot and the solvent was removed under reduced pressure to yield a brown/yellow solid.

Yield: 9.26 g, 59%.

^{1}H NMR (400 MHz, 298 K, DMSO): δ_H ppm 10.15 (s, br, 1H, PyO*H*), 8.03 (d, 1H, $^{4}J_{HH}$ = 2.7 Hz, Py), 7.26 (d, 1H, $^{3}J_{HH}$ = 8.4 Hz, Py), 7.13 (dd, 1H, $^{3}J_{HH}$ = 8.4 Hz, $^{4}J_{HH}$ = 2.7 Hz, Py), 4.44 (s, 1H, CH_2).

^{13}C {^{1}H} NMR (100 MHz, 298K, DMSO): δ_C ppm 152.42, 151.87, 136.44, 122.54, 120.97 (Py), 63.92 (CH_2).

MS (ESI) *m/z* 126 $[M+H]^+$

IR υ cm^{-1} 2845 w, 2366 br, 1760 w, 1570 m, 1491 m, 1455 m, 1336 w, 1269 m, 1208 s, 1128 w, 1117 w, 1070 s, 1026 m, 893 w, 858 w, 829 s, 760 w, 715 w, 658 s.

5-(hydroxyl)picolionaldehyde[4] (**7**)

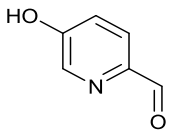

6-(Hydroxymethyl)pyridine-3-ol (**6**) (9.26 g, 74 mmol) was dissolved in isopropanol (200 ml). Activated manganese dioxide (16.10 g, 185 mmol) was added and the solution was heated at reflux (100^{o}C) for 4 h and stirred for a further 18 h at ambient temperature. The reaction mixture was filtered through celite and the solvent was removed under reduced pressure. The pure product was recrystalised from boiling water (50 ml).

Yield: 1.82 g, 20%.

^{1}H NMR (300 MHz, 298 K, DMSO): δ_H ppm 11.07 (s, br, 1H, OH), 9.83 (s, 1H, CHO), 8.32 (d, 1H, $^{4}J_{HH}$ = 2.6 Hz, Py), 7.85 (d, 1H, $3J_{HH}$ = 8.5 Hz, Py), 7.33 (dd, 1H, $^{3}J_{HH}$ = 8.5 Hz, $^{4}J_{HH}$ = 2.7 Hz), 3.38 (s, br, 1H, *Py*OH).

^{13}C {^{1}H} NMR (100 MHz, 298 K, DMSO): δ_C ppm 192.34 (CHO), 158.41, 145.21, 139.25, 124.22, 122.86 (Py).

MS (ESI) *m/z* 124 $[M+H]^+$

IR υ cm^{-1} 2885 w, 2840 w, 1570 s, 1485 m, 1460 w, 1370 w, 1320 w, 1205 s, 1116 m, 1071 s, 1026 m, 886 w, 850 w, 756 w.

L-phenylglycinol[5] (**8**)

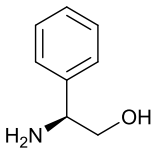

L-phenylglycine (20.0 g, 0.13 mol) was suspended in dry tetrahydrofuran (100 ml) under argon and was added drop-wise to a stirred solution of lithium aluminium hydride (10 g, 0.26 mol) in dry tetrahydrofuran (100 ml) at 0°C. The suspension was allowed to warm to ambient temperature and then heated at reflux (70°C) for 16 h. After cooling to 0°C, the reaction mixture was quenched by drop-wise addintion of saturated potassium carbonate solution (250 ml). The solid was filtered off to obtain a yellow solution. The solvent was removed under reduced pressure to give a yellow solid, which was recrystallized from hot toluene to give the pure product as a white crystalline solid.

Yield: 15.6 g, 87%.

^{1}H-NMR (400 MHz, 298 K, $CDCl_3$): δ_H ppm 7.31 (m, 5H, Ph), 4.04 (dd, 1H, $^{3}J_{HH}$ = 8.3Hz, $^{4}J_{HH}$ = 4.4 Hz, CH), 3.74 (dd, 2H, $^{3}J_{HH}$ = 10.8 Hz, $^{4}J_{HH}$ = 4.4Hz, CH_2), 3.55 (dd, 2H, $^{3}J_{HH}$ = 10.7 Hz, $^{4}J_{HH}$ = 8.3 Hz, CH_2), 2.04 (s, 2H, NH_2).

^{13}C {^{1}H} NMR (101 MHz, 298 K, $CDCl_3$): δ_C ppm 142.74, 128.65, 127.52, 126.47 (Ph), 68.04 (CH_2), 57.35 (CH).

MS (ESI) *m/z* 138 $[M+H]^+$

IR υ cm^{-1}: 3325 w, 2833 s, 1600 m, 1495 m, 1450 m, 1195 w, 1071 m, 1043 m, 970 m, 876 m, 750 s, 701 s.

Elemental analysis found (Calculated for $C_8H_{11}NO$) % C 70.16 (70.04) H 8.12 (8.08) N 10.13 (10.21)

(*E*)-5,5'-(but-2-ene-1,4-diylbis(oxy))dipicolinaldehyde (**9**)

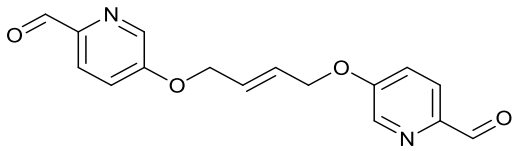

9 was synthesised using the procedure described for **2**, substituting propargyl bromide for 1,4-trans-dibromobut-2-ene with 1 equivalent more 5-(hydroxy)picolinaldehyde added. The resulting beige solid was recrystalised from mixture solvent: methanol/ n-hexane (10:90 v/v).

Yield = 2.24 g, 75%.

^{1}H NMR (300 MHz, 298 K, CD_3CN) δ_H ppm 9.93 (2H, s, CHO), 8.47 (2H, d, $^{3}J_{HH}$ = 2.5 Hz), 7.94 (2H, d, $^{3}J_{HH}$ = 10 Hz), 7.46 (2H, dd, $^{3}J_{HH}$ = 8.7 Hz, $^{4}J_{HH}$ = 2.3 Hz, Py), 6.16 (2H, m CH), 4.80 (4H, m, CH_2).

^{13}C {^{1}H} NMR (75 MHz, 298 K, CD_3CN) δ_C ppm 192.61 (CHO), 139.64, 128.81, 123.68, 121.71 (Py), 68.71 (CH_2).

MS (ESI) *m/z* 321 $[M+Na]^+$

IR υ cm^{-1} 2842 w, 1705 m, 1551 m, 1270 s, 1124 s, 801 m, 610 m.

1-(2-pyridylacetyl)pyridinium iodide[6] (**10**)

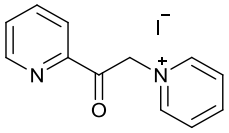

2-Acetylpyridine (26.65 g, 25 ml, 220mmol) was added *via* syringe to a solution of iodine (56.50 g, 220 mmol) in dry pyridine (225 ml) in a 500 ml round bottomed Schlenk vessel. The round bottomed Schlenk was fitted with a condenser and a N_2 bubbler. The reaction mixture was stirred and heated at reflux (130^{o}C) for 2 h and then cooled to to 0^{o}C using an ice/water bath. A 9:1 mixture of diethyl ether/ethanol (20 ml) was then added into the solution. The resulting black precipitate was filtered off, washed with a 9:1 mixture of diethyl ether/ethanol (20 ml), and dried in air. The precipitate was then dissolved in boiling methanol (250 ml) with activated charcoal (30 g) and stirred at reflux for 30 min. The solution was filtered through hot celite in a fritted funnel and the solvent was removed under reduced pressure to leave the crude product. Recrystallisation from hot methanol (100 ml) resulted the final product in light brown crystal which was filtered, washed with cold methanol (25 ml), and dried *in vacuo*.

Yield = 36.25 g, 50%.

^{1}H NMR (400 MHz, 298 K, DMSO) δ_H ppm 9.02 (2H, d, $^{3}J_{HH}$ = 5.7 Hz, Py), 8.88 (1H, d, $^{3}J_{HH}$ = 4.7 Hz, Py), 8.74 (1H, t, $^{3}J_{HH}$ = 7.8 Hz, Py), 8.29 (2H, m, Py), 8.15 (1H, td,

$^{3}J_{HH}$ = 7.7 Hz, $^{4}J_{HH}$ = 1.4 Hz, Py), 8.08 (1H, d, $^{3}J_{HH}$ = 7.7 Hz, Py), 7.85 (1H, m, Py), 6.52 (2H, s, CH_2).

^{13}C {^{1}H} NMR (100 MHz, 298 K, DMSO) δ_C ppm 191.46 (C=O), 150.42, 149.54, 146.32, 146.28, 138.13, 129.12, 127.69, 122.01 (Py), 66.63 (CH_2).

MS (ESI) *m/z* 199 $[M]^+$

IR υ cm^{-1} 3040 w, 1703 m, 1475 m, 990 m, 785 m, 760 m, 695 m, 670 m, 565m.

5-methyl-2,2'-bipyridine[7] (**11**)

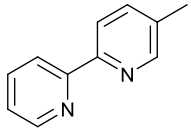

1-(2-Pyridylacetyl)pyridinium iodide (36.25 g, 110 mmol) and ammonium acetate (21.43g, 280 mmol) were dissolved in formamide (250 ml) in argon condition. Freshly distilled methacrolein (7.79 g, 9.17 ml, 110 mmol) was then added *via* syringe and the solution was heated at 80°C for 6 h. After cooled to ambient temperature, water (150 ml) and DCM (3 × 250 ml) were added into the reaction mixture. The organic layer was collected, dried over sodium sulphate and the solvent was removed under reduced pressure to leave a yellow liquid. Distillation under vacuum at 110˚C gave the pure product as a pale yellow oil.

Yield = 11.4 g, 61%.

^{1}H NMR (400 MHz, 298 K, $CDCl_3$) δ_H ppm 8.67 (1H, d, $^{3}J_{HH}$ = 4.6 Hz, Py), 8.52 (1H, s, Py), 8.36 (1H, d, $^{3}J_{HH}$ = 8.0 Hz, Py), 8.29 (1H, d, $^{3}J_{HH}$ = 8.1 Hz, Py), 7.80 (1H, t, $^{3}J_{HH}$ = 7.7 Hz, Py), 7.63 (1H, d, $^{3}J_{HH}$ = 8.1 Hz, Py), 7.29 (1H, t, $^{3}J_{HH}$ = 6.1 Hz, Py), 2.40 (3H, s, CH_3).

^{13}C {^{1}H} NMR (100 MHz, 298K, $CDCl_3$) δ_C ppm 155.67, 153.00, 149.02, 148.50, 136.84, 136.25, 132.80, 122.76, 120.16, 119.97 (Py), 17.74 (CH_3).

MS (ESI) *m/z* 171 $[M+H]^+$, 193 $[M+Na]^+$,

IR υ cm^{-1} 3000 w, 1455 s, 1430 s, 1375 m, 788 s, 741s.

5-((trimethylsilyl)methyl)-2,2'-bipyridine[8] (**12**)

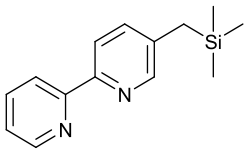

A Schelnk vessel was charged with dry THF (30 ml), diisopropylamine (14.13 ml, 100.8 mmol) and the solution was cooled to -78˚C, at which point n-butyllithium (31.20 ml, 80.7 mmol) was added and the resulting solution was stirred for 10 min before being warmed to 0˚C for a further 10 min. The reaction mixture was then cooled again to -78˚C and a solution of 5-methyl-2,2'-bipyridine(11.44 g, 67.21 mmol) in dry THF was added dropwise. The resulting maroon solution was stirred for 1 h at -78˚C. Chlorotrimethylsilane (10.22 ml, 80.63 mmol) was then added rapidly to the solution and after 1 min the reaction was quenched by the rapid addition of absolute ethanol. The resulting pale yellow/green solution was allowed to warm up to room temperature before a saturated solution of $NaHCO_3$ (150 ml) was added and the reaction mixture was extracted into DCM (3 x 75 ml). The organic fractions were combined, washed with brine, dried over sodium sulphate, filtered and solvents removed under reduced pressure to yield the titular product as a white solid that was used without purification.

Yeild = 13.0 g 80%

^{1}H NMR (400 MHz, 298 K, $CDCl_3$) δ_H ppm 8.69 (1H, dq, $^{3}J_{HH}$ = 4.7 Hz, $^{4}J_{HH}$ = 0.9 Py), 8.41 (2H, m, Py), 8.33 (1H, d, $^{3}J_{HH}$ = 8.3 Hz, Py), 7.78 (1H, td, $^{3}J_{HH}$ = 7.8 Hz, $^{4}J_{HH}$ = 2.0 Hz, Py), 7.46 (1H, dd, $^{3}J_{HH}$ = 8.0 Hz $^{4}J_{HH}$= 2.5, Hz Py), 7.25 (1H, ddd, $^{3}J_{HH}$ = 7.5 Hz $^{3}J_{HH}$ = 4.7 Hz $^{4}J_{HH}$ = 1.2, Py), 2.14 (2H, s, C*H*$_2$), 0.05 (9H, s, $SiMe_3$).

^{13}C {^{1}H} NMR (100 MHz, 298K, $CDCl_3$) δ_C ppm 155.74, 151.54, 148.44, 147.86, 136.93, 136.29, 135.52, 122.58, 120.24, 120.03 (py), 23.39 (*C*H_2), 2.65 (Si*C*H_3).

MS (ESI) *m/z* 243 $[M+H]^+$

IR υ cm^{-1} 3051 w, 1590 m, 1256 s, 1430 s, 1270 w, 1150 w, 870m.

5-(chloromethyl)-2,2'-bipyridine[8] (**13**)

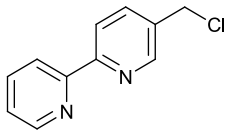

5-((Trimethylsilyl)methyl)-2,2'-bipyridine (22.53 g, 93 mmol), hexachloroethane (44.08 g, 186.18 mmol) and caesium fluoride (28.28 g, 186.12 mmol) were suspended in dry acetonitrile (75 ml) and heated at 60˚C for 4 h. The reaction mixture was cooled to ambient temperature, followed by addition of water (100 ml) and ethyl acetate (3x 150 ml). The organic fractions were combined, washed with brine, dried over sodium sulphate, filtered and solvents were removed under reduced pressure. The product was purified by flash chromatography (petroleum ether/EtOAc/triethylamine, 20:5:1 v/v/v; R_f = 0.50) to furnish the pure product as a white crystal (1.77 g, 4.76 mmol, 98%).

Yield = 16.0 g, 84 %.

^{1}H NMR (300 MHz, 298 K, $CDCl_3$) δ_H ppm 8.69 (2H, d, $^{3}J_{HH}$ = 4.3 Hz Py), 8.43 (2H, t, $^{3}J_{HH}$ = 7.7 Hz Py), 7.92-7.77 (2H, m, Py), 7.38-7.29 (1H, m, Py), 4.66 (2H, s, CH_2).

^{13}C {^{1}H} NMR (75 MHz, 298K, $CDCl_3$) δ_C ppm 156.22, 155.58, 149.26, 149.02, 137.19, 137.00, 133.18, 123.96, 121.24, 121.01 (py), 43.11 (CH_2).

MS (ESI) *m/z* 205 $[M+H]^+$

IR υ cm^{-1} 3000 w, 2696 w,1600 m, 1493 w, 1458 m, 1430 m, 1391 m, 1262 m, 1091 w, 990 w, 855 w, 675s.

(*S*)-2-(2,2'-bipyridin-5-ylmethoxy)-1-phenylethanamine[9] (**14**)

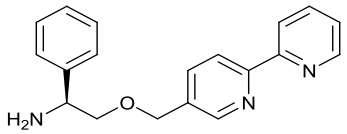

(*S*)-Phenylglycinol (1.00 g, 7.3 mmol) was dissolved in dry THF (20 ml) and added dropwise to a stirred suspension of sodium hydride (0.36 g, 15.0 mmol) in dry THF (10 ml). The solution was stirred for 1 h at room temperature. A solution of 5-(bromomethyl)-2,2'-bipyridine (1.82 g, 7.3 mmol) in dry THF (20 ml) was added dropwise and stirred for 1 h at room temperature before heated to reflux (65˚C) for a further 2 h. The reaction mixture was cooled to ambient temperature followed by addition of brine (40 ml). The product was extracted with diethyl ether (4 × 60 ml), dried over sodium sulphate and the solvent was removed to leave a dark yellow oil. The crude product was purified by flash chromatography (petroleum ether/EtOAc/triethylamine, 8:8:1 v/v/v) to furnish the (*S*)-2-(2,2'-bipyridin-5-ylmethoxy)-1-phenylethanamine as a white solid. R_f = 0.45, (petroleum ether/EtOAc/triethylamine 8:4:1 v/v/v).

Yield 1.8 g, 98%.

^{1}H NMR (300 MHz, $CDCl_3$) δ_H ppm 8.72-8.65 (m, 1H, Ar-H), 8.63 (d, $^{4}J_{HH}$ = 1.3 Hz, 1H, Ar-H), 8.38 (dd, 2H, $^{3}J_{HH}$ = 8.0 Hz, $^{4}J_{HH}$ = 3.9 Hz, Ar-H), 7.86-7.74 (m, 2H, Ar-

H), 7.43-7.23 (m, 6H, Ar-H), 4.62 (s, 2H, OCH_2), 4.26 (dd, 1H, $^3J_{HH}$ = 8.6 Hz, $^4J_{HH}$ = 3.8 Hz, CH), 3.65 (dd, 1H, $^3J_{HH}$ = 9.1 Hz, $^4J_{HH}$ = 3.9 Hz, CH_2), 3.52 (t, 1H, $^3J_{HH}$ = 8.8 Hz, CH_2).

^{13}C {^1H} NMR (75 MHz, 298 K, $CDCl_3$) δ_C ppm 155.97, 155.72, 149.22, 148.57, 142.32, 136.95, 136.40, 133.65, 128.49, 127.52, 126.82, 123.73, 121.10, 120.83 (Ar), 77.35 (CH_2), 70.67 (CH_2), 55.60 (CH).

MS (ESI) *m/z* 306 $[M+H]^+$

IR υ cm^{-1}: 3295 w, 3050 w, 3023 w, 2900 w, 2845 w, 1568 w, 1570 w, 1563 w, 1495 w, 1445 m, 1430 w, 1412 w, 1385 w, 1253 m, 1096 m, 1035 w, 1018 m, 988 w, 933 w.

Elemental Analysis found (Calculated for $C_{19}H_{19}N_3O$) % C 74.53 (74.73), H 6.24 (6.27), N 13.57 (13.75).

(azidomethyl)benzene[10] (**15a**)

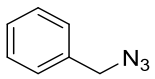

Sodium azide (1.64 g, 25.2 mmol, 1.5 eq.) was added to a solution of benzyl bromide (2.0 ml, 16.8 mmol, 1.0 eq.) in DMSO (25 mL). The reaction mixture was stirred at 80˚C overnight, followed by addition of water (75 mL) and diethyl ether (3 × 150 ml). The combined diethyl ether layers were washed with brine (2 × 150 ml) and water (2 × 200 ml), dried over sodium sulphate and the solvent removed under reduced pressure. The pure product was obtained as a clear colourless oil.

Yield 1.7g, 74%.

^1H NMR (400 MHz, 298 K, $CDCl_3$): δ_H ppm 7.36 (m, 5H, Ph), 4.34 (s, 2 H, CH_2).

^{13}C {^{1}H} NMR (100 MHz, 298 K, $CDCl_3$) δ_C ppm 135.38, 128.86, 128.33, 128.24 (Ph), 54.83 (CH_2).

MS (ESI) *m/z* 289.2 $[2M+Na]^+$

1-(azidomethyl)-4-fluorobenzene (**15b**)

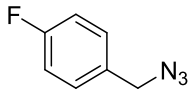

15b was synthesised using the procedure described for **15a**, substituting benzyl bromide for 1-(bromomethyl)-4-fluorobenzene.

Yield = 1.6 g, 73%

^{1}H NMR (300 MHz, 298 K, $CDCl_3$): δ_H ppm 7.32 (t, 2H, $^{3}J_{HH}$ = 6.2 Hz, Ph), 7.10(t, 2H, $^{3}J_{HH}$ = 8.0 Hz, Ph), 4.34 (s, 2 H, CH_2).

^{13}C {^{1}H} NMR (75 MHz, 298 K, $CDCl_3$) δ_C ppm 164.30, 161.03, 130.08, 129.97, 115.94, 115.66 (Ph), 54.07 (CH_2).

MS (+) *m/z* 303.2 $[2M+H]^+$.

4-(azidomethyl)benzonitrile[11] (**15c**)

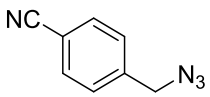

15c was synthesised using the procedure described for **15a**, substituting benzyl bromide for 4-(bromomethy)benzonitrile.

Yield 0.7 g, 88%.

^{1}H NMR (400 MHz, 298 K, $CDCl_3$): δ_H ppm 7.68 (d, 2H, $^{3}J_{HH}$ = 7.5 Hz, Ph), 7.44(d, 2H, $^{3}J_{HH}$ = 7.6 Hz, Ph), 4.45 (s, 2 H, CH_2).

^{13}C {^{1}H} NMR (100 MHz, 298 K, $CDCl_3$) δ_C ppm 140.77, 132.65, 128.50 (Ph), 118.43 (CN), 112.21 (Ph), 54.05 (CH_2).

MS (ESI) *m/z* 181.2 $[M+Na]^+$

1-(azidomethyl)-4-methoxybenzene[12] (**15d**)

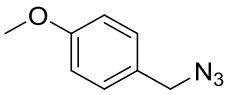

15d was synthesised using the procedure described for **15a**, substituting benzyl bromide for 1-(bromomethy)-4-methoxybenzene.

Yield 1.1g 93%.

^{1}H NMR (300 MHz, 298 K, $CDCl_3$): δ_H ppm 7.27 (d, 2H, $^{3}J_{HH}$ = 7.4 Hz, Ph), 6.94 (d, 2H, $^{3}J_{HH}$ = 7.4 Hz, Ph), 4.30 (s, 2H, CH_2), 3.84 (s, 3H, CH_3).

^{13}C {^{1}H} NMR (75 MHz, 298 K, $CDCl_3$) δ_C ppm 159.65, 129.77, 127.41, 114.22 (Ph), 55.31 (CH_3), 54.41(CH_2).

MS (ESI) *m/z* 365.4 $[2M+K]^+$

4-azidomethyl Benzoic acid[13] (**15e**)

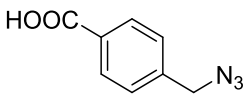

15e was synthesised using the procedure described for **15a**, substituting benzyl bromide for 4-chloromethyl benzoic acid.

Yield 0.9 g, 84%.

^{1}H NMR (300 MHz, 298 K, $CDCl_3$): δ_H ppm 8.16 (d, 2H, $^{3}J_{HH}$ = 7.6 Hz, Ph), 7.47 (d, 2H, $^{3}J_{HH}$ = 7.5 Hz, Ph), 4.48 (s, 2H, CH_2).

^{13}C {^{1}H} NMR (75 MHz, 298 K, $CDCl_3$) δ_C ppm 171.10 (CO), 141.45, 130.79, 129.11, 128.03 (Ph), 54.29 (CH_2).

ESI-MS(+) *m/z* 176.1 $[M-H]^-$.

2,3,4,6-tetra-O-acetyl-α-D-glucopyranosyl bromide[14] (**16**)

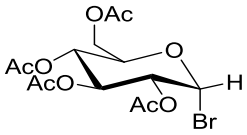

D-glucopyranosylpentaacetate (2.5 g, 6.4 mmol) was dissolved in 33% HBr/AcOH (20 mL) solution and stirred for 3 h. The reaction mixture was then diluted with ethyl acetate (25 mL), cooled to 0 °C, and the solution was neutralized carefully with 10% aqueous NaOH (50 mL) and saturated $NaHCO_3$ solution (5 mL). The solution was extracted with ethyl acetate (3 × 25 mL) after which the organic layer was dried over anhydrous magnesium sulfate, filtered, and evaporated under reduced pressure to a clear syrup that was essentially pure glycosyl bromide.

Yield 2.6 g, 99%.

(*2R,3R,4S,5R,6S*)-2-(acetoxymethyl)-6-((6-formylpyridin-3-yl)oxy)tetrahydro-2H-pyran-3,4,5-triyl triacetate (**17**)

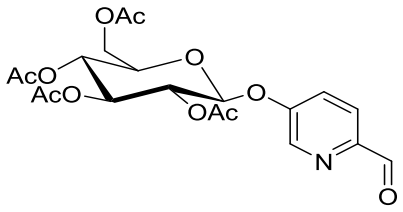

Potassium carbonate (0.59 g, 4.26 mmol) was added to a solution of 5-(hydroxy)picolinaldehyde (0.50 g, 4.06 mmol) in acetonitrile (40 ml), followed by the addition of acetyl protected α-D-glucosyl bromide (1.67g, 4.06mmol). The solution was stirred at reflux (*ca.* 85 °C) overnight, cooled to ambient temperature and passed a short column of silica. The solvent was removed under reduced pressure to leave the product as a white solid.

Yield = 1.5 g, 84%.

^{1}H NMR (500 MHz, 298 K, DMSO) δ_H 9.92 (1H, s, CHO), 8.53 (1H, d, $^{4}J_{HH}$ =2.6 Hz), 7.99 (1H, d, $^{3}J_{HH}$ =8.7 Hz), 7.66 (1H, dd, $^{3}J_{HH}$ = 8.5 Hz, $^{4}J_{HH}$ =2.6 Hz), 5.86 (1H, d, $^{3}J_{HH}$ =7.9Hz, H_{1Glu}), 5.41 (1H, t, $^{3}J_{HH}$ =9.6 Hz, H_{5Glu}), 5.16 (1H, dd, $^{3}J_{HH}$ = 9.7 Hz, 8.0 Hz, H_{2Glu}), 5.06 (1H, t, $^{3}J_{HH}$ =9.8 Hz, H_{4Glu}), 4.35-4.32 (1H, m, H_{3Glu}), 4.21 (1H, dd, $^{3}J_{HH}$ =12.4 Hz, 5.5 Hz, H_{6Glu}), 4.11 (1H, dd, $^{3}J_{HH}$ =12.3 Hz, 2.2 Hz, H_{6Glu}), 2.04 (3H, s, $COCH_3$), 2.03 (3H, s, $COCH_3$), 2.01 (3H, s, $COCH_3$), 1.99 (3H, s, $COCH_3$).

^{13}C {^{1}H} NMR (125 MHz, 298 K, DMSO) δ_C 192.54 (CHO), 170.43, 170.08, 169.77, 169.59 (O*C*OCH$_3$), 156.02, 147.91, 139.82, 124.09, 123.87 (Py), 96.90 (C_{1Glu}), 72.26(C_{5Glu}), 71.65 (C_{3Glu}), 70.86 (C_{2Glu}), 68.22 (C_{4Glu}), 61.93 (C_{6Glu}), 20.92, 20.85, 20.79, 20.74 (CO*C*H$_3$).

MS (ESI) *m/z* 476.2 $[M+Na]^+$

Elemental Analysis found (Calculated for $C_{20}H_{23}NO_{11}$) % C 52.70 (52.98), H 5.01 (5.11), N 2.94 (3.09).

5-(((*2S,3R,4S,5S,6R*)-3,4,5-trihydroxy-6-(hydroxymethyl)tetrahydro-2H-pyran-2-yl)oxy)picolinaldehyde (**18**)

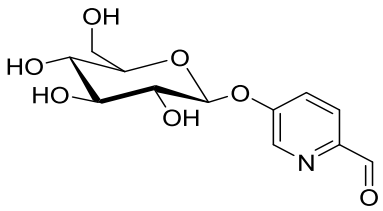

The catalytic amount of sodium methoxide (110 µL, 1M in MeOH, 0.1 eq.) was added to a stirring solution of 2,3,4,6-tetra-*O*-acetyl-β-D-glucopyridealdehyde (500 mg, 1.10 mmol, 1.0 eq) in dry MeOH (6 mL) until pH 9-10 (110 µL). The reaction mixture was stirred at ambient temperature for 24 h. The solution was then neutralized by addition of ion-exchange resin (Dowex® 50WX4 hydrogen form) until pH 7, filtered, and the solvent was removed under reduced pressure to afford the fully acetyl deprotected derivative as a colorless solid.

Yield = 274 mg, 99%

^{1}H NMR (500 MHz, 298 K, D_2O) δ_H 9.80 (1H, s, CHO), 8.43 (1H, d, $^{4}J_{HH}$ =2.4 Hz), 7.99 (1H, d, $^{3}J_{HH}$ =8.7 Hz), 7.65 (1H, dd, $^{3}J_{HH}$ = 8.7 Hz, $^{4}J_{HH}$ =2.5 Hz), 5.23 (1H, d, $^{3}J_{HH}$ =7.2Hz, H_{1Glu}), 5.41 (1H, t, $^{3}J_{HH}$ =9.6 Hz, H_{5Glu}), 3.87 (1H, dd, $^{3}J_{HH}$ =12.3 Hz, 1.7 Hz, H_{6Glu}), 3.74-3.48 (4H, m, $H_{2,3,4,6Glu}$).

^{13}C {^{1}H} NMR (125 MHz, 298 K, D_2O) δ_C 193.25 (CHO), 156.62, 153.19, 139.93, 126.39, 124.02 (Py), 99.55 (C_{1Glu}), 76.29(C_{5Glu}), 75.37 (C_{3Glu}), 72.78 (C_{2Glu}), 69.20 (C_{4Glu}), 60.34 (C_{6Glu}).

MS (ESI) *m/z* 308.2 $[M+Na]^+$; 593.3 $[2M+Na]^+$

Elemental Analysis found (Calculated for $C_{12}H_{15}NO_7 \cdot MeOH$) % C 48.81 (49.21), H 5.65 (6.04), N 4.37 (4.41).

2,3,4,6-tetra-O-acetyl-β-D-glucopyranosylazide (**19**)

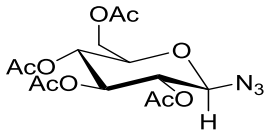

The α-D-glucosyl bromide (2.60 g, 6.32 mmol) was dissolved in a 5:1 acetone and water mixture (70 mL). Sodium azide (1.95 g, 25.0mmol) was added and the solution was stirred overnight at room temperature or until TLC (hexanes: ethyl acetate, 1:1) showed the complete consumption of starting material. The acetone was removed by heating the solution at 50 °C in a water bath, and the remaining slurry was then partitioned between water and ethyl acetate (50 mL each). The organic layer was removed and the aqueous layer was extracted with ethyl acetate (2 x 50 mL). The combined organic extracts were dried over anhydrous magnesium sulfate, filtered, and evaporated to a white solid which was subsequently crystallized from hot methanol or isopropanol to give acetyl-β-D-glucopyranosylazide as a colourless crystalline solid.

Yield 2.2 g, 95%.

^{1}H NMR (400MHz, 298 K, $CDCl_3$) δ_H ppm 5.22 (t, 1H, $^{3}J_{HH}$ =9.5 Hz), 5.11 (t, 1H, $^{3}J_{HH}$ = 9.5Hz), 4.96 (t, 1H, $^{3}J_{HH}$ = 9.6Hz), 4.65(d, 1H, $^{3}J_{HH}$ = 8.8 Hz), 4.28 (dd, 1H, $^{3}J_{HH}$ = 12.5 Hz, $^{4}J_{HH}$ = 4.8 Hz), 4.17 (dd, 1H, $^{3}J_{HH}$ = 12.4 Hz, $^{4}J_{HH}$ = 2.0 Hz), 3.80 (ddd, 1H, $^{3}J_{HH}$ = 10.0 Hz, $^{4}J_{HH}$ = 4.7 Hz, $^{4}J_{HH}$ = 2.2 Hz), 2.11-2.01 (4 × s, 12H, CH_3).

^{13}C {^{1}H} NMR (100 MHz, 298 K, $CDCl_3$) δ_C ppm 170.62, 170.14, 169.32, 169.22 (CO), 87.92 (C_1), 74.03 (C_5), 72.61(C_3), 70.64 (C_2), 67.89 (C_4), 61.66 (C_6), 20.70, 20.57, 20.55 (CH_3).

MS (ESI) *m/z* 396.2 $[M+Na]^+$

β-D-glucopyranosylazide (**20**)

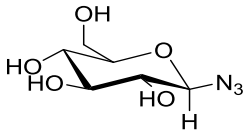

A solution of sodium methoxide (1M in MeOH, 120 μL) was added to a stirring solution of 2,3,4,6-tetra-*O*-acetyl-β-D-glucopyranosylazide (500 mg, 1.34 mmol, 1.0 eq) in dry MeOH (6 mL) until pH 9-10. The reaction mixture was stirred at r.t. for 24 h. The solution was then neutralized by addition of ion-exchange resin (Dowex® 50WX4 hydrogen form) until pH 7, filtered, and the solvent was removed under reduced pressure to afford the fully acetyl deprotected derivative as a colourless syrup.

Yield 254.2 mg, 93%.

^{1}H NMR (400MHz, 298 K, MeOD) δ_H ppm 4.51 (d, 1H, $^{3}J_{HH}$ = 8.6 Hz), 3.90 (d, 1H, $^{3}J_{HH}$ = 12.1 Hz), 3.70 (dd, 1H, $^{3}J_{HH}$ = 12.1 Hz, $^{4}J_{HH}$ = 5.5 Hz), 3.43-3.28 (m, 3H), 3.15 (t, 1H, $^{3}J_{HH}$ = 8.8 Hz).

^{13}C {^{1}H} NMR (100 MHz, 298 K, MeOD) δ_C ppm 92.12 (C_1), 80.21 (C_5), 78.11 (C_3), 74.78 (C_2), 71.12 (C_4), 62.55 (C_6)

MS (ESI) *m/z* 433.2 $[2M+Na]^+$

2,3,4,6-Tetra-O-acetyl-β-D-galactopyranosyl bromide[15] (**21**)

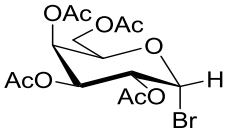

D-galactopyranosylpentaacetate (2.5 g, 6.4 mmol) was dissolved in 33% HBr/AcOH (20 mL) solution and stirred for 3 h. The reaction mixture was then diluted with ethyl acetate (25 mL), cooled to 0 °C, and the solution was neutralized carefully with 10% aqueous NaOH (50 mL) and saturated $NaHCO_3$ solution (5 mL). The mixture was

extracted with ethyl acetate (3 × 25 mL) after which the organic layer was dried over anhydrous magnesium sulfate, filtered, and evaporated under reduced pressure to a clear syrup that was essentially pure glycosyl bromide.

Yield 2.2 g, 82 %.

2,3,4,6-Tetra-O-acetyl-β-D-galactopyranosylazide[15].(**22**)

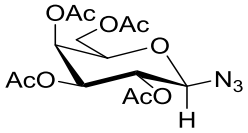

Sodium azide (0.38 g, 5.84 mmol, 1.2 eq.) was added to a solution of 2,3,4,6-tetra-*O*-acetyl-β-D-galactopyranosyl bromide (2.00 g, 4.86 mmol, 1.0 eq.) in dry DMSO (10 mL) and the reaction was allowed to stir at ambient temperature for 30 min. The reaction mixture was then diluted with water (50 mL) and extracted with EtOAc (100 mL). The organic layer was dried over Na_2SO_4 and evaporated to dryness. The residue was purified by flash chromatography (EtOAc/petroleum ether: 1:2) to achieve the desired 2,3,4,6-tetra-*O*acetyl-β-D-galactopyranosylazideas a white solid. R_f = 0.50, hexanes/ethyl acetate: 1:1.

Yield 1.8 g, 98 %.

^{1}H NMR (400MHz, 298 K, $CDCl_3$) δ_H ppm 5.44 (dd, 1H, $^3J_{HH}$ = 3.3 Hz, $^4J_{HH}$ = 0.8 Hz), 5.18 (m, 1H), 5.06 (m, 1H), 4.62(d, 1H, $^3J_{HH}$ = 8.7 Hz), 4.19 (dd, 2H, $^3J_{HH}$ = 6.5 Hz, $^4J_{HH}$ = 3.8 Hz), 4.03 (m, 1H) 2.19-2.01 (4 × s, 12H, CH_3).

^{13}C {^{1}H} NMR (100 MHz, 298 K, $CDCl_3$) δ_C ppm 170.38, 170.12, 170.01, 169.37 (CO), 88.32 (C_1), 72.88 (C_5), 70.74 (C_3), 68.07 (C_2), 66.85 (C_4), 61.23 (C_6), 20.68, 20.67, 20.62, 20.53 (CH_3).

MS (ESI) *m/z* 396.6 $[M+Na]^+$

β-D-galactopyranosylazide[15] (**23**)

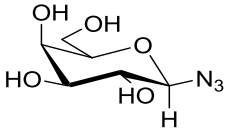

A solution of sodium methoxide (1M in MeOH) was added to a stirring solution of 2,3,4,6-tetra-*O*-acetyl-β-D-galactopyranosylazide (1.00 g, 2.68 mmol,1.0 eq) in dry MeOH (12 mL) until pH 9-10 (250µL). The reaction mixture was stirred at ambient temperature for 24 h. The solution was then neutralized by addition of ion exchange resin (Dowex® 50WX4 hydrogen form) until pH 7, filtered, and the solvent was removed under reduced pressure to yield the fully deprotected derivative as a colourless oil.

Yield 489mg, 89%.

^{1}H NMR (400MHz, 298 K, D_2O) δ_H ppm 4.61 (d, 1H, $^{3}J_{HH}$ = 8.7 Hz), 3.91 (d, 1H, $^{4}J_{HH}$ = 2.0 Hz), 3.78-3.68 (m, 3H), 3.63 (dd, 1H, $^{3}J_{HH}$ = 9.9 Hz, $^{4}J_{HH}$ = 2.4 Hz), 3.46 (t, 1H, $^{3}J_{HH}$ = 9.3 Hz)

^{13}C {^{1}H} NMR (100 MHz, 298 K, MeOD) δ_C ppm 92.64 (C_1), 78.95 (C_5), 74.96 (C_3), 71.98 (C_2), 70.23 (C_4), 62.47 (C_6)

MS (ESI) *m/z* 228.1 $[M+Na]^+$ 433.3 $[2M+Na]^+$

2,3,4,6-tetra-*O*-acetyl-α-D-mannopyranosylazide[15] (**24**)

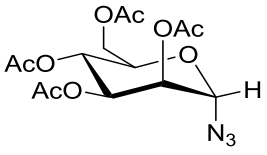

Azidotrimethylsilane ($TMSiN_3$, 11 mL, 9.6 mmol, 4.00 equiv.) and tin tetrachloride ($SnCl_4$, 1M in CH_2Cl_2, 0.62 mL, 0.62 mmol, 0.26 equiv.) were added to a solution of D-mannopyranosylpentaacetate (930 mg, 2.4 mmol, 1.0 eq.) in dry CH_2Cl_2 (3 mL)

under dinitrogen atmosphere and mixture was stirred at ambient temperature. The reaction was monitored by TLC (hexanes/toluene/ethyl acetate: 3:3:4) until complete disappearance of the starting material. DCM (15 mL) was then added and the solution was washed with a saturated aqueous $NaHCO_3$ (10 mL), water (10 mL) and brine (10 mL). The organic phase was dried with Na_2SO_4 and after the evaporation of the solvent, the resulting crude product was purified by flash chromatography (hexanes/ethyl acetate: 3:1) to give 2,3,4,6-tetra-*O*-acetyl-α-D-mannopyranosylazideas a colorless oil.

Yield 276 mg, 96%.

^{1}H NMR (400MHz, 298 K, $CDCl_3$) δ_H ppm 5.20 (s, 1H), 5.08 (m, 2H), 4.96 (s, 1H), 4.12 (dd, 1H, $^3J_{HH}$ = 12.5 Hz, $^4J_{HH}$ = 5.6 Hz), 3.97 (m, 1H), 1.98-1.81 (4 × s, 12H, CH_3).

^{13}C {^{1}H} NMR (100 MHz, 298 K, $CDCl_3$) δ_C ppm 170.65, 169.92, 169.81, 169.67 (CO), 87.45 (*C*$_1$), 70.59 (*C*$_5$), 69.16 (*C*$_2$), 68.22 (*C*$_3$), 65.56 (*C*$_4$), 62.12 (*C*$_6$), 20.86, 20.75, 20.70, 20.65 (CH_3).

MS (ESI) *m/z* 396.4 $[M+Na]^+$

α-D-mannopyranosylazide[15] (**25**)

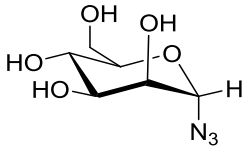

A solution of sodium methoxide (1M in MeOH) was added to a stirring solution of 2,3,4,6-tetra-*O*-acetyl-α-D-mannopyranosylazide (500 mg, 1.34 mmol, 1.0 eq) in dry MeOH (6 mL) until pH 9-10 (120 μL). The reaction mixture was stirred at ambient temperature for 24 h. The solution was then neutralized by addition of ion-exchange resin (Dowex® 50WX4 hydrogen form) until pH 7, filtered, and the solvent was

removed under reduced pressure to afford the fully deprotected derivative as a colorless syrup.

Yield 264.6 mg, 96%.

^{1}H NMR (400MHz, 298 K, D_2O) δ_H ppm 5.42 (s, 1H), 3.86 (m, 2H), 3.73 (m, 3H), 3.61 (t, 1H, $^{3}J_{HH}$ = 9.4 Hz).

^{13}C {^{1}H} NMR (100 MHz, 298 K, D_2O) δ_C ppm 89.68 (C_1), 74.56 (C_5), 69.74 (C_3), 69.69 (C_2), 66.32 (C_4), 60.74 (C_6).

MS (ESI) *m/z* 244.5 $[M+K]^+$

(1-benzyl-1H-1,2,3-triazol-4-yl)methanol[16] (**28a**)

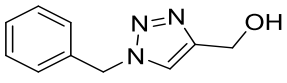

(Azidomethyl)benzene (0.238g, 1.79mmol) was dissolved into methanol, followed by the addition of propargyl alcohol (0.1g, 1.79mmol) and CuI (0.034g, 0.18mmol). The reaction mixture was heated at 60 ℃ overnight while being protected from light. After cooling to ambient temperature, the solution was filtered to remove CuI salt and the solvent was removed under reduced pressure to give a white solid.

Yield 0.30 g, 90%

^{1}H NMR (300 MHz, 298 K, DMSO) δ_H ppm 8.01 (s, 1H, TRZ), 7.34 (dd, 5H, $^{3}J_{HH}$ = 15.5 Hz, $^{4}J_{HH}$ = 6.7 Hz, Ph), 5.57 (s, 2H, Ph-CH_2), 5.15 (t, 1H, $^{3}J_{HH}$ = 5.3 Hz, OH), 4.50 (d, 2H, $^{3}J_{HH}$ = 5.0 Hz, CH_2OH).

^{13}C {^{1}H} NMR (75 MHz, 298 K, DMSO) δ_C ppm 136.70 (*C*=CH (TRZ)), 129.18, 128.55, 128.40 (Ph), 132.32 (C=*C*H (TRZ)), 55.50 (Ph-*C*H_2), 53.16 (CH_2OH).

Elemental Analysis found (Calculated for $C_{10}H_{11}N_3O$) % C 63.56 (63.48), H 5.81 (5.86), N 22.43 (22.20).

MS (ESI) *m/z* 212.2 $[M+Na]^+$, 401.3 $[2M+Na]^+$

(1-(4-fluorobenzyl)-1H-1,2,3-triazol-4-yl)methanol (**28b**)

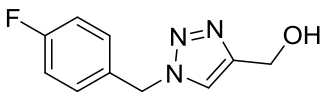

28b was synthesised using the procedure described for **28a**, substituting 1-(azidomethyl)-4-fluorobenzen for (azidomethyl)benzene.

Yield 0.58 g, 92%.

^{1}H NMR (300 MHz, 298 K, DMSO) δ_H ppm 8.02 (s, 1H, TRZ), 7.39 (d, 2H, $^3J_{HH}$ = 8.2 Hz, Ph), 7.21 (d, 2H, $^3J_{HH}$ = 8.2 Hz, Ph), 5.56 (s, 2H, Ph-C*H*$_2$), 5.16 (t, 1H, $^3J_{HH}$ = 5.5 Hz, OH), 4.50 (d, 2H, $^3J_{HH}$ = 5.4 Hz, C*H*$_2$OH).

^{13}C {^{1}H} NMR (75 MHz, 298 K, DMSO) δ_C ppm 163.94 (F-Ph), 160.70 (*C*=CH (TRZ)), 132.98, 130.76, 130.65 (Ph), 123.24 (C=*C*H (TRZ)), 116.16, 115.87 (Ph), 55.50 (Ph-*C*H$_2$), 52.35 (CH$_2$OH).

4-((4-(hydroxymethyl)-1H-1,2,3-triazol-1-yl)methyl)benzonitrile (**28c**)

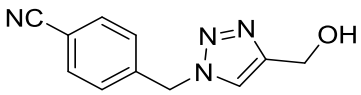

28c was synthesised using the procedure described for **28a**, substituting 4-(azidomethyl)benzonitrile for (azidomethyl)benzene.

Yield 0.50 g, 90%.

^{1}H NMR (300 MHz, 298 K, DMSO) δ_H ppm 8.08 (s, 1H, TRZ), 7.86 (d, 2H, $^{3}J_{HH}$ = 7.5 Hz, Ph), 7.45 (d, 2H, $^{3}J_{HH}$ = 7.6 Hz, Ph), 5.70 (s, 2H, Ph-C*H*$_2$), 5.18 (t, 1H, $^{3}J_{HH}$ = 5.3 Hz, OH), 4.52 (d, 2H, $^{3}J_{HH}$ = 5.4 Hz, C*H*$_2$OH).

^{13}C {^{1}H} NMR (75 MHz, 298 K, DMSO) δ_C ppm 142.19 (*C*=CH (TRZ)), 133.18, 129.10 (Ph), 123.72 (C=*C*H (TRZ)), 119.02 (CN), 111.32 (Ph), 55.48 (Ph-*C*H$_2$), 52.52 (CH$_2$OH).

MS (ESI) *m/z* 237.2 $[M+Na]^+$, 451.3 $[2M+Na]^+$

(1-(4-methoxybenzyl)-1H-1,2,3-triazol-4-yl)methanol (**28d**)

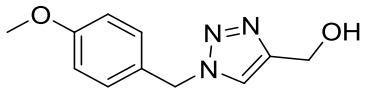

28d was synthesised using the procedure described for **28a**, substituting 1-(azidomethyl)-4-methoxybenzene for (azidomethyl)benzene.

Yield 0.51 g, 85%

^{1}H NMR (300 MHz, 298 K, CDCl$_3$) δ_H ppm 7.43 (s, 1H, TRZ), 7.27 (d, 2H, $^{3}J_{HH}$ = 7.4 Hz, Ph), 6.92 (d, 2H, $^{3}J_{HH}$ = 7.4 Hz, Ph), 5.47 (s, 2H, Ph-C*H*$_2$), 4.78 (s, 2H, C*H*$_2$OH), 3.83 (s, 3H, OCH$_3$).

^{13}C {^{1}H} NMR (75 MHz, 298 K, CDCl$_3$) δ_C ppm 129.74, 126.43, 114.52 (Ph), 56.66 (Ph-*C*H$_2$), 55.36 (OCH$_3$), 53.79 (CH$_2$OH).

4-((4-(hydroxymethyl)-1H-1,2,3-triazol-1-yl)methyl)benzoic acid (**28e**)

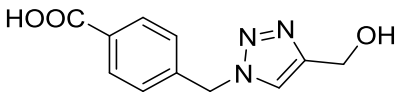

28e was synthesised using the procedure described for **28a**, substituting 4-azidomethyl benzoic acid for (azidomethyl)benzene.

Yield 0.46 g, 87%.

^{1}H NMR (300 MHz, 298 K, DMSO) δ_H ppm 13.01 (s, 1H, COOH), 8.04 (s, 1H, TRZ), 7.94 (d, 2H, $^{3}J_{HH}$ = 5.2 Hz, Ph), 7.40 (d, 2H, $^{3}J_{HH}$ = 5.0 Hz, Ph), 5.67 (s, 2H, Ph-C*H*$_2$), 5.19 (t, 1H, $^{3}J_{HH}$ = 5.0 Hz, OH), 4.52 (d, 2H, $^{3}J_{HH}$ = 5.0 Hz, C*H*$_2$OH).

^{13}C {^{1}H} NMR (75 MHz, 298 K, DMSO) δ_C ppm 141.45 (*C*=CH (TRZ)), 128.61 (Ph), 55.50 (Ph-*C*H$_2$), 52.73 (CH$_2$OH).

1-benzyl-1H-1,2,3-triazole-4-carbaldehyde[16] (**29a**)

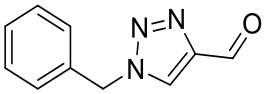

(1-Benzyl-1H-1,2,3-triazol-4-yl)methanol (0.15g, 0.79mmol) was dissolved into 2-propanol, followed by addition of activated manganese dioxide (0.23 g, 2.6 mmol). The reaction mixture was heated at 100℃ overnight. After cooling to ambient tempearture, the solution was filtered to remove MnO_2. The solvent was removed under reduced pressure and the residue was purified by flash chromatography (DCM/MeOH: 100:1 v/v) furnish the 1-benzyl-1H-1,2,3-triazole-4-carbaldehyde as a white solid (0.136 g, 0.73 mmol). R_f = 0.50, DCM/MeOH =100:5 v/v.

Yield 0.14 g 92%.

^{1}H NMR (300 MHz, 298 K, DMSO) δ_H ppm 10.01 (s, 1H, CHO), 8.97 (s, 1H, TRZ), 7.42-7.32 (m, 5H, Ph), 5.70 (s, 2H, Ph-C*H*$_2$).

^{13}C {^{1}H} NMR (75 MHz, 298 K, DMSO) δ_C ppm 185.42 (CHO), 135.81 (*C*=CH (TRZ)), 129.33, 128.86, 128.57 (Ph), 53.66 (Ph-*C*H$_2$).

Elemental Analysis found (Calculated for $C_{10}H_9N_3O$) % C 64.20 (64.16), H 4.69 (4.85), N 22.29 (22.44).

MS (ESI) *m/z* 397.6 $[2M+Na]^+$

1-(4-fluorobenzyl)-1H-1,2,3-triazole-4-carbaldehyde (**29b**)

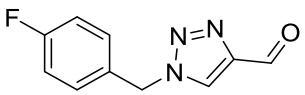

29b was synthesised using the procedure described for **29a**, substituting ((1-(4-fluorobenzyl)-1H-1,2,3-triazol-4-yl)methanol for (1-benzyl-1H-1,2,3-triazol-4-yl)methanol.

Yield 0.36 g, 86%.

^{1}H NMR (300 MHz, 298 K, DMSO) δ_H ppm 10.01 (s, 1H, CHO), 8.96 (s, 1H, TRZ), 7.45 (t, 2H, $^{3}J_{HH}$ = 8.2 Hz, Ph), 7.23 (t, 2H, $^{3}J_{HH}$ = 8.2 Hz, Ph), 5.69 (s, 2H, Ph-C*H*$_2$).

^{13}C {^{1}H} NMR (75 MHz, 298 K, DMSO) δ_C ppm 185.42 (CHO), 164.11 (F-Ph), 147.52 (*C*=CH (TRZ)), 132.03, 131.07, 130.95 (Ph), 128.69 (C=*C*H (TRZ)), 116.32, 116.03 (Ph), 52.87 (Ph-*C*H$_2$).

Elemental Analysis found (Calculated for $C_{10}H_8FN_3O$) % C 58.37 (58.54), H 3.78 (3.93), N 20.02 (20.47).

MS (ESI) *m/z* 433.5 $[2M+Na]^+$

4-((4-formyl-1H-1,2,3-triazol-1-yl)methyl)benzonitrile (**29c**)

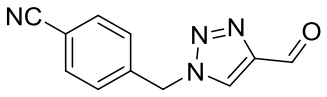

29c was synthesised using the procedure described for **29a**, substituting 4-((4-(hydroxymethyl)-1H-1,2,3-triazol-1-yl)methyl)benzonitrile for (1-benzyl-1H-1,2,3-triazol-4-yl)methanol.

Yield 0.41g, 88%.

^{1}H NMR (300 MHz, 298 K, DMSO) δ_H ppm 10.03 (s, 1H, CHO), 9.01 (s, 1H, TRZ), 7.87 (d, 2H, $^{3}J_{HH}$ = 7.6 Hz, Ph), 7.51 (d, 2H, $^{3}J_{HH}$ = 7.6 Hz, Ph), 5.82 (2H, s, Ph-CH_2).

^{13}C {^{1}H} NMR (75 MHz, 298 K, DMSO) δ_C ppm 185.41 (CHO), 141.15 (*C*=CH (TRZ)), 133.28, 129.38 (Ph), 129.20 (C=*C*H (TRZ)), 118.94 (CN), 111.64 (Ph), 53.03 (Ph-*C*H_2).

Elemental Analysis found (Calculated for $C_{11}H_8N_4O$) % C 61.86 (62.26), H 3.93 (3.80), N 25.79 (26.39).

MS (ESI) *m/z* 447.5 $[2M+Na]^+$

1-(4-methoxybenzyl)-1H-1,2,3-triazole-4-carbaldehyde (**29d**)

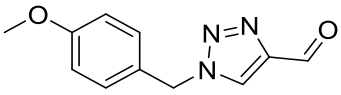

29d was synthesised using the procedure described for **29a**, substituting (1-(4-methoxybenzyl)-1H-1,2,3-triazol-4-yl)methanol for (1-benzyl-1H-1,2,3-triazol-4-yl)methanol.

Yield 0.55 g, 87%.

^{1}H NMR (300 MHz, 298 K, DMSO) δ_H ppm 10.00 (1H, s, CHO), 8.92 (s, 1H, TRZ), 7.35 (d, 2H, $^{3}J_{HH}$ = 7.5 Hz, Ph), 6.94 (d, 2H, $^{3}J_{HH}$ = 7.4 Hz, Ph), 5.61 (s, 2H, Ph-C*H*$_2$), 3.74 (s, 3H, OCH_3).

^{13}C {^{1}H} NMR (75 MHz, 298 K, DMSO) δ_C ppm 185.42 (CHO), 159.78, 130.29(Ph), 128.42 (C=*C*H (TRZ)), 127.70, 114.68 (Ph), 55.63 (OCH_3), 53.23 (Ph-*C*H$_2$).

Elemental Analysis found (Calculated for $C_{11}H_{11}N_3O_2$) % C 60.40 (60.82), H 4.99 (5.10), N 19.21 (19.33).

MS (ESI) *m/z* 457.5 $[2M+Na]^+$

4-((4-formyl-1H-1,2,3-triazol-1-yl)methyl)benzoic acid (**29e**)

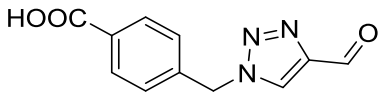

29e was synthesised using the procedure described for **29a**, substituting 4-((4-(hydroxymethyl)-1H-1,2,3-triazol-1-yl)methyl)benzoic acid for (1-benzyl-1H-1,2,3-triazol-4-yl)methanol.

Yield 0.25 g, 50%.

^{1}H NMR (300 MHz, 298 K, DMSO) δ_H ppm 13.09 (s, 1H, COOH), 10.03 (s, 1H, CHO), 9.00 (s, 1H, TRZ), 7.95 (d, 2H, $^{3}J_{HH}$ = 7.4 Hz, Ph), 7.44 (d, 2H, $^{3}J_{HH}$ = 7.5 Hz, Ph), 5.80 (s, 2H, Ph-C*H*$_2$).

^{13}C {^{1}H} NMR (75 MHz, 298 K, DMSO) δ_C ppm 185.42 (CHO), 167.34 (COOH), 147.52 (*C*=CH (TRZ)), 140.48, 131.19, 130.29 (Ph), 129.08 (C=*C*H (TRZ)), 128.57 (Ph), 53.21 (Ph-*C*H$_2$).

Elemental Analysis found (Calculated for $C_{11}H_9N_3O_3$) % C 56.57 (57.14), H 3.77 (3.92), N 18.00 (18.17).

MS (ESI) *m/z* 485.4 $[2M+Na]^+$

acetamido-3,4,6-tri-O-acetyl-2-deoxy-β-D-glucopyranosyl azide.[17] (**30**)

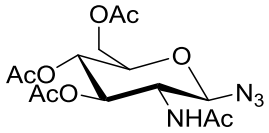

Acetamido-3,4,6-tri-O-acetyl-2-deoxy-β-D-glucopyranosyl chloride (1.01 g 2.74 mmol) was dissolved in DMF (14 mL). Sodium azide (0.5 g, 7.69 mmol) was added slowly and the reaction mixture was heated at 70ºC for 3h. Ethyl acetate (50 mL) and water (2 x 50 mL) were then added to the solution. The organic layer was dried with Na_2SO_4 and solvent removed under reduced pressure. The pure product was achived using column chromatography ethyl acetate: petromleum ether (4:1 v/v) to yield a white solid.

Yield: 0.53 g, 52%.

^{1}H NMR (400 MHz, 298 K, $CDCl_3$) δ_H ppm 5.57 (1H, d, $^3J_{HH}$ = 9.0 Hz, NH), 5.29 (1H, t, $^3J_{HH}$ = 9.0 Hz, H-C_3), 5.11 (1H, t, $^3J_{HH}$ = 10.0, H-C_4), 4.76 (1H, d, $^3J_{HH}$ = 9.0 Hz, H-C_1), 4.27 (1H, dd, *J* = 12.5, 5.0 Hz, H-C_6), 4.14 (1H, m, H-C_6), 3.91 (1H, dd, *J* = 19.5, $^3J_{HH}$ = 9.0 Hz, H-C_2), 3.79 (1H, m, H-C_5), 2.10-2.00 (s, 4 x CH_3)

^{13}C NMR (100 MHz, 298 K, $CDCl_3$) δ_c ppm 171.1, 170.6, 170.4 169.4 (4 x C=O), 88.3 (C_1), 73.8 (C_5), 71.9 (C_3), 67.9 (C_4), 61.7 (C_6) 53.9 (C_2), 23.3, 20.7, 20.6 (4x CH_3)

MS (ESI) *m/z* 395.2 $[M+Na]^+$

IR v cm^{-1} 2117 s, 1752 s, 1731 s, 1368 m, 1236 s, 1211 s, 1056 s, 1037 s, 905 m, 890 m, 878 m

(*2R,3R,4S,5R,6R*)-2-(acetoxymethyl)-6-(4-(hydroxymethyl)-1H-1,2,3-triazol-1-yl)tetrahydro-2H-pyran-3,4,5-triyl triacetate[18] (**31**)

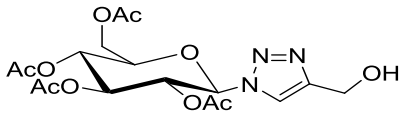

2,3,4,6-Tetra-O-acetyl-β-D-glucopyranosylazide (0.25 g, 6.70 mmol) was dissolved in 1:1 ^{t}BuOH: water (6 mL). $CuSO_4.5H_2O$ (0.008 g, 0.03 mmol) and sodium adsorbate (0.02 g, 0.10 mmol) were added to the reaction mixture, followed by the addition of propargyl alcohol (0.07 mL, 1.08 mmol). The solution was refluxed at 70^{o}C for 24 h. The solvent was removed under reduced pressure and the residue was dispersed in ethyl acetate (50 mL) and water (30 mL). The organic layer was dried with Na_2SO_4 and solvent removed under reduced pressure, to yield a white solid.

Yield 0.60 g, 90%.

^{1}H NMR (300 MHz, 298 K, $CDCl_3$) δ_H ppm 7.79 (1H, s, TRZ), 5.88 (1H, d, $^{3}J_{HH}$ = 8.1 Hz), 5.51-5.35 (2H, m), 5.24 (1H, t, $^{3}J_{HH}$ = 9.0 Hz), 4.79 (2H, s, CH_2), 4.29 (1H, dd, $^{3}J_{HH}$ = 12.6 Hz; $^{4}J_{HH}$ = 4.6 Hz), 4.14 (1H, d, $^{3}J_{HH}$ = 12.6 Hz), 4.06-3.92 (1H, m), 2.07-1.87 (12H, s, 4 × CH_3).

^{13}C {^{1}H} NMR (75 MHz, 298 K, $CDCl_3$) δ_C ppm 170.53, 169.94, 169.93, 169.05 (4 × CO), 148.45 (*C*=CH (TRZ), 120.09 (C=*C*H (TRZ)), 85.74 (C_1), 75.10 (C_5), 72.64 (C_3), 70.32 (C_2), 67.69 (C_4), 61.54 (C_6), 56.55 (CH_2), 20.68, 20.54, 20.52, 20.19 (4 × CH_3).

IR v cm^{-1} 3514 m, 1730 s, 1369 m, 1204 s, 1101 m, 1030 s, 912 m, 846 m, 871 m, 598 m, 505 m

MS (ESI) *m/z* 452.3 [M+Na]$^{+}$

Elemental analysis found (Calculated for $C_{17}H_{23}N_3O_{10}$) % C 47.50 (47.55) H 5.38 (5.40) N 9.51 (9.78)

(*2R,3S,4S,5R,6R*)-2-(acetoxymethyl)-6-(4-(hydroxymethyl)-1H-1,2,3-triazol-1-yl)tetrahydro-2H-pyran-3,4,5-triyl triacetate. (**32**)

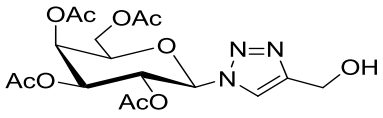

32 was synthesised using the procedure described for **31**, substituting 2,3,4,6-tetra-O-acetyl-β-D-glucopyranosylazide for 2,3,4,6-tetra-O-acetyl-β-D-galactopyranosylazide.

Yield**:** 0.12 g, 41%.

^{1}H NMR (400 MHz, 298 K, $CDCl_3$) δ_H ppm 7.89 (1H, s, TRZ), 5.88 (1H, d, $^3J_{HH}$ = 9.5 Hz, H-C_1), 5.55 (2H, m, H-$C_{3/4}$), 5.27 (1H, t, $^3J_{HH}$ = 9.5 Hz, H-C_2), 4.79 (2H, s, CH_2-OH), 4.26 (1H, m, H-C_5), 4.15 (2H, s, H-C_6), 2.21-1.98 (s, 4 x CH_3)

^{13}C NMR (100 MHz, 298 K, $CDCl_3$) δ_c ppm 170.4, 170.0, 169.8, 169.2, (4 x CO), 120.4 (CH, TRZ), 86.2 (C_1), 73.9 (C_5), 70.6 (C_2), 68.0 (C_3), 66.8 (C_4) 61.0 (C_5), 56.1 (CH_2-OH), 21.0, 20.6, 20.5, 20.2 (4x CH_3)

MS (ESI) *m/z* 452.2 $[M+Na]^+$

IR v cm^{-1} 3518 w, 3128 w, 2941 w, 1739 s, 1367 m, 1208 s, 1042 s, 921 m, 589 m

Elemental analysis found (Calculated for $C_{19}H_{25}N_3O_{12}$) % C 47.39 (46.82) H 5.87 (5.17) N 8.49 (8.62)

(*2R,3S,4R,5R,6R*)-5-acetamido-2-(acetoxymethyl)-6-(4-(hydroxymethyl)-1H-1,2,3-triazol-1-yl)tetrahydro-2H-pyran-3,4-diyl diacetate.[19] (**33**)

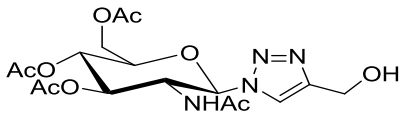

33 was synthesised using the procedure described for **31** substituting 2,3,4,6-tetra-O-acetyl-β-D-glucopyranosylazide for acetamido-3,4,6-tri-O-acetyl-2-deoxy-β-D-glucopyranosyl azide.

Yield: 0.12 g, 41%.

^{1}H NMR (400 MHz, 298 K, $CDCl_3$) δ_H ppm 7.91 (1H, s, HC=C), 6.69 (1H, d, J = 8.0 Hz, NH), 6.05 (1H, d, $^{3}J_{HH}$ = 9.5 Hz, H-C_1), 5.42 (1H, t, $^{3}J_{HH}$ = 9.5 Hz, H-C_3), 5.19 (1H, t, $^{3}J_{HH}$ = 9.5 Hz, H-C_4), 4.73 (2H, s, CH_2-OH), 4.54 (1H, m, H-C_2), 4.23 (1H, dd $^{2}J_{HH}$ = 12.5 Hz, $^{3}J_{HH}$ = 4.0 Hz, H-C_6), 4.09 (1H, d, $^{2}J_{HH}$ = 12.5 Hz, H-C_6), 4.01 (1H, d, $^{3}J_{HH}$ = 7.0 Hz, H-C_5), 2.10 (s, 4 x CH_3)

^{13}C NMR (100 MHz, 298 K, $CDCl_3$) δ_c ppm 171.1, 170.6, 170.4 169.4 (4 x C=O), 88.3 (C_1), 73.8 (C_5), 71.9 (C_3), 67.9 (C_4), 61.7 (C_6) 53.9 (C_2), 23.3, 20.7, 20.6 (4x CH_3)

MS (ESI) *m/z* 451.3 $[M+Na]^+$

IR v cm^{-1} 3270 w, 2926 w, 1741 s, 1664 m, 1369 m, 1218 s, 1101 m, 1034 s, 924 m, 598 m

Elemental analysis found (Calculated for $C_{17}H_{24}N_4O_9$) % C 48.03 (47.66) H 5.70 (5.65) N 10.73 (10.41)

(*2R,3R,4S,5R,6R*)-2-(acetoxymethyl)-6-(4-formyl-1H-1,2,3-triazol-1-yl)tetrahydro-2H-pyran-3,4,5-triyl triacetate (**34)**

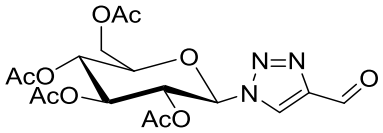

Pyridinium chlorochromate (15.07 mg, 1.2 eq.) was added into the solution of β-glucose-triaozle alchol **31** (25 mg, 1.0 eq.) in DCM. The reaction mixture was stirred at room temperature for 1 h, followed by addition of DCM (3 × 20 mL) and brine (2 × 20 mL). The organic layer was dried over anhydrous Na_2SO_4 and concentrated under reduced pressure. The pure product was obtained by silica gel column chromatography (DCM/MeOH: 20/1 v/v) as white solid.

Yield 23.0 mg, 92%.

^{1}H NMR (400 MHz, 298 K, $CDCl_3$) δ_H ppm 10.15 (1H, s, CHO), 8.37 (1H, s, TRZ), 5.94 (1H, d, $^3J_{HH}$ = 9.0 Hz), 5.43 (2H, m), 5.26 (1H, t, $^3J_{HH}$ = 9.6 Hz), 4.32 (1H, dd, $^3J_{HH}$ = 12.7 Hz; $^4J_{HH}$ = 4.9 Hz), 4.17 (1H, d, $^3J_{HH}$ = 12.6 Hz), 4.04 (1H, dd, $^3J_{HH}$ = 10.0 Hz, $^4J_{HH}$ = 3.0 Hz), 2.10-1.91 (12H, s, 4 × CH_3).

^{13}C {^{1}H} NMR (100 MHz, 298 K, $CDCl_3$) δ_C ppm 184.44 (CHO), 170.45, 169.87, 169.30, 168.91 (4 × CO), 147.97 (*C*=CH (TRZ), 124.17 (C=*C*H (TRZ)), 86.01 (C_1), 75.45 (C_5), 72.25 (C_3), 70.56 (C_2), 67.50 (C_4), 61.36 (C_6), 20.66, 20.52, 20.49, 20.11 (4 × CH_3).

IR v cm^{-1} 2125 s, 1735 s, 1374 s, 1210 s, 1081 s, 1046 m, 951 m

MS (ESI) *m/z* 450.3 $[M+Na]^+$

Elemental analysis found (Calculated for $C_{17}H_{21}N_3O_{10}$) % C 47.59 (47.8) H 4.79 (4.95) N 9.81 (9.83)

(*2R,3S,4S,5R,6R*)-2-(acetoxymethyl)-6-(4-formyl-1H-1,2,3-triazol-1-yl)tetrahydro-2H-pyran-3,4,5-triyl triacetate (**35**)

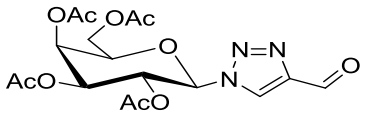

35 was synthesised using the procedure described for **34**, substituting β-glucose-triaozle alchol **31** for β-galactose-triaozle alchol **32**.

Yield: 0.11 g, 35%.

^{1}H NMR (400 MHz, 298 K, $CDCl_3$) δ_H ppm 10.1 (1H, s, H-C=O), 8.35 (1H, s, TRZ), 5.83 (1H, d, $^{3}J_{HH}$ = 9.5 Hz, H-C_1), 5.50 (1H, d, $^{3}J_{HH}$ = 3.0 Hz, H-C_3), 5.42 (1H, t, $^{3}J_{HH}$ = 9.5 Hz, H-C_2), 5.23 (1H, dd, *J* = 10.5 Hz, $^{3}J_{HH}$ = 3.0 Hz, H-C_4), 4.15 (3H, m, H-$C_{5/6}$), 2.16-1.86 (s, 4 x CH_3)

^{13}C NMR (100 MHz, 298 K, $CDCl_3$) δ_c ppm 185.0 (C=O, Aldehyde), 170.3, 169.9 169.8, 161.1 (4 x C=O), 124.2 (TRZ), 86.5 (C_1), 74.3 (C_5), 70.4 (C_4), 68.1 (C_2), 66.7 (C_3) 61.2 (C_6), 20.6, 20.5, 20.2 (4x CH_3)

MS (ESI) *m/z* 450.2 $[M+Na]^+$

IR v cm^{-1} 2124 s, 1736 s, 1374 s, 1211 s, 1081 s, 1045 m, 951 m

Elemental analysis found (Calculated for $C_{17}H_{22}N_4O_9$) % C 47.39 (47.89) H 5.12 (5.20) N 11.39 (13.13).

(*2R,3S,4R,5R,6R*)-5-acetamido-2-(acetoxymethyl)-6-(4-formyl-1H-1,2,3-triazol-1-yl)tetrahydro-2H-pyran-3,4-diyl diacetate (**36**)

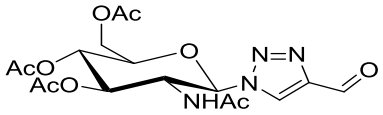

36 was synthesised using the procedure described for **34**, substituting β-glucose-triaozle alchol **31** for β-acetylglucosamine-triaozle alchol **33**.

Yield: 0.15 g, 62%.

^{1}H NMR (400 MHz, 298 K, $CDCl_3$) δ_H ppm 10.1 (1H, s, H-C=O), 8.49 (1H, s, TRZ), 6.50 (1H, s, NH), 6.12 (1H, s, H-C_1), 5.47 (1H, s, H-C_3), 5.20 (1H, s, H-C_4), 4.55 (1H, s, H-C_2), 4.23 (1H, m, H-C_6) 4.10 (2H, d, $^{3}J_{HH}$ = 10.5 Hz, H-$C_{5/6}$), 2.01-1.73 (s, 4 x CH_3)

^{13}C NMR (100 MHz, 298 K, $CDCl_3$) δ_c ppm 184.4 (C=O), 170.9, 170.6, 169.4 (4 x C=O), 147.7 (TRZ), 86.4 (C_1), 75.2 (C_5), 72.3 (C_4), 67.9 (C_3) 61.6 (C_6), 53.8 (C_2), 22.8, 20.7, 20.6 (4x CH_3)

IR v cm^{-1} 3280 w, 2932 w, 2117 w, 1741 s, 1696 m, 1535 m, 1367 m, 1218 s, 1034 s, 922 w, 759 w, 597 m

MS (ESI) *m/z* 449.3 $[M+Na]^+$

Elemental analysis found (Calculated for $C_{17}H_{22}N_4O_9$) % C 47.39 (47.89) H 5.12 (5.20) N 11.39 (13.13)

1-((*2R,3R,4S,5S,6R*)-3,4,5-trihydroxy-6-(hydroxymethyl)tetrahydro-2H-pyran-2-yl)-1H-1,2,3-triazole-4-carbaldehyde (**37**)

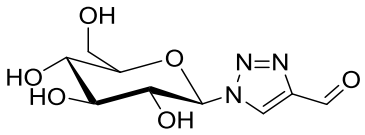

Sodium methoxide (120 µL, 1M in MeOH, 0.1 eq.) was added to a stirring solution of **34** (500 mg, 1.17 mmol, 1.0 eq) in dry MeOH (6 mL) until pH 9-10. The reaction mixture was refluxed at 85°c for 24 h. The solution was then neutralized by addition of ion-exchange resin (Dowex® 50WX4 hydrogen form) until pH 7, filtered, and the solvent was removed under reduced pressure to afford the fully deprotected triazole derivative as a colorless solid.

Yield: 36 mg, 64%.

^{1}H NMR (400 MHz, 298 K, DMSO) δ_H ppm 10.05 (1H, s, CHO), 9.13 (1H, s, TRZ), 5.65 (1H, d, $^{3}J_{HH}$ = 9.0 Hz), 5.55-5.16 (3H, m, 3 x OH), 4.64 (1H, s, OH), 3.87-3.67 (2H, m), 3.51-3.23 (4H, m).

^{13}C {^{1}H} NMR (100 MHz, 298 K, DMSO) δ_C ppm 185.39 (CHO), 147.24 (*C*=CH (TRZ), 128.37 (C=*C*H (TRZ)), 88.34 (C_1), 80.63 (C_5), 77.14 (C_3), 72.55 (C_2), 69.90 (C_4), 61.19 (C_6).

MS (ESI) *m/z* 282.2 $[M+Na]^+$

IR v cm^{-1} 3318 (broad), 2878 w, 1692 s, 1459 w, 1247 w, 1038 s, 897 m, 767 m

Elemental analysis found (Calculated for $C_9H_{13}N_3O_6$) % C 41.63 (41.70) H 5.37 (5.05) N 15.33 (16.20)

1-((*2R,3S,4S,5S,6R*)-3,4,5-trihydroxy-6-(hydroxymethyl)tetrahydro-2H-pyran-2-yl)-1H-1,2,3-triazole-4-carbaldehyde (**38**)

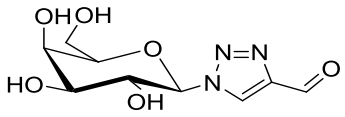

38 was synthesised using the procedure described for **37**, substituting acetyl protected β-glucose triazole aldehyde **34** for acetyl protected β-galactose triazole aldehyde **35**.

Yield**:** 0.10 g, 77%.

^{1}H NMR (400 MHz, 298 K, $CDCl_3$) δ_H ppm 10.1 (1H, s, H-C=O), 8.24 (1H, s, TRZ), 5.63 (1H, d, H-C_1), 4.16 (1H, dd, $^{3}J_{HH}$ = 8.5 Hz, H-C_2), 3.96 (1H, m, H-C_5), 3.83 (1H, m, H-C_4), (3H, 3.77, m, H-$C_{3/6}$)

^{13}C NMR (100 MHz, 298 K, $CDCl_3$) δ_c ppm 184.4 (C=O), 147.4 (**C**=CH TRZ), 120.9 (C=**C**H TRZ), 89.0 (C_1), 78.5 (C_4), 74.5 (C_3), 70.1 (C_2), 69.0 (C_5), 61.0 (C_6)

MS (ESI) *m/z* 282.2 $[M+Na]^+$

IR v cm^{-1} 3262 (broad), 2834 w, 1695 m, 1011 s, 884 m

N-((*2R,3R,4R,5S,6R*)-2-(4-formyl-1H-1,2,3-triazol-1-yl)-4,5-dihydroxy-6-(hydroxymethyl)tetrahydro-2H-pyran-3-yl)acetamide (**39**)

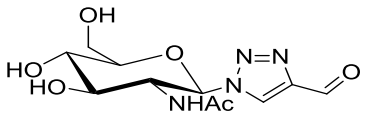

39 was synthesised using the procedure described for **37**, substituting acetyl protected β-glucose triazole aldehyde **34** for acetyl protected β- acetylglucosamine triazole aldehyde **36**.

Yield: 0.09 g, 64%.

^{1}H NMR (400 MHz, 298 K, $CDCl_3$) δ_H ppm 10.0 (1H, s, aldehyde proton), 8.56 (1H, s, TRZ), 5.80 (1H, m, H-C_1), 5.49 (1H, s, N**H**Ac), 4.23 (1H, dd, *J* = 16.5 Hz, $^{3}J_{HH}$ = 10.0 Hz, H-C_2), 3.92 (1H, d, $^{3}J_{HH}$ = 11.5 Hz, H-C_6), 3.74 (2H, dd, *J* = 22.5 Hz, $^{3}J_{HH}$ = 10.0 Hz, H-$C_{4/6}$), 3.58 (2H, d, $^{3}J_{HH}$ = 10.0 Hz, H-$C_{3/5}$), 1.80 (1H, s, CH_3)

^{13}C NMR (100 MHz, 298 K, $CDCl_3$) δ_c ppm 183.4 (C=O Aldehyde), 169.2 (C=O, NHAc), 134.4 (**C**=CH, TRZ), 121.2 (C=**C**H, TRZ), 86.4 (C_1), 79.9 (C_4), 74.5 (C_5), 69.9 (C_3), 61.7 (C_6), 55.6 (C_2), 20.8 (CH_3)

IR v cm^{-1} 3269 (broad), 2927 w, 2381 (broad), 1585 s, 1350 m, 1096 m, 1040 s, 767 w

MS (ESI) *m/z* 325.2 $[M+Na]^+$

6.4 Synthesis of complexes

Synthesis of R_c,Δ_{Zn},$[Zn_2\mathbf{L^1}_3][ClO_4]_4$ [3]

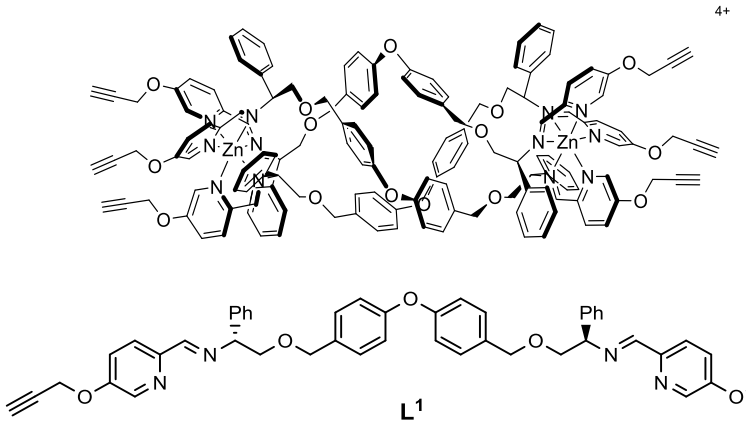

5-(Prop-2-yn-1-yloxy)picolinaldehyde (**2**) (81 mg, 0.50 mmol, 6.0 eq.), and (*R*,*R*)-4,4'-bis[(2-amino-2-phenylethoxy)methyl]-diphenyl ether (**3**) (95 mg, 0.25 mmol, 3 eq.) were dissolved in acetonitrile (30 ml) and stirred at ambient temperature for 2 h. Zinc(II) perchlorate hexahydrate (63 mg, 0.17 mmol, 2 eq.) was added and the yellow solution was stirred for a further 2 h. Upon addition of a few drops of ethyl acetate to the solution, the pure product was precipitated out and isolated by filteration. The off-white crystals were then vacuum filtered and washed with ethyl acetate before drying overnight.

Yield: 0.18 g, 75%

^{1}H NMR (500 MHz, 298 K, CD_3CN) δ_H 8.70 (6H, s, HC=N), 7.47 (12H, d, $^3J_{HH}$ = 8.0Hz, PhO), 7.39 (12H, m, py), 7.33 (12H, d, $^3J_{HH}$ = 8.5 Hz, Ph), 7.07 (6H, t, $^3J_{HH}$ = 7.5Hz, Ph), 6.95 (12H, t, $^3J_{HH}$ = 7.5Hz, Ph), 6.75 (12H, d, $^3J_{HH}$ = 8.5Hz, PhO), 6.66 (12H, d, $^3J_{HH}$ = 8.0Hz, Ph), 5.73 (6H, m, CH), 4.97 (6H, d, $^2J_{HH}$= 12.0Hz, OCH_2Ph), 4.77 (12H, t, $^4J_{HH}$ = 2.0, $CH_2C{\equiv}C$), 4.44 (6H, d, $^3J_{HH}$ = 12.0Hz, OCH_2Ph), 4.19 (6H,

t, J_{HH} = 11.0Hz, OC<u>H</u>$_2$CH), 3.37 (6H, dd, $^2J_{HH}$= 11.0Hz, $^3J_{HH}$= 2.5Hz, OC<u>H</u>$_2$CH), 2.92 (6H, t, $^4J_{HH}$ = 2.0, C≡CH).

^{13}C {^{1}H} NMR (125 MHz,298 K, CD_3CN) δ_C 161.3 (HC=N), 156.8 (q, py), 156.4 (q, PhO), 139.7 (q, py), 137.2 (py), 135.2 (q, Ph), 133.2 (q, PhO), 130.5 (py), 128.5 (Ph/PhO), 128.1 (Ph), 126.1 (Ph), 124.8 (py), 118.3 (PhO), 77.6 (C≡<u>C</u>H), 76.5(q, <u>C</u>≡CH), 71.9 (OCH_2Ph), 71.6 (O<u>C</u>H_2CH), 66.7 (OCH_2<u>C</u>H), 56.4 (<u>C</u>H_2C≡CH);

ESI-MS (+) *m/z* 755.4 $[L+H]^+$, 777.4 $[L+Na]^+$

Elemental Analysis found (Calculated for $C_{144}H_{126}Cl_4N_{12}O_{31}Zn_2 \cdot 4H_2O$) % C 60.32 (60.36), H 4.55 (4.71), N 5.70 (5.87).

IR ν cm^{-1} 3259 (br, m), 2866 (br, m), 1572 (m), 1501 (m), 1223 (m), 1080 (s), 1006 (m), 931 (w), 847 (w), 701 (w), 621 (m).

S_c,Λ_{Zn},HHT-[Zn_2**L**$^3_3$][ClO_4]$_4$ [9]

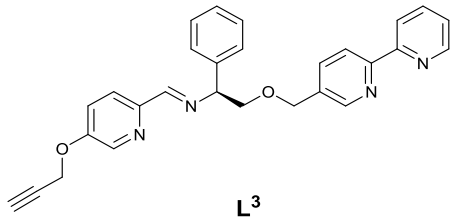

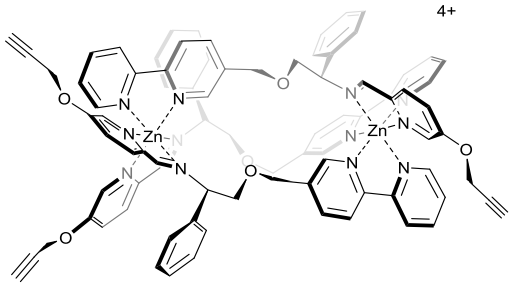

$Zn(ClO_4)_2 \cdot 6H_2O$ (0.11 g, 0.30 mmol) was added to a stirred solution of the 5-(propargyloxy)picolinaldehyde (**2**) (71 mg, 0.44 mmol) and (*S*)-2-(2,2'-bipyridin-5-ylmethoxy)-1-phenylethanamine (**14**) (0.135 g, 0.44 mmol) in acetonitrile (20 ml) at ambient temperature and stirred for 4 h. The resulting yellow solution yielded the desired product as a yellow crystalline solid on the addition of ethyl acetate.

Yield 0.23 g, 72 %.

^{1}H NMR (500 MHz, 298 K, CD_3CN) δ_H 9.26 (1H, s, HC=N), 9.23 (1H, s, bpy), 9.17(1H, s,HC=N), 9.17 (1H, s, bpy), 8.81 (1H, s, HC=N), 8.54 (1H, d, $^{3}J_{HH}$ = 8.0 Hz, bpy), 8.49 (1H, d, $^{3}J_{HH}$ = 8.0 Hz, bpy), 8.39 (1H, s, bpy), 8.30 (1H, d, $^{3}J_{HH}$ = 9.0 Hz, py), 8.28-8.19 (3H, m, py/bpy), 8.13-7.90 (8H, m, bpy), 7.89-7.74 (5H, m, py/bpy), 7.71 (1H, d, $^{4}J_{HH}$ = 2.5 Hz, py), 7.59-7.45 (6H, m, py/bpy), 7.23-7.14 (2H, m, Ph/py), 7.11 (2H, t, $^{3}J_{HH}$ = 7.5 Hz, Ph), 7.03 (1H, t, $^{3}J_{HH}$ = 7.5 Hz, Ph), 6.97 (2H, d, $^{3}J_{HH}$ = 7.5 Hz, Ph), 6.91 (1H, t, $^{3}J_{HH}$ = 7.5 Hz, Ph), 6.72 (2H, t, $^{3}J_{HH}$ = 7.5 Hz, Ph), 6.58 (2H, t, $^{3}J_{HH}$ = 7.5 Hz, Ph), 6.11 (2H, d, $^{3}J_{HH}$ = 7.5 Hz, Ph), 5.99 (2H, d, $^{3}J_{HH}$ = 7.5 Hz, Ph), 5.48 (1H, dd, $^{2}J_{HH}$ = 11.5 Hz, $^{3}J_{HH}$ = 3.0 Hz, C<u>H</u>Ph), 5.22 (1H, d, $^{2}J_{HH}$=13 Hz, OC<u>H</u>$_2$-bpy) 5.21 (1H, d, $^{2}J_{HH}$=13 Hz, OC<u>H</u>$_2$-bpy), 5.16 (1H, d, $^{2}J_{HH}$=13 Hz, OC<u>H</u>$_2$-bpy), 4.97 (1H, dd, $^{3}J_{HH}$ = 11.5 Hz,$^{3}J_{HH}$ =3.5 Hz,C<u>H</u>Ph), 4.88 (2H, d, $^{4}J_{HH}$ = 2.0 Hz, C<u>H</u>$_2$-CCH), 4.84-4.78 (3H, m, C<u>H</u>$_2$-CCH/C<u>H</u>Ph), 4.75 (2H, d, $^{4}J_{HH}$ = 2.0 Hz, C<u>H</u>$_2$-CCH), 4.54 (1H, d, $^{2}J_{HH}$=13 Hz, OC<u>H</u>$_2$-bpy), 4.52 (1H, d, $^{2}J_{HH}$=13 Hz, OC<u>H</u>$_2$-bpy), 4.48 (1H, d, $^{2}J_{HH}$=13 Hz, OC<u>H</u>$_2$-bpy), 4.30 (1H, t, J_{HH} = 11.0 Hz, C<u>H</u>$_2$-CHPh), 4.18 (1H, t, J_{HH} = 11.0 Hz, C<u>H</u>$_2$-CHPh), 4.10 (1H, t, J_{HH} = 11.0 Hz, C<u>H</u>$_2$-CHPh), 3.64 (1H, dd, $^{2}J_{HH}$ = 10.5 Hz, $^{3}J_{HH}$ = 3.5 Hz, C<u>H</u>$_2$-CHPh), 3.54 (1H, dd, $^{2}J_{HH}$ = 10.5 Hz, $^{3}J_{HH}$ = 3.5 Hz, C<u>H</u>$_2$-CHPh), 3.48 (1H, dd, $^{2}J_{HH}$ = 10.5 Hz, $^{3}J_{HH}$ = 3.5 Hz, C<u>H</u>$_2$-CHPh), 3.03 (1H, t, $^{4}J_{HH}$ = 2.0 Hz, C≡CH), 2.92 (1H, t, $^{4}J_{HH}$ = 2.0 Hz, C≡CH), 2.83 (1H, t, $^{4}J_{HH}$ = 2.2 Hz, C≡CH);

^{13}C {^{1}H} NMR (125MHz, 298 K, CD_3CN) δ_C 163.2/ 162.8/ 162.3 (HC=N), 158.6/ 158.2/ 157.8 (q, py), 150.7/ 150.5/ 149.7 (bpy), 149.5/ 149.4/ 149.3 (q, bpy), 148.9(q)/ 148.6/ 148.5(q)/ 148.5/ 148.3/ 148.0 (q, bpy), 143.4/ 143.1/ 143.0 (bpy), 142.3/ 141.9/ 141.8 (bpy), 140.7/ 140.7/ 140.6 (q, py), 138.4/ 138.3/ 138.3 (py), 137.8/ 137.4/ 137.2 (q, bpy), 135.1/ 134.2/ 133.8 (q, Ph), 132.3/132.0/ 131.2 (py), 129.2/ 129.1/ 129.1/ 129.0/ 129.0/ 128.9 (Ph), 127.8/ 127.6/ 127.4 (bpy), 127.2/ 126.5/ 126.4 (Ph), 125.5/

125.5/ 125.3 (py), 124.0/ 123.8/ 123.6/ 123.5/ 123.0/ 122.9 (bpy), 78.4/ 78.4/ 78.3 (C≡CH), 77.1/ 76.9/ 76.9 (q, C≡CH), 70.1/ 70.0 ($\underline{C}H_2$-bpy), 69.5 (CHPh), 69.4 ($\underline{C}H_2$-bpy), 69.3 (CHPh), 69.3/ 69.0/ 68.9 ($\underline{C}H_2$-CHPh), 67.5 (CHPh), 57.3/ 57.2/ 57.1 ($\underline{C}H_2$-C≡CH);

ESI-MS (+) *m/z* 449.3 $[L+H]^+$, 471.3 $[L+Na]^+$, 478.4 $[L+K]^+$

Elemental Analysis found (Calculated for $C_{84}H_{72}Cl_4N_{12}O_{22}Zn_2 \cdot 4H_2O$) % C 52.23 (51.84), H 3.72 (4.14), N 8.53 (8.64).

IR ν cm^{-1} 3568 (br, m), 1572 (m), 1475 (w), 1440 (w), 1220 (m), 1077 (s), 1008 (s), 932 (m), 860 (w), 752 (w), 698 (w), 620 (s).

General procedure for the synthesis of complexes S_c,Λ_{Zn},HHT-$[Zn_2L^{4a\text{-}d}{}_3][ClO_4]_4$

The aromatic azide (4.5 eq.) and $[Zn_2L^3{}_3][ClO_4]_4$ (1 eq.) was addition in acetonitrile (20 ml), followed by the addition of copper (I) iodide (1 eq.). The solution was stirred under partial vacuum and heated at 65 ˚C overnight. After cooling to ambient temperature, the solution was filtered to remove copper salt. The resulting pale yellow solution yielded the desired product as a white or yellow crystalline solid on the addition of ethyl acetate.

S_c,Λ_{Zn},HHT-$[Zn_2L^{4a}{}_3][ClO_4]_4$.

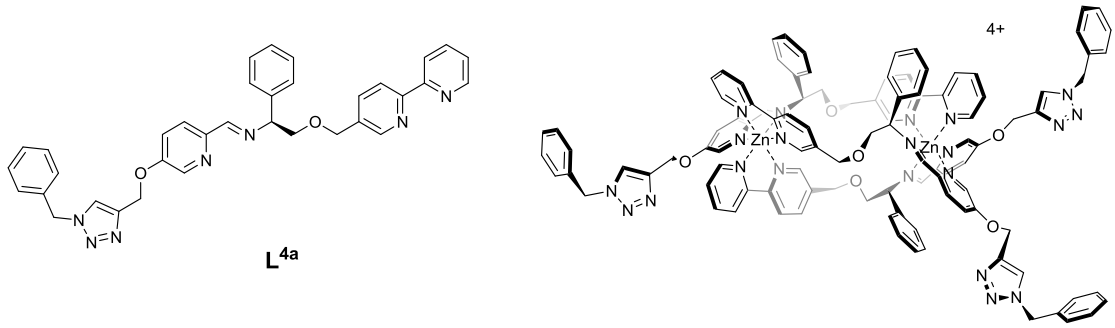

Yield 0.18 g, 82%.

^{1}H NMR (500 MHz, 298 K, CD_3CN) δ_H 9.25 (1H, s, HC=N), 9.20 (1H, s, bpy), 9.14 (1H, s, bpy), 9.11 (1H, s, HC=N), 8.75 (1H, s, HC=N), 8.52 (1H, d,$^3J_{HH}$ = 8.0, bpy), 8.48 (1H, d,$^3J_{HH}$ = 8.0, bpy), 8.36 (1H, s, bpy), 8.28 (1H, d,$^3J_{HH}$ = 9.0 Hz, py), 8.24-7.71 (23H, m, Ph/bpy/py/TRZ), 7.59 (1H, d,$^4J_{HH}$ = 2.5 Hz, py), 7.57-7.23 (27H, m, Ph/bpy/py), 7.10-6.87 (5H, m, Ph/py), 6.82 (1H, d,$^3J_{HH}$ = 8.0 Hz, Ph) 6.70 (2H, t, $^3J_{HH}$ = 8.0 Hz, Ph), 6.56 (2H, t, $^3J_{HH}$ = 8.0 Hz, Ph), 6.09 (2H, d, $^3J_{HH}$ = 8.0 Hz, Ph), 5.96 (2H, d, $^3J_{HH}$ = 8.0 Hz, Ph), 5.60 (2H, s, $PhCH_2TRZ$), 5.57 (2H, s, $PhCH_2TRZ$), 5.48 (2H, s, $PhCH_2TRZ$), 5.42 (1H, dd, $^2J_{HH}$= 11.0Hz, $^3J_{HH}$= 3.0, C<u>H</u>Ph), 5.32-5.09 (10H, m, TRZ-CH_2O/OC<u>H</u>$_2$-bpy), 4.94 (1H, dd, $^2J_{HH}$ = 11.0Hz, $^3J_{HH}$ = 3.0, C<u>H</u>Ph), 4.80 (1H, dd, $^2J_{HH}$ = 11.0Hz, $^3J_{HH}$ = 3.0, C<u>H</u>Ph), 4.53 (2H, d, $^2J_{HH}$= 13.0 Hz, OC<u>H</u>$_2$-bpy), 4.46 (1H, d, $^3J_{HH}$ = 13.0 Hz, OC<u>H</u>$_2$-bpy), 4.29 (1H, t, J_{HH} = 11.0 Hz, C<u>H</u>$_2$-CHPh), 4.15 (1H, t, J_{HH} = 11.0 Hz, C<u>H</u>$_2$-CHPh), 4.07 (1H, t, J_{HH} = 11.0 Hz, C<u>H</u>$_2$-CHPh), 3.60 (1H, dd, $^2J_{HH}$= 10.0Hz,$^3J_{HH}$= 3.5, C<u>H</u>$_2$-CHPh), 3.52 (1H, dd, $^2J_{HH}$= 11.0 Hz,$^3J_{HH}$= 3.0, C<u>H</u>$_2$-CHPh), 3.45 (1H, dd, $^2J_{HH}$= 11.0Hz, $^3J_{HH}$= 3.5, C<u>H</u>$_2$-CHPh).

^{13}C {^{1}H} NMR (125 MHz, 298 K, CD_3CN) δ_C 163.3/ 163.0/ 162.3(HC=N), 159.6/ 159.3/ 158.7 (q, py), 150.8/ 150.6/ 149.8 (bpy), 149.7/ 149.6/ 149.4/ 149.2 (q, bpy), 148.7/ 148.3 (bpy), 148.1 (q, bpy), 143.5/ 143.1/ 143.1 (q, bpy), 142.5/ 142.3 (q, TRZ), 142.0/, 141.7 (bpy), 140.4/ 140.3 (q, py), 138.9/ 138.7/138.4 (py) 137.8/ 137.5/137.2

(q, bpy), 136.2/ 136.1 (q, <u>Ph</u>CH_2), 135.3/ 134.4/ 134.0 (q, Ph), 132.5/ 132.3/131.3 (py), 129.6/ 129.5/129.5/ 129.3/ 129.2/ 129.1/ 129.1/ 129.0/ 129.0/128.8/ 128.7, 128.6 (Ph/bpy),127.2/ 126.6/126.5 (bpy)/ 126.1 (py), 125.3/ 125.4/ 125.1 (TRZ), 124.3/ 124.0/ 123.8/ 123.7/ 123.1/ 123.1 (bpy), 70.2/ 70.2/ 69.6 (<u>C</u>H_2-bpy), 69.6 (<u>C</u>HPh), 69.4 (<u>C</u>H_2-bpy), 69.4 (<u>C</u>HPh), 69.1/ 69.0 (<u>C</u>H_2-CHPh), 67.5 (<u>C</u>HPh), 62.8/ 62.7 (TRZ<u>C</u>H_2O),54.2/ 54.1/ 54.0 (Ph-<u>C</u>H_2-TRZ).

ESI-MS (+) *m/z* 582.4 $[L+H]^+$, 604.3 $[L+Na]^+$

Elemental Analysis found (Calculated for $C_{105}H_{93}Cl_4N_{21}O_6Zn_2 \cdot 30H_2O$) % C 49.03 (49.30), H 3.63 (6.03), N 11.37 (11.50).

IR ν cm^{-1} 3519 (br, m), 3039 (br, m), 1570 (m), 1216 (m), 1076 (s), 933 (w), 794 (w), 752 (w), 697 (w), 621 (m).

S_c,Λ_{Zn},HHT-$[Zn_2L^{4b}{}_3][ClO_4]_4$.

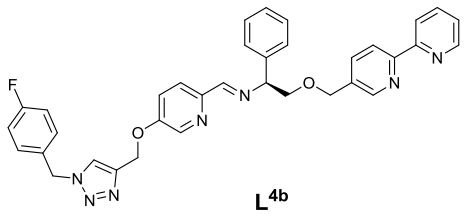

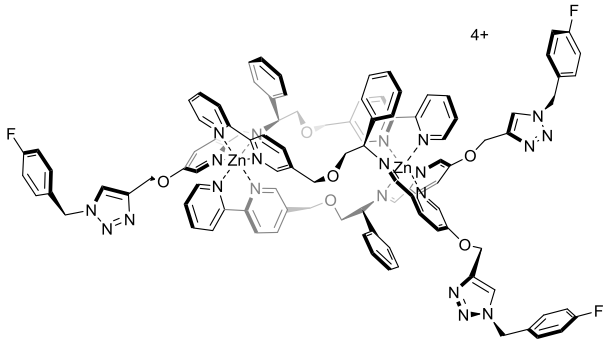

Yield 0.23 g, 66 %.

^{1}H NMR (500 MHz, 298 K, CD_3CN) δ_H 9.24 (1H, s, HC=N), 9.20 (1H, s, bpy), 9.14 (1H, s, bpy), 9.10 (1H, s, HC=N), 8.74 (1H, s, HC=N), 8.52 (1H, d, $^3J_{HH}$ = 8.0 hZ, bpy), 8.49 (1H, d, $^3J_{HH}$ = 8.0 hZ, bpy), 8.36 (1H, s, bpy), 8.28 (1H, d, $^3J_{HH}$ = 9.0 Hz, py), 8.23-8.17 (4H, m, bpy/py), 8.08-7.74 (20H, m, Ph/py/TRZ), 7.62-7.26 (18H, m, Ph/py/bpy), 7.24-6.99 (11H, m, Ph/py/bpy),6.94-6.85 (3H, m, Ph/bpy), 6.78 (2H, d,

$^{3}J_{HH}$ = 8.0 Hz, Ph), 6.71 (2H, t, $^{3}J_{HH}$ = 8.0 Hz, Ph), 6.56 (2H, t, $^{3}J_{HH}$ = 8.0 Hz, Ph), 6.09 (2H, d, $^{3}J_{HH}$ = 8.0 Hz, Ph), 5.96 (2H, d, $^{3}J_{HH}$ = 8.0 Hz, Ph), 5.59 (2H, s, PhCH_2TRZ), 5.55 (2H, s, PhCH_2TRZ), 5.46 (2H, s, PhCH_2TRZ), 5.42 (1H, dd, $^{2}J_{HH}$ = 11.0 Hz, $^{3}J_{HH}$ = 3.0, C<u>H</u>Ph), 5.31-5.08 (10H, m, TRZ-CH_2O/OC<u>H</u>$_2$-bpy), 4.94 (1H, dd, $^{2}J_{HH}$ = 11.0 Hz, $^{3}J_{HH}$ = 3.0, C<u>H</u>Ph), 4.78(1H, dd, $^{2}J_{HH}$ = 11.0 Hz, $^{3}J_{HH}$ = 3.0, C<u>H</u>Ph), 4.53 (4H, d, $^{2}J_{HH}$ = 13.0 Hz,OC<u>H</u>$_2$-bpy), 4.45 (2H, d, $^{2}J_{HH}$ = 13.0 Hz, OC<u>H</u>$_2$-bpy), 4.29 (1H, t, J_{HH} = 11.0 Hz, C<u>H</u>$_2$-CHPh), 4.14 (1H, t, J_{HH} = 11.0 Hz, C<u>H</u>$_2$-CHPh), 4.06 (1H, t, J_{HH} = 11.0 Hz, C<u>H</u>$_2$-CHPh), 3.59 (1H, dd, $^{2}J_{HH}$ = 10.0 Hz, $^{3}J_{HH}$ = 3.5, C<u>H</u>$_2$-CHPh), 3.52 (1H, dd, $^{2}J_{HH}$ = 11.0 Hz, $^{3}J_{HH}$ = 3.0, C<u>H</u>$_2$-CHPh), 3.45 (1H, dd, $^{2}J_{HH}$ = 11.0 Hz, $^{3}J_{HH}$ = 3.5, C<u>H</u>$_2$-CHPh).

^{13}C {^{1}H} NMR (125MHz, 298 K, CD_3CN) δ_C 163.6/ 163.5 (q, F-<u>Ph</u>), 162.7/ 162.4/ 161.7 (HC=N), 161.1 (q, F-<u>Ph</u>), 159.0/ 158.7/ 158.1 (q, py), 150.2/ 150.0/ 149.2 (bpy), 149.1/ 148.9/ 148.6 (q, bpy), 148.1/ 147.7 (bpy), 147.6 (q, bpy), 142.9/ 142.6/ 142.5 (bpy), 141.9/ 141.72 (q, TRZ), 141.70/, 141.4/ 141.1 (bpy), 139.8/ 139.7 (q, py), 138.4/ 138.1/ 137.8 (py), 137.3/ 136.9/ 136.6 (q, <u>Ph</u>CH_2), 134.6/ 133.8/ 133.4 (q, Ph), 131.9/, 131.8/ (py), 130.7/ 130.6/ 130.4/ 130.3/ 130.2/ 128.8/ 128.6/ 128.5/ 128.4/ 128.3 (Ph/bpy), 127.3/ 127.2/ 126.9 (bpy), 126.6/ 126.1/ 126.0 (py), 125.6/ 124.9/ 124.8 (TRZ), 124.7/ 124.5/ 124.4 (bpy), 123.7/ 123.4/ 123.2/ 122.6/ 122.5 (bpy), 155.8/ 155.7/ 155.6/ 155.5 (F-<u>Ph</u>), 69.6/ 69.5 (<u>C</u>H$_2$-bpy), 69.0/ 68.8 (<u>C</u>HPh), 68.5/ 68.4 (<u>C</u>H$_2$-CHPh), 66.9 (<u>C</u>HPh), 62.2/ 62.0 (TRZ<u>C</u>H$_2$O), 52.8/ 52.7/ 52.6 (F-Ph-<u>C</u>H$_2$-TRZ).

ESI-MS (+) *m/z* 600.4 $[L+H]^+$, 622.3 $[L+Na]^+$

Elemental Analysis found (Calculated for $C_{105}H_{90}Cl_4F_3N_{21}O_6Zn_2 \cdot 28H_2O$) % C 49.02 (48.96), H 3.53 (5.71), N 11.39 (11.42).

IR ν cm^{-1} 1602 (w), 1570 (w), 1315 (w), 1218 (m), 1076 (s), 841 (m), 788 (m), 751 (m), 698 (m), 620 (s).

S_c,Λ_{Zn},HHT-$[Zn_2L^{4c}{}_3][ClO_4]_4$.

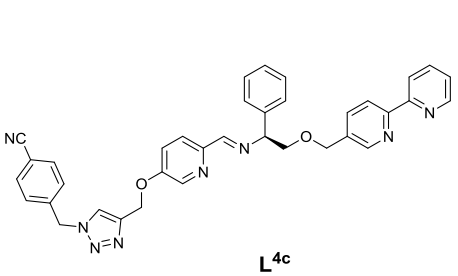

L^{4c}

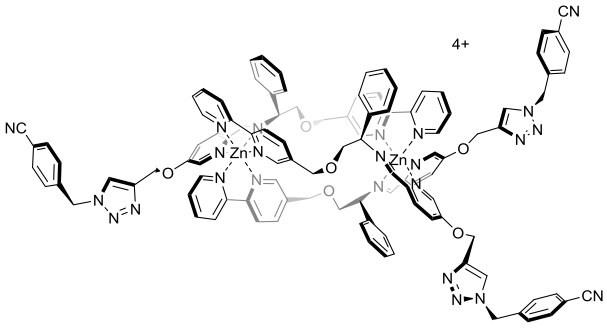

Yield 0.19 g, 74%.

^{1}H NMR (500 MHz, 298 K, CD_3CN) δ_H 9.25 (1H, s, HC=N), 9.21 (1H, s, bpy), 9.14 (1H, s, bpy), 9.10 (1H, s, HC=N), 8.73 (1H, s, HC=N), 8.52 (1H, d, $^3J_{HH}$ = 8.0 Hz, bpy), 8.48 (1H, d, $^3J_{HH}$ = 8.0 Hz, bpy), 8.36 (1H, s, bpy), 8.28 (1H, d,$^3J_{HH}$ = 9.0 Hz, py), 8.24-7.23 (54H, m, Ph/py/bpy/TRZ), 7.02 (2H, t, $^3J_{HH}$ = 7.0 Hz, Ph), 6.91 (2H, t, $^3J_{HH}$ = 7.5 Hz, Ph), 6.85 (2H, d, $^3J_{HH}$ = 8.0 Hz, Ph), 6.76 (2H, d, $^3J_{HH}$ = 8.0 Hz, Ph), 6.71 (2H, t, $^3J_{HH}$ = 8.0 Hz, Ph), 6.57 (2H, t, $^3J_{HH}$ = 8.0 Hz, Ph), 6.06 (2H, d, $^3J_{HH}$ = 8.0 Hz, Ph), 5.96 (2H, d, $^3J_{HH}$ = 8.0 Hz, Ph),5.68 (2H, s, $PhCH_2TRZ$), 5.65 (2H, s, $PhCH_2TRZ$), 5.57 (2H, s, $PhCH_2TRZ$), 5.41(1H, dd, $^2J_{HH}$ = 11.0 Hz,$^3J_{HH}$ = 3.0, C<u>H</u>Ph), 5.36-5.08 (10H, m, TRZ-CH_2O/OC<u>H_2</u>-bpy), 4.94 (1H, dd, $^2J_{HH}$ = 11.0 Hz,$^3J_{HH}$ = 3.0, C<u>H</u>Ph), 4.80 (1H, dd, $^2J_{HH}$ = 11.0 Hz, $^3J_{HH}$ = 3.0, C<u>H</u>Ph), 4.53 (1H, d, $^2J_{HH}$ = 13.0 Hz, OC<u>H_2</u>-bpy), 4.52 (1H, d, $^2J_{HH}$ = 13.0 Hz, OC<u>H_2</u>-bpy), 4.45 (1H, d, $^2J_{HH}$ = 13.0 Hz, OC<u>H_2</u>-bpy), 4.28 (1H, t, J_{HH} = 11.0 Hz, C<u>H_2</u>-CHPh), 4.13 (1H, t, J_{HH} = 11.0 Hz, C<u>H_2</u>-CHPh), 4.06 (1H, t, J_{HH} = 11.0 Hz, C<u>H_2</u>-CHPh), 3.60 (1H, dd, $^2J_{HH}$ = 10.0 Hz, $^3J_{HH}$ = 3.5, C<u>H_2</u>-CHPh), 3.52 (1H, dd, $^2J_{HH}$ = 11.0 Hz, $^3J_{HH}$ = 3.0, C<u>H_2</u>-CHPh), 3.45 (1H, dd, $^2J_{HH}$ = 11.0 Hz, $^3J_{HH}$ = 3.5, C<u>H_2</u>-CHPh).

^{13}C {^{1}H} NMR (125 MHz, CD_3CN) δ_C 162.7/ 162.4/ 161.7 (HC=N), 159.0/ 158.8/ 158.1 (q, py), 150.3/ 150.0/ 149.3 (bpy), 149.1/ 148.9/ 148.6 (q, bpy), 148.1/ 147.7 (bpy), 147.6 (q, bpy), 142.9/ 142.6/ 142.5 (bpy), 142.1/ 141.9 (q, TRZ), 141.7/ 141.4/ 141.2 (bpy), 140.9/ 140.8/ 140.7 (q, PhCN), 139.8/ 139.7 (q, py) 138.4/ 138.2/ 137.7 (py), 137.3/ 137.0/ 136.7 (q, $PhCH_2$), 134.6/ 133.9/ 133.5 (q, Ph), 132.9/ 132.8 (PhCN), 131.9/ 131.8/ 130.7 (py), 129.1/ 128.8/ 128.7/ 128.6/ 128.5/ 128.4/ 128.3 (Ph/bpy), 127.3/ 127.2/ 126.9 (bpy), 126.6/ 126.1/ 126.0 (py), 125.7/ 125.2/ 125.1/ 125.0/ 124.9/ 124.5/ 123.7/ 123.5/ 123.2/ 122.6/ 122.5 (bpy), 118.3 (CN), 112.0 (q, PhCN), 69.7/ 69.6 (CH_2-bpy), 69.03 (CHPh), 69.00 (CH_2-bpy), 68.9 (CH_2-CHPh), 68.8 (CHPh), 68.6/ 68.5 (CH_2-CHPh), 67.0 (CHPh), 62.2/ 62.0/ 61.9 (TRZCH_2O), 53.0/ 52.9/ 52.8 (CNPh-CH_2-TRZ).

ESI-MS (+) *m/z* 607.3 $[L+H]^+$

Elemental Analysis found (Calculated for $C_{108}H_{90}Cl_4N_{24}O_6Zn_2 \cdot 29H_2O$) % C 49.57 (49.60), H 3.36 (5.70), N 12.84 (12.86).

IR ν cm^{-1} 2229 (w), 1571 (m), 1475 (w), 1440 (w), 1317 (w), 1263 (w), 1218 (w), 1080 (s), 827 (m), 792 (m), 753 (m), 698 (m), 622 (s).

S_c,Λ_{Zn},HHT-$[Zn_2L^{4d}{}_3][ClO_4]_4$.

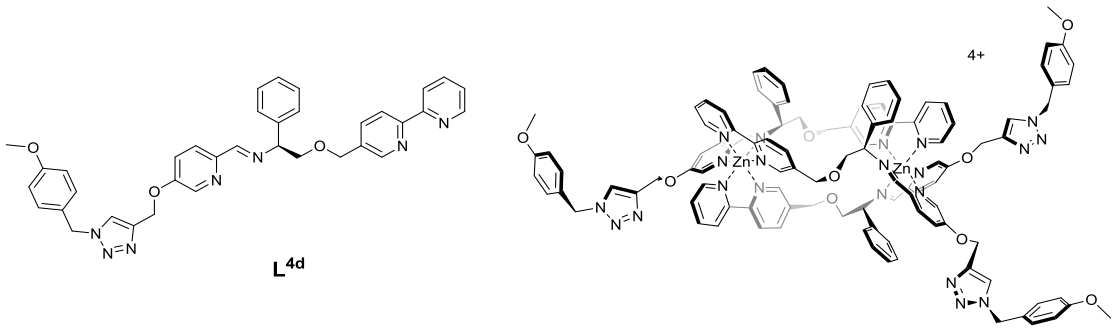

Yield 0.26 g, 90%.

^{1}H NMR (500 MHz, 298 K, CD_3CN) δ_H 9.22 (1H, s, HC=N), 9.17 (1H, s, bpy), 9.11 (1H, s, bpy), 9.06 (1H, s, HC=N), 8.71 (1H, s, HC=N), 8.51 (1H, d,$^{3}J_{HH}$ = 8.0 Hz, bpy), 8.48 (1H, d,$^{3}J_{HH}$ = 8.0 Hz, bpy), 8.34 (1H, s, bpy), 8.25 (1H, d, $^{3}J_{HH}$ = 9.0Hz, py), 8.23-8.15 (4H, m, py), 8.08-7.71 (20H, m, Ph/py/TRZ), 7.56 (1H, d, $^{4}J_{HH}$ = 2.5, py), 7.52-7.45 (3H, m, Ph/py), 7.42-7.25 (10H, m, Ph/bpy/py), 7.20 (2H, d, $^{3}J_{HH}$ = 9.0 Hz, py), 7.06-6.83 (14H, m, Ph/py), 6.74 (2H, d, $^{3}J_{HH}$ = 8.0 Hz, Ph), 6.68 (2H, t, $^{3}J_{HH}$ = 8.0 Hz, Ph), 6.53 (2H, t, $^{3}J_{HH}$ = 8.0 Hz, Ph), 6.06 (2H, d, $^{3}J_{HH}$ = 8.0 Hz, Ph), 5.93 (2H, d, $^{3}J_{HH}$ = 8.0 Hz, Ph), 5.49 (2H, s, $PhCH_2TRZ$), 5.46 (2H, s, $PhCH_2TRZ$), 5.43-5.37 (3H, m, $PhCH_2TRZ$/ CHPh), 5.26-5.06 (10H, m, TRZ-CH_2O/O$C\underline{H}_2$-bpy), 4.91 (1H, dd, $^{2}J_{HH}$ = 11.0Hz, $^{3}J_{HH}$ = 3.0, C$\underline{H}$Ph), 4.77 (1H, dd, $^{2}J_{HH}$ = 11.0Hz, $^{3}J_{HH}$ = 3.0, C$\underline{H}$Ph), 4.52 (2H, d, $^{2}J_{HH}$= 13.0 Hz, O$C\underline{H}_2$-bpy), 4.45 (2H, d, $^{2}J_{HH}$= 13.0 Hz, O$C\underline{H}_2$-bpy)), 4.26 (1H, t, J_{HH} = 11.0 Hz, C$\underline{H}_2$-CHPh), 4.11 (1H, t, J_{HH} = 11.0 Hz, C$\underline{H}_2$-CHPh), 4.03 (1H, t, J_{HH} = 11.0 Hz, C$\underline{H}_2$-CHPh), 3.78 (3H, s, OCH_3), 3.76 (3H, s, OCH_3),3.74 (3H, s, OCH_3), 3.56 (1H, dd, $^{2}J_{HH}$= 10.0 Hz, $^{3}J_{HH}$= 3.5, C$\underline{H}_2$-CHPh), 3.49 (1H, dd, $^{2}J_{HH}$= 11.0 Hz, $^{3}J_{HH}$= 3.0, C$\underline{H}_2$-CHPh), 3.42 (1H, dd, $^{2}J_{HH}$= 11.0 Hz, $^{3}J_{HH}$= 3.5, C$\underline{H}_2$-CHPh).

^{13}C {^{1}H} NMR (125 MHz, 298 K, CD_3CN) δ_C 162.8/ 162.4/ 161.8 (HC=N), 159.9 (q, $\underline{Ph}OCH_3$), 159.1/ 158.8/ 158.2 (q, py), 150.3/ 150.0/ 149.3 (bpy), 149.1/ 148.9/ 148.7 (q, bpy), 148.1/ 147.8 (bpy), 147.6 (q, bpy), 143.0/ 142.6/ 142.5 (bpy), 141.9 (q, TRZ), 141.8 (bpy), 141.7 (q, TRZ), 141.5/ 141.2 (bpy), 139.8/ 139.7 (q, py), 138.4/ 138.2/ 137.7 (py), 137.3/ 137.0/ 136.7 (q, bpy), 134.7/ 133.9/ 133.5 (q, Ph), 131.9/ 131.8/ 130.8 (py), 130.0/ 129.8/ 129.7 ($\underline{Ph}OCH_3$) 128.8/ 128.7/ 128.6/ 128.5/ 128.4 (Ph), 127.6/ 127.5 ($\underline{Ph}OCH_3$), 127.3/ 127.2/ 126.9 (bpy), 126.7/ 126.1/ 126.0 (Ph), 125.8/ 125.0/ 124.6 (py), 124.5/ 124.3 (TRZ), 123.8/ 123.5/ 123.3/ 123.2/ 122.6/ 122.5 (bpy), 114.4/ 114.3/ 114.2 ($\underline{Ph}OCH_3$), 69.7/ 69.6/ 69.1 ($\underline{C}H_2$-bpy), 69.0 ($\underline{C}$HPh), 68.9 ($\underline{C}H_2$-

CHPh), 68.8 (CHPh), 68.6/ 68.5 (CH_2-CHPh), 67.0 (CHPh), 62.3/ 62.1 (TRZCH_2O), 55.1 (OCH_3), 53.3/ 53.2/ 53.1 (CH_3OPh-CH_2-TRZ).

ESI-MS (+) *m/z* 612.4 $[L+H]^+$

Elemental Analysis found (Calculated for $C_{108}H_{99}Cl_4N_{21}O_9Zn_2 \cdot 28H_2O$) % C 49.44 (49.66), H 3.74 (5.98), N 11.10 (11.26).

IR ν cm^{-1} 1571 (m), 1514 (w), 1316 (w), 1248 (m), 1079 (s), 839 (w), 791 (m), 752 (m), 698 (w), 621 (s).

S_c,Λ_{Zn},HHT-$[Zn_2L^5{}_3][ClO_4]_4$.

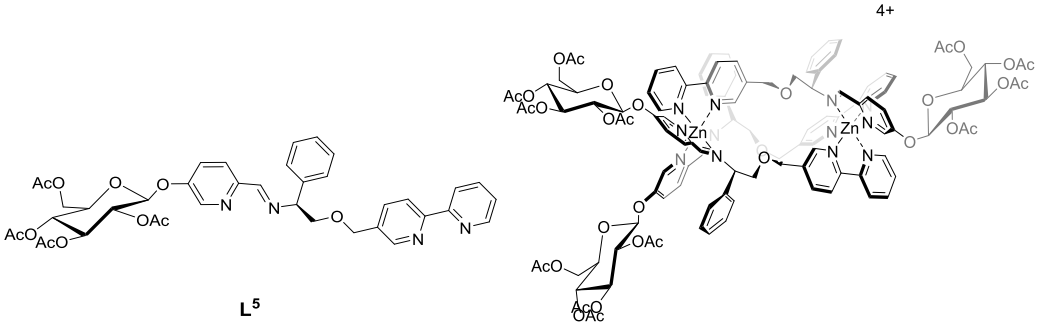

S_c,Λ_{Zn},HHT-$[Zn_2L^5{}_3][ClO_4]_4$ was synthesised using the procedure described for S_c,Λ_{Zn},HHT-$[Zn_2L^3{}_3][ClO_4]_4$, substituting 5-(propargyloxy)picolinaldehyde (**5**) for (*2R,3R,4S,5R,6S*)-2-(acetoxymethyl)-6-((6-formylpyridin-3-yl)oxy)tetrahydro-2H-pyran-3,4,5-triyl triacetate (**21**).

Yield 0.38 g, 85%

^{1}H NMR (500 MHz, 298 K, CD_3CN) δ_H ppm 9.30 (1H, s, HC=N), 9.21 (1H, s, HC=N), 9.19 (1H, s, bpy), 9.13 (1H, s, bpy), 8.85 (1H, s, HC=N), 8.52 (1H, d, $^3J_{HH}$ = 8.2 Hz, bpy), 8.48 (1H, d, $^3J_{HH}$ = 8.2 Hz, bpy), 8.37-8.31 (2H, m, bpy overlapping with py), 8.29-8.18 (3H, m, bpy overlapping with py), 8.12-7.92 (8H, m, bpy overlapping with py), 7.91 (1H, d, $^3J_{HH}$ = 8.2 Hz, bpy), 7.89-7.80 (3H, m, bpy overlapping with py),

7.78 (1H, d, $^{4}J_{HH}$ = 2.5 Hz, bpy), 7.76 (1H, d, $^{3}J_{HH}$ = 8.0 Hz, Py), 7.60-7.48 (5H, m, bpy overlapping with py), 7.44 (1H, d, $^{4}J_{HH}$ = 2.5 Hz, py), 7.24 (1H, t, $^{3}J_{HH}$ = 7.4 Hz, Ph), 7.17 (1H, d, $^{4}J_{HH}$ = 2.5 Hz, py), 7.09 (2H, t, $^{3}J_{HH}$ = 7.7 Hz, Ph), 7.02 (1H, t, $^{3}J_{HH}$ = 7.4 Hz, Ph), 6.96-6.89 (3H, m, Ph overlapping with py), 6.71 (2H, t, $^{3}J_{HH}$ = 7.7 Hz, Ph), 6.58 (2H, t, $^{3}J_{HH}$ = 7.7 Hz, Ph), 6.09 (2H, d, $^{3}J_{HH}$ = 7.6 Hz, Ph), 5.97 (2H, d, $^{3}J_{HH}$ = 7.6 Hz, Ph), 5.51-5.41 (4H, m, H_{glu} overlapping with C<u>H</u>Ph), 5.38-5.04 (12H, m, H_{glu} overlapping with C<u>H</u>$_2$-bpy), 4.95 (1H, d, $^{3}J_{HH}$ = 9.1 Hz, C<u>H</u>Ph), 4.79 (1H, d, $^{2}J_{HH}$ = 9.1Hz, C<u>H</u>Ph), 4.55 (2H, d, $^{2}J_{HH}$ = 13.0 Hz, C<u>H</u>$_2$-bpy), 4.48 (1H, d, $^{2}J_{HH}$ = 12.9 Hz, C<u>H</u>$_2$-bpy), 4.34-3.94 (12H, m, H_{glu} overlapping with C<u>H</u>$_2$-CHPh), 3.66 (1H, dd, $^{2}J_{HH}$ = 10.3 Hz, $^{3}J_{HH}$ = 3.5 Hz, C<u>H</u>$_2$-CHPh), 3.53 (1H, dd, $^{2}J_{HH}$ = 11.0 Hz, $^{3}J_{HH}$ = 2.8 Hz, C<u>H</u>$_2$-CHPh), 3.45 (1H, dd, $^{2}J_{HH}$ = 11.1 Hz, $^{3}J_{HH}$ = 3.4 Hz, C<u>H</u>$_2$-CHPh), 2.08-1.83 (36H, m, 12 × $COCH_3$).

^{13}C {^{1}H} NMR (126 MHz, 298 K, CD_3CN) δ_C ppm 170.8, 170.8, 170.8, 170.5, 170.4, 170.4, 170.1, 170.0, 170.0, 169.9, 169.8, 169.7 (12 × CO), 163.5, 163.1, 162.7 (HC=N), 157.8, 157.3, 157.0 (q, py), 150.9, 150.7, 149.8 (bpy), 149.7, 149.5, 149.4, 149.0 (q, bpy), 149.0, 148.9, 148.8 (bpy), 148.6, 148.1 (q, bpy), 143.6, 143.3, 143.2, 142.5 (bpy), 142.2, 142.1 (q, py), 142.0, 141.9, 140.4, 139.9, 139.9 (py), 137.9, 137.5, 137.4 (q, bpy), 135.2, 134.2, 133.8 (q, Ph), 132.7, 132.3, 131.7 (py), 129.4, 129.2, 129.2, 129.2, 129.1 (Ph), 127.9, 127.8 (bpy), 127.5 (Ph), 127.3 (bpy), 126.9, 126.8 (py), 126.7, 126.5 (Ph), 124.0, 123.8, 123.7, 123.7, 123.2, 123.1 (bpy), 98.5, 98.2 (C_{1Glu}), 72.6, 72.6 (C_{5Glu}), 72.2, 72.2 (C_{3Glu}), 71.1, 70.9, 70.7 (<u>C</u>HPh), 70.2, 70.2 (<u>C</u>H_2-bpy), 69.6, 69.6 (C_{2Glu}), 69.5, 69.1, 69.0 (<u>C</u>H_2-CHPh), 68.0, 67.7 (C_{4Glu}), 61.7, 61.7, 61.6 (C_{6Glu}), 20.7, 20.5, 20.5, 20.5, 20.5, 20.4, 20.4, 20.4 (12 × CH_3).

Elemental Analysis found (Calculated for $C_{117}H_{120}Cl_4N_{12}O_{49}Zn_2 \cdot 4H_2O$) % C 49.47 (49.78), H 4.23 (4.57), N 6.04 (5.95).

S_c,Λ_{Zn},HHT-$[Zn_2L^6{}_3][ClO_4]_4$.

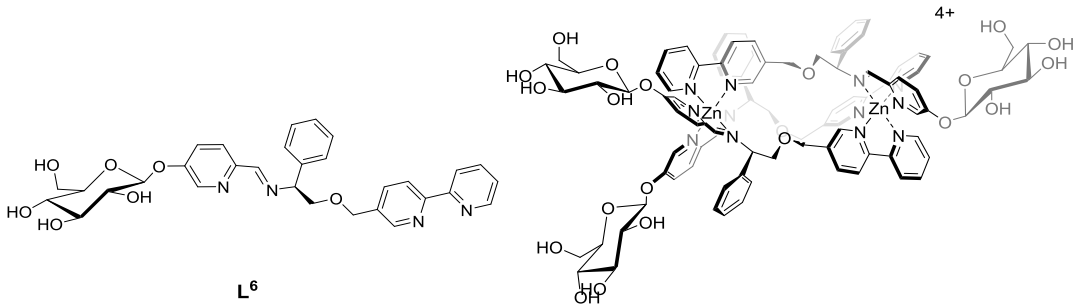

S_c,Λ_{Zn},HHT-$[Zn_2L^6{}_3][ClO_4]_4$ was synthesised using the procedure described for S_c,Λ_{Zn},HHT-$[Zn_2L^3{}_3][ClO_4]_4$, substituting 5-(propargyloxy)picolinaldehyde (**5**) for 5-(((*2S,3R,4S,5S,6R*)-3,4,5-trihydroxy-6-(hydroxymethyl)tetrahydro-2H-pyran-2-yl)oxy)picolinaldehyde (**22**)

Yield 0.30 g, 80%

^{1}H NMR (500 MHz, 298 K, CD_3CN) δ_H ppm 9.29 (1H, s, HC=N), 9.21 (1H, s, bpy), 9.18 (1H, s, HC=N), 9.15 (1H, s, bpy), 8.85 (1H, s, HC=N), 8.55 (1H, d, $^3J_{HH}$ = 8.2 Hz, bpy), 8.50 (1H, d, $^3J_{HH}$ = 8.2 Hz, bpy), 8.38 (1H, s, bpy), 8.32 (1H, d, $^3J_{HH}$ = 8.7 Hz, Py), 8.23 (4H, m, Py/bpy), 8.12-7.89 (11H, m, bpy), 7.89-7.79 (5H, m, $^3J_{HH}$ = 8.2 Hz, bpy), 7.76 (1H, d, $^4J_{HH}$ = 2.2 Hz, Py), 7.61-7.42 (9H, m, Py), 7.25 (1H, d, $^4J_{HH}$ = 2.3 Hz, Py), 7.19 (1H, t, $^3J_{HH}$ = 7.3 Hz, Ph), 7.11 (2H, t, $^3J_{HH}$ = 7.6 Hz, Ph), 7.02 (1H, t, $^3J_{HH}$ = 7.5 Hz, Ph), 6.79 (2H, d, $^3J_{HH}$ = 7.6 Hz, Ph), 6.91 (1H, t, $^3J_{HH}$ = 7.4 Hz, Ph), 6.71 (2H, t, $^3J_{HH}$ = 7.7 Hz, Ph), 6.57 (2H, t, $^3J_{HH}$ = 7.7 Hz, Ph), 6.11 (2H, d, $^3J_{HH}$ = 7.6 Hz, Ph), 5.98 (2H, d, $^3J_{HH}$ = 7.6 Hz, Ph), 5.46 (1H, dd, $^2J_{HH}$ = 11.5 Hz, $^3J_{HH}$ = 3.0 Hz, C<u>H</u>Ph), 5.22 (1H, d, $^2J_{HH}$=13 Hz, C<u>H</u>$_2$-bpy) 5.20 (1H, d, $^2J_{HH}$=13 Hz, C<u>H</u>$_2$-bpy), 5.17 (1H, d, $^2J_{HH}$=13 Hz, OC<u>H</u>$_2$-bpy), 4.99-4.91 (3H, m, C<u>H</u>Ph overlapping with H_{glu}), 4.88-4.81 (2H, m, C<u>H</u>Ph overlapping with H_{glu}), 4.55 (1H, d, $^2J_{HH}$=13 Hz, C<u>H</u>$_2$-bpy), 4.49 (1H, d, $^2J_{HH}$=13 Hz, C<u>H</u>$_2$-bpy), 4.31 (1H, t, J_{HH} = 11.0 Hz, C<u>H</u>$_2$-CHPh), 4.18 (1H,

t, J_{HH} = 11.0 Hz, C<u>H</u>$_2$-CHPh), 4.14-3.20 (38H, m, C<u>H</u>$_2$-CHPh overlapping with H_{glu}), 3.15 (1H, s, OH), 3.06 (1H, s, OH), 2.90 (1H, s, OH).

^{13}C {^{1}H} NMR (125MHz, 298 K, CD_3CN) δ_C 163.1/ 162.7/ 162.1 (HC=N), 158.0/ 157.7/ 157.6 (q, py), 150.5/ 150.2/ 149.5 (bpy), 149.3/ 149.1/ 149.1 (q, bpy), 148.7 (q)/ 148.4/ 148.3 (bpy), 148.26 (q, bpy) 147.9 (bpy), 147.8 (q, bpy), 143.2/ 142.9/ 142.8 (bpy), 142.0/ 141.7/ 141.5 (bpy), 141.2/ 141.2/ 141.1 (q, py), 138.3/ 138.1 (py), 137.6/ 137.2/ 137.0 (q, bpy), 134.9/ 133.9/ 133.6 (q, Ph), 132.2/ 132.1/ 131.1 (py), 129.4/ 129.0/ 128.9/ 128.9/ 128.8/ 128.7 (Ph), 127.7/ 127.5/ 127.5 (bpy), 127.3/ 127.1/ 127.0 (Ph), 126.7/ 126.3/ 126.2 (py), 124.0/ 123.7/ 123.5/ 123.4/ 122.8 (bpy), 100.5, 100.1, 99.9 (C_{1Glu}), 76.9, 76.9, 76.8 (C_{5Glu}), 76.4, 76.3 (C_{3Glu}), 73.3, 73.2 (C_{2Glu}), 70.2, 70.1 (C_{4Glu}), 69.9 (C<u>H</u>$_2$-bpy), 69.8 (C_{4Glu}), 69.8 (C<u>H</u>$_2$-bpy), 69.4/ 69.1 (C<u>H</u>Ph), 69.1/ 68.7/ 68.7 (C<u>H</u>$_2$-CHPh), 67.4 (C<u>H</u>Ph), 61.7/ 61.5/ 61.4 (C_{6Glu})

MS (ESI) *m/z* 573.3 $[L + H]^+$; 595.3 $[L + Na]^+$

Elemental Analysis found (Calculated for $C_{93}H_{96}Cl_4N_{12}O_{37}Zn_2 \cdot 10H_2O$) % C 46.05 (46.03), H 4.17 (4.82), N 6.96 (6.93).

R_c,Δ_{Zn},HHT-[$Zn_2L^{7a}_3$][ClO_4]$_4$

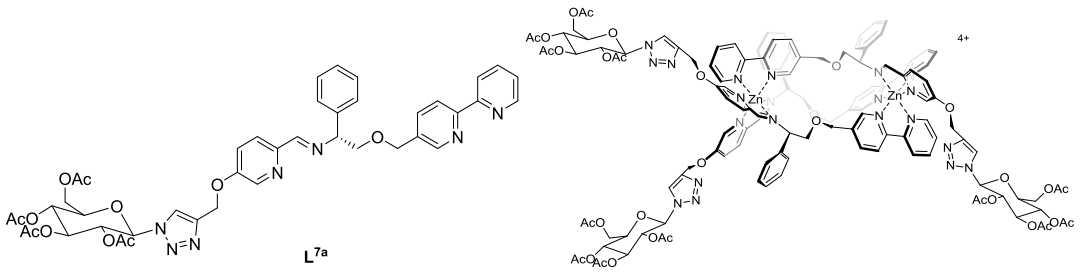

R_c, Δ_{Zn},HHT-[$Zn_2L^{7a}_3$][ClO_4]$_4$ was synthesised using the procedure described for S_c,Λ_{Zn},HHT-[$Zn_2L^{3}_3$][ClO_4]$_4$, substituting 5-(propargyloxy)picolinaldehyde (**5**) for

(*2R,3R,4S,5R,6R*)-2-(acetoxymethyl)-6-(4-formyl-1H-1,2,3-triazol-1-yl)tetrahydro-2H-pyran-3,4,5-triyl triacetate (**46**)

Yield 0.21 g, 83%

^{1}H NMR (500 MHz, 298 K, CD_3CN) δ_H ppm 9.22 (1H, s, HC=N), 9.18 (1H, s, bpy), 9.12 (2H, s, bpy overlapping with HC=N), 8.75 (1H, s, HC=N), 8.49 (1H, t, $^{3}J_{HH}$ = 9.0 Hz, bpy), 8.35 (1H, s, bpy), 8.24 (1H, d, $^{3}J_{HH}$ = 8.7 Hz, py), 8.22-8.15 (5H, m, bpy overlapping with TRZ), 8.10 (1H, s, TRZ), 8.07-7.73 (19H, m, bpy overlapping with TRZ and py), 7.61-7.42 (7H, m, bpy overlapping with py), 7.40 (1H, d, $^{3}J_{HH}$ = 8.6 Hz, py), 7.30 (1H, d, $^{4}J_{HH}$ = 2.5 Hz, py), 7.06 (1H, t, $^{3}J_{HH}$ = 7.4 Hz, Ph), 6.99 (2H, t, $^{3}J_{HH}$ = 7.4 Hz, Ph), 6.93 (2H, t, $^{3}J_{HH}$ = 7.4 Hz, Ph), 6.88 (1H, t, $^{3}J_{HH}$ = 7.4 Hz, Ph), 6.83 (2H, d, $^{3}J_{HH}$ = 7.5 Hz, Ph), 6.68 (2H, t, $^{3}J_{HH}$ = 7.7 Hz, Ph), 6.54 (2H, t, $^{3}J_{HH}$ = 7.6 Hz, Ph), 6.06 (2H, d, $^{3}J_{HH}$ = 7.4 Hz, Ph), 6.09-5.92 (7H, m, Ph overlapping with H_{glu}), 5.75 (1H, t, $^{3}J_{HH}$ = 9.5 Hz, H_{glu}), 5.65-5.08 (28H, m, H_{glu} overlapping with C<u>H</u>Ph and C<u>H</u>$_2$-bpy), 4.92 (1H, d, $^{3}J_{HH}$ = 10.9 Hz, C<u>H</u>Ph), 4.79 (1H, d, $^{3}J_{HH}$ = 7.4 Hz, C<u>H</u>Ph), 4.50 (2H, d, $^{2}J_{HH}$ = 12.9 Hz, C<u>H</u>$_2$-bpy), 4.44 (1H, d, $^{2}J_{HH}$ = 12.9 Hz, C<u>H</u>$_2$-bpy), 4.31-4.00 (20H, m, H_{glu} overlapping with C<u>H</u>$_2$-CHPh), 3.56 (1H, dd, $^{2}J_{HH}$ = 11.0 Hz, $^{3}J_{HH}$ = 3.0 Hz, C<u>H</u>$_2$-CHPh), 3.51 (1H, dd, $^{2}J_{HH}$ = 11.0 Hz, $^{3}J_{HH}$ = 3.0 Hz, C<u>H</u>$_2$-CHPh), 3.43 (1H, dd, $^{2}J_{HH}$ = 11.0 Hz, $^{3}J_{HH}$ = 3.0 Hz, C<u>H</u>$_2$-CHPh), 2.05-1.65 (36H, m, 12 × $COCH_3$).

^{13}C {^{1}H} NMR (125 MHz, 298 K, CD_3CN) δ_C ppm 170.6, 170.3, 170.2, 170.1, 169.3, 169.3, 169.2 (12 × CO), 163.1, 162.2, 162.2 (HC=N), 159.2, 159.0, 158.3 (q, py), 150.6, 150.4, 149.7 (bpy), 149.5, 149.3, 149.1 (q, bpy), 148.6 (bpy), 148.5 (q, bpy), 148.2 (bpy), 148.0 (q, bpy), 143.4, 143.3, 142.9 (bpy), 142.8, 142.7, 142.5 (q, TRZ), 142.2, 141.8, 141.6 (bpy), 140.4, 140.3, 140.2 (q, py), 138.9, 138.4, 138.3 (py), 137.7, 137.4, 137.1 (q, bpy), 135.1, 134.3, 133.8 (q, Ph), 132.3, 132.3, 131.2 (py), 129.2,

129.1, 129.0, 128.8 (Ph), 127.7, 127.6, 127.3 (bpy), 127.2, 126.5, 126.4 (Ph), 126.0, 125.3, 124.9 (py), 124.8, 124.3, 124. 3, 124.2, 123.9, 123.7 (bpy), 123.6, 123.0 (TRZ), 85.3, 85.2 (C_{1Glu}), 74.9, 74.8 (C_{5Glu}), 72.8, 72.6 (C_{3Glu}), 70.5, 70.4 (C_{2Glu}), 70.1, 70.0 ($\underline{C}H_2$-bpy), 69.4 ($\underline{C}$HPh), 69.3 ($\underline{C}H_2$-CHPh), 69.2 ($\underline{C}$HPh), 69.0, 68.9 ($\underline{C}H_2$-CHPh), 68.1, 68.0, 68.0 (C_{4Glu}), 67.4 ($\underline{C}$HPh), 62.4, 62.2, 62.1 (TRZ-$\underline{C}H_2$), 61.9, 61.9 (C_{6Glu}), 20.1, 20.3, 20.2, 12.0, 19.9, 19.8

(12 × CH_3).

R_c,Δ_{Zn},HHT-[$Zn_2L^{8a}{}_3$][ClO_4]$_4$

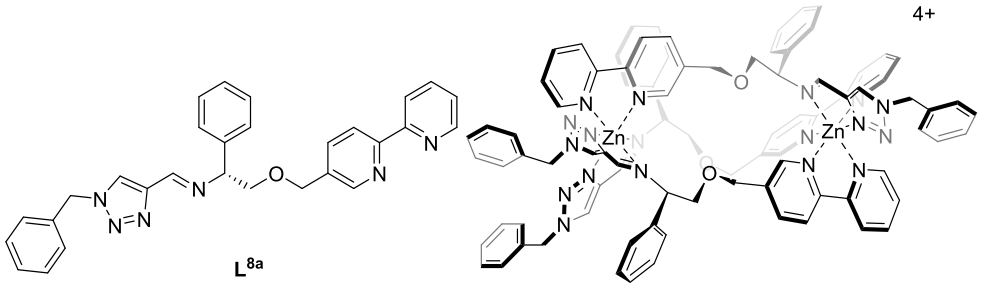

R_c,Δ_{Zn},HHT-[$Zn_2L^{8a}{}_3$][ClO_4]$_4$ was synthesised using the procedure described for S_c,Λ_{Zn},HHT-[$Zn_2L^{3}{}_3$][ClO_4]$_4$, substituting 5-(propargyloxy)picolinaldehyde (**5**) for 1-benzyl-1H-1,2,3-triazole-4-carbaldehyde (**37**)

Yield 0.29 g, 90%

^{1}H NMR (500 MHz, 298 K, CD_3CN) δ_H ppm 9.21 (1H, s, HC=N), 9.17 (2H, s, HC=N/bpy), 9.14 (1H, s, bpy), 8.83 (1H, s, HC=N), 8.60 (1H, s, TRZ), 8.54 (1H, s, TRZ), 8.48 (1H, s, bpy), 8.45 (2H, d, $^3J_{HH}$ =8.2 Hz, bpy), 8.42 (2H, d, $^3J_{HH}$ =8.3 Hz, bpy), 8.24-7.77 (15H, m, bpy/TRZ), 7.66-7.28 (17H, m, bpy/Ph), 7.22-6.94 (10H, m, bpy/Ph), 6.89 (2H, t, $^3J_{HH}$ =7.4 Hz, Ph), 6.74 (2H, t, $^3J_{HH}$ =7.7 Hz, Ph), 6.56 (2H, t, $^3J_{HH}$ =7.7 Hz, Ph), 6.11 (2H, d, $^3J_{HH}$ =7.5 Hz, Ph), 5.98 (2H, d, $^3J_{HH}$ =7.5 Hz, Ph), 5.61-

5.46 (6H, m, PhC$\underline{H}_2$), 5.43 (1H, dd, $^3J_{HH}$ = 11.4 Hz $^4J_{HH}$ = 3.2, C$\underline{H}$Ph), 5.26-5.10 (3H, m, C$\underline{H}_2$-bpy), 4.88 (1H, d, $^3J_{HH}$ =9.0 Hz, C$\underline{H}$Ph), 4.79 (1H, d, $^3J_{HH}$ =8.2 Hz, C$\underline{H}$Ph), 4.54-4.43 (3H, m, C$\underline{H}_2$-bpy), 4.18 (1H, t, J_{HH} =11.2 Hz, C$\underline{H}_2$-CHPh), 4.09 (1H, t, J_{HH} =10.8 Hz, C$\underline{H}_2$-CHPh), 4.03 (1H, t, J_{HH} =10.9 Hz, C$\underline{H}_2$-CHPh), 3.66 (1H, dd, $^2J_{HH}$ = 10.4 Hz $^3J_{HH}$ = 3.5, C$\underline{H}_2$-CHPh), 3.53 (1H, dd, $^2J_{HH}$ = 11.2 Hz $^3J_{HH}$ = 3.1, C$\underline{H}_2$-CHPh), 3.47 (1H, dd, $^2J_{HH}$ = 11.2 Hz $^3J_{HH}$ = 3.4, C$\underline{H}_2$-CHPh).

^{13}C {^1H} NMR (125 MHz, 298 K, CD_3CN) δ_C ppm 157.1, 156.6, 156.1 (HC=N), 150.4, 150.2, 149.9 (bpy), 149.4, 149.3, 149.0, 148.7, 148.5 (q, bpy), 148.1 (bpy), 147.6 (q, bpy), 147.5 (bpy), 143.6, 143.0, 142.9, 142.1, 142.1 (bpy), 141.9, 141.8 (q, TRZ), 141.6 (bpy), 141.5 (q, TRZ), 138.0, 137.5, 137.4 (q, bpy), 135.0, 134.5, 134.4, 134.0, 133.8, 133.7 (q, Ph), 130.1, 129.7, 129.7, 129.5, 129.5, 129.5, 129.3, 129.1, 129.0, 128.8, 128.5, 128.4, 128.2 (Ph/TRZ), 127.8, 127.4, 127.3 (bpy), 127.2, 126.5, 126.4 (Ph), 123.6, 123.2, 123.1, 123.1, 122.7 (bpy), 70.0, 69.9 (C$\underline{H}_2$-bpy), 69.7 (C$\underline{H}$Ph), 69.5 (C$\underline{H}$Ph), 69.1 (C$\underline{H}_2$-bpy), 69.0, 68.9 (C$\underline{H}_2$-CHPh), 67.8 (C$\underline{H}$Ph), 55.5, 55.3, 55.1 (PhC$\underline{H}_2$).

Elemental Analysis found (Calculated for $C_{87}H_{78}Cl_4N_{18}O_{19}Zn_2 \cdot 4H_2O$) % C 51.61 (51.62), H 4.04 (4.28), N 12.39 (12.45).

ESI-MS (+) *m/z* 475.4 $[L+H]^+$, 497.3 $[L+Na]^+$

IR *v* cm^{-1} 1603 (w), 1440 (w), 1224 (w), 1069 (s), 843 (m), 791 (m), 722 (m), 700 (m), 620 (s).

R_c,Δ_{Zn},HHT-$[Zn_2L^{8b}{}_3][ClO_4]_4$

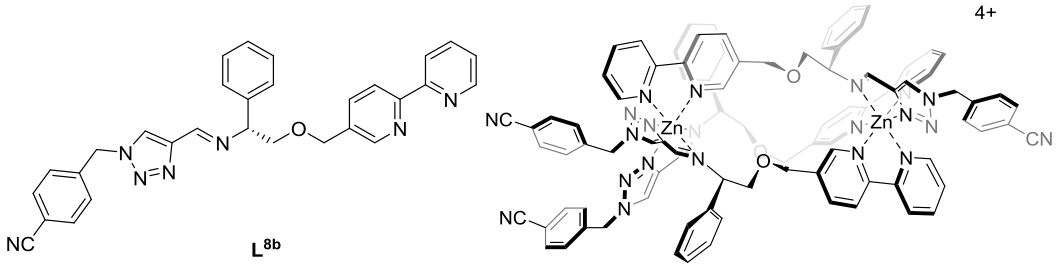

R_c,Δ_{Zn},HHT-$[Zn_2L^{8b}{}_3][ClO_4]_4$ was synthesised using the procedure described for S_c,Λ_{Zn},HHT-$[Zn_2L^{3}{}_3][ClO_4]_4$, substituting 5-(propargyloxy)picolinaldehyde (**5**) for 4-((4-formyl-1H-1,2,3-triazol-1-yl)methyl)benzonitrile (**39**)

Yield 0.28 g, 83%

^{1}H NMR (500 MHz, 298 K, CD_3CN) δ_H ppm 9.24 (1H, s, HC=N), 9.21 (1H, s, HC=N), 9.18 (1H, s, bpy), 9.14 (1H, s, bpy), 8.89 (1H, s, HC=N), 8.68 (1H, s, TRZ), 8.61 (1H, s, TRZ), 8.49 (1H, s, bpy), 8.44 (2H, d, $^3J_{HH}$ =8.5 Hz, bpy), 8.42 (2H, d, $^3J_{HH}$ =8.5 Hz, bpy) 8.24-6.98 (37H, m, Ph/bpy/TRZ), 6.89 (2H, t, $^3J_{HH}$ =7.4 Hz, Ph), 6.75 (2H, t, $^3J_{HH}$ =7.7 Hz, Ph), 6.56 (2H, t, $^3J_{HH}$ =7.7 Hz, Ph), 6.12 (2H, d, $^3J_{HH}$ =7.6 Hz, Ph), 6.00 (2H, d, $^3J_{HH}$ =7.6 Hz, Ph), 5.72-5.55 (6H, m, CNPhC$\underline{H}_2$), 5.44 (1H, dd, $^3J_{HH}$ = 11.3 Hz $^4J_{HH}$ = 3.2, C$\underline{H}$Ph), 5.27-5.11 (3H, m, C$\underline{H}_2$-bpy), 4.90 (1H, d, $^3J_{HH}$ =9.2 Hz, C$\underline{H}$Ph), 4.81 (1H, d, $^3J_{HH}$ =8.2 Hz, C$\underline{H}$Ph), 4.57-4.45 (3H, m, C$\underline{H}_2$-bpy), 4.20 (1H, t, J_{HH} =11.2 Hz, C$\underline{H}_2$-CHPh), 4.11 (1H, t, J_{HH} =10.8 Hz, C$\underline{H}_2$-CHPh), 4.06 (1H, t, J_{HH} =10.9 Hz, C$\underline{H}_2$-CHPh), 3.68 (1H, dd, $^2J_{HH}$ = 10.4 Hz $^3J_{HH}$ = 3.5, C$\underline{H}_2$-CHPh), 3.54 (1H, dd, $^2J_{HH}$ = 11.2 Hz $^3J_{HH}$ = 3.0, C$\underline{H}_2$-CHPh), 3.49 (1H, dd, $^2J_{HH}$ = 11.3 Hz $^3J_{HH}$ = 3.4, C$\underline{H}_2$-CHPh).

^{13}C {^{1}H} NMR (125 MHz, 298 K, CD_3CN) δ_C ppm 157.2, 156.6, 156.2 (HC=N), 150.4, 150.3, 149.9 (bpy), 149.3, 149.3, 149.0, 148.6, 148.5 (q, bpy), 148.1, 147.5 (bpy), 147.5 (q, bpy), 143.6, 143.1, 143.0, 142.1, 142.1 (bpy), 142.0, 142.0 (q, TRZ), 141.6 (bpy), 141.6 (q, TRZ), 139.6, 138.9, 138.1 (q, CN$\underline{Ph}$), 137.5, 137.5, 133.9 (q, bpy),

133.8, 133.5, 133.3, 133.2 (q, Ph), 129.9, 129.2, 129.0 (CN<u>Ph</u>), 128.9, 128.9, 128.7 (Ph, TRZ), 127.9, 127.7, 127.4 (bpy), 127.3, 126.5, 126.5 (Ph), 123.6, 123.2, 123.1, 123.0, 122.6 (bpy), 118.6, 118.6, 118.5 (q, CN<u>Ph</u>), 113.1, 112.8, 112.7 (CN), 70.0, 70.0 (<u>C</u>H$_2$-bpy), 69.8, 69.5 (<u>C</u>HPh), 69.0 (<u>C</u>H$_2$-bpy), 69.0, 68.9 (<u>C</u>H$_2$-CHPh), 67.8 (<u>C</u>HPh), 54.7, 54.5, 54.3 (CNPh-<u>C</u>H$_2$).

Elemental Analysis found (Calculated for $C_{90}H_{75}Cl_4N_{18}O_{19}Zn_2 \cdot 8H_2O$) % C 49.36 (49.78), H 3.81 (4.22), N 12.36 (13.55).

ESI-MS (+) *m/z* 500.3 $[L+H]^+$, 522.3 $[L+Na]^+$

IR *v* cm^{-1} 1602 (w), 1475 (w), 1440 (w), 1073 (s), 792 (m), 752 (m), 700 (m), 620 (s), 546 (m).

R$_c$,Δ$_{Zn}$,HHT-$[Zn_2L^{8c}{}_3][ClO_4]_4$

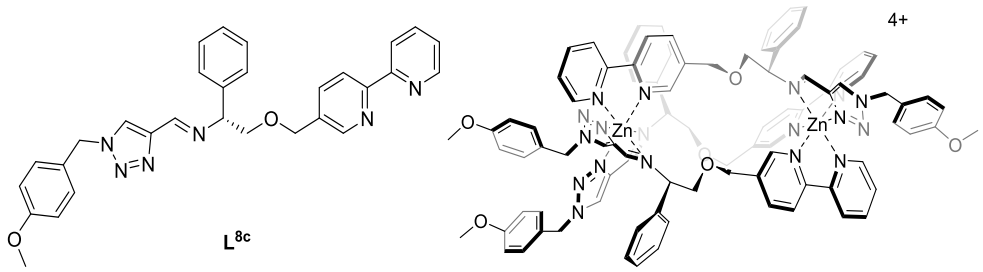

R$_c$,Δ$_{Zn}$,HHT-$[Zn_2L^{8c}{}_3][ClO_4]_4$ was synthesised using the procedure described for *S*$_c$,Λ$_{Zn}$,HHT-$[Zn_2L^3{}_3][ClO_4]_4$, substituting 5-(propargyloxy)picolinaldehyde (**5**) for 1-(4-methoxybenzyl)-1H-1,2,3-triazole-4-carbaldehyde (**40**)

Yield 0.30 g, 88%

^{1}H NMR (500 MHz, 298 K, CD_3CN) δ_H ppm 9.20 (1H, s, HC=N), 9.17 (1H, s, HC=N), 9.16 (1H, s, bpy), 9.13 (1H, s, HC=N), 8.81 (1H, s, bpy), 8.59-6.85 (55H, m, Ph/bpy/TRZ), 6.74 (2H, t, $^3J_{HH}$ =7.7 Hz, Ph), 6.56 (2H, t, $^3J_{HH}$ =7.7 Hz, Ph), 6.10 (2H,

d, $^{3}J_{HH}$ =7.6 Hz, Ph), 5.97 (2H, d, $^{3}J_{HH}$ =7.6 Hz, Ph), 5.58-5.38 (7H, m, PhCH_2 overlapping with C<u>H</u>Ph), 5.23-5.02 (3H, m, C<u>H</u>$_2$-bpy), 4.88 (1H, d, $^{3}J_{HH}$ = 9.1 Hz C<u>H</u>Ph), 4.78 (1H, d, $^{3}J_{HH}$ =7.9 Hz, C<u>H</u>Ph), 4.56-4.41 (3H, m, C<u>H</u>$_2$-bpy), 4.18 (1H, t, $^{3}J_{HH}$ =11.2 Hz, C<u>H</u>$_2$-CHPh), 4.08 (1H, t, $^{3}J_{HH}$ =10.8 Hz, C<u>H</u>$_2$-CHPh), 4.04 (1H, t, $^{3}J_{HH}$ =10.9 Hz, C<u>H</u>$_2$-CHPh), 3.87 (3H, s, OCH_3), 3.85 (3H, s, OCH_3), 3.79 (3H, s, OCH_3), 3.66 (1H, dd, $^{2}J_{HH}$ = 10.4 Hz $^{3}J_{HH}$ = 3.5, C<u>H</u>$_2$-CHPh), 3.52 (1H, dd, $^{2}J_{HH}$ = 11.1 Hz $^{3}J_{HH}$ = 3.0, C<u>H</u>$_2$-CHPh), 3.46 (1H, dd, $^{2}J_{HH}$ = 11.2 Hz $^{3}J_{HH}$ = 3.4, C<u>H</u>$_2$-CHPh).

^{13}C {^{1}H} NMR (125 MHz, 298 K, CD_3CN) δ_C ppm 160.9, 160.6, 160.5 (q, <u>Ph</u>OCH_3), 157.1, 156.6, 156.0 (HC=N), 150.4, 150.2, 149.9 (bpy), 149.4, 149.2, 149.1, 148.7, 148.5 (q, bpy), 148.1, 148.1 (bpy), 147.6 (q, bpy), 147.5 (bpy), 143.6, 143.0, 142.9, 142.3, 142.1, 142.0 (bpy), 141.9, 141.7 (q, TRZ), 141.6 (bpy), 141.5 (q, TRZ), 137.9, 137.5, 137.4 (q, bpy), 135.0, 134.0, 133.8 (q, Ph), 131.2, 130.3, 130.2, 130.1 (<u>Ph</u>OCH_3), 129.8, 129.4, 129.2, 129.1, 129.0, 128.9, 128.8, 128.2 (Ph/TRZ), 127.8, 127.4, 127.3 (bpy), 127.2, 126.5, 126.4 (Ph), 126.3, 126.2, 125.5 (q, <u>Ph</u>OCH_3), 123.6, 123.3, 123.1, 123.1, 122.7 (bpy), 114.9, 114.8, 114.7 (<u>Ph</u>OCH_3), 70.0, 69.9 (<u>C</u>H$_2$-bpy), 69.7 (<u>C</u>HPh), 69.4 (<u>C</u>HPh), 69.1 (<u>C</u>H$_2$-bpy), 69.0, 68.9, 68.9 (<u>C</u>H$_2$-CHPh), 67.7 (<u>C</u>HPh), 55.6, 55.5, 55.5 (OCH_3), 55.0, 54.9, 54.7 (Anisole-<u>C</u>H$_2$).

Elemental Analysis found (Calculated for $C_{90}H_{84}Cl_4N_{18}O_{22}Zn_2 \cdot 8H_2O$) % C 49.09 (49.44), H 3.82 (4.61), N 10.87 (11.53).

ESI-MS (+) *m/z* 505.3 $[L+H]^+$, 527.3 $[L+Na]^+$

IR *v* cm^{-1} 1604 (w), 1513 (w), 1440 (w), 1249 (w), 1070 (s), 791 (w), 750 (m), 700 (m), 620 (s).

R_c,Δ_{Zn},HHT-$[Zn_2L^{8d}{}_3][ClO_4]_4$

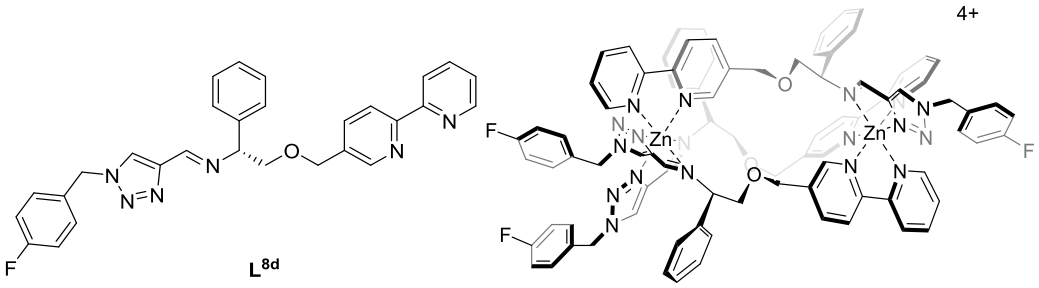

R_c,Δ_{Zn},HHT-$[Zn_2L^{8d}{}_3][ClO_4]_4$ was synthesised using the procedure described for S_c,Λ_{Zn},HHT-$[Zn_2L^{3}{}_3][ClO_4]_4$, substituting 5-(propargyloxy)picolinaldehyde (**5**) for 1-(4-fluorobenzyl)-1H-1,2,3-triazole-4-carbaldehyde (**38**)

Yield 0.31 g, 92%

^{1}H NMR (500 MHz, 298 K, CD_3CN) δ_H ppm 9.22 (1H, s, HC=N), 9.18 (1H, s, HC=N), 9.17 (1H, s, bpy), 9.13 (1H, s, bpy), 8.85 (1H, s, HC=N), 8.68 (1H, s, TRZ), 8.61 (1H, s, TRZ), 8.54 (1H, s, bpy), 8.50-6.98 (36H, m, Ph/bpy/TRZ), 6.89 (1H, t, $^3J_{HH}$ =7.4 Hz, Ph), 6.74 (2H, t, $^3J_{HH}$ =7.7 Hz, Ph), 6.56 (2H, t, $^3J_{HH}$ =7.7 Hz, Ph), 6.11 (2H, d, $^3J_{HH}$ =7.6 Hz, Ph), 5.98 (2H, d, $^3J_{HH}$ =7.6 Hz, Ph), 5.63-5.40 (7H, m, F-PhC<u>H</u>$_2$ overlapping with C<u>H</u>Ph), 5.26-5.12 (3H, m, C<u>H</u>$_2$-bpy), 4.88 (1H, d, $^3J_{HH}$ =9.1 Hz, C<u>H</u>Ph), 4.79 (1H, d, $^3J_{HH}$ =8.1 Hz, C<u>H</u>Ph), 4.56-4.43 (3H, m, C<u>H</u>$_2$-bpy), 4.19 (1H, t, $^3J_{HH}$ =11.2 Hz, C<u>H</u>$_2$-CHPh), 4.10 (1H, t, $^3J_{HH}$ =10.8 Hz, C<u>H</u>$_2$-CHPh), 4.04 (1H, t, $^3J_{HH}$ =10.9 Hz, C<u>H</u>$_2$-CHPh), 3.67 (1H, dd, $^2J_{HH}$ = 10.4 Hz $^3J_{HH}$ = 3.5, C<u>H</u>$_2$-CHPh), 3.53 (1H, dd, $^2J_{HH}$ = 11.2 Hz $^3J_{HH}$ = 3.1, C<u>H</u>$_2$-CHPh), 3.47 (1H, dd, $^2J_{HH}$ = 11.2 Hz $^3J_{HH}$ = 3.4, C<u>H</u>$_2$-CHPh).

^{13}C {^{1}H} NMR (125 MHz, 298 K, CD_3CN) δ_C ppm 164.5, 164.2, 164.1, 162.5, 162.3, 162.2 (q, F-<u>Ph</u>), 157.2, 156.6, 156.1 (HC=N), 150.4, 150.2, 149.9 (bpy), 149.3, 149.3, 149.0, 148.6, 148.5 (q, bpy), 148.1 (bpy), 147.6 (q, bpy), 147.5 (bpy), 143.6, 143.0,

142.9, 142.1, 142.1 (bpy), 141.9, 141.8 (q, TRZ), 141.6 (bpy), 141.5 (q, TRZ), 138.0, 137.5, 137.4 (q, bpy), 135.0, 134.0, 133.8 (q, Ph), 131.8, 131.8, 130.8, 130.7, 130.7 (F-Ph), 130.5, 130.5 (q, F-Ph), 130.1 (TRZ), 129.9 (q, F-Ph), 129.7 (TRZ), 129.3, 129.1, 129.0, 128.9, 128.8 (Ph), 128.5 (TRZ), 127.8, 127.4, 127.3 (bpy), 127.2, 126.5, 126.4 (Ph), 123.6, 123.2, 123.1, 123.1, 122.6 (bpy), 116.5, 116.3, 116.3, 116.3, 116.2, 116.1 (F-Ph), 70.0, 70.0 ($\underline{C}H_2$-bpy), 69.7 (CHPh), 69. 5 (CHPh), 69.1 ($\underline{C}H_2$-bpy), 69.0, 68.9 ($\underline{C}H_2$-CHPh), 67.8 (CHPh), 54.6, 54.5, 54.3 (PhF-*C*H_2).

Elemental Analysis found (Calculated for $C_{87}H_{75}Cl_4F_3N_{18}O_{19}Zn_2 \cdot 6H_2O$) % C 49.52 (49.42), H 3.61 (4.15), N 11.58 (11.92).

ESI-MS (+) *m/z* 493.3 $[L+H]^+$, 515.3 $[L+Na]^+$

IR ν cm^{-1} 1603 (w), 1510 (w), 1475 (w), 1440 (w), 1224 (w), 1071 (s), 841 (m), 791 (m), 750 (m), 700 (m), 620 (s).

S_c,Λ_{Zn},HHT-$[Zn_2L^{9a}{}_3][ClO_4]_4$.

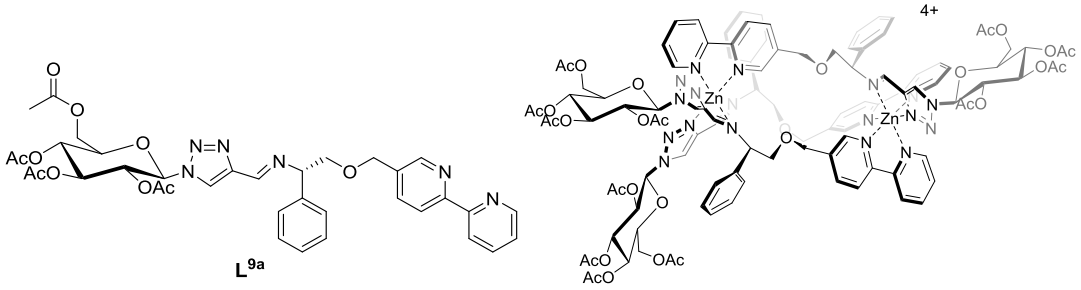

S_c,Λ_{Zn},HHT-$[Zn_2L^{9a}{}_3][ClO_4]_4$ was synthesised using the procedure described for S_c,Λ_{Zn},HHT-$[Zn_2L^{3}{}_3][ClO_4]_4$, substituting 5-(propargyloxy)picolinaldehyde (**5**) for (*2R,3R,4S,5R,6R*)-2-(acetoxymethyl)-6-(4-formyl-1H-1,2,3-triazol-1-yl)tetrahydro-2H-pyran-3,4,5-triyl triacetate (**46**)

Yield: 28 mg, 45%.

^{1}H NMR (500 MHz, 298 K, MeCN) δ_H ppm 9.30 (1H, s, CHN), 9.25 (1H, s, CHN), 9.19 (1H, s, bpy), 9.12 (1H, s, bpy), 8.85 (1H, s, CHN), 8.84 (1H, s, TRZ), 8.77 (1H, s, TRZ), 8.53 (3H, t, $^{3}J_{HH}$ =10.0 Hz, bpy), 8.45 (1H, s, bpy), 8.25 (3H, t, $^{3}J_{HH}$ =7.9 Hz, bpy), 8.14-7.94 (9H, m, bpy/TRZ), 7.87 (2H, d, $^{3}J_{HH}$ =8.1 Hz, bpy), 7.81 (2H, t, $^{3}J_{HH}$ =10.0 Hz, bpy), 7.62 (1H, dd, $^{3}J_{HH}$ = 7.2 Hz, $^{4}J_{HH}$ = 5.5, bpy), 7.54 (2H, dd, $^{3}J_{HH}$ = 12.6 Hz, $^{4}J_{HH}$ = 5.3, bpy), 7.31-7.21 (4H, m, bpy/Ph), 7.05 (1H, t, $^{3}J_{HH}$ = 7.4 Hz, Ph), 6.97 (2H, d, $^{3}J_{HH}$ = 7.4 Hz, Ph), 6.91 (1H, t, $^{3}J_{HH}$ = 7.5 Hz, Ph), 6.74 (2H, t, $^{3}J_{HH}$ = 7.7 Hz, Ph), 6.57 (2H, t, $^{3}J_{HH}$ = 7.7 Hz, Ph), 6.11 (2H, d, $^{3}J_{HH}$ = 7.6 Hz, Ph), 6.02-5.95 (4H, m, Ph overlapping with H_{glu}), 5.89 (1H, d, $^{3}J_{HH}$ = 8.7 Hz, H_{glu}), 5.58 (1H, t, $^{3}J_{HH}$ = 9.6 Hz, H_{glu}), 5.50 (1H, t, $^{3}J_{HH}$ = 9.6 Hz, H_{glu}), 5.45-5.11 (12H, m, H_{glu} overlapping with C<u>H</u>Ph/ OC<u>H</u>$_2$-bpy), 4.92 (1H, d, $^{3}J_{HH}$ = 11.2 Hz, C<u>H</u>Ph), 4.80 (1H, d, $^{3}J_{HH}$ = 8.5 Hz, C<u>H</u>Ph), 4.57-4.44 (4H, m, H_{glu} overlapping with OC<u>H</u>$_2$-bpy), 4.36-4.31 (2H, m, H_{glu}), 4.26-4.17 (6H, m, C<u>H</u>$_2$-CHPh overlapping with H_{glu}), 4.15-4.05 (5H, m, C<u>H</u>$_2$-CHPh overlapping with H_{glu}), 3.73 (1H, dd, $^{2}J_{HH}$ = 10.4 Hz $^{3}J_{HH}$ = 3.4, C<u>H</u>$_2$-CHPh), 3.53 (1H, dd, $^{2}J_{HH}$ = 11.2 Hz $^{3}J_{HH}$ = 2.8, C<u>H</u>$_2$-CHPh), 3.48 (1H, dd, $^{2}J_{HH}$ = 11.2 Hz $^{3}J_{HH}$ = 3.2, C<u>H</u>$_2$-CHPh), 2.16-1.50 (36H, m, 12 × COC<u>H</u>$_3$).

^{13}C {^{1}H} NMR (126 MHz, 298 K, CD_3CN) δ_C ppm 170.8, 170.6, 170.6, 170.2, 170.1, 170.1, 167.0, 169.9, 169.5, 168.5 (12 × CO), 157.3, 156.6, 156.0 (CHN), 150.5, 150.4, 149.9 (bpy), 149.4, 149.3, 149.0, 148.7, 148.6 (q, bpy), 148.0 (bpy), 147.8 (q, bpy), 147.7, 146.6, 143.7, 143.2, 143.2, 142.2 (bpy), 142.0, 141.9 (q, TRZ), 141.7 (bpy), 141.3 (q, TRZ), 138.0, 137.5 (q, bpy), 134.5, 133.7, 133.6 (q, Ph), 129.4, 129.3, 129.2, 129.1, 128.9 (Ph/TRZ), 127.8, 127.5, 127.3 (bpy), 127.0, 126.5, 126.4 (Ph), 123.8, 123.5, 123.5, 123.4, 123.2, 123.0 (bpy), 86.7, 86.4, 85.9 (C_{1Glu}), 75.3, 75.3, 75.2 (C_{5Glu}), 72.3, 72.1, 71.8 (C_{3Glu}), 71.6, 71.0, 70.1 (C_{2Glu}), 70.0, 70.0 (<u>C</u>H$_2$-bpy), 69.7,

69.7 (CHPh), 69.1, 68.9, 68.7 (CH_2-CHPh), 68.2 (CHPh), 67.7, 67.6, 67.6 (C_{4Glu}), 62.2, 61.7, 61.6 (C_{6Glu}), 20.5, 20.3, 20.3, 20.2, 20.2, 20.1, 19.7 (12 × CH_3).

MS (ESI) *m/z* 715.4 $[L + H]^+$

IR v cm^{-1} 1745 s, 1369 m, 1221 s, 1064 m, 925 w, 752 s

Elemental Analysis found (Calculated for $C_{108}H_{114}Cl_4N_{18}O_{46}Zn_2 \cdot 6H_2O$) % C 46.60 (46.65), H 4.12 (4.57), N 8.79 (9.07).

S_c,Λ_{Zn},HHT-$[Zn_2L^{9b}{}_3][ClO_4]_4$.

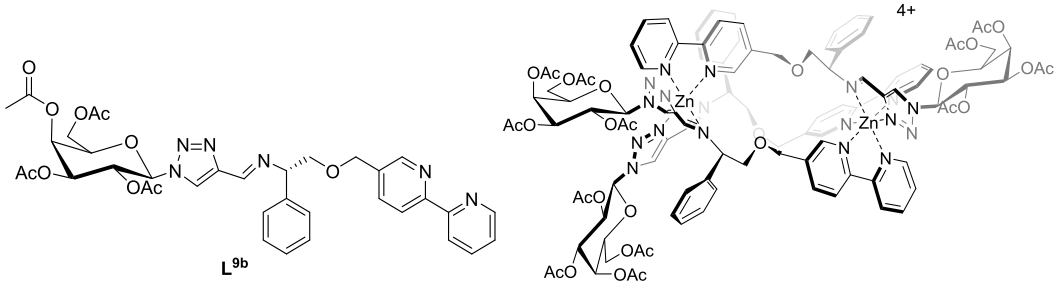

S_c,Λ_{Zn},HHT-$[Zn_2L^{9b}{}_3][ClO_4]_4$ was synthesised using the procedure described for S_c,Λ_{Zn},HHT-$[Zn_2L^{3}{}_3][ClO_4]_4$, substituting 5-(propargyloxy)picolinaldehyde (**5**) for (*2R,3S,4S,5R,6R*)-2-(acetoxymethyl)-6-(4-formyl-1H-1,2,3-triazol-1-yl)tetrahydro-2H-pyran-3,4,5-triyl triacetate (**47**)

Yield: 45 mg, 54 %.

^{1}H NMR (500 MHz, 298 K, CD_3CN) δ_H ppm 9.33 (1H, s, HC=N), 9.27 (1H, s, HC=N), 9.23 (1H, s, bpy), 9.16 (1H, s, bpy), 8.91 (1H, s, TRZ), 8.87 (1H, s, TRZ), 8.83 (1H, s, HC=N), 8.56 (2H, m, bpy), 8.41 (1H, s, bpy), 8.27 (3H, m, bpy), 8.11 (2H, d, $^3J_{HH}$ = 8.5 Hz, bpy), 8.06 (2H, m, bpy), 7.99 (3H, m, bpy), 7.84 (3H, dd, $^2J_{HH}$ = 12.0, $^3J_{HH}$ = 7.5 Hz, bpy), 7.63 (1H, m, bpy), 7.55 (2H, m, bpy), 7.36 (1H, t, $^3J_{HH}$ = 7.5 Hz, Ph), 7.28 (2H, t, $^3J_{HH}$ = 7.5 Hz, Ph), 7.06 (1H, t, $^3J_{HH}$ = 7.5 Hz, Ph), 7.01 (2H, d, $^3J_{HH}$ = 7.5

Hz, Ph), 6.94 (1H, t, $^{3}J_{HH}$ = 7.5 Hz, Ph), 6.74 (2H, t, $^{3}J_{HH}$ = 7.5, Ph), 6.59 (2H, t, $^{3}J_{HH}$ = 7.5 Hz, Ph), 6.11 (2H, d, $^{3}J_{HH}$ = 7.5 Hz, Ph), 6.03 (1H, d, $^{3}J_{HH}$ = 9.0 Hz, H_{gal}), 5.98 (2H, d, $^{3}J_{HH}$ = 7.5 Hz, Ph), 5.91 (2H, m, H_{gal}), 5.61 (2H, m, H_{gal}), 5.52 (1H, d, $^{3}J_{HH}$ = 3.0 Hz, H_{gal}), 5.46 (3H, m, H_{glu} overlapping with C<u>H</u>Ph), 5.36 (2H, m, H_{gal}), 5.22 (4H, m, H_{glu} overlapping with C<u>H</u>$_2$-bpy), 4.92 (1H, d, $^{3}J_{HH}$ = 9.5 Hz, C<u>H</u>Ph), 4.77 (1H, d, $^{3}J_{HH}$ = 8.5 Hz, C<u>H</u>Ph), 4.63-4.29 (8H, m, H_{glu} overlapping with C<u>H</u>$_2$-bpy), 4.25 (1H, t, $^{3}J_{HH}$ = 11.0 Hz, C<u>H</u>$_2$-CHPh), 4.18-4.06 (6H, m, H_{glu} overlapping with C<u>H</u>$_2$-CHPh), 3.76 (1H, dd, $^{2}J_{HH}$ = 10.0 Hz, $^{3}J_{HH}$ = 3.0 Hz, C<u>H</u>$_2$-CHPh), 3.56 (1H, dd, $^{2}J_{HH}$ = 11.0 Hz, $^{3}J_{HH}$ = 3.0 Hz, C<u>H</u>$_2$-CHPh), 3.49 (1H, dd, $^{2}J_{HH}$ = 11.0 Hz, $^{3}J_{HH}$ = 3.0 Hz, C<u>H</u>$_2$-CHPh), 2.19-1.78 (36H, s, 12 x CH_3)

^{13}C NMR (125 MHz, 298 K, CD_3CN) δ_c ppm 170.6, 170.5, 170.4, 170.0, 169.9, 169.8, 169.5, 168.9 (12 x C=O), 157.3, 156.6, 156.2 (HC=N), 150.7, 150.3, 149.8 (bpy), 149.4, 149.3, 148.9, 148.7, 145.5 (q, bpy), 148.2, 147.6 (bpy), 147.4 (q, bpy), 143.6, 143.4, 142.3, 142.1, 141.9 (bpy), 140.8 (q, TRZ), 137.9, 137.5 (q, bpy), 134.6, 133.8, 133.6 (q, Ph), 129.5, 129.4, 129.3, 129.1, 129.0 (Ph/TRZ), 127.9, 127.7, 127.5 (bpy), 127.1, 126.5, 126.4 (Ph), 123.7, 123.6, 123.5, 123.3, 123.1, 122.9 (bpy), 86.8, 86.7, 86.5 (C_{1Gal}), 74.9, 74.7, 74.6 (C_{5Gal}), 70.8, 70.6, 70.4 (C_{3Gal}), 70.0 (<u>C</u>H$_2$-bpy), 69.9, 69.7 (<u>C</u>HPh), 69.2 (<u>C</u>H$_2$-bpy), 69.1, 68.9, 68.8 (<u>C</u>H$_2$-CHPh), 68.7, 68.53, 68.49 (C_{2Gal}) 68.1 (<u>C</u>HPh), 67.6, 67.3, 67.3, (C_{4Gal}), 62.1, 61.7, 61.6 (C_{6Gal}), 20.4, 20.3, 20.2, 20.1, 20.0, 19.9 (12 x CH_3)

IR v cm^{-1} 1742 s, 1440 w, 1367 m, 1214 s, 1041 s, 922 m, 621 s

MS (ESI) *m/z* 715.4 $[L + H]^+$

Elemental analysis found (Calculated for $C_{108}H_{114}N_{18}O_{46}Cl_4Zn_2$).4$H_2O$ % C 47.27 (47.26) H 5.29 (4.48) N 9.19 (9.19)

S_c,Λ_{Zn},HHT-$[Zn_2L^{9c}_3][ClO_4]_4$.

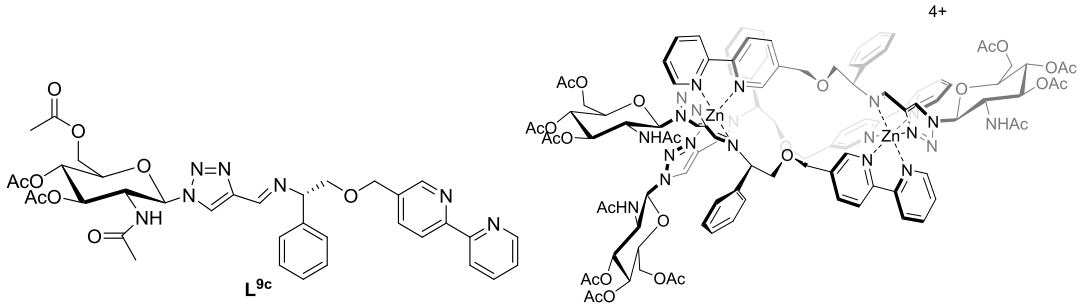

S_c,Λ_{Zn},HHT-$[Zn_2L^{9c}_3][ClO_4]_4$ was synthesised using the procedure described for S_c,Λ_{Zn},HHT-$[Zn_2L^{3}_3][ClO_4]_4$, substituting 5-(propargyloxy)picolinaldehyde (**5**) for (*2R,3S,4R,5R,6R*)-5-acetamido-2-(acetoxymethyl)-6-(4-formyl-1H-1,2,3-triazol-1-yl)tetrahydro-2H-pyran-3,4-diyl diacetate (**48**)

Yield: 86 mg, 85%.

^{1}H NMR (500 MHz, 298 K, CD_3CN) δ_H ppm 9.31 (1H, s, HC=N), 9.25 (1H, s, HC=N), 9.22 (1H, s, bpy), 9.15 (1H, s, bpy), 8.83 (1H, s, TRZ), 8.80 (1H, s, HC=N), 8.78 (1H, s, TRZ), 8.53 (2H, dd, $^3J_{HH}$ = 8.0, 5.0 Hz, bpy), 8.40 (1H, s, bpy), 8.26 (2H, m, bpy), 8.16-7.96 (6H, m, bpy/TRZ), 7.93 (1H, d , $^3J_{HH}$ = 8.0 Hz, bpy), 7.87-7.78 (3H ,m, bpy), 7.63 (1H, m, bpy), 7.58-7.45 (2H, m, bpy), 7.32 (1H, t, $^3J_{HH}$ = 7.5 Hz, Ph), 7.25 (2H, t, $^3J_{HH}$ = 7.5 Hz, Ph), 7.04 (1H, t, $^3J_{HH}$ = 7.5 Hz, Ph), 6.96 (2H, d, $^3J_{HH}$ = 7.5 Hz, Ph), 6.92 (1H, t, $^3J_{HH}$ = 7.5 Hz, Ph), 6.72 (2H, m, Ph/NH), 6.57 (1H, t, $^3J_{HH}$ = 7.5 Hz, Ph), 6.52 (1H, d, $^3J_{HH}$ = 9.0 Hz, NH), 6.44 (1H, d, $^3J_{HH}$ = 9.0 Hz, NH), 6.13-6.04 (4H, m, Ph/H_{GlcNAc}), 6.00-5.91 (3H, m, Ph/H_{GlcNAc}), 5.49-5.12 (10H, m, H_{GlcNAc} overlapping with C<u>H</u>Ph/ C<u>H</u>$_2$-bpy), 4.91 (1H, d, $^3J_{HH}$ = 9.0 Hz, C<u>H</u>Ph), 4.77 (1H, d, $^3J_{HH}$ = 9.0 Hz, C<u>H</u>Ph), 4.68-4.36 (6H, m, H_{GlcNAc} overlapping with C<u>H</u>$_2$-bpy), 4.29-4.02 (13H, m, H_{GlcNAc} overlapping with C<u>H</u>$_2$-CHPh), 3.74 (1H, dd, $^2J_{HH}$ = 11.0 Hz, $^3J_{HH}$ = 3.0 Hz, C<u>H</u>$_2$-CHPh), 3.55, (1H, dd, ^{2}J$_{HH}$ = 11.0 Hz, $^3J_{HH}$ = 3.0 Hz, C<u>H</u>$_2$-CHPh), 3.47 (1H, dd, ^{2}J$_{HH}$ = 11.0 Hz, $^3J_{HH}$ = 3.0, Hz, C<u>H</u>$_2$-CHPh), 2.20-1.78 (36H, s, 12x CH_3)

^{13}C NMR (125 MHz, 298 K, CD_3CN) δ_c ppm 170.7, 170.6, 170.5, 170.4, 170.3, 170.0 (12 x C=O), 157.3, 156.7, 156.1 (HC=N), 150.7, 150.3, 147.7 (bpy), 149.4, 149.3, 148.9, 148.7, 148.4 (q, bpy), 148.2 (bpy), 147.4 (q, bpy), 143.6, 143.4, 142.3, 142.0, 141.7 (bpy), 141.6, 141.4, 140.5 (q, TRZ), 137.9, 137.5 (q, bpy), 134.5, 133.9, 133.7 (q, Ph), 129.5, 129.1, 128.9 (Ph/TRZ), 128.0, 127.7, 127.5 (bpy), 127.0, 126.5, 126.4 (Ph), 123.6, 123.4, 123.3, 123.1, 123.0, 122.8 (bpy), 87.1, 86.9, 86.6 ($C_{1GlcNAc}$), 75.4, 75.2, 75.1 ($C_{5GlcNAc}$), 72.4, 71.7, 71.4 ($C_{4GlcNAc}$), 70.0 ($\underline{C}H_2$-bpy), 69.8, 69.6 ($\underline{C}$HPh), 69.1 ($\underline{C}H_2$-bpy), 69.0, 68.9, 68.8 ($\underline{C}H_2$-CHPh), 68.4, 68.2, 68.1 ($C_{3GlcNAc}$), 62.2, 61.8 ($C_{6GlcNAc}$), 54.0, 53.2 ($C_{2GlcNAc}$), 22.4, 22.3, 22.0, 20.4, 20.3, 20.2 (12 x CH_3)

IR v cm^{-1} 1741 s, 1367 m, 1224 s, 1038 s, 925 w, 621 s

MS (ESI) *m/z* 714.4 $[L + H]^+$

Elemental analysis found (Calculated for $C_{108}H_{117}N_{21}O_{43}Cl_4Zn_2 \cdot 10H_2O$) % C 45.68 (45.52) H 4.77 (4.85) N 10.04 (10.32)

R$_c$,Δ_{Fe},-[Fe_2**L**$^1{}_3$]Cl_4·

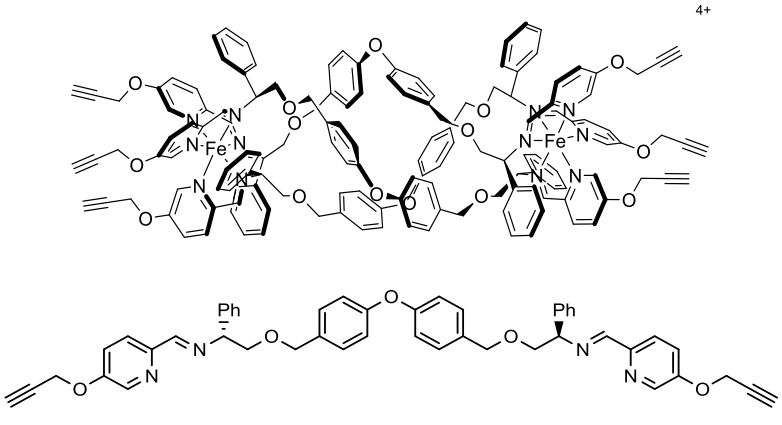

L^1

5- (Prop-2-yn-1-yloxy)picolinaldehyde (0.14 g, 0.85 mmol, 6.0 eq.) and (*R*,*R*)-bis(4-{[2-amino-2-phenylethoxy]methyl}phenyl)ether (0.2 g, 0.43 mmol, 3.0 eq.) were

dissolved in methanol followed by addition of anhydrous $FeCl_2$ (0.036 g, 0.29 mmol, 2 eq.). The solution was heated at reflux for 48 h. The dark purple solid was isolated under reduced pressure.

Yield = 0.3 g, 78%.

^{1}H NMR (500 MHz, 298 K, CD_3OD) δ_H 9.24 (6H, s, HC=N), 7.54 (6H, d, $^3J_{HH}$ =9.0 Hz, py), 7.46 (12H, d, $^3J_{HH}$ =8.5 Hz, OPh), 7.37 (6H, d, $^3J_{HH}$ = 8.0 Hz, py), 7.12 (6H, t, $^3J_{HH}$ = 7.0 Hz Ph), 7.04 (12H, t, $^3J_{HH}$ = 7.5 Hz, Ph), 6.79 (12H, d, $^3J_{HH}$ =7.0 Hz, Ph), 6.71 (12H, d, $^3J_{HH}$ = 8.0 Hz, OPh), 6.48 (6H, s, py), 5.93 (6H, d, $^3J_{HH}$ = 10.0 Hz, C<u>H</u>Ph), 5.02 (6H, d, $^2J_{HH}$ = 12.0 Hz, OCH_2Ph), 4.73 (12H, d, $^4J_{HH}$ = 3.5 Hz, $CH_2C{\equiv}C$), 4.50 (6H, t, $^3J_{HH}$ = 11.0 Hz, C<u>H</u>$_2$-CHPh), 4.42 (6H, d, $^2J_{HH}$ = 12.0 Hz, OCH_2Ph), 3.26 (6H, d, $^3J_{HH}$ = 9.0 Hz, C<u>H</u>$_2$-CHPh), 3.22 (6H, s, CH),

$^{13}C\{^1H\}$ NMR (125 MHz, 298K, CD_3OD) δ_C ppm 169.9 (HC=N), 157.0 (q, OPh), 155.8 (q, py), 152.5 (q, py), 141.2 (py), 135.4 (q, Ph), 132.82 (q, OPh), 129.8 (py), 128.8 (Ph), 128.7(OPh), 128.2/ 125.7 (Ph), 123.8 (py), 118.5 (OPh), 78.1 (C≡<u>C</u>H),76.6 (q, <u>C</u>≡CH), 72.7 (OCH_2Ph), 72.3 (O<u>C</u>H_2CH), 70.9 (OCH_2<u>C</u>H), 55.9 (<u>C</u>$H_2C{\equiv}CH$).

Elemental analysis found (calculated for $C_{144}H_{126}Cl_4Fe_2N_{12}O_{15}{\cdot}9H_2O$) % C 64.74 (64.53), H 4.81 (5.42), N 6.05 (6.27)

S_c,Λ_{Fe},-[$Fe_2\mathbf{L^2}_3$]Cl_4·

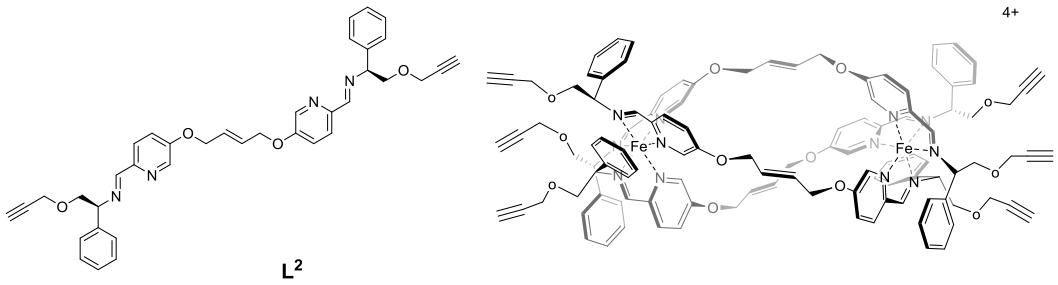

$\mathbf{L^2}$

(*S*)-1-phenyl-2-(prop-2-ynyloxy)ethanamine (**8**) (0.1 g, 0.57 mmol) and (*E*)-5,5'-(but-2-ene-1,4-diylbis(oxy))dipicolinaldehyde (**9**) (85 mg, 0.29 mmol) were dissolved in methanol followed by the addition of $FeCl_2$ (23.9 mg, 0.19 mmol). After reflux for 48 h, the solution was filted through celite and the solvent was removed under reduced pressure to obtain the dark purple compound.

Yield 0.17 g, 82%

^{1}H NMR (500 MHz, 298 K, CD_3OD) δ_H ppm 9.03 (6H, s, CHN), 7.53-7.30 (14H, m), 7.23-7.01 (18H, m), 6.87 (10H, d, $^3J_{HH}$ = 7.4 Hz), 6.50 (6H, s), 6.03 (6H, s), 5.87 (6H, d, $^3J_{HH}$ =9.2 Hz), 4.74-4.42 (30H, m), 3.72 (6H, d, $^3J_{HH}$ =9.1 Hz), 3.17 (6H, s, CH).

^{13}C {^{1}H} NMR (125 MHz, 298 K, CD_3OD) δ_C ppm 170.2 (CHN), 157.1, 151.6, 143.5, 135.3, 130.0, 129.2, 128.9, 128.8, 128.5 (*C*HCH), 128.1. 127.0, 125.8, 120.0 (Ar), 78.9, 76.1 (C*C*H), 71.0 (CH*C*H_2), 69.7 (*C*HCH_2), 68.7 (O*C*H_2CHCH), 58.2 (*C*H_2CCH).

HRMS Calculated for [$Fe_2L^2_3$]$^{4+}$ *m/z* 487.1724, found *m/z* 487.1722

Elemental Analysis found (Calculated for $C_{114}H_{108}Cl_4Fe_2N_{12}O_{12}$·$14H_2O$) % C 58.32 (58.42), H 4.69 (5.85), N 7.12 (7.17).

R_c,Δ_{Fe},-[$Fe_2\mathbf{L^2}_3$]Cl_4·

Yield 0.18 g, 85%

HRMS Calculated for $[Fe_2L^2{}_3]^{4+}$ *m/z* 487.1724, found *m/z* 487.1724

Elemental Analysis found (Calculated for $C_{114}H_{108}Cl_4Fe_2N_{12}O_{12}\cdot 13H_2O$) % C 58.94 (58.87), H 4.93 (5.81), N 7.20 (7.23).

Synthesis of S_c,Λ_{Fe},HHT-$[Fe_2L^3{}_3]Cl_4$

$FeCl_2$ (0.10 g, 0.82 mmol) was added to a stirred solution of the 5-(propargyloxy)picolinaldehyde (**2**) (0.20 g, 1.24 mmol) and (*S*)-2-(2,2'-bipyridin-5-ylmethoxy)-1-phenylethanamine (**14**) (0.38 g, 1.24 mmol) in methanol (50 ml) at ambient temperature to give a purple solution that was then refluxed for 48 h. The reaction was cooled to room temperature, filtered through a Celite plug prior to the solvents being removed *in vaccuo* to yield the desired product as a purple solid.

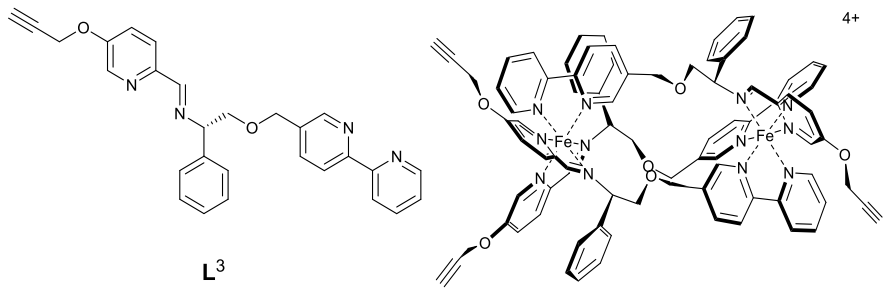

L^3

Yield 0.61 g, 90%.

^{1}H NMR (500 MHz, 298 K, D_2O) δ_H 9.57 (1H, s, HC=N), 9.48 (1H, s, HC=N), 9.16 (1H, s, bpy),9.15 (1H, s, bpy), 9.06 (1H, s, HC=N), 8.44 (2H, d, $^3J_{HH}$ = 10.0 Hz, bpy), 8.37 (1H, d, $^3J_{HH}$ = 10.0 Hz, py), 8.25 (1H, d, $^3J_{HH}$ = 10.0 Hz, py), 8.04-7.98 (2H, m, bpy), 7.89 (1H, d, $^3J_{HH}$ = 5.0 Hz, bpy), 7.86-7.62 (9H, m, Ph/bpy/py), 7.54 (1H, s, bpy), 7.50 (1H, d, $^3J_{HH}$ = 10.0 Hz, py), 7.35-6.84 (15H, m, Ph/py/bpy), 6.65 (2H, t, $^3J_{HH}$=7.5, Ph), 6.54 (2H, t,$^3J_{HH}$ =7.5 Hz, Ph), 6.41(1H, d, $^4J_{HH}$=0.4 Hz, py), 5.77 (2H, s, Ph), 5.32

(1H, dd, $^{2}J_{HH}$ = 11.0Hz,$^{3}J_{HH}$ = 3.5, C<u>H</u>Ph), 5.21 (1H, d, $^{2}J_{HH}$= 15.0 Hz, OC<u>H</u>$_2$-bpy), 5.19 (1H, d, $^{2}J_{HH}$= 15.0 Hz, OC<u>H</u>$_2$-bpy), 4.96 (2H, d, $^{2}J_{HH}$= 15.0 Hz, OC<u>H</u>$_2$-bpy), 4.73-4.60 (4H, m, C<u>H</u>$_2$-CCH overlapping with D_2O), 4.55-4.51 (4H, m, C<u>H</u>$_2$-CCH/CHPh), 4.45-4.38 (3H, m, OC<u>H</u>$_2$-bpy/C<u>H</u>$_2$-CHPh), 4.45-4.38 (2H, m, OC<u>H</u>$_2$-bpy/ C<u>H</u>$_2$-CHPh), 4.21 (1H, t, $^{3}J_{HH}$ =10.0 Hz, C<u>H</u>$_2$-CHPh), 3.54 (1H, dd, $^{2}J_{HH}$ = 10.5 Hz, $^{3}J_{HH}$ = 3.5 Hz, C<u>H</u>$_2$-CHPh), 3.35 (1H, dd, $^{2}J_{HH}$ = 10.5 Hz, $^{3}J_{HH}$ = 3.5 Hz, C<u>H</u>$_2$-CHPh), 3.25 (1H, dd, $^{2}J_{HH}$ = 10.5 Hz, $^{3}J_{HH}$ = 3.5 Hz, C<u>H</u>$_2$-CHPh), 3.05 (1H, s, CH), 2.84 (1H, s, CH), 2.79 (1H, s, CH).

^{13}C {^{1}H} NMR (125 MHz, 298 K, D_2O) δ_C 170.4/ 170.0/ 169.5 (HC=N), 159.7/ 158.9/ 158.6/ 158.3/ 157.9/ 157.8 (q, bpy)/ 157.5/ 157.4 (bpy), 156.0/ 155.9/ 155.6 (q, py), 154.5/ 153.8/ 153.4/ 153.3 (bpy), 152.3/ 152.0/ 151.8 (q, py), 142.6/ 141.8/ 141.7 (py), 140.0/ 139.7/ 139.6/ 138.9/ 138.6/ 138.6 (bpy), 136.9/ 136.7/ 136.3 (q, bpy), 134.1/ 132.5/ 132.2 (q, Ph), 131.1/ 130.7/ 130.2 (py), 129.1/ 129.0/ 128.9/ 128.8/ 128.7/ 128.6 (Ph), 127.3/ 127.2/ 127.1 (bpy), 124.3 (py), 123. 9/ 123.8/ 123.7/ 123.6/ 123.5 (py/bpy), 122.7/ 122.5/ 121.9 (bpy), 78.4/ 78.3/ 78.2 (C≡<u>C</u>H), 77.0/ 76.8/ 76.7 (q, <u>C</u>≡CH), 72.6/ 72.5/ 70.4 (<u>C</u>HPh), 69.2/ 69.1/ 68.7 (<u>C</u>H$_2$-bpy), 68.5/ 68.4/ 67.9 (<u>C</u>H$_2$-CHPh), 56.5/ 56.4 (<u>C</u>H$_2$-C≡CH).

HRMS Calculated for $[Fe_2L^{3}_3]^{4+}$ *m/z* 364.1095, found *m/z* 364.1103

IR *v* cm^{-1} 3366 (br, m), 1606 (m), 1590 (m), 1557 (s), 1467 (m), 1403 (w), 1363 (m), 1277 (m), 1227 (s), 1109 (m), 1074 (s), 1002 (s), 933 (m), 842 (m), 791 (m), 754 (m), 697 (s).

Elemental Analysis found (Calculated for $C_{84}H_{72}Cl_4Fe_2N_{12}O_6 \cdot 11H_2O$) % C 56.41 (56.14), H 4.68 (5.27), N 9.31 (9.35).

R_c,Δ_{Fe} HHT-$[Fe_2L^{3}_3]Cl_4$

HRMS Calculated for $[Fe_2L^3{}_3]^{4+}$ *m/z* 364.1095, found *m/z* 364.1098

IR *v* cm^{-1} 3370 (br, m), 1606 (m), 1591 (m), 1556 (s), 1493 (m), 1468 (m), 1404 (w), 1364 (w), 1276 (m), 1227 (s), 1109 (w), 1074 (s), 1002 (s), 932 (m), 841 (m), 791 (m), 755 (m), 697 (s).

Elemental Analysis found (Calculated for $C_{84}H_{72}Cl_4Fe_2N_{12}O_6 \cdot 11H_2O$) % C 56.31 (56.14), H 4.67 (5.27), N 9.28 (9.35).

General synthesis of clicked HHT-$[Fe_2L^{4a\text{-}e;\ 7a\text{-}i}]Cl_4$

The azide (4.5 eq.) and $[Fe_2L^3{}_3]Cl_4$ (1 eq.) was dissolved in methanol (20 ml), followed by the addition of copper (I) iodide (1 eq.). The solution was stirred under partial vacuum and heated at 65 ˚C overnight. The solution was filtered to remove copper salt. The resulting purple solution yielded the desired product as a purple solid on the addition of ethyl acetate.

S_c,Λ_{Fe},HHT-$[Fe_2L^{4a}{}_3]Cl_4$.

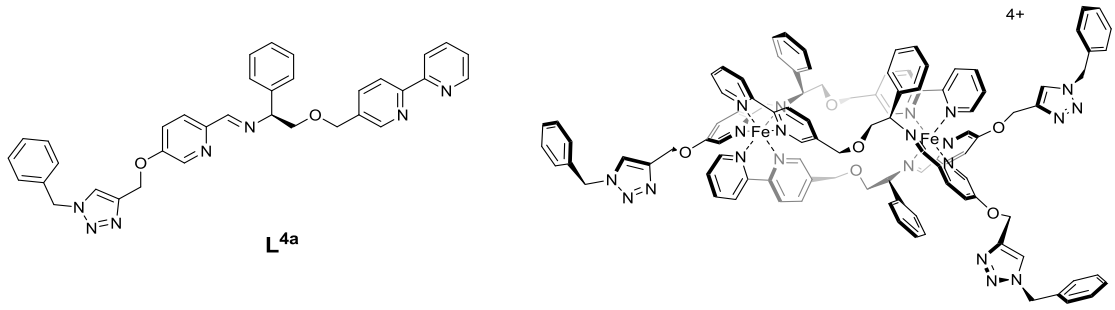

Yield 0.19 g, 82%.

^{13}C {^1H} NMR (125 MHz, 298K, CD_3OD) δ_C 171.2/ 171.1/ 170.3 (HC=N), 159.8/ 159.2/ 158.9/ 158.8/ 158.3/ 158.2 (q, bpy), 157.54 (bpy), 157.51 (q, py), 157.4 (bpy), 157.3/ 156.8 (q, py), 155.0 (bpy), 154.1/ 153.5/ 152.9 (py), 151.9/ 151.7/ 151.6 (q, py), 143.2/ 142.6/ 142.2 (py), 134.0/ 139.9/ 139.7/ 138.8/ 138.5/ 138.2 (bpy), 137.3/ 137.0/

136.9 (q, bpy), 135.3/ 135.2/ 135.1 (q, PhCH$_2$), 134.4/ 132.9/ 132.6 (q, Ph), 131.7/ 131.4/ 130.3 (py), 129.8/ 128.9/ 128.8/ 128.7/ 128.6/ 128.5/ 128.4/ 128.3/ 128.2/ 128.1/ 128.0/ 127.8/ 127.7 (Ph), 127.5/ 127.4/ 127.3/ 127.1 (bpy), 125.5/ 125.0/ 124.7 (TRZ), 124.3/ 124.1/ 123.6 (py), 123.4/ 123.1 122.8/ 122. 6/ 122.1 (bpy), 72.4/ 72.3/ 70.3 (CHPh), 69.3/ 69.2/ 69.0 (CH$_2$-bpy), 68.9/ 68.6/ 68.4 (CH$_2$-CHPh), 61.8/ 61.5/ 61.4 (TRZCH$_2$O), 53.7/ 53.6/ 53.5 (Ph-CH$_2$-TRZ).

HRMS Calculated for $[Fe_2L_n]^{4+}$ *m/z* 463.9076, found *m/z* 463.9073

IR *v* cm^{-1} 3381 (br, s), 3031 (br, s), 1603 (m), 1556 (s), 1495 (m), 1468 (s), 1403 (m), 1361 (m), 1301 (m), 1220 (s), 1076 (s), 984 (m), 937 (m), 840 (w), 791 (w), 755 (w), 723 (w), 696 (m), 536 (w), 451 (m).

Elemental Analysis found (Calculated for $C_{105}H_{93}Cl_4Fe_2N_{21}O_6 \cdot 19H_2O$) % C 53.90 (53.88), H 4.53 (5.64), N 12.54 (12.57).

R$_c$,Δ_{Fe},HHT-$[Fe_2L^{4a}{}_3]Cl_4$.

Yield 0.18 g, 79%.

HRMS Calculated for $[Fe_2L_n]^{4+}$ *m/z* 463.9076, found *m/z* 463.9073

IR *v* cm^{-1} 3356 (br, s), 1604 (m), 1556 (s), 1468 (s), 1221 (s), 1111 (w), 1076 (s), 985 (m), 936 (w), 840 (w), 791 (w), 754 (w), 726 (w), 697 (m).

Elemental Analysis found (Calculated for $C_{105}H_{93}Cl_4Fe_2N_{21}O_6 \cdot 22H_2O$) % C 52.65 (52.66), H 4.25 (5.77), N 12.18 (12.28).

S_c,Λ_{Fe},HHT-[$Fe_2L^{4b}{}_3$]Cl_4.

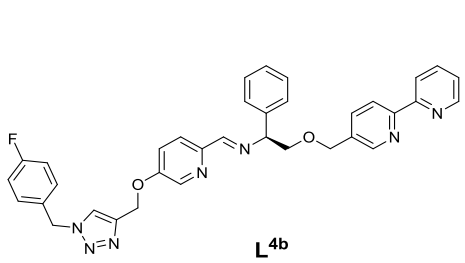

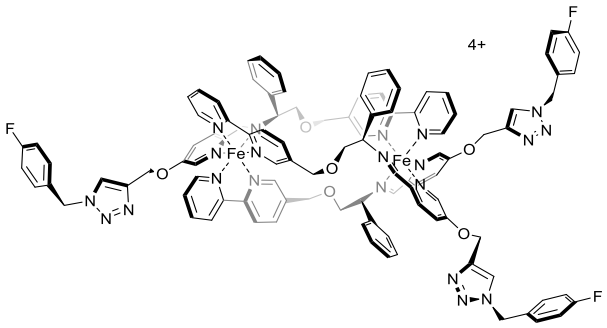

Yield 0.23 g, 75%.

^{13}C {^1H} NMR (125 MHz, 298K, CD_3OD) δ_C 171.4/ 171.3/ 170.5 (HC=N), 163.8/ 163.7/ 161.8/ 161.8 (q, F-Ph), 159.8/ 159.2/ 158.9/ 158.8/ 158.3/ 158.2 (q, bpy), 157.6 (bpy), 157.5 (q, py), 157.5 (bpy), 157.3/ 156.7 (q, py), 155.0 (bpy), 154.1/ 153.6/ 152.9 (py), 151.9/ 151.7/ 151.6 (q, py), 143.3/ 142.7/ 142.3 (py), 140.0/ 139.9/ 139.8/ 138.9/ 138.5/ 138.3 (bpy), 1374/ 137.1/ 136.9 (q, bpy), 134.4/ 132.9/ 132.6 (q, Ph), 131.8/ 131.6 (py), 131.4/ 131.3/ 131.2 (q, F-Ph), 130.5/ 130.4/ 130.2/ 130.1/ 130.0 (F-Ph), 128.9/ 128.7/ 128.6/ 128.5 (Ph), 128.2/ 127.5/ 127.1 (bpy), 125.5/ 125.0/ 124.8 (TRZ), 124.3/ 124.0/ 123.6/ 123.5 (py/ bpy), 122.9/ 122.7/ 122.6/ 122.2 (bpy), 115.6, 115./ 115.4/ 115.3 (F-Ph), 72.4/ 72.3/ 70.3 (CHPh), 69.6/ 69.5/ 69.0 (CH_2-bpy), 68.9/ 68.7/ 68.5 (CH_2-CHPh), 61.8/ 61.6/ 61.5 (TRZCH_2O), 52.9/ 52.8/ 52.8 (F-Ph-CH_2-TRZ).

HRMS Calculated for $[Fe_2L_n]^{4+}$ *m/z* 477.4004, found *m/z* 477.4004

IR *v* cm^{-1} 3348 (br, m), 1603 (w), 1556 (s), 1509 (m), 1468 (m), 1218 (s), 1075 (s), 983 (m), 936 (m), 841 (m), 788 (m), 754 (m), 698 (s), 530 (s), 489 (s), 418 (s).

Elemental Analysis found (Calculated for $C_{105}H_{90}Cl_4F_3Fe_2N_{21}O_6 \cdot 19H_2O$) % C 52.75 (52.66), H 3.96 (5.39), N 12.17 (12.28).

R_c,Δ_{Fe},HHT-$[Fe_2L^{4b}{}_3]Cl_4$.

Yield 0.25 g, 82%.

HRMS Calculated for $[Fe_2L_n]^{4+}$ *m/z* 477.4005, found *m/z* 477.4003

IR *v* cm^{-1} 3363 (br, m), 1603 (w), 1556 (s), 1510 (m), 1468 (m), 1218 (s), 1076 (s), 984 (m), 936 (m), 839 (m), 788 (m), 754 (m), 697 (s), 533 (s), 421 (s).

Elemental Analysis found (Calculated for $C_{105}H_{90}Cl_4F_3Fe_2N_{21}O_6 \cdot 17H_2O$) % C 53.58 (53.47), H 4.20 (5.30), N 12.31 (12.47).

S_c,Λ_{Fe},HHT-$[Fe_2L^{4c}{}_3]Cl_4$.

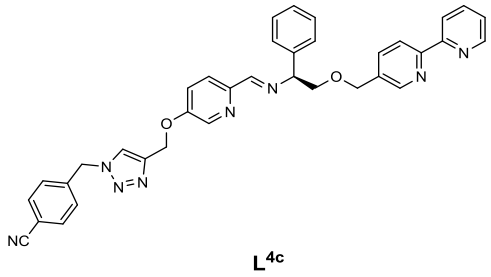

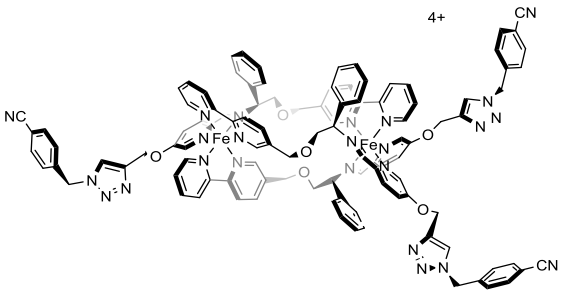

Yield 0.26 g, 84%.

^{13}C {^1H} NMR (125 MHz, 298K, CD_3OD) δ_C 171.3/ 171.2/ 170.4 (HC=N), 159.8/ 159.2/ 158.9/ 158.8/ 158.3/ 158.2 (q, bpy), 157.6 (bpy), 157.5 (q, py), 157.4 (bpy), 157.3/ 156.7 (q, py), 155.0 (bpy), 154.1/ 153.6/ 152.9 (py), 152.0, 151.7/ 151.6 (q, py), 143.3/ 142.6/ 142.3 (py), 140.7/ 140.6 (q, CN-Ph), 140.0/ 139.9/ 139.8/ 138.9/ 138.5/ 138.3 (bpy), 137.4/ 137.1/ 136.9 (q, bpy), 134.4/ 132.9 (q, Ph), 132.6 (CN-Ph), 132.6 (q, Ph), 132.5/ 132.5 (CN-Ph), 131.8/ 131.6/ 130.4 (py), 129.1/ 129.0/ 128.9/ 128.7/ 128.7/ 128.6/ 128.5/ 128.4/ 128.3/ 128.2/ 128.1 (Ph), 127.5/ 127.1 (bpy), 125.5/ 125.2/ 125.1 (TRZ), 124.3/ 124.1/ 123.6/ 123.5 (py/ bpy), 122.9/ 122.6/ 122.2 (bpy), 117.9/ 117.86/ 117.84 (CN), 112.1/ 112.0 (q, CN-Ph), 72.4/ 72.36/ 70.32 (CHPh), 69.5/ 69.3/

69.0 ($\underline{C}H_2$-bpy), 68.9/ 68.7/ 68.4 ($\underline{C}H_2$-CHPh), 61.7/ 61.6/ 61.4 (TRZ$\underline{CH_2}$O), 53.0/ 52.8/ 52.7 (CN-Ph-$\underline{C}H_2$-TRZ).

HRMS Calculated for $[Fe_2L_n]^{4+}$ *m/z* 482.6541, found *m/z* 482.6539

Elemental Analysis found (Calculated for $C_{108}H_{90}Cl_4Fe_2N_{24}O_6 \cdot 17H_2O$) % C 54.85 (54.51), H 4.15 (5.25), N 14.00 (14.13).

IR *v* cm^{-1} 3356 (br, s), 2226 (m), 1606 (m), 1556 (s), 1468 (s), 1221 (s), 1111 (w), 1076 (s), 985 (m), 936 (w), 840 (w), 788 (m), 754 (m), 697 (m), 544 (s).

R_c,Δ_{Fe},HHT-$[Fe_2L^{4c}{}_3]Cl_4$.

Yield 0.25 g, 80%.

HRMS Calculated for $[Fe_2L_n]^{4+}$ *m/z* 482.6541, found *m/z* 482.6526

IR *v* cm^{-1} 3348 (br, s), 2227 (S), 1605 (S), 1557 (s), 1468 (s), 1220 (s), 1112 (w), 1076 (s), 985 (m), 937 (w), 840 (w), 789 (m), 754 (m), 697 (m), 545 (M).

Elemental Analysis found (Calculated for $C_{108}H_{90}Cl_4Fe_2N_{24}O_6 \cdot 20H_2O$) % C 53.36 (53.30), H 4.07 (5.38), N 13.56 (13.81).

S_c,Λ_{Fe},HHT-$[Fe_2L^{4d}{}_3]Cl_4$.

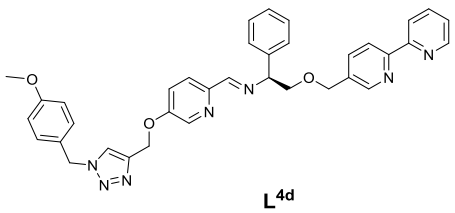

L^{4d}

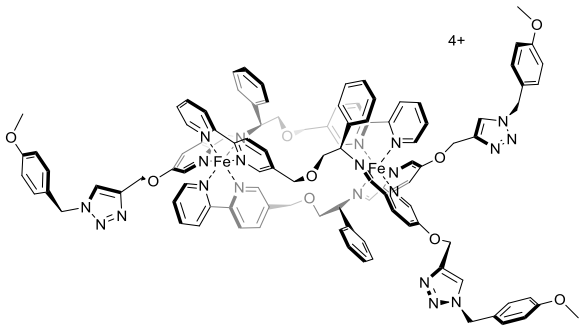

Yield 0.18 g, 88%.

^{13}C {^{1}H} NMR (125 MHz, 298K, CD_3OD) δ_C 171.4/ 171.3/ 170.5 (HC=N), 160.0 (q, PhOCH_3), 159.9/ 159.2/ 158.9/ 158.8/ 158.7/ 158.3/ 158.2 (q, bpy), 157.6 (bpy), 157.5 (q, bpy), 157.4 (bpy), 157.3/ 157.2/ 156.7/ 156.6 (q, py), 155.0 (bpy), 154.1/ 153.6/ 152.9 (py), 152.0/ 151.7/ 151.6 (q, py) 143.2/ 142.5/ 142.3 (py) 139.9/ 139.8/ 139.3/ 138.9/ 138.5/ 138.3 (bpy), 137.4/ 137.1/ 136.9 (q, bpy), 134.4/ 132.9/ 132.6 (q, Ph), 131.78/ 131.6/ 130.4 (py), 128.9/ 129.8/ 129.7/ 129.6/ 129.5/ 129.4 (PhOCH_3), 129.1/ 128.9/ 128.7/ 128.6/ 128.5/ 128.2/ 127.5 (Ph), 127.2/ 127.1/ 127.0 (q, PhOCH_3), 125.5/ 124.8/ 124.4 (TRZ), 124.3/ 124.2/ 123.6 (py), 123.5/ 123.4/ 123.0/ 122.7/ 122.6/ 122.2 (bpy), 114.1/ 114.0/ 113. 9/ 113.8 (PhOCH_3), 72.4/ 72.4/ 70.3 (CHPh), 69.5/ 69.4/ 69.0 (CH_2-bpy), 69.0/ 68.7/ 68.5 (CH_2-CHPh), 61.9/ 61.6/ 61.5 (TRZCH_2O), 54.5 (OCH_3), 53.3/ 53.2/ 53.1 (CH_3OPh-CH_2-TRZ).

HRMS Calculated for $[Fe_2L_n]^{4+}$ *m/z* 486.4155, found *m/z* 486.4154

IR *v* cm^{-1} 3361 (br, s), 1607 (m), 1556 (s), 1512 (s), 1467 (s), 1302 (m), 1241 (s), 1178 (m), 1076 (s), 1025 (m), 937 (w), 839 (w), 788 (m), 755 (m), 698 (m).

Elemental Analysis found (Calculated for $C_{108}H_{99}Cl_4Fe_2N_{21}O_9 \cdot 22H_2O$) % C 52.18 (52.20), H 4.35 (5.80), N 11.53 (11.84).

R_c,Δ_{Fe},HHT-$[Fe_2L^{4d}{}_3]Cl_4$.

Yield 0.17 g, 85%.

HRMS Calculated for $[Fe_2L_n]^{4+}$ *m/z* 486.4155, found *m/z* 486.4150

IR *v* cm^{-1} 3362 (br, s), 1607 (m), 1557 (s), 1513 (s), 1467 (s), 1302 (m), 1242 (s), 1177 (m), 1076 (s), 1025 (m), 937 (w), 840 (w), 788 (m), 755 (m), 698 (m).

Elemental Analysis found (Calculated for $C_{108}H_{99}Cl_4Fe_2N_{21}O_9 \cdot 21H_2O$) % C 52.83 (52.58), H 4.46 (5.76), N 11.68 (11.92).

S_c,Λ_{Fe},HHT-[$Fe_2L^{4e}_3$]Cl_4.

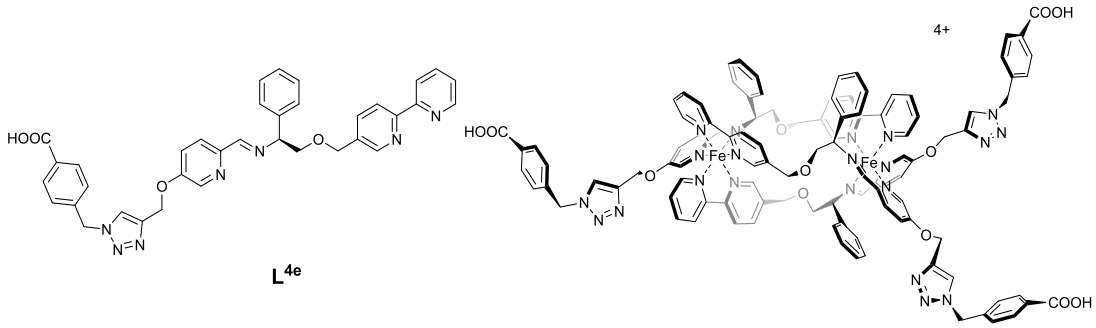

Yield 0.26 g, 77%.

^{13}C {^1H} NMR (125 MHz, 298K, CD_3OD) δ_C 171.3/ 170.4 (HC=N), 159.8/ 159.2/ 158.8/ 158.3/ 158.2 (q, bpy), 157.5 (bpy), 157.46 (q, py), 157.4 (bpy), 157.2/ 156.7 (q, py), 155.0 (bpy), 154.1/ 153.5/ 152.9 (py), 152.0/ 151.7/ 151.5 (q, py), 143.3/ 142.3/ 142.1 (py), 140.1/ 140.0 (q, PhCOOH), 139.9/ 139.7/ 138.9/ 138.5/ 138.3 (bpy), 137.4/ 137.0/ 136.9 (q, bpy), 134.3/ 132.9/ 132.6 (q, Ph), 131.7/ 130.3 (py), 128.9/ 128.7/ 128.6 128.5/ 128.1/ 128.0/ 127.5/ 127.1 (Ph), 125.5/ 125.1 (TRZ), 124.6/ 124.3/ 123.6 (py), 123.5/ 123.1/ 122.8/ 122.6/ 122.1 (bpy), 72.4/ 72.3/ 70.3 (CHPh), 69.3/ 69.0 (CH_2-bpy), 68.9/ 68.6/ 68.4 (CH_2-CHPh), 61.8/ 61.6/ 61.4 (TRZCH_2O), 53.2/ 53.1/ 53.0 (COOHPh-CH_2-TRZ)

HRMS Calculated for $[Fe_2L_n]^{4+}$ *m/z* 496.9000, found *m/z* 496.9020

IR *v* cm^{-1} 3360 (br, w), 1699 (m), 1606 (m), 1556 (s), 1467 (m), 1373 (m), 1220 (s), 1178 (m), 1110 (m), 1076 (s), 1053 (m), 984 (m), 936 (m), 839 (m), 750 (s), 731 (s), 697 (s).

Elemental Analysis found (Calculated for $C_{108}H_{93}Cl_4Fe_2N_{21}O_{12}\cdot16H_2O$) % C 53.67 (53.63), H 4.18 (5.21), N 11.95 (12.16).

R_c,Δ_{Fe},HHT-[$Fe_2L^{4e}_3$]Cl_4.

Yield 0.25 g, 75%.

HRMS Calculated for $[Fe_2L_n]^{4+}$ *m/z* 496.9000, found *m/z* 496.8998

IR *v* cm^{-1} 3339 (br, m), 1700 (m), 1605 (m), 1555 (s), 1468 (m), 1405 (m), 1372 (m), 1220 (s), 1109 (m), 1075 (s), 985 (m), 936 (m), 840 (m), 752 (s), 731 (s), 697 (s).

Elemental Analysis found (Calculated for $C_{108}H_{93}Cl_4Fe_2N_{21}O_{12}\cdot 17H_2O$) % C 53.25 (53.23), H 4.17 (5.25), N 11.98 (12.07).

S_c,Λ_{Fe},HHT-$[Fe_2L^5{}_3][ClO_4]_4$

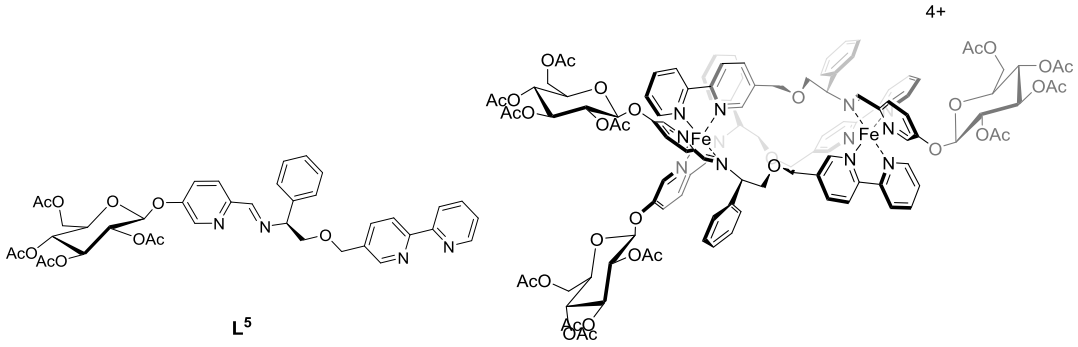

S_c,Λ_{Fe},HHT-$[Fe_2L^5{}_3][ClO_4]_4$ was synthesised using the procedure described for S_c,Λ_{Fe},HHT-$[Fe_2L^3{}_3]Cl_4$, substituting 5-(propargyloxy)picolinaldehyde (**5**) for (*2R,3R,4S,5R,6S*)-2-(acetoxymethyl)-6-((6-formylpyridin-3-yl)oxy)tetrahydro-2H-pyran-3,4,5-triyl triacetate (**21**).

Yield 89 mg, 89%

^{1}H NMR (500 MHz, 298 K, CD_3CN) δ_H 9.58 (1H, s, HC=N), 9.46 (1H, s, HC=N), 9.15 (1H, s, bpy),9.13 (1H, s, bpy), 9.09 (1H, s, HC=N), 8.56-8.49 (3H, m, bpy/py), 8.46 (1H, d, $^3J_{HH}$ = 9.0 Hz, py), 8.10-8.08 (2H, m, bpy), 7.99-7.60 (13H, m, Ph/bpy/py), 7.47-6.90 (17H, m, Ph/bpy/py), 6.74-6.68 (3H, m, py/Ph), 6.61 (2H, t, $^3J_{HH}$=7.5, Ph), 6.24 (1H, d, $^4J_{HH}$=2.0 Hz, py), 6.11-5.67 (3H, br, Ph), 5.42 (1H, t, $^3J_{HH}$=10.0, H_{glu}), 5.38-4.96 (15H, m, H_{glu} overlapping with OC<u>H</u>$_2$-bpy), 4.57-3.85 (17H, m, H_{glu} overlapping with OC<u>H</u>$_2$-bpy, C<u>H</u>$_2$-CHPh and C<u>H</u>Ph), 3.74 (1H, dd, $^2J_{HH}$ =

11.0Hz,$^{3}J_{HH}$ = 3.5, C<u>H</u>Ph), 3.57 (1H, dd, $^{2}J_{HH}$ = 10.5 Hz, $^{3}J_{HH}$ = 4.0 Hz, C<u>H</u>$_2$-CHPh), 3.41 (1H, dd, $^{2}J_{HH}$ = 11.0 Hz, $^{3}J_{HH}$ = 3.0 Hz, C<u>H</u>$_2$-CHPh), 3.30 (1H, dd, $^{2}J_{HH}$ = 11.0 Hz, $^{3}J_{HH}$ = 3.0 Hz, C<u>H</u>$_2$-CHPh), 2.09-1.88 (36H, m, 12 × $COCH_3$).

^{13}C {^{1}H} NMR (125 MHz, 298 K, CD_3CN) δ_C 171.3/ 171.0/ 170.4 (HC=N), 170.4/ 170.1/170.1/ 169.9/ 169.8/ 169.7/ 169.5/ 169.4/ 169.4/ 169.2/ 169.1/ 169.0 (q, CO), 159.3/ 158.9/ 158.6/ 158.3/ 158.0/ 157.9 (q, bpy)/ 157.8/ 157.5/ 155.5 (bpy), 155.4/ 155.4/ 155.0 (q, py), 154.3/ 154.0 (bpy), 153.7/ 153.5 (q, py), 153.2 (bpy), 144.1/ 143.7/ 142.6 (py), 140.2/ 140.1/ 139.9/ 139.0/ 138.6/ 138.5 (bpy), 137.4/ 137.0/ 136.6 (q, bpy), 134.2/ 132.5/ 132.3 (q, Ph), 132.0/ 131.8/ 130.7 (py), 128.9/ 128.8/ 128.8/ 128.6/ 128.5 (Ph), 127.5/ 127.4/ 127.2 (bpy),125.3/ 125.1/ 124.7 (py), 124.1/ 123.9/ 123.6/ 123.5/ 122.5/ 122.4 (bpy), 98.0/ 97.6 (C_{1Glu}), 72.5/ 72.4 (C_{5Glu}), 72.0/ 71.9/ 71.8 (C_{3Glu}), 71.5/ 71.4/ 70.6 (<u>C</u>HPh), 70.5/ 70.2/ 70.1 (C_{2Glu}), 69.4/ 69.3/ 69.2 (O<u>C</u>H$_2$-bpy), 68.7/ 68.6/ 68.5 (<u>C</u>H$_2$-CHPh), 67.4/ 67.4 (C_{4Glu}), 61.4/ 61.2/ 61.1 (C_{6Glu}), 12.0/ 12.0/ 19.9/ 19.8/ 19.8/ 19.8 (12 × CH_3).

MS (ESI) *m/z* 763.4 $[L + Na]^+$

Elemental Analysis found (Calculated for $C_{117}H_{120}Cl_4N_{12}O_{49}Fe_2 \cdot 6H_2O$) % C 49.30 (49.48), H 4.31 (4.69), N 6.10 (5.92).

S_c,Λ_{Fe},HHT-$[Fe_2L^6{}_3][ClO_4]_4$

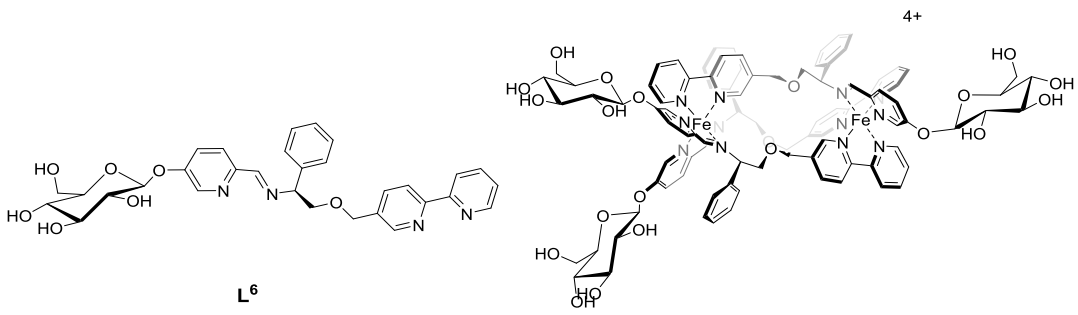

S_c,Λ_{Fe},HHT-$[Fe_2L^6{}_3][ClO_4]_4$ was synthesised using the procedure described for S_c,Λ_{Fe},HHT-$[Fe_2L^3{}_3]Cl_4$, substituting 5-(propargyloxy)picolinaldehyde (**5**) for 5-(((*2S,3R,4S,5S,6R*)-3,4,5-trihydroxy-6-(hydroxymethyl)tetrahydro-2H-pyran-2-yl)oxy)picolinaldehyde (**22**)

Yield 70 mg, 83%

^{1}H NMR (500 MHz, 298 K, CD_3CN) δ_H 9.53 (1H, s, HC=N), 9.38 (1H, s, HC=N), 9.15 (1H, s, bpy),9.13 (1H, s, bpy), 9.00 (1H, s, HC=N), 8.54-8.48 (3H, m, bpy/py), 8.37 (1H, d, $^3J_{HH}$ = 9.0 Hz, py), 8.17-8.08 (2H, m, bpy), 7.94-7.63 (13H, m, Ph/bpy/py), 7.55 (1H, d, $^3J_{HH}$ = 9.0 Hz, py), 7.45-6.89 (19H, m, Ph/bpy/py), 6.80 (1H, d, $^4J_{HH}$=2.0 Hz, py), 6.70 (2H, t, $^3J_{HH}$=7.5, Ph), 6.58 (2H, t, $^3J_{HH}$=7.5, Ph), 6.29 (1H, d, $^4J_{HH}$=2.0 Hz, py), 6.06-5.65 (2H, br, Ph), 5.31 (1H, dd, $^2J_{HH}$ = 11.0Hz,$^3J_{HH}$ = 3.5, C<u>H</u>Ph), 5.22 (2H, d, $^2J_{HH}$ = 12.5 Hz, C<u>H</u>$_2$-bpy), 5.09 (1H, d, $^2J_{HH}$ = 13.0 Hz, OC<u>H</u>$_2$-bpy), 4.89 (1H, d,$^3J_{HH}$ = 7.0 Hz, H_{glu}), 4.82 (1H, d,$^3J_{HH}$ = 7.0 Hz, H_{glu}), 4.64 (1H, d,$^3J_{HH}$ = 7.0 Hz, H_{glu}), 4.56-4.34 (6H, m, H_{glu} overlapping with C<u>H</u>$_2$-bpy, C<u>H</u>$_2$-CHPh and C<u>H</u>Ph), 4.26 (1H, t, $^3J_{HH}$= 11.0, C<u>H</u>$_2$-CHPh), 4.17 (1H, t, $^3J_{HH}$= 11.0, C<u>H</u>$_2$-CHPh), 3.81-3.11 (32H, m, H_{glu} overlapping with C<u>H</u>$_2$-bpy, C<u>H</u>$_2$-CHPh and C<u>H</u>Ph).

^{13}C {^{1}H} NMR (125 MHz, 298 K, CD_3CN) δ_C 171.7/ 171.4/ 170.7 (HC=N), 156.0/ 159.4/ 159.2/ 156.0/ 158.6 (q, bpy)/ 158.3/ 158.0 (bpy), 156.7/ 156.6/ 156.3 (q, py), 156.1/ 155.0/ 154.5/ 154.1 (bpy), 153.5/ 153.3/ 153.2 (q, py), 143.5/ 143.3/ 141.9 (py), 140.8/ 140.5/ 140.4/ 139.5/ 139.1/ 139.0/ (bpy), 138.0/ 137.6/ 137.2 (q, bpy), 134.9/ 133.3/ 133.0 (q, Ph), 132.5/ 132.3/ 131.1 (py), 129.5/ 129.5/ 129.3/ 129.2/ 129.1 (Ph), 128.2/ 128.1/ 127.9/ 125.9/ 125.5/ 125.4 (bpy), 124.6/ 124.4/ 124.2 (py), 124.1/ 123.1/ 122.9 (bpy), 100.7/ 100.2/ 99.9 (C_{1Glu}), 77.1/ 77.0 (C_{5Glu}), 76.6/ 76.6/ 76.5 (C_{3Glu}),

73.6/ 73.5/ 73.4 (C_{2Glu}), 73.0/ 72.9/ 71.1 (C_{4Glu}), 70.3/ 70.2 (CHPh), 70.0 (CH_2-bpy), 69.8 (CHPh), 69.3/ 69.2 (CH_2-CHPh), 61.8/ 61.5 (C_{6Glu}).

MS (ESI) *m/z* 573.4 $[L + H]^+$; 595.3 $[L + Na]^+$

Elemental Analysis found (Calculated for $C_{93}H_{96}Cl_4N_{12}O_{37}Fe_2 \cdot 10H_2O$) % C 46.40 (46.40), H 4.27 (4.86), N 7.15 (6.98).

S_c,Λ_{Fe},HHT-$[Fe_2L^{7a}{}_3]Cl_4$

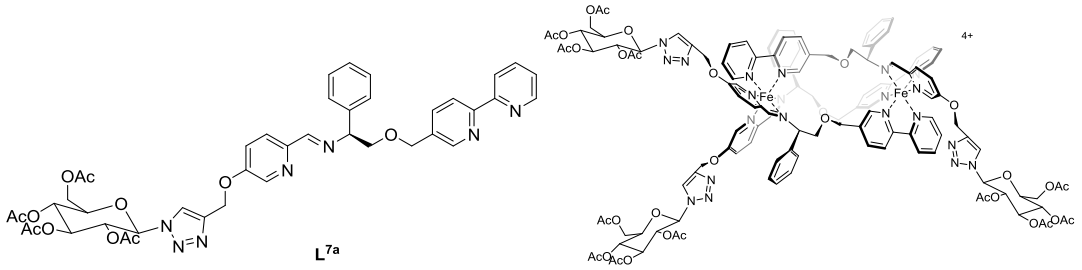

Yield 0.15 g, 87%.

HRMS Calculated for $[Fe_2L_n]^{4+}$ *m/z* 644.1943, found *m/z* 644.1914

Elemental Analysis found (Calculated for $C_{126}H_{129}Cl_4Fe_2N_{21}O_{33} \cdot 25H_2O$) % C 47.78 (47.75), H 4.49 (5.69), N 9.52 (9.28).

IR *v* cm^{-1} 3381 (br, w), 1737 (s), 1559 (m), 1468 (m), 1366 (m), 1213 (s), 1077 (m), 1035 (s), 921 (m), 791 (w), 755 (w), 699 (w).

R_c,Δ_{Fe},HHT-$[Fe_2L^{7a}{}_3]Cl_4$

Yield 0.14 g, 82%.

HRMS Calculated for $[Fe_2L_n]^{4+}$ *m/z* 644.1943, found *m/z* 644.1939

IR *v* cm^{-1} 3386 (br, w), 1737 (s), 1562 (m), 1469 (m), 1366 (m), 1214 (s), 1076 (m), 1036 (s), 921 (m), 791 (w), 755 (m), 698 (m).

Elemental Analysis found (Calculated for $C_{126}H_{129}Cl_4Fe_2N_{21}O_{33}\cdot 26H_2O$) % C 47.30 (47.48), H 4.47 (5.72), N 9.43 (9.23).

S_c,Λ_{Fe},HHT-$[Fe_2L^{7b}{}_3]Cl_4$

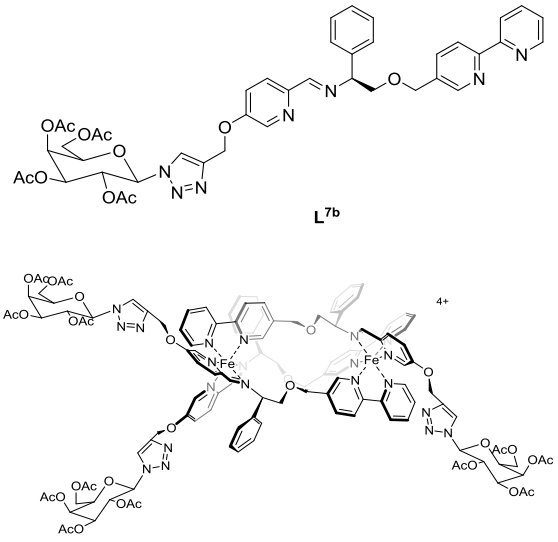

L^{7b}

Yield 0.18 g, 79%.

Elemental Analysis found (Calculated for $C_{126}H_{129}Cl_4Fe_2N_{21}O_{33}\cdot 24H_2O$) % C 48.07 (48.02), H 4.45 (5.66), N 9.64 (9.33).

IR ν cm^{-1} 3369 (br, m), 1750 (s), 1677 (w), 1603 (w), 1555 (m), 1455 (m), 1367 (m), 1217 (s), 1060 (s), 913 (m), 838 (w), 752 (w), 698 (w), 541 (w).

HRMS Calculated for $[Fe_2L_n]^{4+}$ *m/z* 644.1942, found *m/z* 644.1944

R_c,Δ_{Fe},HHT-$[Fe_2L^{7b}{}_3]Cl_4$

Yield 0.18 g, 81%.

Elemental Analysis found (Calculated for $C_{126}H_{129}Cl_4Fe_2N_{21}O_{33}\cdot 26H_2O$) % C 47.35 (47.48), H 4.30 (5.72), N 9.57 (9.23).

HRMS Calculated for $[Fe_2L_n]^{4+}$ *m/z* 643.9438, found *m/z* 643.9423

IR *v* cm^{-1} 3357 (br, m), 1740 (s), 1607 (w), 1558 (m), 1469 (w), 1367 (m), 1216 (s), 1050 (s), 922 (m), 840 (w), 775 (w), 698 (w), 537 (w).

S_c,Λ_{Fe},HHT-$[Fe_2L^{7c}{}_3]Cl_4$

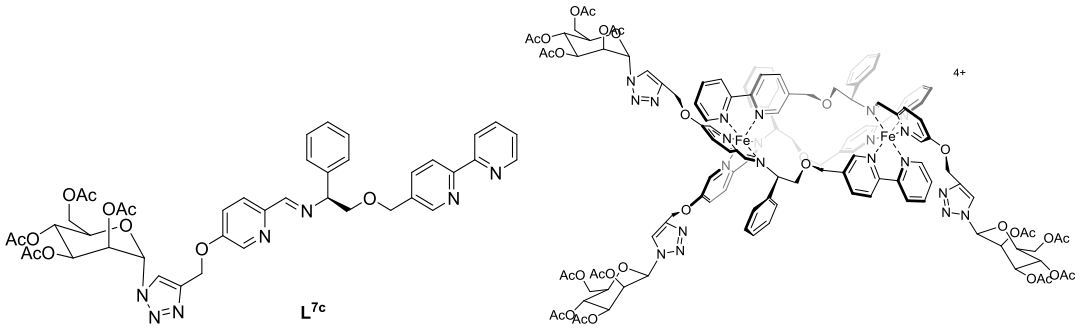

Yield 0.22 g, 84%.

Elemental Analysis found (Calculated for $C_{126}H_{129}Cl_4Fe_2N_{21}O_{33}\cdot 19H_2O$) % C 49.42 (49.44), H 4.47 (5.50), N 10.20 (9.61).

IR *v* cm^{-1} 3376 (br, S), 1750 (s), 1557 (m), 1468 (m), 1367 (m), 1217 (s), 1121 (m), 1075 (s), 1043 (s), 936 (w), 840 (w), 788 (w), 755 (w), 698 (w).

HRMS Calculated for $[Fe_2L_n]^{4+}$ *m/z* 644.1943, found *m/z* 644.1940

R_c,Δ_{Fe},HHT-$[Fe_2L^{7c}{}_3]Cl_4$

Yield 0.23 g, 86%.

Elemental Analysis found (Calculated for $C_{126}H_{129}Cl_4Fe_2N_{21}O_{33}\cdot 19H_2O$) % C 49.50 (49.44), H 4.52 (5.50), N 10.05 (9.61).

IR *v* cm^{-1} 3380 (br, S), 1739 (s), 1557 (m), 1469 (m), 1368 (m), 1217 (s), 1121 (m), 1075 (s), 1043 (s), 937 (w), 839 (w), 789 (w), 755 (w), 698 (w).

HRMS Calculated for $[Fe_2L_n]^{4+}$ *m/z* 643.9438, found *m/z* 643.9431

S_c,Λ_{Fe},HHT-[$Fe_2L^{7d}{}_3$]Cl_4

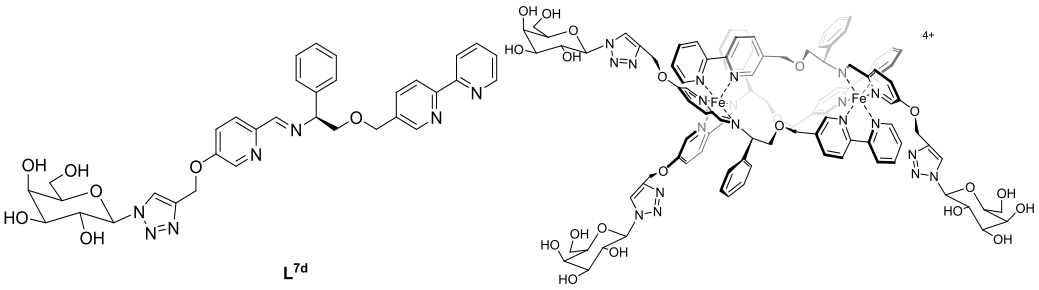

L^{7d}

Yield 0.16 g, 92%.

^{1}H NMR (500 MHz, 298 K, D_2O)δ_H 9.55 (1H, s, HC=N), 9.40 (1H, s, HC=N), 9.11 (1H, s, bpy),9.09 (1H, s, bpy), 9.00 (1H, s, HC=N), 8.41-8.36 (3H, m, bpy), 8.30 (1H, s, triazole), 8.27 (1H, d, $^3J_{HH}$ =8.8 Hz, py), 8.06-8.01 (2H, m, triazole/Ph), 7.93 (1H, t, $^3J_{HH}$ = 7.5 Hz, bpy), 7.88-6.76 (24H, m, Ph/py/bpy), 6.63 (2H, t, $^3J_{HH}$ = 7.0 Hz, Ph), 6.50 (2H, t, $^3J_{HH}$ = 7.5 Hz, Ph), 6.27 (1H, s, py), 5.66 (1H, d, $^3J_{HH}$ =9.2 Hz, H_{Gal}), 5.60 (1H, d, $^3J_{HH}$ =9.3 Hz, H_{Gal}), 5.55 (1H, d, $^3J_{HH}$ =9.2 Hz, H_{Gal}), 5.26-5.08 (8H, m), 4.92 (1H, d, $^2J_{HH}$ =12.7 Hz, C<u>H</u>$_2$-bpy), 4.48-4.36 (5H, m), 4.28-3.64 (24H, m), 3.50-3.20 (3H, m).

^{13}C {^{1}H} NMR (126 MHz, 298 K, D_2O) δ_C ppm 170.3, 170.0, 169.4 (CHN), 159.6, 158.7, 158.5, 158.2, 157.9, 157.6, 157.4 (bpy), 157.2 (bpy), 156.8, 156.7, 156.1, 154.5 (bpy), 153.8, 153.3, 153.2, 152.0, 151.9, 151.6, 143.1, 142.8, 142.4 (<u>C</u>=CH (triazole)), 142.2 (<u>C</u>=CH (triazole)), 142.0 (<u>C</u>=CH (triazole)), 141.7, 139.9, 139.7, 138.8, 138.6, 136.9, 136.7, 136.3, 134.2, 132.5, 132.2, 131.2, 130.8, 130.2, 129.0, 128.9, 128.8, 128.8, 128.6, 127.3, 127.2, 127.0, 124.5 (C=<u>C</u>H (triazole)), 123.8 (C=<u>C</u>H (triazole)), 123.7, 123.5 (C=<u>C</u>H (triazole)), 123.4, 123.4, 123.3, 122.8, 122.5, 121.9 (Ar), 88.0, 88.0 (C_{1Gal}), 78.4, 78.3, 78.3 (C_{5Gal}), 73.0, 72.8 (C_{3Gal}), 72.5, 72.4, 70.3 (<u>C</u>HPh), 69.7, 69.7, 69.6 (C_{2Gal}), 69.3, 69.2, 68.7 (<u>C</u>H$_2$-bpy), 68.5 (C_{4Gal}), 68.4, 67.9 (<u>C</u>H$_2$-CHPh), 61.9, 61.7, 61.4 (TRZ-CH$_2$), 60.9, 60.8 (C_{6Glu}).

HRMS Calculated for $[Fe_2L_3]^{4+}$ *m/z* 518.1626, found *m/z* 518.1619

IR *v* cm^{-1} 3275 (br, s), 2874 (br, s), 2114 (w), 1605 (w), 1556 (s), 1468 (m), 1402 (w), 1364 (m), 1303 (m), 1223 (s), 1073 (s), 1053 (s), 1010 (s), 983 (s), 936 (m), 883 (m),840 (m), 791 (m), 745 (m), 698 (s), 534 (s).

Elemental Analysis found (Calculated for $C_{102}H_{105}Cl_4Fe_2N_{21}O_{21}\cdot 21H_2O$) % C 47.19 (47.25), H 4.68 (5.71), N 11.31 (11.34).

R_c,Δ_{Fe},HHT-$[Fe_2L^{7d}_3]Cl_4$

Data as for *S*-enantiomer

Yield 0.13 g, 77%.

Elemental Analysis found (Calculated for $C_{102}H_{105}Cl_4Fe_2N_{21}O_{21}\cdot 19H_2O$) % C 47.90 (47.92), H 4.62 (5.64), N 11.48 (11.50).

S_c,Λ_{Fe},HHT-$[Fe_2L^{7e}_3]Cl_4$

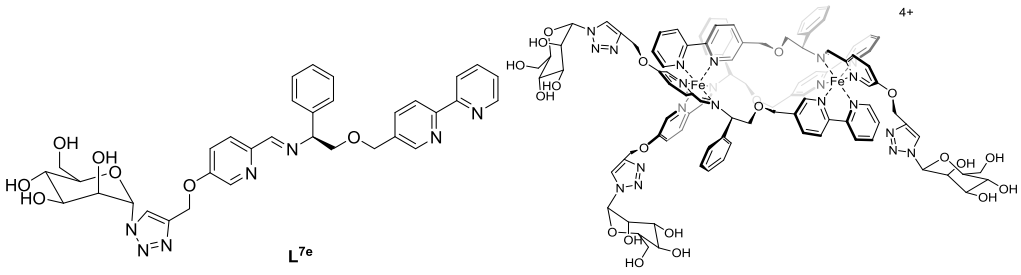

Yield 0.21 g, 88%.

^{1}H NMR (500 MHz, 298 K, D_2O) δ_H 9.56 (1H, s, HC=N), 9.41 (1H, s, HC=N), 9.12 (1H, s, bpy),9.10 (1H, s, bpy), 9.01 (1H, s, HC=N), 8.41-8.37 (3H, m, bpy), 8.26 (2H, m, py/triazole), 8.09 (1H, s, triazole), 8.04-8.01 (2H, m, triazole/Ph), 7.96-6.63 (30H, m, Ph/py/bpy), 6.52 (2H, t, $^3J_{HH}$ = 7.3 Hz, Ph), 6.37 (1H, s, py), 6.08 (1H, s, H_{Man}), 5.98 (1H, s, H_{Man}), 5.92 (1H, s, H_{Man}), 5.26-5.08 (8H, m), 4.93 (1H, d, $^2J_{HH}$ =12.3 Hz,

C$\underline{H}_2$-bpy), 4.65-4.24 (11H, m), 4.17 (1H, t, $^3J_{HH}$ =10.7 Hz, C$\underline{H}_2$-CHPh), 4.10-3.95 (3H, m, H_{Man}), 3.79-3.67 (9H, m, H_{Man}), 3.51 (1H, d, $^3J_{HH}$ =7.0 Hz, C$\underline{H}_2$-CHPh), 3.34-3.14 (5H, m, H_{Man}).

^{13}C {^1H} NMR (126 MHz, 298 K, D_2O) δ_C ppm 170.4, 170.0, 169.5 (CHN), 159.6, 158.9, 158.6, 158.2, 157.9, 157.8, 157.5 (bpy), 157.3 (bpy), 156.8, 156.2, 154.5, 153.8 (bpy), 153.2, 153.2, 152.0, 151.7, 151.5, 143.7, 143.1, 142.6, 142.3 ($\underline{C}$=CH (triazole)), 142.2 ($\underline{C}$=CH (triazole)), 142.2 ($\underline{C}$=CH (triazole)), 139.9, 139.7, 138.8, 138.6, 136.9, 136.7, 136.3, 134.3, 132.5, 132.2, 131.2, 130.8, 130.3, 129.0, 128.8, 128.8, 128.6, 127.3, 127.0, 125.3 (C=$\underline{C}$H (triazole)), 124.9 (C=$\underline{C}$H (triazole)), 124.8 (C=$\underline{C}$H (triazole)), 123.7, 123.6, 123.5, 123.2, 122.8, 122.7, 122.5, 121.9 (Ar), 86.6, 86.6, 86.5 (C_{1Man}), 76.5, 76.4, 76.3 (C_{5Man}), 72.5 ($\underline{C}$HPh), 72.4 ($\underline{C}$HPh), 70.6, 70.5, 70.4 (C_{3Man}), 69.3, 69.2, ($\underline{C}H_2$-bpy) 68.7, 68.4 ($\underline{C}H_2$-CHPh), 67.9 ($\underline{C}H_2$-bpy) 68.3, 68.2 (C_{2Man}), 66.6, 66.5 (C_{4Man}), 61.7, 61.6, 61.3 (TRZ-CH$_2$), 60.4, 60.3 (C_{6Man}).

HRMS Calculated for $[Fe_2L_3]^{4+}$ *m/z* 518.1626, found *m/z* 518.1612

IR *v* cm^{-1} 3277 (br, s), 1559 (s), 1468 (m), 1226 (s), 1110 (m), 1075 (s), 1010 (m), 936 (w), 791 (w), 755 (w), 698 (w).

Elemental Analysis found (Calculated for $C_{102}H_{105}Cl_4Fe_2N_{21}O_{21}\cdot 15H_2O$) % C 49.41 (49.30), H 4.65 (5.48), N 12.16 (11.84).

R_c,Δ_{Fe},HHT-$[Fe_2L^{7e}_3]Cl_4$

Data as for *S*-enantiomer

Yield 0.20 g, 84%.

Elemental Analysis found (Calculated for $C_{102}H_{105}Cl_4Fe_2N_{21}O_{21}\cdot 14H_2O$) % C 49.69 (49.66), H 4.68 (5.43), N 11.83 (11.92).

S_c,Λ_{Fe},HHT-$[Fe_2L^{7f}{}_3]Cl_4$

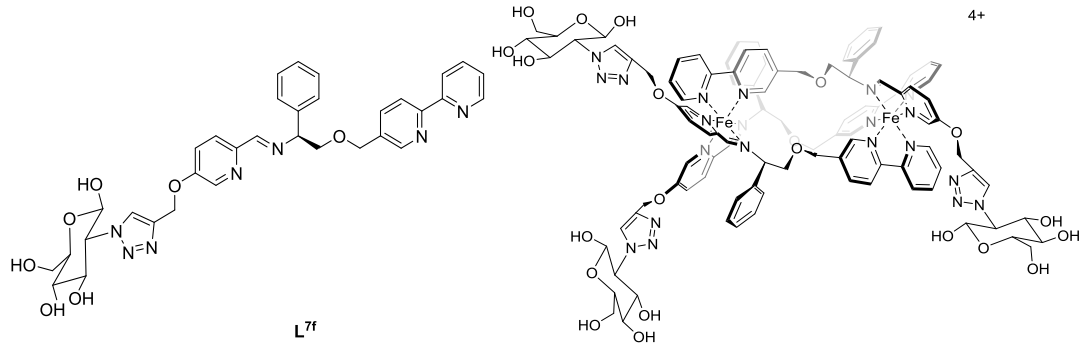

Yield. 0.17g, 83%.

HRMS Calculated for $[Fe_2L_3]^{4+}$ *m/z* 518.1626, found *m/z* 518.1633

IR *v* cm^{-1} 3239 (br, s), 1556 (s), 1468 (m), 1360 (m), 1303 (m), 1224 (s), 1074 (s), 936 (m), 836 (m), 791 (m), 753 (s), 698 (s).

Elemental Analysis found (Calculated for $C_{102}H_{105}Cl_4Fe_2N_{21}O_{21}\cdot 14H_2O$) % C 49.85 (49.66), H 4.78 (5.43), N 12.33 (11.92).

R_c,Δ_{Fe},HHT-$[Fe_2L^{7f}{}_3]Cl_4$

Data as for *S*-enantiomer

Yield 0.19 g, 91%.

Elemental Analysis found (Calculated for $C_{102}H_{105}Cl_4Fe_2N_{21}O_{21}\cdot 14H_2O$) % C 49.48 (49.66), H 4.77 (5.43), N 12.32 (11.92).

S_c,Λ_{Fe},HHT-$[Fe_2L^{7g}{}_3]Cl_4$

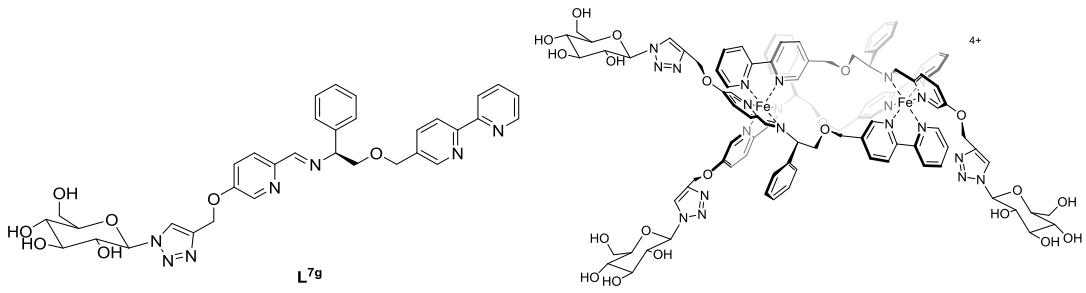

Yield 0.21 g, 88%.

^{1}H NMR (500 MHz, 298 K, D_2O) δ_H 9.55 (1H, s, HC=N), 9.40 (1H, s, HC=N), 9.11 (1H, s, bpy),9.09 (1H, s, bpy), 8.95 (1H, s, HC=N), 8.41-8.35 (3H, m, bpy), 8.30 (1H, s, triazole), 8.26 (1H, d, $^{3}J_{HH}$ =8.8 Hz, Py), 8.01 (2H, m, triazole/Ph), 7.92 (1H, t, $^{3}J_{HH}$ = 7.8 Hz, bpy), 7.88-6.62 (29H, m, Ph/py/bpy), 6.50 (2H, t, $^{3}J_{HH}$ = 7.5 Hz, Ph), 6.27 (1H, s, py), 5.73 (1H, d, $^{3}J_{HH}$ =9.3 Hz, H_{Glu}), 5.66 (1H, d, $^{3}J_{HH}$ =9.3 Hz, H_{Glu}), 5.60 (1H, d, $^{3}J_{HH}$ =9.3 Hz, H_{Glu}), 5.26-5.08 (8H, m), 4.92 (1H, d, $^{2}J_{HH}$ =12.9 Hz, C$\underline{H}_2$-bpy), 4.16 (1H, t, $^{3}J_{HH}$ =10.6 Hz, C$\underline{H}_2$-CHPh), 3.97 (1H, t, $^{3}J_{HH}$ =9.2 Hz, C$\underline{H}_2$-CHPh), 3.87-3.47 (21H, m), 3.33-3.19 (2H, m)

^{13}C {^{1}H} NMR (126 MHz, 298 K, D_2O) δ_C ppm 170.4, 170.0, 169.4 (CHN), 159.6, 158.7, 158.5, 158.2, 157.9, 157.6, 157.4 (bpy), 157.2 (bpy), 156.8, 156.7, 156.0, 154.5 (bpy), 153.8, 153.3, 153.2, 152.0, 151.9, 151.7, 143.0, 142.8, 142.3 (C=CH (triazole)), 142.2 (C=CH (triazole)), 142.0 (C=CH (triazole)), 141.6, 139.9, 139.7, 138.8, 138.6, 136.9, 136.7, 136.3, 134.2, 132.5, 132.2, 131.2, 130.8, 130.2, 129.0, 128.8, 128.8, 128.8, 128.6, 127.2, 127.2, 126.9, 124.9 (C=CH (triazole)), 124.0 (C=CH (triazole)), 123.9 (C=CH (triazole)), 123.7, 123.6, 123.5, 123.4, 123.3, 122.8, 122.5, 121.8 (Ar), 87.5, 87.4, 87.4 (C_{1Glu}), 78.4, 78.9 (C_{5Glu}), 76.0, 75.8, 75.8 (C_{3Glu}), 72.5, 72.4 (CHPh), 72.2 (C_{2Glu}), 70.3 (CHPh), 69.2 (CH_2-bpy), 69.1 (CH_2-bpy), 69.0, 68.9 (C_{4Glu}), 68.7 (CH_2-bpy), 68.5, 68.4, 67.9 (CH_2-CHPh), 61.9, 61.7, 61.3 (TRZ-CH_2), 60.4, 60.4, 60.3 (C_{6Glu})

HRMS Calculated for $[Fe_2L_3]^{4+}$ *m/z* 518.1626, found *m/z* 518.1625

IR *v* cm^{-1} 3307 (br, s), 1557 (m), 1468 (m), 1363 (w), 1227 (s), 1075 (s), 1010 (s), 937 (m), 989 (m), 838 (m), 791 (m), 754 (s), 698 (s).

Elemental Analysis found (Calculated for $C_{102}H_{105}Cl_4Fe_2N_{21}O_{21}\cdot 17H_2O$) % C 48.81 (48.60), H 4.62 (5.56), N 11.67 (11.67).

R_c,Δ_{Fe},HHT-$[Fe_2L^{7g}{}_3]Cl_4$

Data as for *S*-enantiomer

Yield 0.21 g, 89%.

Elemental Analysis found (Calculated for $C_{102}H_{105}Cl_4Fe_2N_{21}O_{21}\cdot 19H_2O$) % C 47.91 (47.92), H 4.70 (5.64), N 11.38 (11.50).

S_c,Λ_{Fe},HHT-$[Fe_2L^{7h}{}_3]Cl_4$

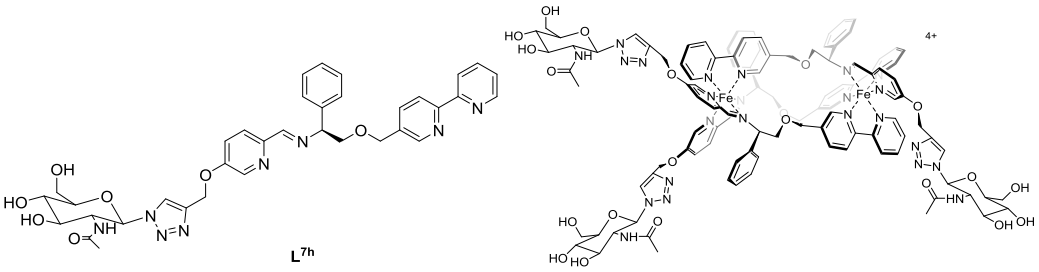

Yield 0.16 g, 79%.

^{1}H NMR (500 MHz, 298 K, D_2O) δ_H 9.54 (1H, s, HC=N), 9.40 (1H, s, HC=N), 9.10 (1H, s, bpy),9.07 (1H, s, bpy), 9.00 (1H, s, HC=N), 8.41-8.33 (4H, m, bpy/triazole), 8.24 (1H, d, $^3J_{HH}$ = 9.0 Hz, py), 8.09 (1H, s, triazole), 8.02-8.00 (2H, m, triazole/Ph), 7.94 (1H, t, $^3J_{HH}$ =7.5 Hz, Ph), 7.87-7.34 (13H, m, Ph/py/bpy), 7.30 (1H, t, $^3J_{HH}$ = 7.55 Hz, Ph), 7.22-6.62 (15H, m, Ph/py/bpy), 6.51 (2H, t, $^3J_{HH}$ = 7.5 Hz, Ph), 6.32 (1H, s, py), 5.85 (1H, d, $^3J_{HH}$ =10.0 Hz), 5.70 (2H, t, $^3J_{HH}$ =9.6 Hz), 5.25-5.05 (8H, m), 4.92 (1H, d, $^2J_{HH}$ =13.1 Hz, C$\underline{H}_2$-bpy), 4.47-4.14 (11H, m), 4.03 (2H, t, $^3J_{HH}$ =10.0 Hz), 3.85-3.55 (19H, m), 3.98 (1H, d, $^3J_{HH}$ =10.0 Hz, C$\underline{H}_2$-CHPh), 3.31 (1H, d, $^3J_{HH}$ =10.0 Hz, C$\underline{H}_2$-CHPh), 3.19 (1H, d, $^3J_{HH}$ =10.0 Hz, C$\underline{H}_2$-CHPh), 1.68 (1H, s, COC$\underline{H}_3$), 1.60 (1H, s, COC$\underline{H}_3$), 1.57 (1H, s, COC$\underline{H}_3$).

^{13}C {^{1}H} NMR (126 MHz, 298 K, D_2O) δ_C ppm 174.1, 173.7, 173.7 ($\underline{C}OCH_3$), 170.4, 170.0, 169.4 (CHN), 159.6, 158.8, 158.5, 158.2, 157.9, 157.7, 157.4 (bpy), 157.2 (bpy), 156.7, 156.6, 156.0, 154.5 (bpy), 153.7, 153.2, 153.1, 151.9, 151.7, 151.5, 143.5, 142.9, 142.4 ($\underline{C}$=CH (triazole)), 142.2, 142.0 ($\underline{C}$=CH (triazole)), 141.9 ($\underline{C}$=CH (triazole)), 139.9, 139.7, 138.8, 138.5, 136.8, 136.7, 136.3, 134.2, 132.5, 132.2, 131.2, 130.8, 130.3, 129.4, 129.0, 128.8, 128.8, 128.6, 127.3, 127.2, 127.0, 127.0, 124.2, 123.7 (C=$\underline{C}$H (triazole)), 123.6, 123.6 (C=$\underline{C}$H (triazole)), 123.5 (C=$\underline{C}$H (triazole)), 123.2, 123.2, 123.1, 122.8, 122.5, 121.9 (Ar), 86.5, 86.5 ($C_{1GlcNac}$), 79.0, 78.9 ($C_{5GlcNac}$), 73.5, 73.3, 73.3 ($C_{3GlcNac}$), 72.5, 72.4, 70.2 ($\underline{C}$HPh), 69.3, 69.2 ($C_{4GlcNac}$), 68.7, 68.4, 67.8 ($\underline{C}H_2$-bpy), 61.7, 61.6, 61.2 ($\underline{C}H_2$-CHPh/TRZ-CH_2), 60.5, 60.4 ($C_{6GlcNac}$), 55.4, 55.4, 55.3 ($C_{2GlcNac}$), 21.7, 21.5, 21.5 (CO$\underline{C}H_3$).

HRMS Calculated for $[Fe_2L_3]^{4+}$ *m/z* 548.9324, found *m/z* 548.9324

IR *v* cm^{-1} 3257 (br, m), 3055 (br, m), 1654 (m), 1556 (s), 1468 (s), 1371 (m), 1304 (m), 1225 (s), 1107 (s), 1075 (s), 1002 (s), 937 (m), 900 (w), 837 (w), 793 (m), 754 (m), 698 (s).

Elemental Analysis found (Calculated for $C_{108}H_{114}Cl_4Fe_2N_{24}O_{21}\cdot 17H_2O$) % C 49.02 (49.06), H 4.91 (5.64), N 12.61 (12.71).

R_c,Δ_{Fe},HHT-$[Fe_2L^{7h}_3]Cl_4$

Data as for *S*-enantiomer

Yield 0.18 g, 91%.

Elemental Analysis found (Calculated for $C_{108}H_{114}Cl_4Fe_2N_{24}O_{21}\cdot 18H_2O$) % C 48.55 (48.73), H 4.90 (5.68), N 12.57 (12.63).

S_c,Λ_{Fe},HHT-[$Fe_2L^{7i}{}_3$]Cl_4

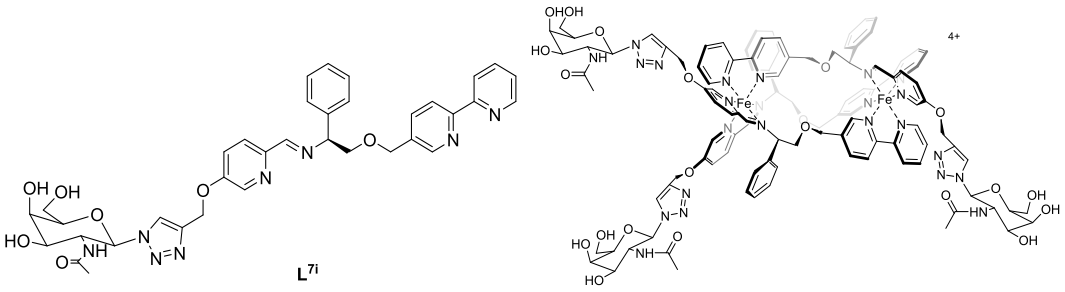

L^{7i}

Yield 0.17 g, 85%.

^{1}H NMR (500 MHz, 298 K, D_2O)δ_H 9.54 (1H, s, HC=N), 9.47 (1H, s, HC=N), 9.13 (1H, s, bpy),9.10 (1H, s, bpy), 9.01 (1H, s, HC=N), 8.42-8.35 (3H, m, bpy), 8.28-8.24 (2H, m, py/ triazole), 8.17 (1H, s, triazole), 8.06 (1H, s, triazole), 8.03-6.79 (28H, m, Ph/py/byp), 6.63 (2H, t, $^3J_{HH}$ = 7.4 Hz, Ph), 6.50 (2H, t, $^3J_{HH}$ = 7.8 Hz, Ph), 6.29 (1H, d, $^4J_{HH}$ =2.4 Hz, py), 5.76-5.62 (3H, m, H_{GalNAc}), 5.27-5.03 (9H, m), 4.92 (1H, d, $^2J_{HH}$ =13.0 Hz, C$\underline{H}_2$-bpy), 4.47-4.36 (6H, m), 4.29-4.15 (5H, m), 4.05-4.01 (3H, m), 3.69-3.87 (6H, m), 3.76-3.71 (6H, m), 3.48 (1H, d, $^3J_{HH}$ = 9.0 Hz, C$\underline{H}_2$-CHPh), 3.31 (1H, d, $^3J_{HH}$ =9.0 Hz, C$\underline{H}_2$-CHPh), 3.20 (1H, d, $^3J_{HH}$ = 9.0 Hz, C$\underline{H}_2$-CHPh), 1.71 (3H, s, OC$\underline{H}_3$), 1.55 (3H, s, OC$\underline{H}_3$), 1.51 (3H, s, OC$\underline{H}_3$).

^{13}C {^{1}H} NMR (126 MHz, 298 K, D_2O) δ_C ppm 174.2, 173.9, 173.8 (C$\underline{O}$CH$_3$), 170.3, 170.0, 169.4 (CHN), 159.6, 158.8, 158.6, 158.2, 157.9, 157.6, 157.4 (bpy), 157.2 (bpy), 156.7, 156.6, 156.2, 154.5 (bpy), 153.8, 153.3, 153.2, 151.8, 151.7, 151.4, 143.6, 143.5, 142.4 (C$\underline{}$=CH (triazole)), 142.2, 142.1 (C$\underline{}$=CH (triazole)), 142.0 (C$\underline{}$=CH (triazole)), 139.9, 139.7, 138.8, 138.5, 136.8, 136.7, 136.3, 134.2, 132.5, 132.2, 131.2, 130.7, 130.2, 129.0, 128.9, 128.8, 128.8, 128.6, 127.3, 127.2, 127.0, 124.2 (C=C$\underline{}$H (triazole)), 123.7, 123.5, 123.4 (C=C$\underline{}$H (triazole)), 123.3 (C=C$\underline{}$H (triazole)), 122.9, 122.8, 122.5, 121.9 (Ar), 87.0 ($C_{1GalNAc}$), 78.5, 78.4, 78.4 ($C_{5\ GalNAc}$), 72.5 (C$\underline{}$HPh), 72.4 (C$\underline{}$HPh), 70.6, 70.5, 70.4 ($C_{3GalNAc}$), 70.3 (C$\underline{}$HPh), 69.2, 69.1, 68.7 (C$\underline{}$H$_2$-bpy),

68.5, 68.4, 67.9 (<u>C</u>H$_2$-CHPh), 67.6 ($C_{4GalNAc}$), 61.6, 61.5, 61.3 (TRZ-CH$_2$), 61.0, 60.9 ($C_{6GalNAc}$), 52.0, 52.0, 51.9 ($C_{2GalNAc}$), 21.7, 21.5 (CO<u>C</u>H$_3$).

HRMS Calculated for $[Fe_2L_3]^{4+}$ *m/z* 548.9325, found *m/z* 548.9335

IR ν cm^{-1} 3242 (br, s), 2987 (br, s), 1654 (m), 1556 (s), 1467 (m), 1370 (m), 1304 (m), 1225 (s), 1076 (s), 1056 (s), 936 (w), 886 (w), 754 (w), 698 (m).

Elemental Analysis found (Calculated for $C_{108}H_{114}Cl_4Fe_2N_{24}O_{21}\cdot 19H_2O$) % C 48.64 (48.40), H 4.72 (5.72), N 12.70 (12.54).

R_c,Δ_{Fe},HHT-$[Fe_2L^{7i}{}_3]Cl_4$

Data as for *S*-enantiomer

Yield 0.18 g, 90%.

Elemental Analysis found (Calculated for $C_{108}H_{114}Cl_4Fe_2N_{24}O_{21}\cdot 17H_2O$) % C 49.04 (49.06), H 4.76 (5.64), N 12.57 (12.71).

S_c,Λ_{Fe},HHT-$[Fe_2L^{8a}{}_3]Cl_4$

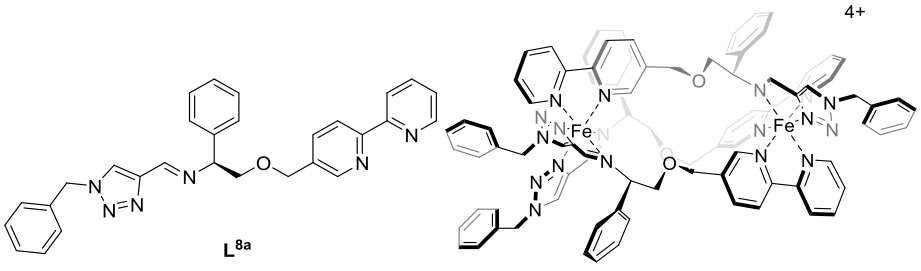

S_c,Λ_{Fe},HHT-$[Fe_2L^{8a}{}_3]Cl_4$ was synthesised using the procedure described for S_c,Λ_{Fe},HHT-$[Fe_2L^{3}{}_3]Cl_4$, substituting 5-(propargyloxy)picolinaldehyde (**5**) for 1-benzyl-1H-1,2,3-triazole-4-carbaldehyde (**37**)

Yield 0.58 g, 81%

^{1}H NMR (500 MHz, 298 K, MeOD) δ_H ppm 9.65 (1H, s, HC=N), 9.47 (1H, s, HC=N), 9.39 (1H, s, bpy), 9.30 (1H, s, bpy), 9.20 (1H, s, HC=N), 9.19 (1H, s, TRZ), 9.01 (1H, s, TRZ), 8.75-8.56 (5H, m, bpy), 8.35 (1H, s, TRZ), 8.26-7.89 (13H, m, bpy), 7.78-7.74 (2H, m, bpy), 7.50-6.93 (42H, m, Ph/bpy), 6.78 (2H, t, $^{3}J_{HH}$ =7.6 Hz, Ph), 6.60 (2H, t, $^{3}J_{HH}$ =7.7 Hz, Ph), 5.90 (1H, s, Ph), 5.68 (2H, s, PhC$\underline{H}_2$), 5.64-5.50 (4H, m, PhC$\underline{H}_2$), 5.34 (1H, dt, $^{3}J_{HH}$=15.1, 7.4 Hz, C$\underline{H}$Ph), 5.25 (2H, d, $^{2}J_{HH}$=13.0 Hz, C$\underline{H}_2$-bpy), 5.14 (1H, d, $^{2}J_{HH}$=18.1 Hz, C$\underline{H}_2$-bpy), 4.78 (1H, d, $^{3}J_{HH}$=11.3 Hz, C$\underline{H}$Ph), 4.60-4.48 (6H, m, C$\underline{H}$Ph / C$\underline{H}_2$-bpy), 4.28 (1H, t, $^{3}J_{HH}$=11.0 Hz), 3.54-3.51 (3H, m, C$\underline{H}_2$-CHPh), 3.43-3.41 (1H, m, C$\underline{H}_2$-CHPh), 3.37 (1H, C$\underline{H}_2$-CHPh overlap with MeOD).

^{13}C {^{1}H} NMR (125 MHz, 298 K, CD_3OD) δ_C ppm 163.4, 163.1, 162.6 (HC=N), 160.1, 159.9, 159.3, 159.2, 158.5, 158.4 (q, bpy), 157.9, 157.2, 155.8, 154.3, 154.0, 153.3 (bpy), 149.5, 149.5, 149.4 (q, TRZ), 139.9, 139.8, 139.5, 138.7, 138.5, 138.3, 137.7 (bpy), 137.4, 136.8, 136.8 (q, bpy), 134.4, 134.2, 134.1, 134.0, 133.4, 132.9, 132.5 (q, Ph), 130.2 (TRZ), 129.3, 129.2, 129.0 (Ph), 129.0 (TRZ), 128.9, 128.9, 128.8, 128.7, 128.6 (Ph), 128.3 (TRZ), 127.9, 127.5, 127.3, 127.2, 127.2, 127.2 (Ph), 126.9, 126.3, 125.8, 125. 6, 123. 5, 123.0, 122.7, 122.5, 122.4, 121.6 (bpy), 72.9, 72.6 (C$\underline{H}$Ph), 71.3 (C$\underline{H}_2$-bpy), 70.8 (C$\underline{H}$Ph), 69.1, 69.1 (C$\underline{H}_2$-bpy), 68.7, 68.5, 68.5 (C$\underline{H}_2$-CHPh), 55.6, 55.5, 55.2 (Ph$\underline{C}H_2$).

HRMS Calculated for $[Fe_2L_n]^{4+}$ *m/z* 383.6292, found *m/z* 383.6297

Elemental Analysis found (Calculated for $C_{87}H_{78}Cl_4Fe_2N_{18}O_3 \cdot 13H_2O \cdot EtOAc$) % C 54.44 (54.66), H 5.12 (5.65), N 12.31 (12.61).

IR *v* cm^{-1} 3371 (br, s), 3028 (br, s), 1603 (m), 1468 (m), 1359 (w), 1076 (s), 1010 (w), 933 (w), 697 (s).

R_c,Δ_{Fe},HHT-$[Fe_2L^{8a}{}_3]Cl_4$

Yield 0.57 g, 79%

HRMS Calculated for $[Fe_2L_n]^{4+}$ *m/z* 383.6297, found *m/z* 383.6297

Elemental Analysis found (Calculated for $C_{87}H_{78}Cl_4Fe_2N_{18}O_3 \cdot 13H_2O \cdot EtOAc$) % C 54.20 (54.66), H 5.17 (5.65), N 12.24 (12.61).

S_c,Λ_{Fe},HHT-$[Fe_2L^{8b}{}_3]Cl_4$

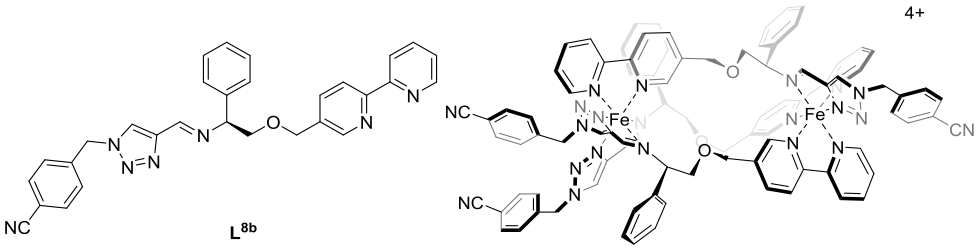

S_c,Λ_{Fe},HHT-$[Fe_2L^{8b}{}_3]Cl_4$ was synthesised using the procedure described for S_c,Λ_{Fe},HHT-$[Fe_2L^{3}{}_3]Cl_4$, substituting 5-(propargyloxy)picolinaldehyde (**5**) for 4-((4-formyl-1H-1,2,3-triazol-1-yl)methyl)benzonitrile (**39**)

Yield 0.65 g, 88%

^{1}H NMR (500 MHz, 298 K, MeOD) δ_H 9.69 (1H, s, HC=N), 9.54 (1H, s, HC=N), 9.40 (1H, s, bpy), 9.31 (1H, s, bpy), 9.30 (1H, s, HC=N), 9.29 (1H, s, TRZ), 9.12 (1H, s, TRZ), 8.76-6.93 (42H, m, Ph/TRZ/bpy), 6.79 (2H, t, $^3J_{HH}$ =7.6 Hz, Ph), 6.61 (2H, t, $^3J_{HH}$ =7.6 Hz, Ph), 5.93 (1H, brs, Ph), 5.82-5.65 (6H, m, CNPhC$\underline{H}_2$), 5.42-5.32 (1H, m, C$\underline{H}$Ph), 5.28 (2H, d, $^2J_{HH}$=12.7 Hz, C$\underline{H}_2$-bpy), 5.18 (1H, d, $^2J_{HH}$=12.9 Hz, C$\underline{H}_2$-bpy), 4.79 (1H, d, $^3J_{HH}$=12.9 Hz, C$\underline{H}$Ph), 4.68-4.35 (8H, m, C$\underline{H}$Ph/C$\underline{H}_2$-bpy), 3.86-3.61 (3H, m, C$\underline{H}_2$-CHPh), 3.57-3.54 (1H, m, C$\underline{H}_2$-CHPh), 3.43 (1H, d, $^3J_{HH}$=8.6 Hz, C$\underline{H}_2$-CHPh), 3.37 (1H, C$\underline{H}_2$-CHPh overlap with MeOD).

^{13}C {^{1}H} NMR (125 MHz, 298 K, CD_3OD) δ_C ppm 163.5, 163.3, 162.8 (HC=N), 160.1, 159.8, 159.2, 159.1 (q, bpy), 158.4, 158.4, 158.3, 157.9, 157.3, 155.8, 154.4, 154.1, 153.9, 153.7, 153.3 (bpy), 149.8, 149.6, 149.5 (q, TRZ), 140.0, 139.9, 139.6 (bpy), 139.4, 139.2 (q, bpy), 138.7, 138.7, 138.5 (bpy), 138.4 (q, bpy), 137.8 (bpy), 137.5, 137.0, 136.8 (q, bpy), 134.5, 134.2 (q, Ph), 132.8, 132.8, 132.6, 132.5, 132.4 (CNPh), 130.7 (TRZ), 129.4, 129.3 (Ph), 129.0 (TRZ), 128.9, 128.7, 128.6, 128.4 (Ph), 128.4 (TRZ), 128.3, 127.3, 127.2, 127.2, 127.2, 126.9 (Ph), 126.4, 125.9, 125.6, 123.9, 123.7, 123.6, 123.5, 123.0, 122.7, 122.5, 122.4, 121.5 (bpy), 117.8, 117.7, 117.6 (q, CNPh), 112.8, 112.6, 112.3 (CN), 73.0 (CHPh), 72.6 (CHPh), 71.4 (CH_2-bpy), 70.9 (CHPh), 69.2, 69.0 (CH_2-bpy), 68.7, 68.6, 68.5 (CH_2-CHPh), 54.8, 54.6, 54.4 (Benzonitrile-CH_2).

HRMS Calculated for $[Fe_2L_n]^{4+}$ *m/z* 402.3761, found *m/z* 402.3748

Elemental Analysis found (Calculated for $C_{90}H_{75}Cl_4Fe_2N_{21}O_3 \cdot 12H_2O \cdot 3EtOAc$) % C 54.81 (54.87), H 4.79 (5.55), N 13.26 (13.17).

IR *v* cm^{-1} 3394 (br, s), 3028 (br, s), 1603 (m), 1467 (m), 1078 (s), 934 (w), 790 (s), 755 (s), 698 (s).

R_c,Δ_{Fe},HHT-$[Fe_2L^{8b}{}_3]Cl_4$

Yield 0.59 g, 80%

HRMS Calculated for $[Fe_2L_n]^{4+}$ *m/z* 402.3761, found *m/z* 402.3758

Elemental Analysis found (Calculated for $C_{90}H_{75}Cl_4Fe_2N_{21}O_3 \cdot 11H_2O \cdot 3EtOAc$) % C 55.44 (55.32), H 4.73 (5.51), N 13.36 (13.28).

S_c,Λ_{Fe},HHT-$[Fe_2L^{8c}{}_3]Cl_4$

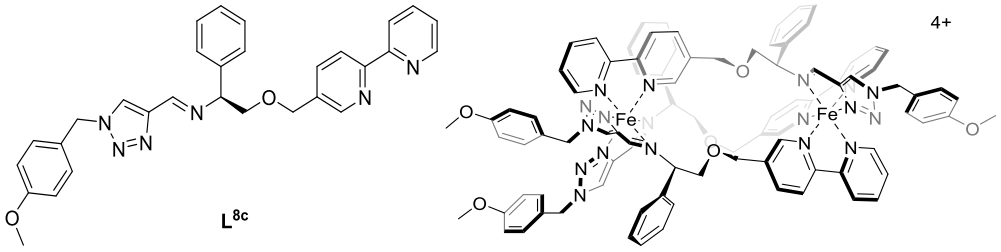

S_c,Λ_{Fe},HHT-$[Fe_2L^{8c}{}_3]Cl_4$ was synthesised using the procedure described for S_c,Λ_{Fe},HHT-$[Fe_2L^{3}{}_3]Cl_4$, substituting 5-(propargyloxy)picolinaldehyde (**5**) for 1-(4-methoxybenzyl)-1H-1,2,3-triazole-4-carbaldehyde (**40**)

Yield 0.42 g, 83%

^{1}H NMR (500 MHz, 298 K, MeOD) δ_H ppm 9.65 (1H, s, HC=N), 9.47 (1H, s, HC=N), 9.39 (1H, s, bpy), 9.30 (1H, s, bpy), 9.19 (1H, s, HC=N), 9.12 (1H, s, TRZ), 8.96 (1H, s, TRZ), 8.85-8.51 (7H, m, bpy), 8.26 (1H, s, TRZ), 8.25-7.73 (18H, m, TRZ/bpy), 7.57-6.82 (50H, m, Ph/bpy), 6.78 (2H, t, $^3J_{HH}$ =7.7 Hz, Ph), 6.60 (2H, t, $^3J_{HH}$ =7.7 Hz, Ph), 5.90 (1H, brs, Ph), 5.68-5.42 (6H, m, C$\underline{H}_2$PhOCH$_3$), 5.34 (1H, dd, $^3J_{HH}$=11.3, $^4J_{HH}$=3.7 Hz, C$\underline{H}$Ph), 5.25 (2H, d, $^2J_{HH}$=11.9 Hz, C$\underline{H}_2$-bpy), 5.16 (1H, d, $^2J_{HH}$=13.0 Hz, C$\underline{H}_2$-bpy), 4.77 (1H, d, $^3J_{HH}$=8.6 Hz, C$\underline{H}$Ph), 4.68-4.42 (6H, m, C$\underline{H}$Ph / C$\underline{H}_2$-bpy), 4.29 (1H, t, $^3J_{HH}$=10.9 Hz C$\underline{H}_2$-CHPh), 3.90-3.61 (9H, m, OCH$_3$/ C$\underline{H}_2$-CHPh), 3.56-3.49 (1H, m, C$\underline{H}_2$-CHPh), 3.44-3.39 (1H, m, C$\underline{H}_2$-CHPh), 3.37 (1H, C$\underline{H}_2$-CHPh overlap with MeOD).

^{13}C {^{1}H} NMR (125 MHz, 298 K, CD$_3$OD) δ_C ppm 163.4, 163.1, 162.5 (HC=N), 160.7, 160.4, 160.3 (q, $\underline{Ph}$OCH$_3$), 160.1, 159.9, 159.3, 159.2, 158.5, 158.4 (q, bpy), 157.9, 157.3, 155.7, 154.3, 154.0, 153.3 (bpy), 149.4, 149.4, 149.3 (q, TRZ), 139.9, 139.8, 139.5, 138.7, 138.5, 138.3, 137.7 (bpy), 137.4, 136.8 (q, bpy), 134.4, 132.9, 132.5 (q, Ph), 130.6, 129.6, 129.3, 129.0, 129.0, 128.7, 128.6, 128.3, 128.3, 127.3, 127.2, 127.2,

127.2 (TRZ/ PhOCH$_3$/ Ph), 126.3 (bpy), 126.0 (q, PhOCH$_3$), 125.8 (bpy), 125.7 (q, PhOCH$_3$), 125.6 (bpy), 125.2 (q, PhOCH$_3$), 123.9, 123.7, 123.5, 123.0, 122.7, 122.5, 122.4, 121.5 (bpy), 114.2, 114.1, 114.0 (PhOCH$_3$), 72.9 (CHPh), 72.6 (CHPh), 71.5 (CH$_2$-bpy), 70.8 (CHPh), 69.1, 68.9 (CH$_2$-bpy), 68.8, 68.5, (CH$_2$-CHPh), 55.3, 55.1, 54.9 (Anisole-CH$_2$), 54.6, 54.5, 54.4 (OCH$_3$).

HRMS Calculated for $[Fe_2L_n]^{4+}$ *m/z* 406.1376, found *m/z* 406.1380

Elemental Analysis found (Calculated for $C_{90}H_{84}Cl_4Fe_2N_{18}O_6 \cdot 14H_2O \cdot EtOAc$) % C 53.31 (53.57), H 5.01 (5.74), N 11.75 (11.96).

IR *v* cm^{-1} 3375 (br, s), 3026 (br, s), 1604 (m), 1512 (m), 1466 (m), 1246 (m), 1076 (s), 1023 (s), 755 (s), 697 (s).

R$_c$,Δ$_{Fe}$,HHT-[Fe$_2$L$^{8c}{}_3$]Cl$_4$

Yield 0.44 g, 87%

HRMS Calculated for $[Fe_2L_n]^{4+}$ *m/z* 406.1376, found *m/z* 406.1380

Elemental Analysis found (Calculated for $C_{90}H_{84}Cl_4Fe_2N_{18}O_6 \cdot 14H_2O \cdot EtOAc$) % C 53.46 (53.57), H 5.03 (5.74), N 11.52 (11.96).

S$_c$,Λ$_{Fe}$,HHT-[Fe$_2$L$^{8d}{}_3$]Cl$_4$

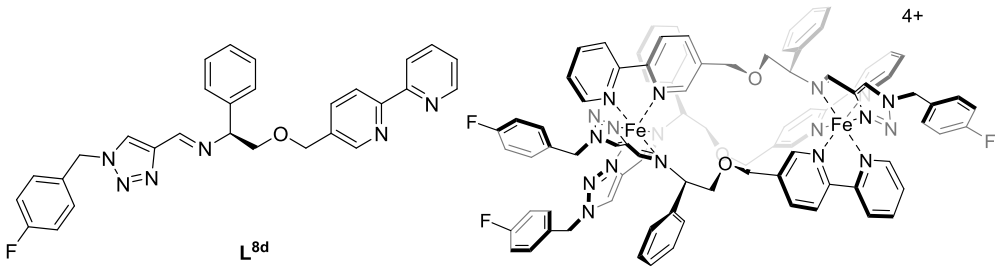

S_c,Λ_{Fe},HHT-[$Fe_2L^{8d}{}_3$]Cl_4 was synthesised using the procedure described for S_c,Λ_{Fe},HHT-[$Fe_2L^{3}{}_3$]Cl_4, substituting 5-(propargyloxy)picolinaldehyde (**5**) for 1-(4-fluorobenzyl)-1H-1,2,3-triazole-4-carbaldehyde (**38**)

Yield 0.38 g, 78%

^{1}H NMR (500 MHz, 298 K, MeOD) δ_H ppm 9.67 (1H, s, HC=N), 9.50 (1H, s, HC=N), 9.38 (1H, s, bpy), 9.30 (1H, s, bpy), 9.23 (1H, s, HC=N), 9.20 (1H, s, TRZ), 9.03 (1H, s, TRZ), 8.79-8.52 (7H, m, bpy), 8.34 (1H, s, TRZ), 8.29-7.72 (18H, m, bpy), 7.55-6.85 (50H, m, Ph/F-Ph/bpy), 6.78 (2H, t, $^3J_{HH}$ =7.6 Hz, Ph), 6.60 (2H, t, $^3J_{HH}$ =7.6 Hz, Ph), 6.19-5.82 (4H, m, Ph), 5.73-5.46 (6H, m, F-PhC$\underline{H}_2$), 5.35 (1H, dd, $^3J_{HH}$=11.4, $^4J_{HH}$=3.5 Hz, C$\underline{H}$Ph), 5.25 (2H, d, $^2J_{HH}$=13.1 Hz, C$\underline{H}_2$-bpy), 5.16 (1H, d, $^3J_{HH}$=13.0 Hz, C$\underline{H}_2$-bpy), 4.77 (1H, d, $^3J_{HH}$=8.8 Hz, C$\underline{H}$Ph), 4.67-4.43 (6H, m, C$\underline{H}$Ph/ C$\underline{H}_2$-bpy), 4.30 (1H, t, $^3J_{HH}$=11.0 Hz $\underline{C}H_2$-CHPh), 3.88-3.63 (3H, m, $\underline{C}H_2$-CHPh)3.54 (1H, dd, $^3J_{HH}$=10.4, 3.6 Hz $\underline{C}H_2$-CHPh), 3.42 (1H, d, $^3J_{HH}$=8.4 Hz $\underline{C}H_2$-CHPh), 3.37 (1H, $\underline{C}H_2$-CHPh overlap with MeOD).

^{13}C {^{1}H} NMR (125 MHz, 298 K, CD_3OD) δ_C ppm 164.3, 164.0, 163.9 (q, F-Ph), 163.4, 163.2, 162.6 (HC=N), 162.3, 162.1, 161.9 (q, F-Ph), 160.1, 159.8, 159.3, 159.1, 158.5, 158.4 (q, bpy), 157.9, 157.3, 155.7, 154.3, 154.0, 153.3 (bpy), 149.6, 149.5, 149.4 (q, TRZ), 139.9, 139.8, 139.5, 138.7, 138.5, 138.3, 137.7 (bpy), 137.4, 136.9, 136.8 (q, bpy), 134.4, 132.9, 132.5 (q, Ph), 131.2, 131.1, 130.4, 130.3, 130.0, 129.9 (F-Ph), 129.3, 129.0, 129.0, 128.9, 128.8, 128.7, 128.6, 128.6, 128.3, 127.3, 127.2, 127.2, 127.2, 126.9 (TRZ/ Ph), 126.3, 125.8, 125.6, 123.5, 123.0, 122.7, 122.5, 122.4, 121.5 (bpy), 115.8, 115.7, 115.6, 115.5, 115.5, 115.3 (F-$\underline{Ph}$), 72.9 ($\underline{C}$HPh), 72.6 ($\underline{C}$HPh), 71.3 ($\underline{C}H_2$-bpy), 70.8 ($\underline{C}$HPh), 69.1, 69.0 ($\underline{C}H_2$-bpy), 68.7, 68.5, 68.5 ($\underline{C}H_2$-CHPh), 54.8, 54.6, 54.4 (PhF-$\underline{C}H_2$).

HRMS Calculated for $[Fe_2L_n]^{4+}$ *m/z* 397.1226, found *m/z* 397.1221

Elemental Analysis found (Calculated for $C_{87}H_{75}Cl_4F_3Fe_2N_{18}O_3 \cdot 13H_2O \cdot EtOAc$) % C 53.23 (53.23), H 4.91 (5.35), N 11.98 (12.28).

IR *v* cm^{-1} 3374 (br, s), 3026 (br, s), 1602 (m), 1509 (m), 1468 (m), 1220 (m), 1077 (s), 1009 (m), 753 (s), 697 (s).

R_c,Δ_{Fe},HHT-$[Fe_2L^{8d}{}_3]Cl_4$

Yield 0.36 g, 75%

HRMS Calculated for $[Fe_2L_n]^{4+}$ *m/z* 397.1226, found *m/z* 397.1224

Elemental Analysis found (Calculated for $C_{87}H_{75}Cl_4F_3Fe_2N_{18}O_3 \cdot 13H_2O \cdot EtOAc$) % C 53.45 (53.23), H 4.69 (5.35), N 11.75 (12.28).

S_c,Λ_{Fe},HHT-$[Fe_2L^{8e}{}_3]Cl_4$

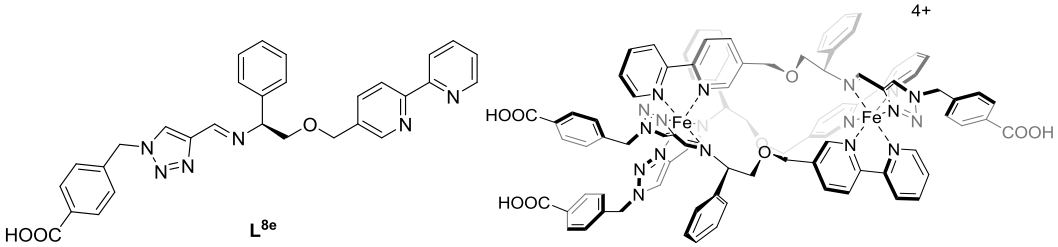

S_c,Λ_{Fe},HHT-$[Fe_2L^{8e}{}_3]Cl_4$ was synthesised using the procedure described for S_c,Λ_{Fe},HHT-$[Fe_2L^{3}{}_3]Cl_4$, substituting 5-(propargyloxy)picolinaldehyde (**5**) for 4-((4-formyl-1H-1,2,3-triazol-1-yl)methyl)benzoic acid (**39**)

Yield 0.44 g, 86%

^{13}C {^1H} NMR (125 MHz, 298 K, CD_3OD) δ_C ppm 163.4, 163.2, 162.6 (HC=N), 160.1, 159.8, 159.3, 159.2, 159.0, 158.5, 158.4, 158.3, 158.2, 157.9 (bpy), 157.3 (bpy), 155.8 (bpy), 154.4, 153.9, 153.7, 153.3, 153.1, 152.5, 151.9, 149.6 (q, TRZ), 149.6 (q, TRZ),

149.5 (q, TRZ), 139.9, 139.8, 139.6, 138.7, 138.5, 138.3, 138.3, 138.0, 137.8, 137.5, 136.9, 136.8, 134.4, 134.0, 134.0, 133.9, 132.8, 132.5, 130.0 (TRZ), 129.3, 129.3, 129.3, 129.0 (TRZ), 129.0, 128.7, 128.6, 128.3 (TRZ), 127.7, 127.6, 127.4, 127.2, 127.2, 127.2, 126.4, 125.9, 125.6, 123.9, 123.7, 123.6, 123.5, 123.0, 122.7, 122.5, 121.5 (Ar), 73.0 (CHPh), 72.6 (CHPh), 71.3 (CH_2-bpy), 70.8 (CHPh), 69.2, 69.1 (CH_2-bpy), 69.0, 68.7, 68.5 (CH_2-CHPh), 55.0, 55.0, 54.7 (Ph-CH_2).

HRMS Calculated for $[Fe_2L_n]^{4+}$ *m/z* 416.6221, found *m/z* 416.6219

Elemental Analysis found (Calculated for $C_{90}H_{78}Cl_4Fe_2N_{18}O_9 \cdot 15H_2O \cdot EtOAc$) % C 52.05 (52.09), H 4.76 (5.39), N 11.13 (11.63).

IR *v* cm^{-1} 3371 (br, s), 2851 (br, s), 1694 (m), 1591 (m), 1525 (m), 1467 (m), 1401 (s), 1077 (s), 753 (s), 698 (s).

R_c,Δ_{Fe},HHT-$[Fe_2L^{8e}{}_3]Cl_4$

Yield 0.42 g, 82%

HRMS Calculated for $[Fe_2L_n]^{4+}$ *m/z* 416.6221, found *m/z* 416.6227

Elemental Analysis found (Calculated for $C_{90}H_{78}Cl_4Fe_2N_{18}O_9 \cdot 16H_2O \cdot EtOAc$) % C 51.49 (51.66), H 4.69 (5.44), N 11.35 (11.54).

S_c,Λ_{Fe},HHT-$[Fe_2L^{10}{}_3]Cl_4$

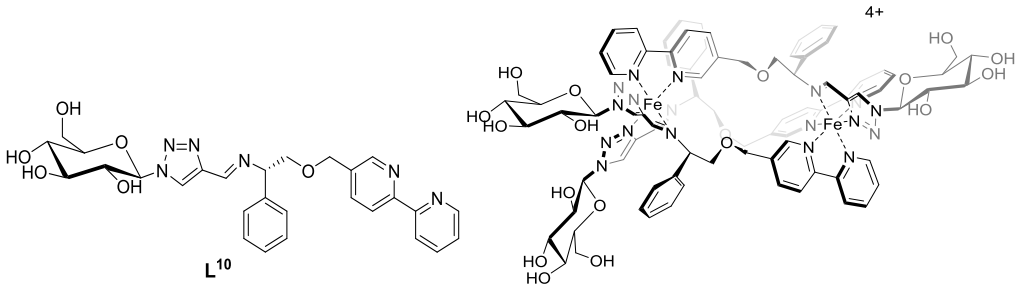

S_c,Λ_{Fe},HHT-[$Fe_2L^{10}{}_3$]Cl_4 was synthesised using the procedure described for S_c,Λ_{Fe},HHT-[$Fe_2L^{3}{}_3$]Cl_4, substituting 5-(propargyloxy)picolinaldehyde (**5**) for 1-((*2R,3R,4S,5S,6R*)-3,4,5-trihydroxy-6-(hydroxymethyl)tetrahydro-2H-pyran-2-yl)-1H-1,2,3-triazole-4-carbaldehyde (**49**)

Yeild: 99 mg, 58 %.

^{1}H NMR (500 MHz, 298 K, MeOD) δ_H ppm 9.75 (s, 1H), 9.53 (s, 1H), 9.51 (s, 1H), 9.44 (s, 1H), 9.36 (s, 1H), 9.26 (s, 1H), 9.17 (s, 1H), 8.67 (m, 4H), 8.20 (m, 12H), 8.05 (m, 2H), 7.99 (s, 1H), 7.92 (s, 2H), 7.74 (s, 2H), 7.40 (m, 10H), 7.07 (m, 2H), 6.94 (s, 1H), 6.88 (s, 1H), 6.78 (s, 2H), 6.60 (s, 2H), 5.88 (s, 1H), 5.66 (d, $^3J_{HH}$ = 8.0 Hz, 1H), 5.61 (d, $^3J_{HH}$ = 8.0 Hz, 2H), 5.55 (d, $^3J_{HH}$ = 9.0 Hz, 1H), 5.42 (t, $^3J_{HH}$ = 11.5 Hz, 2H), 5.29 (t, $^3J_{HH}$ = 19.5 Hz, 2H), 5.19 (d, $^3J_{HH}$ = 12.5 Hz, 2H), 4.52 (m, 6H), 4.01 (t, $^3J_{HH}$ = 18.5 Hz, 2H), 3.66 (m, 13H).

^{13}C NMR (125 MHz, 298 K, MeOH) δ_c ppm 164.9, 164.8, 164.1 (HC=N), 161.4, 161.3, 160.6, 160.5, 159.8, 159.7 (q, bpy), 159.2, 158.7, 157.0, 155.6, 154.6 (bpy), 151.2, 151.1, 150.7 (q, TRZ), 141.6, 141.3, 140.2, 139.9, 139.2 (bpy), 138.7, 138.3, 138.2 (q, bpy), 135.3, 134.2, 133.8 (q, Ph), 130.9, 130.7, 130.1, 129.7, 128.6 (Ph/TRZ), 127.8, 127.3, 126.9, 125.3, 124.9, 124.6, 124.2, 124.1, 124.0, 123.2 (bpy), 89.3, 89.1, 89.1 (C_{1Glu}), 80.3, 80.2, 80.0 (C_{5Glu}), 77.4, 76.8, 76.7 (C_{3Glu}), 74.5, 74.3 (CHPh), 74.1, 74.0 (C_{2Glu}), 73.9 (CHPh), 72.6 (OCH_2-bpy), 72.5, 70.9 (C_{4Glu}), 70.3, 69.9 (CH_2-CHPh), 62.4, 62.2, 62.0 (C_{6Glu}).

IR v cm^{-1} 3242 (br, s), 2864 w, 1604 m, 1360 m, 1219 m, 1016 s

MS (ESI) *m/z* 547.3 $[L + H]^+$

HRMS Calculated for $[Fe_2L_n]Cl_2^{2+}$ *m/z* 910.2376, found *m/z* 910.2362

Elemental analysis found (Calculated for $C_{84}H_{90}N_{18}O_{18}Cl_4Fe_2 \cdot 15H_2O$) % C 46.37 (46.63) H 4.90 (4.79) N 10.78 (11.65)

R_c,Δ_{Fe},HHT-$[Fe_2L^{10}{}_3]Cl_4$

Yeild: 88 mg, 70 %.

IR v cm^{-1} 3242 (br, s), 2859 w, 1604 w, 1441 w, 1357 w, 1225 w, 1073 s, 699 m

MS (ESI) *m/z* 547.4 $[L + H]^+$

Elemental analysis found (Calculated for $C_{84}H_{90}N_{18}O_{18}Cl_4Fe_2 \cdot 10H_2O$) % C 48.74 (48.66) H 5.03 (5.35) N 11.48 (12.16)

6.5 Circular dichroism

Samples were dissolved in methanol to 0.1 mg/mL and the spectra were measured on a Jasco J-815 spectrometer. Measurements were collected using a 0.1 cm path-length quartz cuvette. The parameters used were; bandwidth 1 nm, response time 1 sec, wavelength scan range 200-800 nm, data pitch 0.2 nm, scanning speed 100 nm/min and accumulation 10.

6.6 Absorbance spectroscopy and stability

UV-vis absorbance spectra for stability studies were recorded using a Carey IE spectrometer. Measuerments were collected in a 1 cm path-length polystyrene cuvette and the standard parameters used were bandwidth 1 nm, response time 1 sec, wavelength scan rang 200-800 nm, data pitch 1 nm, scanning speed 200 nm/min and accumulation 1. A concentration of each compound (0.01 mg/mL) was measured in pH 7 aqueous solution.

6.7 Chemosensitivity (MTT assay)

HCT116 p^{53++} (human colon carcinoma) cells or ARPE19 (human retinal pigment epithelial) cells were incubated in 96-well plates at a cell concentration of 0.5×10^4 cells/ml. The cells were used when between 50 and 80% confluent in the stock flasks. Complete cell media containing DMEM, supplemented with 10% foetal calf serum and L-glutamine (2 mM), was used to prepare the desired cell concentration and reference wells. Plates containing cells were incubated for 24 h at 37°C in an atmosphere of 5% CO^2, prior to drug exposure. Cell media (200 µl) was added to the reference cells and differing concentrations of drug solution (200 µl) were added to the remaining wells. The plates were incubated for a further 96 h at 37°C in an atmosphere of 5% CO_2. 3- (4,5-Dimethylthiazol-1-yl)-2,5-diphenyltetrazolium bromide (MTT) solution (0.5 mg/ml, 20µl per well) was added to each well and incubated for a further 4 h at 37°C in an atmosphere of 5% CO^2. Upon completion all solutions were removed from the wells and dimethyl sulfoxide (150 µl) was added to each well to dissolve the purple formazan crystals. A Thermo Scientific Multiskan EX microplate photometer was used to measure the absorbance at 540 nm. Lanes containing 100% cell media and untreated cells were used as a blank and 100% cell survival respectively. Cell survival was determined as the absorbance of treated cells minus the blank cell media, divided by the absorbance of the untreated control; this value was expressed as a percentage. The IC_{50} values were determined from a plot of percentage cell survival against drug concentration (µM). All assays were conducted in triplicate and the mean IC_{50} ± standard deviation was determined.

6.8 References

1. S. E. Howson, L. E. Allan, N. P. Chmel, G. J. Clarkson, R. van Gorkum and P. Scott, *Chem. Commun.*, 2009, 1727-1729.
2. S. M. Bakunova, S. A. Bakunov, T. Wenzler, T. Barszcz, K. A. Werbovetz, R. Brun and R. Tidwell, *J. Med. Chem.*, 2009, **52**, 4657-4667.
3. S. E. Howson, A. Bolhuis, V. Brabec, G. J. Clarkson, J. Malina, A. Rodger and P. Scott, *Nat. Chem.*, 2012, **4**, 31-36.
4. M. Seredyuk, A. Gaspar, V. Ksenofontov, Y. Galyametdinov, J. Kusz and P. Gütlich, *J. Am. Chem. Soc.*, 2008, **130**, 1431-1439.
5. Y. Hsiao and L. Hegedus, *J. Org. Chem.*, 1997, **62**, 3586-3591.
6. P. Das, A. Ghosh, M. K. Kesharwani, V. Ramu, B. Ganguly and A. Das, *Eur. J. Inorg. Chem.*, 2011, **2011**, 3050-3058.
7. R. Ballardini, V. Balzani, M. Clemente-León, A. Credi, M. T. Gandolfi, E. Ishow, J. Perkins, J. F. Stoddart, H.-R. Tseng and S. Wenger, *J. Am. Chem. Soc.*, 2002, **124**, 12786-12795.
8. C. Dallaire, I. Kolber and M. Gingras, *Org. Synth.*, 2002, 42-42.
9. A. D. Faulkner, R. A. Kaner, Q. M. Abdallah, G. Clarkson, D. J. Fox, P. Gurnani, S. E. Howson, R. M. Phillips, D. I. Roper and D. Simpson, *Nat. Chem.*, 2014, **6**, 797.
10. W. G. Kim, M. E. Kang, J. B. Lee, M. H. Jeon, S. Lee, J. Lee, B. Choi, P. M. Cal, S. Kang and J.-M. Kee, *J. Am. Chem. Soc.*, 2017, **139**, 12121-12124.
11. Y. Liu, Q. Xiao, Y. Liu, Z. Li, Y. Qiu, G. B. Zhou, Z. J. Yao and S. Jiang, *Eur. J. Med. Chem.*, 2014, **78**, 248-258.
12. S. Lal, H. S. Rzepa and S. Diez-Gonzalez, *ACS Catal.*, 2014, **4**, 2274-2287.
13. M. I. Montanez, Y. Hed, S. Utsel, J. Ropponen, E. Malmstrom, L. Wagberg, A. Hult and M. Malkoch, *Biomacromolecules*, 2011, **12**, 2114-2125.
14. O. G. Adesoye, I. N. Mills, D. P. Temelkoff, J. A. Jackson and P. Norris, *J. Chem. Educ.*, 2012, **89**, 943-945.
15. V. Percec, P. Leowanawat, H. J. Sun, O. Kulikov, C. D. Nusbaum, T. M. Tran, A. Bertin, D. A. Wilson, M. Peterca, S. Zhang, N. P. Kamat, K. Vargo, D. Moock, E. D. Johnston, D. A. Hammer, D. J. Pochan, Y. Chen, Y. M. Chabre, T. C. Shiao, M. Bergeron-Brlek, S. Andre, R. Roy, H. J. Gabius and P. A. Heiney, *J. Am. Chem. Soc.*, 2013, **135**, 9055-9077.
16. M. M. Pisal, R. A. Annadate, M. C. Athalye, D. Kumar, S. P. Chavan, D. Sarkar and H. Borate, *Bioorg. Med. Chem. Lett.*, 2017, **27**, 979-988.
17. H. P. Mangunuru, J. R. Yerabolu and G. Wang, *Tetrahedron Lett.*, 2015, **56**, 3361-3364.
18. H. P. Mangunuru, J. R. Yerabolu, D. Liu and G. Wang, *Tetrahedron Lett.*, 2015, **56**, 82-85.
19. S. Dedola, D. L. Hughes, S. A. Nepogodiev, M. Rejzek and R. A. Field, *Carbohydr. Res.*, 2010, **345**, 1123-1134.